The Role of Nanomaterial-Protein Interactions in Determining the Toxic Consequences of Nanomaterial Exposure

Eva J. Gubbins

A thesis submitted in partial fulfilment of the requirements for Heriot Watt University for the degree of Doctor of Philosophy.

January 2014

The copyright in this thesis is owned by the author. Any quotation from the thesis or use of any of the information contained in it must acknowledge this thesis as the source of the quotation or information.

Abstract

As early biological responses to foreign objects in the body can be influenced by their bound proteins, the nanomaterial hard protein corona (the collection of slow exchange proteins that associate with nanomaterials) is an emerging area of interest in nanotoxicology. There is a limited but growing appreciation of the role these interactions have in influencing nanomaterial toxicity.

This research dealt with (i) the characterisation of iron oxide and silica particles with and without a plasma, serum and lung lining fluid protein hard corona, (ii) the identification of the proteins in the hard corona that associate with the particles and (iii) the effect of the hard corona on influencing particle cytotoxicity in a J774.A1 macrophage cell line.

Initial investigation of the particles illustrates the advantages in using a variety of characterisation techniques to better elucidate particle properties. Subsequent characterisation of the hard corona protein profile demonstrated a clear difference in the biological identity of the particles in a plasma, serum and in a lung lining fluid corona. Although it is difficult to associate the impact of any individual protein identified in the hard corona to cytotoxicity this study indicates that the binding of proteins plays a significant role in altering the cytotoxic potential (as determined by LDH release) in macrophages. The work also demonstrates the hard corona has an impact on macrophage chemotaxis, which further strengthens the hypothesis that the corona is a key consideration in nanoparticle toxicity.

Ultimately this thesis finds that the nanomaterial hard corona is an important element to consider in experimental design and highlights the concept of creating particle preparation protocols to mimic the corona composition *in vivo* when examining *in vitro* cellular responses. This research highlights the implications for interpretation of data from *in vitro* cell culture tests that do not take the protein corona into consideration.

Aitheantas

B’é ullmhú an trácht seo mo pas chun an domhan mealltach, aisteach, fíorspéisiúil na heolaíochta. Thug an domhan seo go tíortha agus saotharlanna ar fud na hEorpa mé. Bhí an tádh orm, freisin, bheith ag obair trasna ceithre ollscoil le trí bliana anuas. Bhuail go leor scoláire agus eolaí liom ar an slí agus ba mhaith liom mo bhuíochas a gabháil le gach éinne a cabhraig liom le mo taighde agus mo ceisteanna teibí. Bhí a lán maoirseoir agam i rith an t-am sin agus ba mhaith liom “go raibh maith agat” a rá leo, go mór mór, Ollamh Vicki Stone, Dr.David Brown, agus Dr.Marco Monolopi nár chaill tuarisc ar mo dul cun cinn trasna saotharlanna difriúil. Buíochas freisin le foireann Ollamh Yuri Volkov ag an IMM i gColáiste na Trinóide, Baile Átha Cliath, go speisíalta Dr. Adriele Prina Mello agus Dr.Steven Paul a thug spreaga agus misneach dom faoin tionscadal nuair a bhí sé de dhíth orm.

Beadh an saol sa saotharlann an dúr, aonarach gan an caint agus comhrá, míle buíochas, mar sin, do gach éinne a bhí páirteach liom ó Ollscoil Napier agus Heriot Watt, Dún Éideann agus T.C.D. agus U.C.D., Baile Átha Cliath as an caibidil, an taca, agallamh agus an díospóireacht ar eolaíocht. Le Shona, Ali agus an HB, le Heli a cuir a lán cruinniú d’en scoth ar súil, Tatsiana Keiran, Omar, Diana, Navain agus na daoine as an IMM cabhraigh sibh go léir leis an turas a dhéanamh suimiúil agus táirbheach. Le mo chairde Maria, Susie, Edel, Gillian, Rosie agus Orfhlaith as mé a choimeád im’ cheartmheabhar, agus ar an bothar caol agus direach. Le Durka Durka ón Isiltír a thug ar strae mé, anois is aris, chun an domhan mór, iontach a feicheáil Go raibh maith agaibh go léir. Ni féidir liom chríochniú gan cúpla focal le mo chlann, Brian agus Sarah go speisíalta a fhiafriann na ceisteanna eolaíochta is fearr. Beidh na freagraí agam lá éigin – bfhéidir!

An Colt Foundation a thug infheistiú don tionscadal seo a bhí ar súil i gceangail le ollscoil Napier, Heriot Watt, Dún Éideann agus UCD, TCD, Baile Átha Cliath

THE COLT FOUNDATION
OCCUPATIONAL & ENVIRONMENTAL MEDICINE
The Foundation is a charity, registered No. 277189

Acknowledgments

The preparation of this thesis has been my passport to the engaging, curious and fascinating world of science. This world has brought me to many countries and laboratories across Europe and I have been lucky to work across four universities over the last three years. I have met with many scholars and scientists along the way and to everyone who has assisted me – with my sometimes abstract research queries and interests I am indebted. I have had many supervisors and in particular I would like to thank Professor Vicki Stone, Dr. David Brown and Dr. Marco Monolopi who have tracked my progress across many labs. Also I would like to thank Professor Yuri Volkov's team at the Institute for Molecular Medicine in Trinity College Dublin in particular Dr. Adriele Prina-Mello and Dr. Steven Paul for the motivation and enthusiasm for my project just when I needed it the most.

Life in the laboratory would be very dull and isolated without engagement and discussion. For all the chats, support, dialogue, meetings, scientific arguments and general 'banter' I have to say a big thanks to everyone who has been in some way or another involved (from Edinburgh Napier University, University College Dublin, Trinity College Dublin and Heriot Watt University) in making this journey an exciting interesting and beneficial one, in particular to Shona, Ali, and the HB. To Heli who organised many fantastic talks and meetings to keep us all up date. To Tatsiana, Keiran, Omar, Diana, Navain, Namrata and the entire IMM contingent. To Maria, Susie, Edel, Gillian, Rosie and Orflaith who kept me sane and on the right path in the big smoke that is Dublin City and Durka Durka for taking me off the path every now and then to see the big world outside. I can't really finish without adding a few lines to my family for their support - in particular Brian and Sarah who asked the best science questions which some day I might be able to answer.

Financial support for this work was provided by the Colt Foundation and was carried out in affiliation with Heriot-Watt University, Edinburgh Napier University, Trinity College Dublin and University College Dublin.

THE COLT FOUNDATION
OCCUPATIONAL & ENVIRONMENTAL MEDICINE
The Foundation is a charity, registered No. 277189

ACADEMIC REGISTRY

Research Thesis Submission

Name:	Eva J. Gubbins		
School/PGI:	School of Life Sciences.		
Version: (i.e. First, Resubmission, Final)	Final	Degree Sought (Award and Subject area)	Doctor of Philosophy

Declaration

In accordance with the appropriate regulations I hereby submit my thesis and I declare that:

1) The thesis embodies the results of my own work and has been composed by myself
2) Where appropriate, I have made acknowledgement of the work of others and have made reference to work carried out in collaboration with other persons
3) The thesis is the correct version of the thesis for submission and is the same version as any electronic versions submitted*.
4) my thesis for the award referred to, deposited in the Heriot-Watt University Library, should be made available for loan or photocopying and be available via the Institutional Repository, subject to such conditions as the Librarian may require
5) I understand that as a student of the University I am required to abide by the Regulations of the University and to conform to its discipline.

* Please note that it is the responsibility of the candidate to ensure that the correct version of the thesis is submitted.

Signature of Candidate: Date:

Submission

Submitted By (name in capitals):	
Signature of Individual Submitting:	
Date Submitted:	

For Completion in the Student Service Centre (SSC)

Received in the SSC by (name in capitals):			
Method of Submission (Handed in to SSC; posted through internal/external mail):			
E-thesis Submitted (mandatory for final theses)			
Signature		Date:	

Table of Contents

List of Figures

List of Tables

Abbreviations

Chapter 1

NP	Nanoparticle
NM	Nanomaterial
nm	Nanometre
TiO_2	Titanium Dioxide
EC	European Commission
UFP	Ultra Fine Particle
ROS	Reactive Oxygen Species
DNA	Deoxyribonucleic acid
H_20_2	Hydrogen Peroxide
ATP	Adenosine Triphosphate
NF	Nuclear Factor
RNS	Reactive Nitrogen Species
AM	Alveolar Macrophage
TNF-α	Tumour Necrosis Factor
CB	Carbon Black
CNT	Carbon Nanotube
ZP	Zeta Potential

Chapter 2

DLS	Dynamic Light Scattering
TEM	Transmission Electron Microscopy
SEM	Scanning Electron Microscopy
BET	Brunner-Emmet-Teller
PCS	Photon Correlation Spectroscopy
AFM	Atomic Force Microscopy
NTA	Nanoparticle Tracking Analysis
mW	Milliwatts
EDX/EDS	Energy Dispersive X-ray Spectroscopy
ZS	Zetasizer
DCS	Differential Centrifugation Sedimentation
IEP	Isoelectric Point
kHz	Kilohertz

g	g Force (unit of Measurement Gravity * Force or g force)
HCL	Hydrochloric Acid
NaOH	Sodium Hydroxide
WPMN	Working Party for Manufactured Nanomaterials
EU	European Union
PSD	Particle Size Distribution
Pdi	Polydispersity Index
RPMI	Culture Media named after Roswell Park Memorial Institute
BSA	Bovine Serum Albumin
NIH	National Institute of Health (USA)
ANOVA	Analysis of Variance
LLF	Lung Lining Fluid
FCS	Foetal Calf Serum

Chapter 3

kDa	Kilodalton
LDH	Lactate Dehydrogenase
WST	Tetrazolium Salt
DMSO	Dimethyl Sulfoxide
PPM	Parts Per Million
SDS-PAGE	Sodium Dodecyl Sulfate Polyacrylamide Gel Electrophoresis
MS	Mass Spectroscopy
mA	Milliampere
DDT	Dichlorodiphenyltrichloroethane
USPIO	Ultrasmall Superparamagnetic Iron Oxides
MTT	Tetrazolium dye
10%P	100µg/ml particles incubated in plasma and PBS (final conc.10% plasma)
55% P	100µg/ml particles incubated in plasma and PBS (final conc.55% plasma)
10%S	100µg/ml particles incubated in plasma and PBS (final conc.10% plasma)
LLF/ 10%P	Particles incubated with LLF and separately with 10% plasma
LLF/ 55%P	Particles incubated as per LLF, after incubation centrifuged and supernatant removed. Then incubated with 55% plasma

LLF/ 10%S	Particles incubated as per LLF, after incubation centrifuged and supernatant removed. Then incubated with 10% serum

Chapter 4

SMN	Silica Nanomaterials
NH_2	Amino Functional Group
MCP-1	Monocyte Chemotactic Protein-1
IL-10	Interleukin 10
IL-1β	Interleukin-1 beta
FACS	Fluorescence-Activated Cell Sorter
HaCaT	Human Keratinocyte Cell Line
HeLa	Henrietta Lacks -Human Cervical Carcinomal Cell Line
A549	Adenocarcinomic Human Alveolar Epithelial Cell Line
HcMEC/D3	Human Brain Endothelial Capillary Cell Line

Chapter 5

MAC	Membrane Attack Complex
C1-C9	Complement Proteins
TM	Trade Mark
PEG	Poly (Ethylene Glycol)
GPCR	G protein Coupled Receptors
MTS	Methanethiosulfonate
ZAC	Zymosan Activated Serum

Publications

Investigating the relationship between nanomaterial hazard and physicochemical properties: Informing the exploitation of nanomaterials within therapeutic and diagnostic applications [1]

Chapter 1 Introduction

1.1 Nanotechnology and Nanomaterials

The ‘nano-revolution’ that nominally began with the Feynman Lecture of 1959 ‘Plenty of room at the bottom’ [2] has progressed considerably in the last fifty years. Today the applications of nanotechnology represent a vast potential for innovation. The ability to design at the nanoscale, to create tailor made nanomaterials (NMs) means technology can be developed to have real and significant socioeconomic, health and environmental benefits. The current state of nanotechnology is a long way from the promise of what the technology holds (to transform communications, in medical diagnostics and treatments, the way energy is generated, the way all our materials, consumer goods and food are manufactured, etc.) but one sector of nanotechnology that is progressing rapidly is the production of engineered nanoparticles (NPs) and NMs.

According to the European Commission’s definition a “nanomaterial” refers to any ‘natural, incidental or manufactured material containing particles, in an unbound state or as an aggregate or as an agglomerate and where, for 50% or more of the particles in the number size distribution, one or more external dimensions is in the size range 1nm – 100nm’[3]. Clearly this definition focuses on the size criterion as opposed to other nano specific properties of NMs. The purpose of such a definition which applies to a heterogeneous set of materials is primarily to have consistent terminology. From a scientific context this is important to allow consistency across the published literature, it is also important in a legal context. Size is a measurable criterion can be applied to all NMs. It is an evolving definition and it will be reviewed again by the European Commission in 2014. The definition differs subtly from the definition of a NP, in that NPs are distinct entities which have one or more dimensions of the order of 100nm or less [4]. When materials are synthesized at the nanoscale their properties often change in comparison to larger particles - for example, the magnetism of iron NMs can be greatly enhanced in the nano scale as opposed to their bulk form [5], the large surface area of nano silica gives them superior absorbent properties [6] and gold NMs have enhanced optical properties at the nanoscale.

These unique properties make NMs useful in developing new materials with applications in almost every sector of the world's economy (see figure 1.1). For example, NMs are used in healthcare (magnetic resonance imaging and anticancer treatments [7]), in consumer products (see figure 1.2), in the electronics and construction industry (sensors and creation of durable light weight resistance materials [8]), in the food industry [9], in environmental remediation [10] and in the energy sector (efficient energy storage) [11].

NMs have occurred in the environment for millennia as they can be generated in a wide variety of biogenic processes, for example, biological synthesis by bacteria, geological processes such as the generation of volcanic ash and anthropogenic processes such as industrial or combustion derived and manufactured/engineered NMs. While we have been exposed to NMs for a long time the types and routes of this exposure have been limited, however today increasing production and use of a wide variety of NMs that vary in composition and physicochemical characteristics are raising concerns about the impact of engineered NMs on human health and in the environment [12].

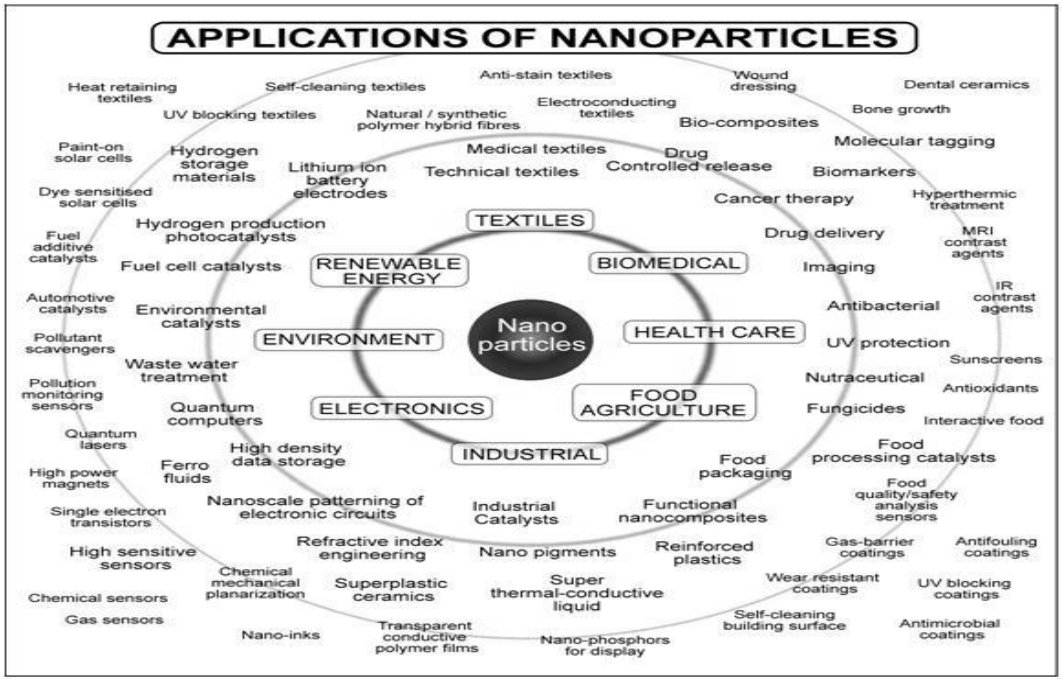

Figure 1.1: The applications of nanomaterials in a diverse range of fields (source: Tsuzuki 2009[13]).

There is still a lot of uncertainty on the quantities of NMs being manufactured globally. A recent report by the European Commission (EC) shows that the main NMs on the market today include carbon based NMs, metallic and non metallic NMs, organic NMs, and composites. Table 1.2 shows the quantities produced annually by tonnage as reported by the EC's staff working paper on the types and uses of NMs [14].

Table 1.1: Global quantities of nanomaterials produced annually as reported in European Commission's report on 'types and uses of nanomaterials'[14].

NM Produced Per Year	**Tonnage**
Global Quantity	11.5 million
Carbon Black (CB)	9.6 million
Amorphous Silica	1.5 million
Aluminium Oxide	200,000
Barium Titanate	15,000
Titanium Dioxide	10,000 t
Cerium Oxide	10,000
Zinc Oxide	8,000
Carbon Nanotubes(CNTs)/Nanofiber	>100 tonnes
Nanosilver	20 tonnes

Many of the current applications of NMs are in consumer products. According to the Inventory of Nanotechnology over 1000 products containing NMs are now on the market [15]. Figure 1.2 illustrates how the number of products available continues to increase steadily over the years, tripling in number from 2006 - 2009. It is expected that the widespread and expanding use of NMs will result in increased human and environmental exposure [16].

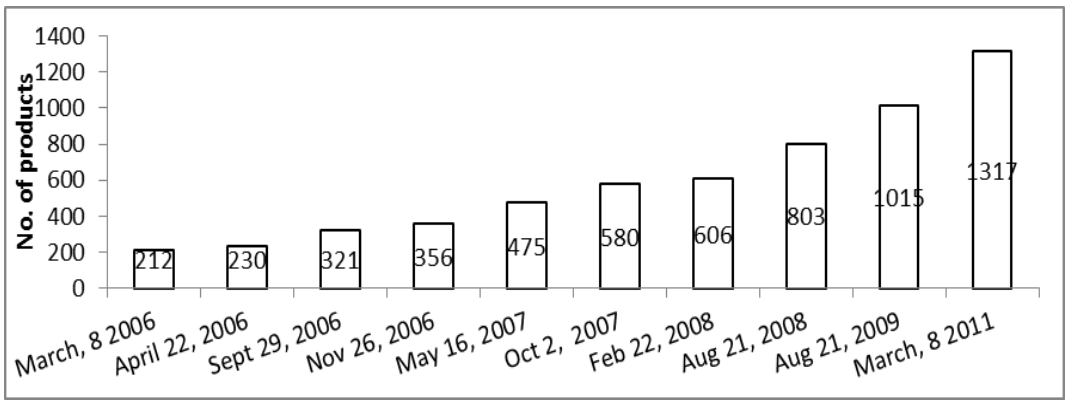

Figure 1.2: The number of consumer products on the market incorporating NMs from 2006 – 2011 [15].

These projections on global production and availability of NMs are compounded by a lack of regulatory guidelines in dealing with new novel NMs. Increasing mass production and use of NMs will likely lead to their appearance in the environment, air, water, soil and organisms, which in turn raises concern regarding potential human exposure and environmental contamination. Awareness is increasing and studies are being published in a diverse range of journals at an accelerated and unprecedented rate as can be seen in figure 1.3.

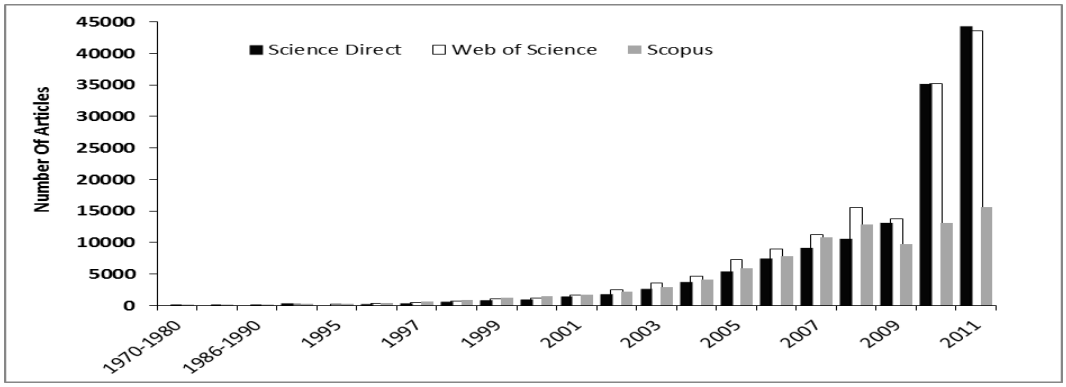

Figure 1.3: Review of articles (from Science Direct, Web of Science and Scopus) spanning from 1970 to 2011 searching the terms nanotoxicology, nanotoxicity and nanoparticles) n increase in the amount of published articles can be seen from nineteen ninety onwards. The numbers from the earlier decades may be underestimated as they would not include ultrafine particle literature due to the nano specific search terms used.

If the promise of nanotechnology is to be realised it is important to address the questions of health and environmental risks. There is still a considerable amount of uncertainty regarding how NMs behave in biological systems. An ever increasing amount of *in vitro* studies find NMs of many types in various treatments are taken up by a wide variety of mammalian cell types (e.g. hepatocytes, macrophages, fibroblasts, epithelial cells, red blood cells [17-20] and *in vivo* studies show evidence that NMs, due to their nanoscale size, can cross barriers from lungs and the gastrointestinal tract into the blood stream and migrate to other parts of the body such as the liver [21-24]. NMs have been shown to lead the production of reactive oxygen species (ROS - see section 1.2.). Such events can lead to altered cell signalling [25] causing enhanced transcription of defence genes, inflammation and activation of apoptotic pathways or necrosis. It is important to address potential exposure now while production of these materials is still relatively low, to mitigate any potential long term risks. A further understanding of how NMs are taken up in the body, how they are distributed, how they stimulate an immune response and how they are cleared from the body is essential, as this research will maximise the potential of engineered NMs.

1.2 Nanotoxicity

The study of the toxicity of NMs or nanotoxicity has evolved from the knowledge gained from particulate toxicology and from research in air pollution studies - focusing on respirable and atmospheric particulate matter or ultra-fine particles [22]. Ultra fine particles defined as particles less than 100nm are nano sized however; they are generally not manufactured intentionally and typically are not of a uniform size or composition. Particulate toxicology has a long history dating back to the middle ages where writings observing lung health in miners were first recorded by Paracelsus (1493 -1541) and Agricola (1494–1555) [26]. It was becoming apparent in the late 1900's that air pollution could be associated with adverse effects and by the late 1990's epidemiology evidence had proven that ambient air particle exposure lead to disease and mortality [27]. More recently research on biopersistent synthetic vitreous fibres and naturally occurring fibres such as asbestos has shown modern particle toxicology to be a multidisciplinary

science which ultimately aims to relate particle characteristics to pathological/physiological effects.

Today we know that it is the smallest fractions of atmospheric particulate matter (i.e. solid or liquid particles found in the air) such as particulate matter 2.5μm or less in size and ultra fine particles which are the most toxic on a per mass basis and an increase in particulate matter has been found to correlate with morbidity and mortality from cardiovascular and respiratory causes in humans [28-31]. This has led to the 'ultrafine hypothesis' that very small particles can be associated with distinct biological effects [28]. There are potentially various toxicological mechanisms by which particles exert their effect which of course will depend on exposure, the particle type (shape and chemistry), the initial deposition site and translocation. Pathological paradigms of particle toxicity have evolved to include physical (penetration), biological (phagocytosis, inflammation, cell signalling) as well as chemical processes (free radical production and oxidative stress) [32-34]. Nanotoxicology must now evolve to consider additional factors such as translocation from the lung into the blood/potential target organs and the effect of surface area for a wide range of ever increasing novel materials. It has been suggested that the ultrafine paradigm of particle toxicology may also be applicable to NMs and thus the emergence of nanotoxicology as a discipline essentially follows on from the well-established particle toxicology field.

1.2.1 Mechanisms of Toxicity

Tissues, cells and organs have well defined ways in which they react to any exposure. In nanotoxicology areas of interest include, (i) the association of NMs with cells - how they interact with cell membranes at the bio-nano interface and their uptake into cells, (ii) direct toxicological effects such as the production of free radicals and oxidative stress, (iii) indirect effects such as the ability of reactive oxygen species (ROS) to induce inflammation and (iv) damage to DNA or genotoxic potential is also a concern as it is known that some low soluble fibres/particles such as asbestos and crystalline silica are known carcinogens [35, 36]

1.2.1.1 Interaction of Nanomaterials with Cells

The fate of NMs in the body will depend not only on the physicochemical properties of the NMs but also on the forces acting in the interface between the NM and the cell [25, 37]. After NM exposure to the body this interface offers a first line of defence acting as a barrier protecting the tissues/cells/cell organelles, thus, studying the interaction of NM with cell membranes is a crucial step in understanding nanotoxicity. A recent review by Nel *et al.* [25] lists 'hydrodynamic, electrodynamic, electrostatic (or ionic), solvent and steric interactions and polymer binding' as the main forces governing the NM-cell interactions. As these interactions will vary according to the physicochemical makeup of the NM - this in some way begins to explain why, if we are to understand NM behaviour at the cell interface, a good degree of knowledge on the NMs physicochemical makeup is desirable. It is known that NMs do penetrate cell membranes and transport into cells such as endothelial, pulmonary, macrophage and neuronal cells [38]. Mechanisms of membrane penetration by NMs are not fully elucidated as it will vary depending on the NMs and cell type. NMs may cross the cellular membrane lipid bilayer by active uptake mechanisms (e.g. phagocytosis, pinocytosis and by clathrin and caveolin-mediated endocytosis) or by passive penetration (see figure 1.4) [39, 40]. If NMs enter the cell by endocytosis, NM are enclosed by endocytic vesicles and are not directly in contact with the cytosol of the cell, however NM internalized by membrane penetration enter the cytosol directly. As targeted entry of NMs into cells is an important feature of drug delivery this is the subject of much on-going research and many cellular uptake pathways have been described for particle uptake (as well as drugs, bacteria and viruses) [1, 41, 42]. In general literature has reported a great (and sometimes conflicting) variety in the uptake mechanism - some examples are reported in table 1.2.

Table 1.2 Particle uptake mechanisms reported in literature for various nanomaterials and cell types.

Uptake Mechanism	**Particles**	**Cell Type**	**Author and Year**
Clathrin-Mediated Endocytosis	Latex beads 50-200nm	murine melanoma B16-F10	Rejman *et al.*, 2004[42].
Caveolin-Dependent Endocytosis	Latex beads ≤ 500nm	murine melanoma cell line B16-F10	Rejman *et al.*, 2004 [42]
Endocytosis	50nm Magnetic NP coated in SiO_2	human lung cancer cells - A549	Kim *et al.*, 2006 [43]
Endocytosis – possible macropinocytosis	18 ± 5nm Polymer NP	Murine macrophage cells - J774A.1	Fernando *et al.*, [44]
Suggested Several Uptake Pathways (e.g., clathrin and caveolae-mediated endocytosis, and macropinocytosis)	Hydrophobic glycol chitosan NPs (359nm)	Human HeLa cells	Nam *et al.*, 2009 [45].
Pinocytosis/Macropinocytosis	polystyrene NP (113 nm)	Human HeLa Cells	Dausen *et al.*, 2008 [46]
Phagocytosis	Metallofullerenol (100-157nm)	macrophages, and lymphocytes	Liu *et al.*, 2009[47]
Passive Uptake Mechanism (diffusion, transmembrane channels, or adhesive interactions)	22nm TiO_2	*In vivo* (rat inhalation)	Geiser et al., 2005 [48]
Passive uptake (membrane penetration without pore formation)	QDs coated with zwitterionic thiol ligand D-penicillamine.	Red Blood Cells	Wang et al., 2012 [49]

A recent study investigating a range of cell types including HeLa (cervical cancer), A549 (lung carcinoma) and 1321N1 (brain astrocytoma) cells concluded that no one mechanism of transport was responsible for uptake and suggested that even for one type of NM the uptake mechanism could be different depending on the cell type [50].

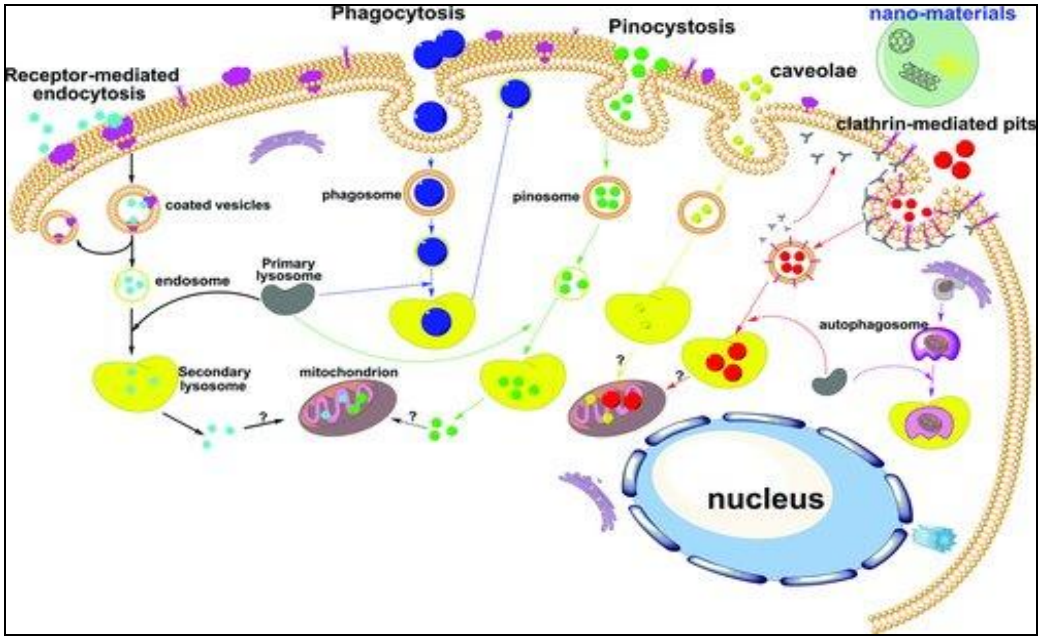

Figure 1.4: Possible mechanisms of NM cellular uptake – image taken from Zhao et al. [38].

One emerging area of investigation is the concept of the NM 'corona' or the ability of NM to absorb biomolecules onto their surface (particularly proteins, therefore termed the protein corona). This is central in shaping the surface properties, charges, aggregation behaviour and size of NMs within a biological system and has been found to effect the amount of uptake into cells [51]. Hypothetically this could also affect the interaction of NMs with cell surface receptor proteins. An interaction such as this may lead to denaturation/malformation of these cell membrane receptors leading to the induction of a biological response causing changes in the signalling pathway of target cells [52]. However this hypothesis does lead away from the current paradigm of nanotoxicity which is the role of oxidative stress induced toxicity.

1.2.1.2 Oxidative Stress

To date oxidative stress has emerged as the leading paradigm of NM toxicity [53]. When an atom has unpaired electrons it is termed a free radical - free radicals are highly volatile and in a cell will react with cellular molecules (lipids, nucleic

acids, etc.) leading to oxidation. There are many types of radicals and those that derive from oxygen are collectively called ROS, examples include the hydroxyl radical ($^{\cdot}OH$), superoxide radical ($^{\bullet}0_2^-$) and hydrogen peroxide (H_20_2). The main source of ROS *in vivo* is in the mitochondria - produced during oxidative metabolism leading to adenosine triphosphate (ATP) production. ROS is also a feature of many tissues [54] for example many oxidases produce ROS during xenobiotic metabolism.

As protection against the damaging effects of ROS cells have evolved to deal with these radicals - for example antioxidant enzymes (such as superoxide dismutase, catalase and glutathione peroxidase) counteract the effects of ROS [55]. Generation of ROS is an important cellular function, however oxidative stress results when ROS overwhelms the antioxidant system of the cell [56]. This increased oxidative stress depletes cellular antioxidants and leads the activation of transcription factors for pro-inflammatory mediators such as nuclear factor kB (NF kB) and pro-inflammatory cytokines and chemokines [57], causing inflammation. Nel *et al.* [58] describes the hierarchical oxidative stress hypothesis where a lower level of oxidative stress is associated with the induction of antioxidant and detoxification enzymes and at higher levels of oxidative stress activation of pro-inflammatory mediators can lead to inflammation and cytotoxicity and prolonged or excessive ROS generation can lead to cell death. Although this hierarchical oxidative stress hypothesis is a basic concept of what is no doubt a complex mechanism in vitro it is universally accepted that ROS can damage virtually any biomolecules present and oxidative stress is a significant event in the mechanism for inflammation based chronic degenerative diseases [59] and it has been implicated in diseases such as pulmonary fibrosis, atherosclerosis, cancer, neurodegenerative diseases and in aging [56].

The oxidative stress paradigm for NM toxicity emerged from research in the 1980s by Mossman *et al.* [35, 36] who discovered the direct carcinogenic effects of asbestos. They saw that the high iron content of the asbestos resulted in the generation of reactive species which they suggested could initiate cell signalling events to induce cell damage. One of the first published reports of nanotoxicity was conducted in the rat lung by Oberdörster *et al.* [60] and found that ultrafine

TiO_2 particles induced a greater inflammatory reaction than fine TiO_2. This led Stone *et al.* (1998) to investigate the potential of ultrafine particles to generate ROS and the role of this ROS production in the toxicity of the particles [61]. Today there is evidence from many published studies [22, 32, 62, 63] that NMs have the ability to induce oxidative stress and inflammation. NMs may cause oxidative stress either by non-cellular mediated ROS production or by particle mediated cellular ROS and reactive nitrogen species (RNS) production [62]. Non cellular oxidative stress results from or is enhanced by transition metals. The mechanism of toxic action of asbestos for example has been shown to involve the ability of iron present in asbestos to form hydroxyl radicals due to iron catalysed reactions (Fenton chemistry). These hydroxyl radicals can go on to cause peroxidation and DNA strand breaks.

1.2.1.3 Inhalation Toxicology - The Role of Macrophages

A major source of particle exposure to the body is via inhalation. Such an exposure may occur at the synthesis stage in an occupational setting or due to wear and tear from a product containing NMs. The lung not only has physical defence mechanisms which can filter and eliminate particles (i.e. nasal hairs and the mucocilliary escalator) but also specialised cells such as Type I and Type II epithelial cells and macrophages (interstitial intravascular and alveolar macrophages (AM)). Macrophages are derived from the circulating blood monocyte population and are distributed ubiquitously throughout the body where they have various roles, for example in phagocytosis and antigen presentation and also in cytokine production [64]. AM are large macrophages (12-40μm) [65] and continually deal with inhaled foreign substances due to their location in the alveolar space. Their ability to ingest and degrade particulate matter using the molecular mechanism of phagocytosis is key in their defence of the lung. Macrophages express a variety of cell-surface receptors that can bind to antigens. Upon ligand binding, the macrophage cell-surface receptors become activated and trigger phagocytosis. Most of our understanding of the signalling pathways leading to phagocytosis in macrophages comes from studies of the Fc receptor [66]. Each receptor is involved in a specific response thus macrophages can produce a variety of functions depending on the receptors involved in the

particular response. This variety of receptors capable of stimulating phagocytosis (e.g. Fc and complement receptors etc.) makes it a complex action to elucidate – however recently much progress has been made in understanding the signalling pathways that induce phagocytosis [67]. As the cell moves, filopodia up to 20 μm in length can be seen, these are supported by actin filaments and these actin filaments, in association with structural and regulatory proteins, create the molecular mechanics of cell movement [67]. Besides their phagocytic ability macrophages (like many other cells of the immune system) have the ability to secrete products such as cytokines [68].

Cytokines are soluble cell-signalling proteins which functions in intercellular communication regulating cellular responses such as proliferation, differentiation, immunoregulation. Upon antigen stimulation macrophages can synthesize/release a variety of cytokines (such as IL-1, IL-6, IL-8, IL-10, IL-12, TNF-α, MCP-1), which are involved in immune responses, inflammation and other homeostatic processes [69]. Cytokines act by binding to their specific cell surface receptors which results in a cascade of intracellular signalling. This can result in processes such as upregulation and/or downregulation of genes and their transcription factors, resulting in the production of other/more cytokines or in their suppression. Macrophages can also secrete chemokines a type of cytokine enabling chemotaxis or the recruitment of circulating monocytes within tissues [69]. This will be discussed in more detail in Chapter 5. The presence or absence of cytokines in the body's biological fluids at any time reflects a complex relationship between activation/production and inhibitory signals acting on the macrophage (or indeed any other producer cell) [70].

1.3 Physicochemical Characteristics of Nanomaterials

The inherent toxicity of NMs and their ability to interact with a biological system will vary depending on their individual physicochemical properties [71]. It has become apparent that even when NMs are composed of the same elements as their bulk counterparts (i.e. uniform particles of similar/same chemical makeup but of a larger size); they behave differently as mentioned in 1.1. It is important to ascertain if there is any relationship between the physico-chemical properties of

NMs and the induction of any toxic responses in biological systems. The physicochemical properties in question are: small particle size, size distribution, specific surface-area, surface structure, molecular and crystal structure, chemical composition (including surface coating), physical form, particle density, solubility, colloidal stability, bulk density, agglomeration state, porosity and surface charge [72, 73]. The particle size can influence the fate of the NM in the body and thus the body's response to the exposure [74]. For example, much research in the area of inhaled particles, which have been obtained predominately from the rodent model, find that the mechanism of inhaled particle deposition is to a great extent dependent on the diameter of the inhaled particles [75]. When particles are inhaled the size will determine not only the mechanism of deposition but also where in the lung it is deposited. Particles in the µm range will deposit in the upper airways or mouth and throat whereas those smaller in size deposit in the alveolar region [75]. *Oberdörster* et al. [22, 76] reported that the situation for NMs is a little more complicated and the deposition behaviour in the respiratory system is not linear with size – with NMs in the size range 10 and 50 nm being deposited mainly in the alveoli, while smaller and larger ones are more efficiently deposited in the higher regions. This suggests that NMs of different sizes can have different effects in different parts of the lungs. NMs will not necessarily remain at their sites of deposition in the respiratory tract. They may undergo numerous transport processes within the various tissues of the lungs, including clearance from the lungs. A study by Moller et al. [77] on the retention times of NMs in the airways also points to a size relationship. For example, a human inhalation study of 100nm carbon particles found that 25% of the particles were cleared after 1 day (due to mucocilliary action) and 75% of the particles were persistent in the airways for more than 48 hours. The mechanism proposed for such retention was that deposition of the particles meant they were no longer accessible for clearance [75].

It has been suggested that a particle greater than 100nm in size will not enter cells via receptor mediated processes [78, 79]. Other sizes that have been noted as important in nanotoxicity are those below 40nm which may have greater access to the nucleus and the mitochondria [78] and Elder *et al.* did show that size was important in the neuronal uptake of 31nm Mn oxide NP [80]. *In vitro*

experiments have also demonstrated this size specific effect for example, in the rat alveolar macrophages and human blood monocyte cells, 14nm carbon black (CB) NPs were shown to induce a calcium influx, which was found to activate transcription factors and stimulate the production of pro-inflammatory cytokine (TNF-α), significantly compared to treatment with 260nm CB, indicating that the effect is size specific [81]. However these size observations will be specific to the NM and the cell type employed thus such observations are best used as a general guideline.

Size is also related to surface area, as the size of NM decreases, the surface area per unit mass increases and so forces such as gravity may not be as significant when compared with surface forces like van der Waals, electrostatic forces and chemical bonding [82]. As the size of the particle decreases and the surface area increases more of its atoms or molecules are exposed at the surface rather than the interior of the material. The surface to bulk ratio has been linked to the increased biological reactivity of NMs [62, 63]. This large surface to bulk ratio will thus allow for binding of proteins and other biomolecules available in the living system. Toxicity data from a pulmonary toxicity study in rats shows that inhalation exposures to NMs (TiO_2, polystyrene beads and CB) results in enhanced toxicity responses when compared with micro-sized particles with a comparable chemical composition [22, 83, 84]. For example, in the case of TiO_2 at high dose concentrations the ultrafine TiO_2 caused inflammation, and at low doses resulted in proinflammatory effects suggesting that the NMs may have a greater biological activity than larger particles [34, 85]. The positive effects of the large surface to bulk ratio is in creating novel ways of enabling drug delivery, but it may also have possible negative cytotoxic effects, given that the interaction of NMs with subcellular structures may be different from that of the bulk material. For this reason it is important when considering dose and effect that properties such as size and surface area are investigated [24, 62, 63].

Shape is an important factor to consider in NM toxicity as evidence from investigating materials such as asbestos has shown that shape drives the biological response [36, 86]. Fibre-like NMs such as carbon nanotubes (CNTs) have been investigated for shape related toxic effects. For example Brown *et al.* [87] demonstrated the connection between morphology and cellular response in a

monocyte cell line finding monocytes exposed to long straight multiwall CNTs produced significantly more TNF-α and ROS compared with highly curved materials. Poland *et al.* [88] showed a similar result *in vivo*, where long straight nanotubes injected into the abdominal cavity of mice produced a similar result to that of asbestos, causing an inflammatory response. This was again in contrast to the entangled nanotubes which did not produce a significant inflammatory response. Hamilton *et al.* [89] study on TiO_2 NMs of different shapes concluded that AM had more difficulty in processing longer fibers than the shorter fibers and concluded that toxicity was altered by the shape of the NM. In recent years much research has been carried out investigating if fibres such as CNTs, due to their fibre shape, translocate in a similar way to biopersistent asbestos. There is growing evidence that shows CNT do translocate. For example, multi walled CNTs *in vivo* (inhalation or aspiration) translocate to sub pleural tissue, where they caused fibrosis [90, 91]. The charge of NMs is another aspect that needs consideration. The surface charge of NMs can be measured in solution using zeta potential analysis (ZP). ZP is a measure of the electrostatic forces and so will vary depending on the material of interest. Of course any surface coatings or adsorbed material will effect this ZP measurement and as such a single ZP measurement without regard to the biological environment (pH, adsorbed molecules, etc.) will not be relevant. As the cell wall has a negative surface charge [92] it may seem that positively charged particles would be more likely to be drawn to the cell and thus could be more toxic. Many *in vivo* and *in vitro* studies have found that cationic particles are more cytotoxic [25], for example Goodman *et al*. found cells exposed to Au NMs were more likely to induce haemolysis and platelet aggregation than anionic particles [93]. However the role of surface charge in toxicity has been reported for both anionic and cationic particles in the literature [94].

1.4 *In vitro* Cytotoxicity Testing of Nanomaterials

In toxicology we aim to relate the basal cytotoxicity of a compound *in vitro* to its toxicity *in vivo*, however there are factors which can complicate this correlation and optimisation of *in vitro* assays is a major concern in toxicology. It is important to ascertain how the physico-chemical properties mentioned in 1.3 will

express themselves in biological systems. As NMs can consist of a wide variety of materials characterisation and classification is the first step in addressing potential toxicity but of course additional factors are also important when considering nanotoxicity. For example, the nominal NM concentration is difficult to determine given the complex nature of NMs and NMs may be influenced by the *in vitro* assay components and properties. There is a need to develop and design assays to consider not just the nominal dose but the free dose available to and recognised by the cells.

The route of entry and fate of the NM must be considered; NMs can enter the body via inhalation, dermal contact and ingestion, injection or implantation. The lung represents a major route of entry for NMs, where both micro sized particles and NM will be cleared via the mucocilliary escalator. Particles are also cleared or undergo phagocytosis by macrophages (as mention previously section 1.2.1.3) and transported to the throat where they are cleared. Renwick *et al.* [95] showed a significant reduction in the ability of macrophages (J774.A1.2) to phagocytose particles (fine and ultrafine TiO_2, CB and ultrafine CB) and attributed this slowed clearance in part to a particle-mediated impairment of macrophage phagocytosis. Such an effect may lead to persistence, translocation to other body compartments, interaction with other cell types and induction of the biological response. Compounding this is the ability of transition metals (for example zinc and iron) to potentiate the toxic NM effects [96]. NMs that are effectively cleared from the lungs may potentially exert toxic effects in the gut or may translocate via the circulatory system to a different tissue or organ. When designing *in vitro* toxicology assays there is a need to consider a potential target tissue or organs. NMs given their size have a greater ability to reach many organs and tissues in the body. If a potential target can be identified the mechanism by which the material can produce its effect must be considered. The rate and frequency of exposure, and the fate of the NM once in the body, the absorption, distribution, metabolism and elimination are crucial factors when considering the toxicity of NMs. Borm *et al.* [97] suggested looking at the 5 D's of particle toxicity *in vivo*; dose, deposition, dimension, durability and defence, when examining nanotoxicity.

Many *in vivo* studies have focused on pulmonary toxicity ([21, 79, 87-89, 98]) but NM such as those designed for drug delivery (e.g. iron oxides NMs used in magnetic hyperthermia) can also be deliberately introduced into the body by injection. In such cases NMs are generally developed to have specific coatings to allow increase blood circulation time, reduce adsorption of protein and promote phagocytosis to specific tumour cells [99]. Combinations of both *in vivo* and *in vitro* studies are useful in elucidating the mechanisms of toxicity. *In vitro* it can be difficult to determine the actual exposure dose and to correlate any findings with the effect as it is difficult to determine the effect of reagents used and the effectiveness of the model. It has thus proven to be difficult to elucidate the mechanisms of toxicity of NMs. This emerging complex issue is compounded by the fact that different studies reveal differences in NM cytotoxicity ranging from non-toxic to highly toxic [100, 101]. NMs cannot be seen as a consistent or uniform set of materials with specific toxicity. The aim must be to understand the physicochemical characteristics that drive NM toxicity. It would seem unlikely that given the large diversity in NMs being produced there will be a universal biological response. However the key parameters of concern for most types of NMs are emerging to be, good characterisation of NMs, the surface area of the NM, the mechanism by which particles binds to biological materials *in vivo*, the identification and affinity of absorbed biological material to NMs *in vitro*/*in vivo*, their fate, their biopersistance and of course exposure. Individualised testing of every individual NM in production is not a possibility considering the amount of experimental work, time, money, and animals that would be required. However understanding the mechanism of nano induced toxicity is something that needs to be considered in order to ascertain if any paradigms or trends exist - for example the ability of NMs to generate oxidative stress can be an indicator of how toxic it may be and could be employed as a screening tool to identify NMs which warrant a closer examination.

One area that is emerging to be a big factor in nanotoxicity is the ability of NMs to bind biological molecules such as proteins and lipids once in the body. Once particles and NMs enter the body they immediately come into contact with biological fluids, the content of which is dependent upon the route of entry [78, 102-104]. It is well known that early biological responses to foreign objects in the

body are influenced by their attached protein [105]. In fact considerable research has been done in the medical device field to coat the surfaces of medical devices with compounds to prevent and avoid the formation of a biopolymer coating between the device or foreign material and the body's tissues [106, 107]. Conversely, the ability to control NM binding leads to numerous NM applications, for example in nanobiotechnology and drug design [108, 109]. Although much research has been carried out on these protein-surface interactions in the bio-medical industry, to date there is limited understanding of the role of these interactions in influencing NM toxicity. The aim of this thesis is to address one of these issues by investigating particle and NM–protein interactions. Beginning to understand more about these key concepts will address the gap in our knowledge on the role of these interactions in influencing NM induced toxicity. In the long term this may help to close the gap in our knowledge of NMs mechanism of toxicity which may result in being able to abandon our case by case approach in light of a less time consuming, economical predicative model, which would allow for not only faster toxicity assessments but also aid commercialisation and bring the field one step closer to realisation of the power of nanotechnology.

1.5 Aims and Objectives

- This study aims to characterize a set of nanomaterials and investigate how their properties (size, composition and charge) may affect their cytotoxicity in a J774.A1 macrophage cell line. Chapter 2 exclusively deals with the characterisation of the NM and Chapter 3 and four explores NM toxicity on a J774.A1 macrophage cell line

- Use protein characterization techniques to investigate the interactions of NMs with proteins and examine how the size, composition and charge influence the affinity and degree of protein binding. Chapter 3 explores this aim with respect to iron oxide particles and Chapter 4 with respect to silica particles

- Chapter 5 investigates if the interaction of NMs with biological fluids causes a change in the function of the proteins and ultimately aims to understand the role this protein-NM interaction has in influencing toxicity of the NMs.

- To develop a better understanding of nanotoxicity by considering the *in vivo* situation. Thus enabling superior *in vivo-in vitro* extrapolations to be made and gaining more relevant toxicity data.

Chapter 2 Characterisation of Nanomaterials

2.1 Characterisation

In order to gain relevant data from *in vitro* toxicity assessments which are reproducible and reliable NMs must be well characterised. Many of the physicochemical characteristics of NMs are still not fully understood/elucidated making this a challenging and complex issue. Thorough characterisation of NMs includes measurements before and after dispersion of size, size distribution, surface area, morphological features (such as shape, surface roughness and porosity), particle chemistry (such as surface chemistry, particle composition, solubility) and contamination testing (such as metal analysis and endotoxin testing) [110, 111]. Thorough characterisation however may not always be possible given the interdisciplinary nature of nanotoxicology. Knowledge, facilities, time and costs are obstacles that may not allow for such exhaustive characterisation. Although not every aspect of the NMs can be meticulously characterised at a minimum, key parameters such as charge, shape, size and surface area should be known in order to relate any results to exposure.

Many NMs can be purchased commercially for toxicological testing and are supplied with manufacturer specifications (for example detailing size and composition information). However simply reporting manufacturers specifications is no longer deemed sufficient for a nanotoxicological study, Park *et al.* [112] highlighted that there can be significant differences in values obtained for independently characterised NMs and those provided by the supplier or manufacturer.

Ideally knowledge of how the NMs behave in the test system (*in situ*) is of interest, for example how the test media or other modifications (such as sonicating) will affect the NMs. If this is not possible, at minimum, the detailed experimental conditions should be reported and as much characterisation data as possible in the relevant biological media should be completed, without this information results from toxicological studies can be meaningless or have limited significance. The addition of serum, for example, is routine in cell culture studies,

Murdock *et al.* [113] found that metal oxide NMs not only tend to agglomerate in solution but the addition of serum in the culture media can affect the toxicity *in vitro*. In general serum in cell culture systems has been reported to interfere with *in vitro* tests, as it can affect the uptake rate of the NMs in question [114-117], can coat the particle surface [118] allow binding of test particles to serum proteins, may act as an antioxidant and may alter differentiation/cell cycle state of cells [119]. It should also be noted that NMs dispersed and sonicated in water and then added into dispersant/media/serum may produce different results than NMs sonicated in dispersant/media/serum alone and the effect of the dispersant is of importance as it may impact on toxicity of the NMs, for example Wang *et al.* [120] found that degradation of dispersants during sonication can be toxic to cells. It is known that the serum content in cell culture media varies not only between laboratories, but also will vary depending on what cell type is used, which can further complicate comparison of results. NMs characterised in their dry state and those characterised in suspension will offer two entirely different sets of data. It is also important to check if NM interacts with the assay components or the detection system. Kroll *et al.* [121] lists many important properties of NM that can interact with the test system such as high adsorption capacity, optical properties, catalytic activity and in the specific case of iron oxide NMs factors such as magnetism and dissolution must also be considered.

In addition to the fact that NMs samples are not homogenous and that there are no nano specific standard characterisation methods, another issue arises from the variety of manufacturers producing NMs. Manufactured NMs are engineered in an ever increasing variety of ways and using a wide variety of materials. They are also often produced in relatively small quantities. This increases the chance of having batch to batch variations. Successful measurement will depend on accurate and precise sampling, sample preparation and sample measurement. Thus the first task is to accurately obtain a representative sample of the bulk for characterisation and experimentation. Characterisation particularly *in situ* is a complex procedure and the list of available methodologies becomes larger as our understanding grows. It has been suggested that there is a need for guidelines or standard methodologies for basic characterisation of NMs [110] however as the term NM potentially encompasses such a large diversity of materials each with their own

unique properties, each individual NM may require its own unique set of characterisation for optimum results on its detailed structure. For example, popular methods such as dynamic light scattering (DLS) for size analysis are only suitable for spherical particles, for non-spherical particles alternatives such as imaging with transmission electron microscope (TEM) or scanning electron microscope (SEM) will be required.

2.1.1 Dispersion

Once sampled, NMs need to be exposed to the test model using a relevant method of dispersal in a suitable non toxic media. The measured size distribution is highly dependent on the degree of dispersal [110] and NMs can agglomerate when dispersed in high ionic strength or protein rich environments [110]. Agglomeration/aggregation of NMs need to be considered in experimental design so as best to simulate the *in vivo* behaviour of NMs although the dispersal method should not aim to manipulate the sample to produce dispersed NMs that are not relevant to real life exposures [110]. Agglomerates can be defined as a 'collection of loosely bound particles or aggregates or mixtures of the two where the external surface area is similar to the sum of the surface area of the individual components'. An aggregate can be defined as a 'particles comprising of strongly bonded or fused particles where the external surface area may be significantly smaller than the sum of the calculated surface areas of the individual components' [122]. So whereas agglomerates may be easily dispersed using sonication or the addition of dispersants, aggregates may not so easily be dispersed. This leads to the question of dose. The dose *in vitro* is related to the behaviour of NMs in the test media, if for example NMs agglomerate they can settle quicker than their monodispersed counterpart onto cells *in vitro* and may not be available for uptake into cells. Any resulting dose-response curves produced from exposures that do not consider dispersal (i.e. transport of NM to cell and time frame to reach cells) may be untrustworthy as these variations would be expected to impact the magnitude of a cellular response [123]. In summary, an overall understanding of the implications of dispersal on the delivered dose is important and whichever method of dispersal is used will depend on the type of NM, the state in which it is produced (e.g. powder, liquid) and the model system used.

2.1.2 Size Measurements

Many techniques are available for measuring the size of NMs. Today global standards from the International Organisation for Standardisation exist not only with respect to sampling and dispersion of particles but also for particle size analysis [124]. They include information on how to represent the results from particle size analysis, determination of specific surface area of solids by gas adsorption using a technique known as Brunner-Emmet-Teller (BET), particle size analysis using photon correlation spectroscopy (PCS) and particle size using image analysis methods. These methods are not considered a 'gold standard' for nanotechnology as they relate to diverse particle sizes, however it is generally accepted that some form of microscopy such as TEM, SEM or atomic force microscopy (AFM)) and one other method, such as dynamic light scattering (DLS) or surface area measurements etc., should be used when assessing NM size.

PCS, such as DLS, is a common method to measure hydrodynamic diameter of spherical NMs. A Malvern Zetasizer Nano ZS measures size within a 0.6nm to 6µm range [125]. It determines the size by measuring the Brownian motion of the particles in a sample. Brownian motion is defined as: 'the random movement of particles in a liquid due to the bombardment by the molecules that surround them' [125]. Thus DLS works by illuminating the particles with a laser and analysing the intensity fluctuations in the scattered light. An important feature of Brownian motion for DLS is that small particles move quicker than larger particles. The relationship between the size of a particle and its speed due to Brownian motion is defined in the Stokes-Einstein equation. Due to this relationship and that between the diffusion speed and size of a particle, the size can be determined.

Nanoparticle tracking and analysis (NTA) is an instrumental technique that allows NMs to be sized in a liquid. According to manufacturer's specifications NMs in liquid suspension with range of 10nm to 1000nm; and with concentration of 0.1ppm to 40% w/v, in any non-corrosive solvent can be measured. The sample cell has an optical window and a laser beam (40mW, 635nm) is focused through the optical flat window on the sample [126]. Particles in the liquid sample pass

through the beam and are seen via a microscope as small points of light moving due to Brownian motion. This motion of the particles in Brownian motion is captured by camera and recorded - thus what is obtained is a recording of each particle being tracked over time. The recording can be analysed via NTA software and the mean square of the displacement over time is determined. From this information the diffusion coefficient and hence the sphere equivalent (the hydrodynamic diameter) can be determined again (as with DLS) using the Stokes-Einstein equations. As the NTA separately tracks each individual particle the size distributions generated reflect the actual number of particles seen in the sample and this is a big advantage over PCS, a method where a large number of particles are analysed simultaneously and result in a 'Z-average' thus being more suited to more polydisperse samples [127]. When using PCS if there are aggregates present it will lead to a shift in the distribution to the right hiding or obscuring any smaller particles present in the sample. Thus according to the manufacturer, NTA analysis allows for a higher resolution and a better understanding of aggregation behaviour [128]. An advantage over PCS also lies in the fact that little knowledge of the particle properties (i.e. refractive index) is required - and knowledge of parameters such as sample viscosity and temperature are sufficient data to input when analysing a sample. In this way the advantage of NTA is that it allows for particle populations to be separated by size and intensity and allows complex heterogeneous samples to be fully characterised without the intensity bias towards large particles [128]. It is important to emphasize that the particles themselves are not visualised - the Brownian motion is. An inherent problem with NM imaging analysis is that NMs are too small to be imaged by light dependent microscopy.

Differential centrifugation sedimentation is another method that can be used for size analysis for particles that range in size from 5nm to 75µm [129]. Particles in a liquid are centrifuged at known speed and allowed to settle. The particles will settle due to gravity according to Stokes law, larger particles will settle faster than smaller ones [130]. The system can be optimised for different materials by knowing the density of the particles and adjusting the speed of centrifugation.

Size information can also be determined from image analysis of images obtained from TEM and SEM. TEM and SEM can be used to image particles of size from

0.3nm up to 1mm. Visual imaging is one of the most instinctive methods for size determination. Its advantages lie in the fact that it can provide information not only on size but also on possible contamination, on composition (using EDX metal analysis - see section 2.1.3) and morphology. Using image analysis programmes the size can be estimated and surface area modelled. However the sample preparation process can be complicated and time consuming and can introduce artefacts, also due to the fact that the sample is imaged under a high vacuum the actual process of imaging can cause agglomeration. It is also an expensive technique and in order to get any meaningful results a large number of images may be required for image analysis.

It is important to consider that different methods of sizing can give different values, especially if the sample is polydispersed. Some techniques may measure the particle size (e.g. TEM) and other techniques measure hydrodynamic diameter (e.g. DLS), thus it is important to gain as much knowledge about a sample before analysis.

2.1.3 Other Physicochemical Properties

2.1.3.1 Zeta Potential

When a charged particle is introduced into liquid, ions of an opposite charge will be attracted to its surface. Ions close to the surface of the particle will bind more than ions that are further away and will form what is called a 'diffuse layer'[125]. Within the diffuse layer there is a boundary around which any ions within the boundary will move with the particle when it moves in the liquid and any ions outside the boundary will stay where they are. This boundary is called the 'slipping plane' [125]. The potential that exists at this boundary is known as the zeta potential (ZP). It is important to ascertain the ZP as it gives an understanding of the stability of the particle in solution, making ZP a powerful characterisation tool. The ZP is not an actual measurement of the NM surface charge, or a measurement of the atomic charge at the surface of the NM. As described above ZP will help in gaining an understanding of how a particle will react in a solution. If all particles have a large positive or negative ZP then they will repel each other

and these types of particles tend not to agglomerate. Conversely particles with low ZP values will tend to agglomerate as there are no forces stopping them from combining. Particles with a ZP more positive or negative than 30mV are considered stable [125].

There are many factors which will affect the ZP, for example the pH. ZP should always be quoted at its pH, and when doing initial research a ZP versus pH plot should be constructed. The point where this plot passes through zero is called the isoelectric point (IEP) [125]. This IEP is normally the point where the particle suspension is least stable. For this reason it is essential to consider the pH when carrying out cell studies. Here again it is necessary to consider routes of exposure and the model for NM exposure. If using NMs in solution with a pH that is the same as the pH at the IEP the NMs may agglomerate more than when the pH is greater or less than the IEP. If the route of exposure is via the skin the pH is 5.5 whereas the blood has a physiological range of pH 7.34 - 7.45. As NM behaviour, including its size, shape and ZP will be affected by pH and this may alter their fate and behaviour in the body. Other issues to be considered in terms of charge and pH is that altering the pH also has effects in the amount of soluble ions that may be released from the NM again adding another layer of complexity to understanding NM toxicity, i.e. differentiating between ion effects and NM effects.

ZP can be measured by a variety of techniques. One such way is by using the Malvern Zetasizer Nano instrument. This instrument uses a combined technique of electrophoresis and laser doppler velocimetry, i.e. it uses a laser which is passed through the sample to measure 'the velocity of the particles in an applied electric field of known value (electrophoretic mobility)' [125]. Once the velocity of the particle is known and the electrical field applied by using two other known constants of the sample (viscosity and dielectric constant) the ZP can be calculated.

2.1.3.2 Metal Analysis

Knowledge of NM composition is extremely useful for characterization, allowing contaminants or unknown elements present in the sample to be identified and possibly quantified. Energy dispersive X-ray spectroscopy (EDS or EDX) is a technique used in conjunction with SEM which can identify the elemental composition of a sample. This SEM/EXD method has been used extensively to characterize the size, morphology and elemental composition of ambient aerosols [131] and is finding increasing use in nano specific studies. It is a relatively simple yet powerful technique with the added advantage of being nondestructive. The technique works by bombarding the sample with an electron beam to produce x-rays that are detected and analysed. Each element has a unique atomic structure - the atoms from every element release x-rays with unique amounts of energy and as the x-ray energy is characteristic of the element from which it was emitted from the elemental composition can be determined. The output shows unique peaks corresponding to the energy levels for the X-rays received. The higher the peak in the output spectrum, the more concentrated the presence of the element in the specimen.

In summary, it is important to have a range of techniques in order to elucidate the most important aspects of the NM characterisation. Each technique will give its own unique model or view of the particles and together this combined approach can help to build and an understanding of the complex nature of particles at the nanoscale.

2.1.4 Iron Oxide Nanomaterials

Iron NMs have been highlighted by the Organisation for Economic Co-operation and Development's Working Party on Manufactured Nanoparticles' (WPMN) as one of the thirteen NMs they intend to analyse further to examine their physicochemical properties, environmental fate, environmental toxicology and mammalian toxicology [132]. Chosen for their relevance (in commercialisation, production volume and availability) the objective as set out by the WPMN is to

provide ‘information on intrinsic properties that may be relevant for exposure and effects of NMs through testing’ [132].

The unique characteristics of iron oxide NMs (e.g. their superior magnetic potential at the nanoscale) mean that they are being employed in a vast array of applications. Besides the considerable attention they have received in the biomedical field (for example in targeted drug delivery and as magnetic resonance imaging contrast agents for example) their magnetic qualities also make them useful in a broad range of applications such as pigments in cosmetics and the automotive industry, sealants, inks and catalysts [133]. Coated magnetic particles also have uses in industrial water treatment, bioremediation and labelling where iron oxide NMs allow for effective cell separating techniques [134, 135]. Currently the biggest use of iron oxide NMs is in magnetic recording media (such as magnetic tape, hard drives and removable storage devices) [136]. The current global production for iron oxide NMs is estimated to 100 tonnes, however this value should be taken as an estimate only as it is difficult to distinguish between bulk and nano form materials when making these projections. With increasing applications, ease of production and high production value, human and environmental exposure to these NM is likely to increase.

Iron oxide NMs have the greatest potential in medical applications. Recently they are finding applications in targeted drug delivery where cells labelled with the NMs can be located and tracked. This application is useful in cancer treatment where current treatments are not as specific and thus not as effective. They are also used as contrast agents in magnetic resonance imaging and their magnetic properties are exploited for use in bioassays [134, 137, 138]. Recently it has become the first NM to gain European Union (EU) regulatory approval [139] for a novel therapy that involves the direct instillation of a fluid containing iron oxide NMs into a tumour. The NM can then be manipulated by an external magnetic field causing them to generate heat and kill cancer cells in a technique termed magnetic hyperthermia. The clinical evidence that lead to the approval of this treatment has recently been published [140]. The treatment had a significant effect on prolonging the life span of patients with recurrent glioblastoma multiforme (an aggressive brain tumour). Side effects of this treatment were

noted to include sweating, increased body temperature, tachycardia fluctuations in blood pressure, headaches and convulsions). Fourteen out of sixty six patients exhibited motor disturbances; in four of these cases the symptoms appeared following the NM instillation. Overall, the authors reported no prolonged side effects and reported no indication of iron being released from the tumour [140]. Medical treatments do involve the direct injection of large amounts of iron oxide NMs into the body [135]. The dose in currently approved treatments (magnet resonance imaging contrast agents) can be 50-200mg of iron [141]. Although many papers report iron is well tolerated in the body [134, 142] and biocompatible, the effects of higher intracellular concentrations of iron NMs on cell function is not a topic that has been studied sufficiently. This is important to consider as although the body can lose small amounts of iron there are no dedicated pathways by which the body can excrete iron (iron not used in the body will be excreted in the faeces over a 3 month period), therefore in mammals iron levels are mostly controlled by regulating uptake. The body (on average) stores 3500mg iron, of which 0.2mg/g is in the liver and liver toxicity can occur when iron levels reach 4mg/g [141]. Although iron oxide NMs have been found to have a low level of toxicity, their use has been associated with production of inflammatory factors observed in some studies [143-145]. Now that these procedures are gaining medical approval it's important to address the potential effects of such large concentrations in the body so as to increase their effectiveness as therapeutic agents.

2.1.5 Chapter 2 Aims

- To characterise three types of iron particles 280 and 22nm Fe_2O_3 and 45nm Fe_3O_4 (using a variety of techniques) with regards to size, dispersion stability and elemental analysis

- To examine the above mentioned particles for the effect of time, sonication, particle concentration, ionic strength, pH and the presence of foetal calf serum (FCS) on their dispersion stability.

2.2 Materials and Methods

2.2.1 Chemicals

Iron oxide nanoparticles Fe_2O_3 (280nm and 22nm) and Fe_3O_4 (45nm) were received in 2009 from Prof. Chunying Chen (Laboratory for Bio-Environmental Effects of Nanomaterials and Nanosafety and Key Laboratory of Nuclear Analytical Techniques, Institute of High Energy Physics, Chinese Academy of Sciences, Beijing, China). The particles were provided as a dry powder and were previously reported [146, 147] to have the following characteristics:

Table 2.1: Properties of iron oxide (Fe_2O_3) particles (280nm and 22nm) as previously reported by Zhu et al.[146, 147]. These particles were obtained and used for this study. After characterisation (see section 2.3) however the 22nm Fe_2O_3 particles were discovered to have different properties from those described below.

280nm Ferric oxide (α form)	
Purchased from :	Zunye Nanomaterials Co. Ltd Shenzhen, China
Primary Particle Size (TEM)	280nm
Structure (X-Ray diffraction)	Rhombohedral Crystal Structure
Surface Area (BET)	4.25m^2/g
Purity (ICP-IES)	99%
22nm Ferric oxide (α form)	
Purchased from :	Haoyun Industrial and Trade Co. Ltd Beijing, China
Primary Particle Size (TEM)	22nm
Structure (X-Ray Diffraction)	Rhombohedral Crystal Structure
Surface Area(BET)	53.27m^2/g
Purity (ICP-IES)	95%
Hydrodynamic Diameter (in RPMI Cell Culture Media with 10% Serum)	144.36nm

2.2.2 Sample and Media Preparation.

Particles were weighed in a Sartorius safety weighing cabinet (Model: SWC900). Before removal from the cabinet, the particles were suspended in sterile filtered water at a concentration of 1mg/ml. Each sample was sonicated at 200W (32 kH_Z) for five minutes using a bath sonicator (Ultrawave Q series).

For dispersion experiments a 100µg/ml particle solution from the stock was prepared in water, RPMI (RPMI 1640 media developed by Moore *et al.* at Roswell Park Memorial Institute obtained from Sigma, UK) and in RPMI with increasing amounts of bovine serum albumin (BSA) (0, 0.1, 0.5 and 1%), 5mls of this solution was added to 7ml vials. Each of these vials were vortexed and then sonicated for 10 minutes. These vials were then pictured over time using a digital camera (Canon 40D) at 0, 0.15,0, 30, 1, 3, 4, 18 and 24 hours.

For size measurements the 1mg/ml stock solutions were diluted to 1, 10 and 100µg/ml in filtered sterile deionised water, filtered RPMI (supplemented with 1% pen/strep) and filtered RPMI (supplemented with 1% Penicillin/Streptomycin) with added (1%) BSA. These were vortexed, sonicated (200W) for 10 minutes and analysed immediately.

Sample preparation for light microscopy and SEM involved preparing a glass slide with the NMs spun onto their surface (cytospin centrifuge). A slide was prepared by placing a glass cover slip between a glass slide and a cytospin cuvette loader and placing in a metal cytospin holder. Each cuvette loader was loaded with 100 µl of sample and spun at 215g for 3 minutes. After 3 minutes the slide was dismantled and the glass cover slide with attached particles was recovered. Each cover slip was examined by microscopy to determine the degree of agglomeration and coverage. These samples were imaged by use of a Canon 40D camera attached to an inverted microscope. Once examined under light microscopy the same glass slide was used for SEM analysis. The glass slides were mounted onto an aluminium stub. The slides were attached to the stub using silver paint/glue. Each sample was then introduced into a chamber and coated with a very thin film of platinum before SEM imaging.

A 10µg/ml dilution of all particle types in water, RPMI and RPMI +1% BSA were prepared and deposited on copper grids (Agar Scientific, UK) for TEM analysis. The grids were placed in eppendorfs with 200mls of each sample and spun at 500g to coat the grid. The slides were recovered and placed in a holder until analysis by TEM (Hitachi H -7600).

The samples for the sonication study were prepared as follows. A 100µg/ml sample of each particle type was prepared in sterile deionised water. The samples were placed in a sonication bath and sampled after 5, 10, 15, 20, 30 and 40 minutes sonication. The size and zeta potential was measured using the zetasizer (Malvern Instruments).

2.2.3 Dynamic Light Scattering Size Measurements

DLS for characterisation of hydrodynamic size was performed using a Malvern Zetasizer Nano-ZS instrument. The instrument was turned on 30 minutes before measurements to allow the laser to stabilise. A 100µl volume of each sample was pipetted into a 1ml disposable low volume cuvette care was taken to avoid bubbles which can interfere with measurements. A cap was used to ensure thermal stability and to prevent dust interference which can greatly affect sample readings. The sample was placed in the chamber. Before analysis the specifications (material absorption, viscosity and refractive index) were adjusted to reflect the material being measured. The Malvern Zetasizer Nano used dispersion technology software (Version 5.1) for data collection and analysis. The software collected and interpreted the data and the report gave various interpretations for the sample such as volume, size and intensity graphs as well as statistical analysis and expert advice on the quality of the sample. The standard report for size measurements is an intensity particle size distribution (PSD). For each measurement the mean particle size was calculated and reported as the Z average, it is only comparable to other techniques if the sample is monodispersed, spherical and monomodal. The polydispersity index (Pdi) which is a measurement of the size distribution in the sample was also reported. The Pdi scale ranges from 0 to 1, 0 being monodisperse and 1 being polydisperse. The

software calculated the PD1 and the Z average from parameters defined in International Standards Organisation documentation (13321: 1996 E).

2.2.4 Zeta Potential Measurements

Zeta potential was measured using the Malvern Zetasizer Nano. Samples were prepared as previously described (2.2.2), vortexed briefly and sonicated for 10 minutes and then transferred to a 1ml Malvern clear zeta potential cell. A titration was carried out using hydrochloric acid (HCL) and sodium hydroxide (NaOH) to determine the IEP, the NM were titrated from acidic pH (pH = 1) to a basic pH (pH = 12) and at every 2 pH units (± 0.5 U) the zeta potential were determined. The zeta potential measurements were plotted against pH to determine the IEP.

2.2.5 Nanosight Size Measurements

NTA was carried out on a NanoSight LM20 (NanoSight Ltd., UK). Samples were prepared in ultra-pure filtered water. The sample chamber was removed from the unit, dismantled and cleaned first by rinsing with ethanol, then with deionised water and then cleaned with lens grade paper. The sample chamber was reassembled and using a 1ml syringe (without a needle) the sample was introduced carefully to avoid high pressure and bubbles from forming. The chamber was placed in the unit and aligned to the laser beam. Using NTA 2.0 software, the viscosity, temperature and length of film to be captured (166 seconds) was specified. The auto settings were used to allow software to determine appropriate shutter and gain settings. The expert mode was used to adjust settings such as minimum expected size. When the quality of the picture was deemed “good” and when the settings were saved, the motion was captured. The NTA 2.0 software automatically opened in processing mode when a video was opened. The videos were processed and a report was saved to excel and exported as a PDF.

2.2.6 Differential Centrifugal Sedimentation Measurements

Measurements were carried out using DCS. A volume of 100μg/ml of each of the three particles in water was made up and injected into a differential centrifuge (CPS instruments USA) at a speed of 18747g. Using specific parameters for iron oxide NMs the density was specified as 5.24g/cm^3 (Fe_2O_3) and 5.17g/cm^3 (Fe_3O_4) and particle absorbance at 0.5nm. The sample settled according to the size of the particles and the mean size from the resulting peaks was used as the average size of the sample.

2.2.7 Light Microscopy

Light microscopy was carried out on an inverted microscope. A digital camera (Canon 40D) was attached to capture the images. Samples were prepared as described (2.2.2), these slides were then analysed under 10, 20 and 100x magnification to gain information regarding dispersion state.

2.2.8 Scanning Electron Microscopy (SEM) and EDX

Samples were prepared as described (2.2.2). SEM was carried out on a Hitachi S-4800 II. The resulting images were analysed using Image J (freeware from NIH-USA)

2.2.9 Transmission Electron Microscopy (TEM)

TEM characterisation was performed to obtain size, size distribution and morphology on a Hitachi H -7600. The samples were prepared as described (2.3.2). Information on mean size and standard deviation was calculated using Image J analysis of the images.

2.3 Results

2.3.1 Dispersion

A.  B. 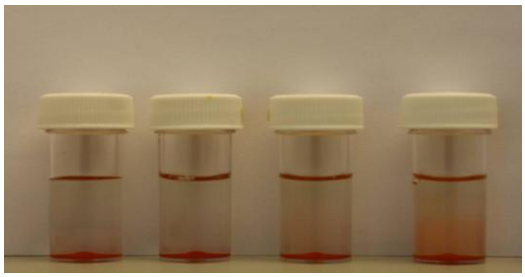

Figure 2.1: 280 nm Fe_2O_3 particles suspended in phenol red free RPMI at 0 minutes (A) and after 24 hours (B) from left to right in 0, 0.1, 0.5 and 1% BSA.

A.  B. 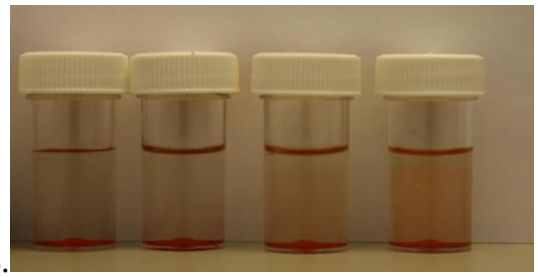

Figure 2.2: 22 nm Fe_2O_3 NM suspended in phenol red free RPMI at 0 minutes (A) and after 24 hours (B), from left to right in 0, 0.1, 0.5 and 1% BSA.

A. 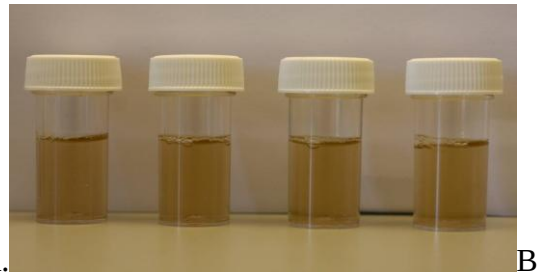 B. 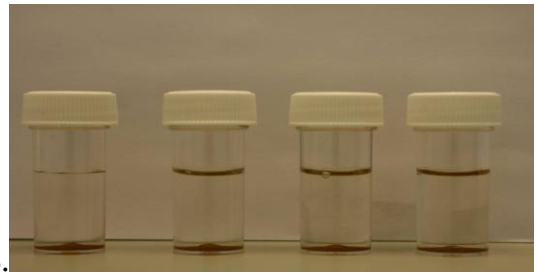

Figure 2.3: 45 nm Fe_3O_4 NMs suspended in phenol red free RPMI at 0 minutes (A) and after 24 hours (B), from left to right in 0, 0.1, 0.5 and 1% BSA.

A.  B. 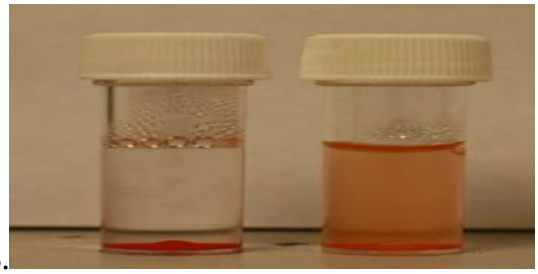

Figure 2.4: 280 nm Fe_2O_3 particles suspended in phenol red free RPMI at (A)0 minutes and (B) after 48 hours, left to right phenol red free RPMI and phenol red free RPMI+10% FCS.

Figures 2.1 - 2.4 show images at time 0 and time 24 hours for comparison purposes. The particles of all sizes tend to settle out of solution after 24 hours. The addition of extra protein had a stabilising/dispersing effect keeping the particles in suspension and dispersed for longer. This can be particularly seen in figure 2.4 which shows the 280nm Fe_2O_3 particles dispersed in RPMI with 10% foetal calf serum (FCS). The 45nm Fe_3O_4 NM behaved in a different manner to the Fe_2O_3, in that they seem to settle faster out of solution.

2.3.2 Cytospin and Light Microscopy

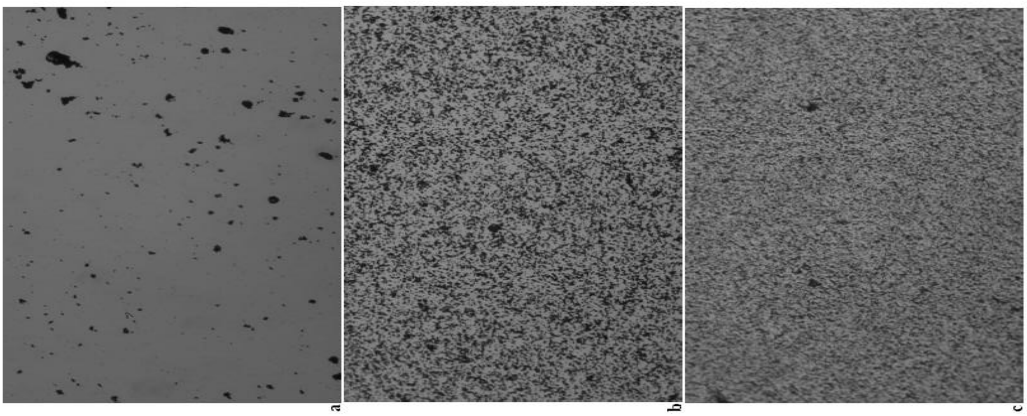

Figure 2.5: Light microscopy at 20X magnification of 280nm Fe_2O_3 particles in (a) water, (b) RPMI and in (c) RPMI with 1% BSA showing evidence of improved dispersion in cell culture media and cell culture media with added protein.

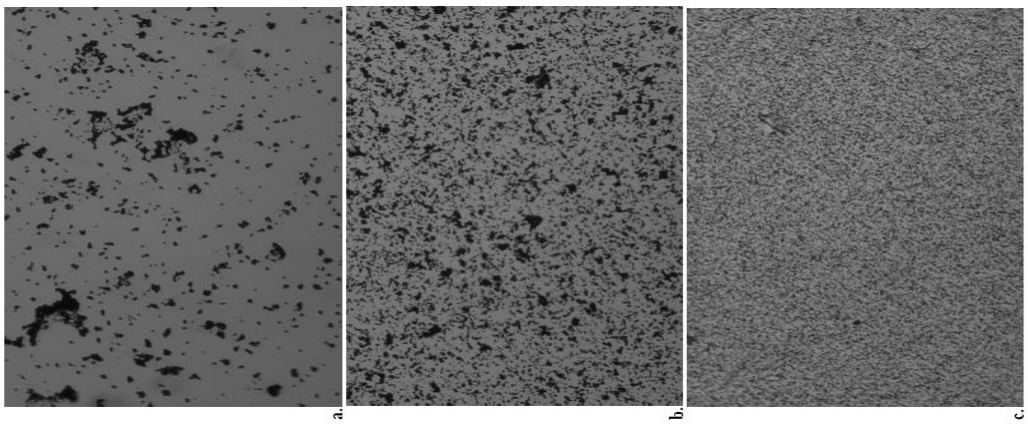

Figure 2.6: Light microscopy (20X) of 22nm Fe_2O_3 particles in (a) water (b) RPMI and (c) in RPMI with 1% BSA.

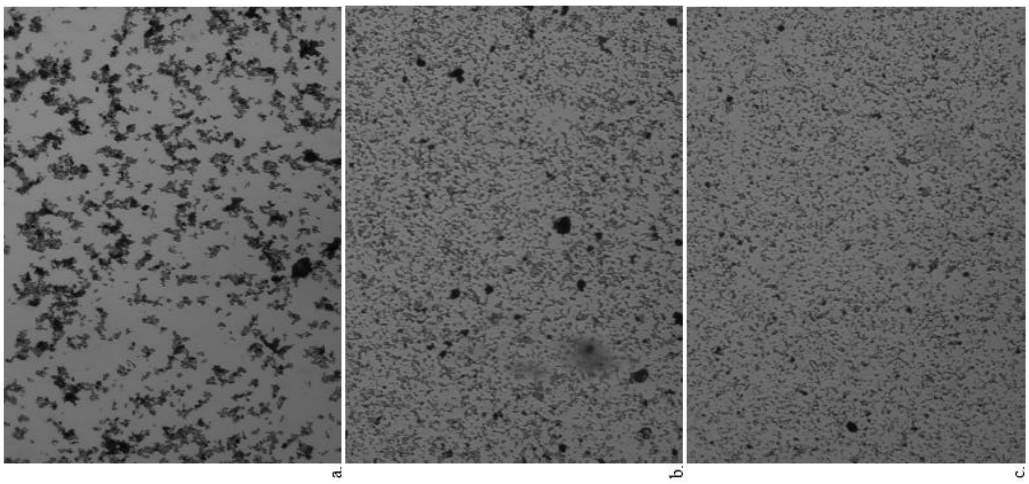

Figure 2.7: Light microscopy (20X) of 45nm Fe_3O_4nm particles in (a) water, (b) RPMI and (c) RPMI with 1% BSA.

Figure 2.5 - 2.7 shows the 280nm, 22nm and 45nm iron particle dispersions in different media. It appears that all particles are more dispersed in RPMI cell culture media and medium with added BSA than in water alone (figures 2.5(a), 2.6(a) and 2.7(a)). These figures also indicate that agglomeration to some degree occurred in all of the media. This was investigated further using electron microscopy.

2.3.3 SEM

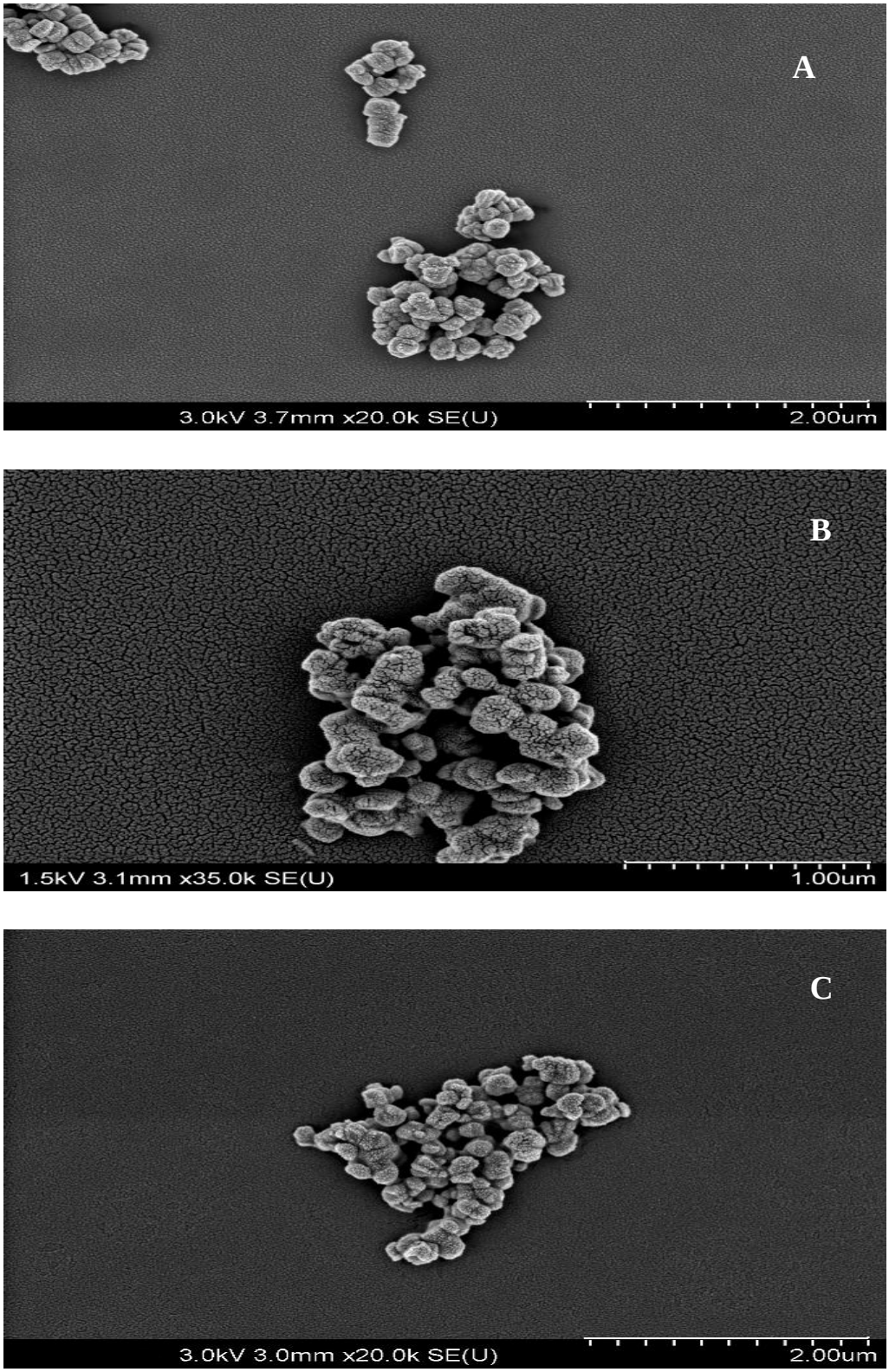

Figure 2.8: SEM micrograph showing 280nm Fe_2O_3 particles in (A) water, (B) RPMI AND (C) RPMI with 1% BSA. With scale bar on the right and voltage specified on the left.

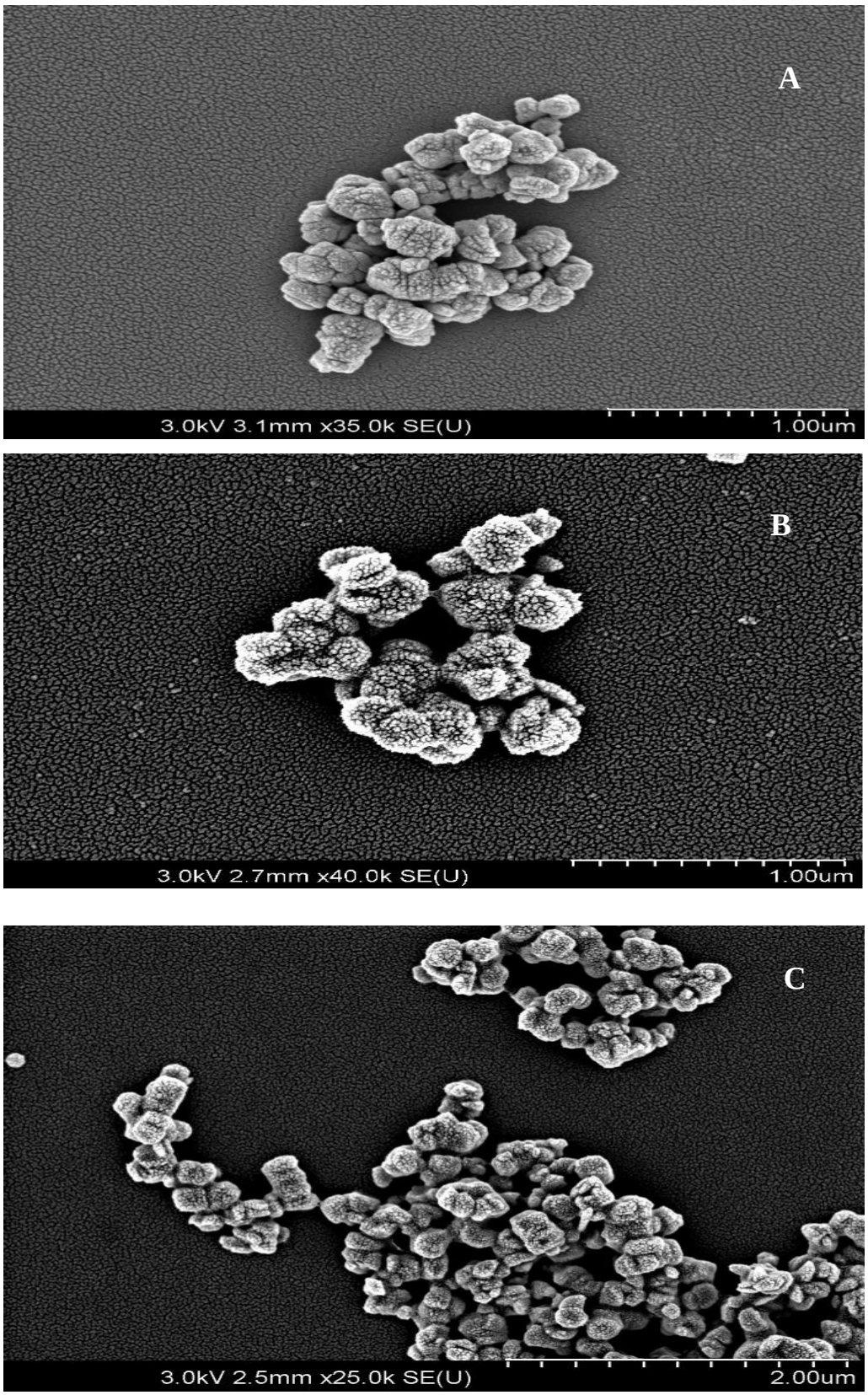

Figure 2.9: SEM micrograph showing 22nm Fe_2O_3 particles in (A) water, (B) RPMI and (c) RPMI with 1% BSA. With scale bar on the right and voltage specified on the left.

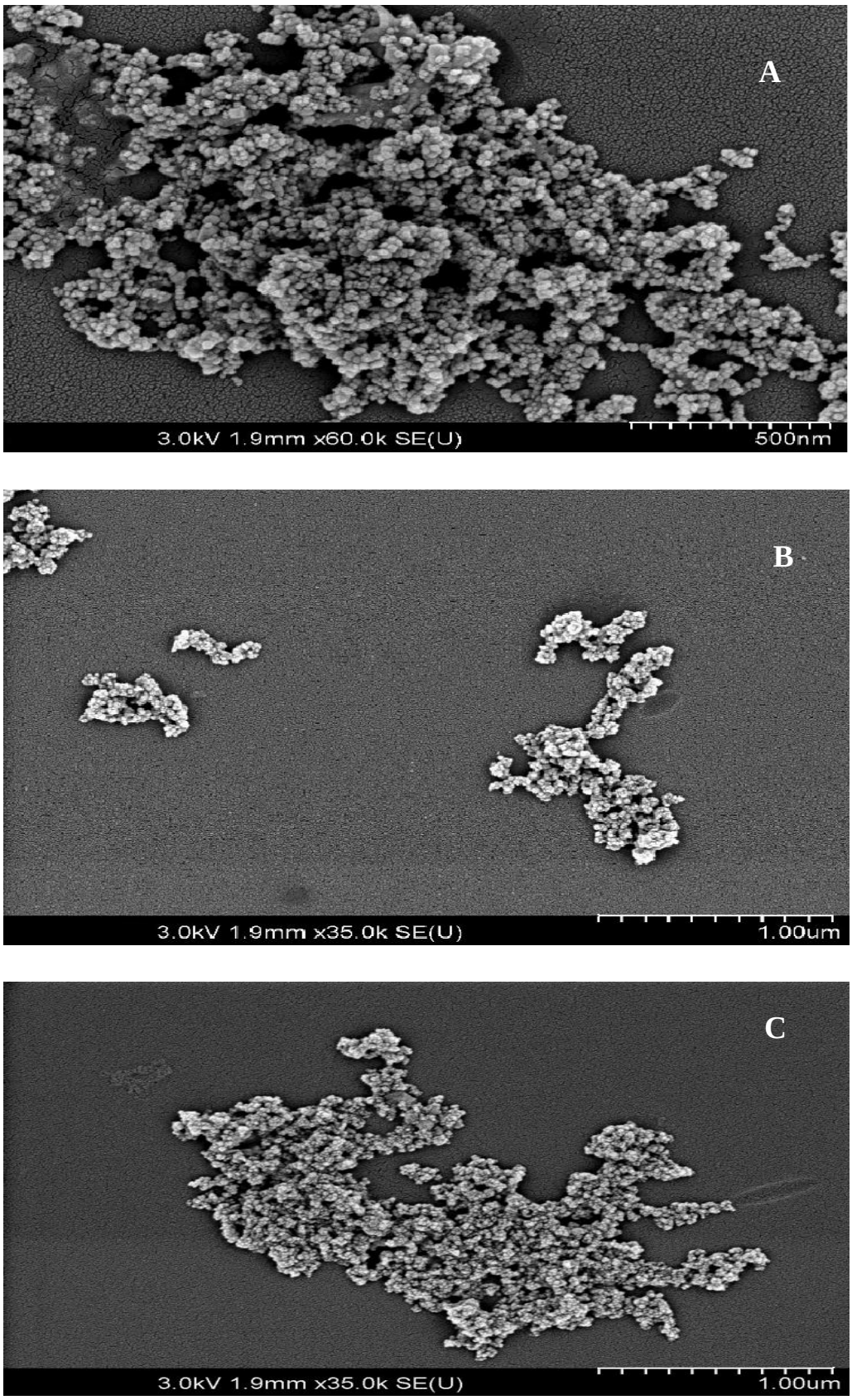

Figure 2.10: SEM micrograph showing 45nm Fe_3O_4 particles in (A) water (B) RPMI (C) and RPMI with 1% BSA. With scale bar on the right and voltage specified on the left.

The SEM pictures reveal the particles morphology to be nearly spherical in nature with a tendency to agglomerate in all media types. Both the 280nm and the 22nm Fe_2O_3 look very similar in terms of particle size and morphology and the images reveal a slight difference in appearance in the 45nm Fe_3O_4 iron oxide NMs, which appear to be far more agglomerated than the 280 nm Fe_2O_3 particles. At this high magnification it is difficult to see any differences when the particles are dispersed in water, RPMI or RPMI with added protein. But in all media types the particles appear to be agglomerated with a range of particle diameters described in table 2.2. Calculating size from SEM images was achieved in two ways. Manually counting every particle visually and using a scale bar to estimate particle size and also using open source software Image J.

Table 2.2: Particle hydrodynamic diameter as determined from SEM micrographs, calculated using Image J software before and after using watershed feature.

Particle Type	**Diameter (nm)**	**Diameter (nm)as Determined by Image J**
22nm in water	**643.43±84.23**	**272.39±115.95**
22nm in RPMI	**612.90±253.15**	**228.18±74.55**
22nm in RPMI+0.1%BSA	**702.82±129.26**	**203.08±81.06**
280nm in water	**611.96±103.78**	**253.12±54.07**
280nm in RPMI	**231.80±137.59**	**90.01±9.07**
280nm in RPMI+0.1% BSA	**532.27±107.00**	**185.22±57.31**
45nm in water	**1284.51±58.10**	**59.00±13.88**
45nm in RPMI	**356.52±73.15**	**128.85±170.30**
45nm in RPMI+BSA	**388.60±365.40**	**76.69±105.29**

2.3.4 TEM

TEM revealed not only size data but also important morphological and structural characteristics as can be seen from the figure 2.12 - 2.15. For example, the Fe_2O_3 particles (figure 2.12 and 2.14) images clearly show a polydispersed particle size distribution.

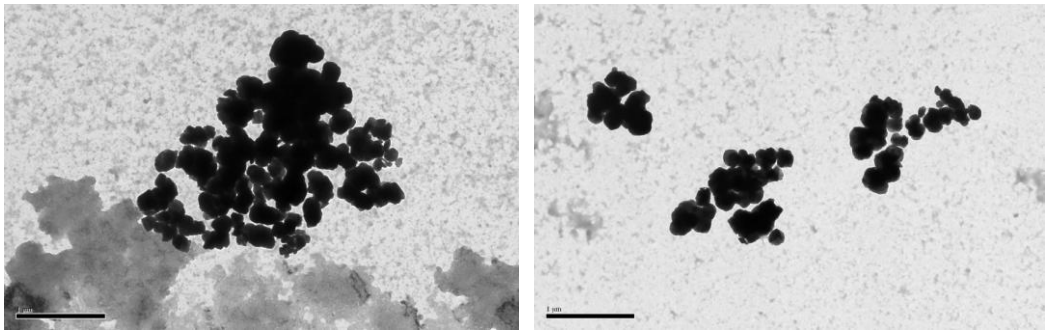

Figure 2.11: TEM micrograph of 280nm Fe_2O_3 particles dispersed in water. Size bar represents 1 µm.

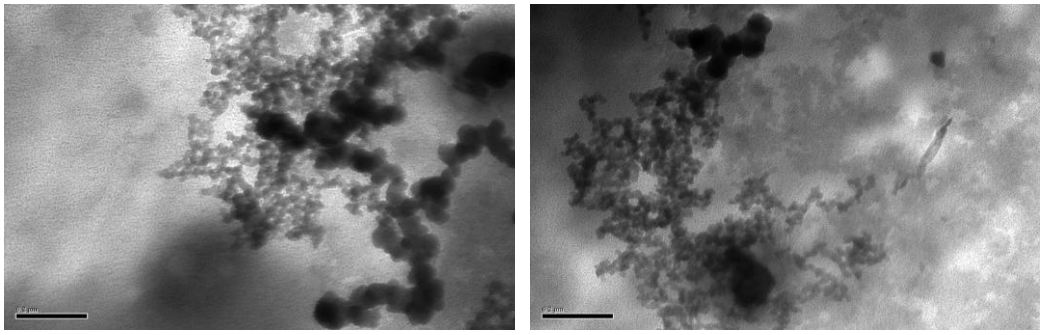

Figure 2.12: TEM micrograph showing 22nm particles dispersed in water Size bar represents 200nm.

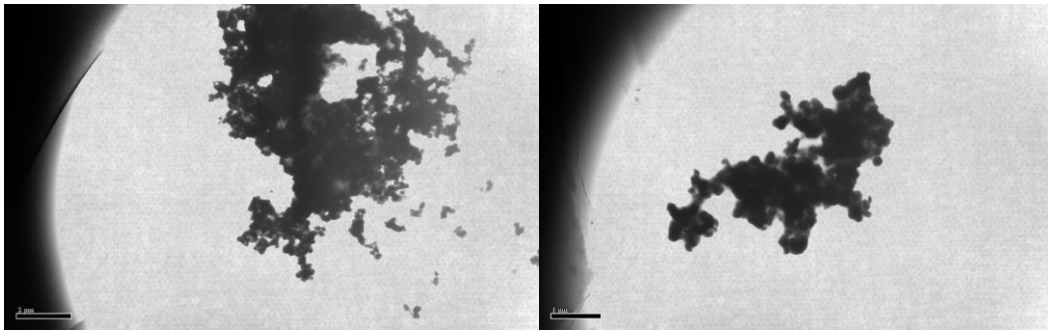

Figure 2.13: TEM micrograph showing 45nm Fe_3O_4 particles dispersed in water. Size bar represents 1 µm.

2.3.5 DLS

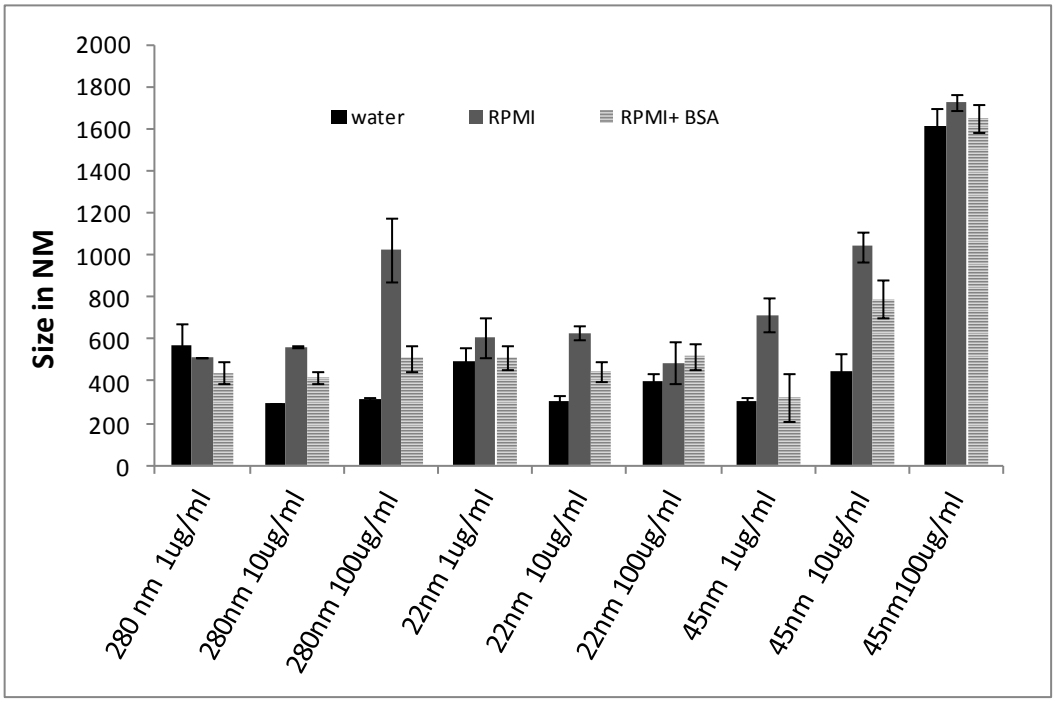

Figure 2.14: Graph showing DLS hydrodynamic diameter of 280, 22 and 45nm particles at 100, 10 and 1 µg/ml in water, RPMI and in RPMI with 0.1% BSA. Values represent the means of 3 experiments ± SEM (See appendix 8.1 for full set of data).

One way analysis of variance (ANOVA) was preformed to investigate the DLS measurements further and revealed that there was a significant difference between the size (i.e. hydrodynamic diameter) in water, RPMI and RPMI with BSA for the 280nm particles at 100µg/ml (P=0.00), with the largest particle size observed in RPMI. There was a significant difference between the size of the 22nm Fe_2O_3 particles in water, RPMI and RPMI with 1% BSA at 100µg/ml (p=0.00) and again the largest size was to be found when the NMs were measured in RPMI (with and without BSA). ANOVA also found there was no significant difference between the size of the 45nm Fe_3O_4 NM in water, RPMI and RPMI with 0.1% BSA at 100µg/ml (p=0.253). The graph shows that there is a clear influence of particle concentration on the hydrodynamic size for all three particle types (22nm, 280nm and 45nm) and there is an effect of media on hydrodynamic size for the 22nm and 280nm particle. The higher concentration of 100µg/ml gives a higher Z average reading then the lowest 1 µg/ml reading. This result was found in all media types.

2.3.6 Nanoparticle Tracking Analysis (NTA)

Table 2.3: Hydrodynamic diameter of two particle types Fe_2O_3 (280nm) and Fe_3O_4 (45nm) at 10µg/ml (n=3) data obtained from NTA analysis as explained in 2.2.5

Fe_2O_3 280nm	**Mean**	**Mode**	**St dev**	**Concentration (i.e. NTA estimation of number of particles/ml)**	
1	216.00	216.00	45	4.58E+08	
2	291.00	241.00	92	4.85E+08	
3	263.00	274.00	76	5.82E+08	
Average	256.67	243.67	71.00	5.08E+08	6.52E+07

Fe_3O_4 45nm	**Mean**	**Mode**	**St dev**	**Concentration (i.e. NTA estimation of number of particles/ml)**	
1	232	42	169	4.06E+08	
2	228	47	184	1.39E+08	
3	154	31	115	3.17E+08	
Average	204.67	40	156	2.87E+08	1.36E+08

The NTA model generates an alternative model of the NM hydrodynamic diameter compared to DLS. Upon further investigation of the NTA graphs the 280 nm particles can be seen to be a monomeric sample, whereas it is clear there are aggregates or agglomerates present in the 45nm sample. This can be seen quite clearly in the graphical output from the NTA as seen in the below figure (2.15-2.16)

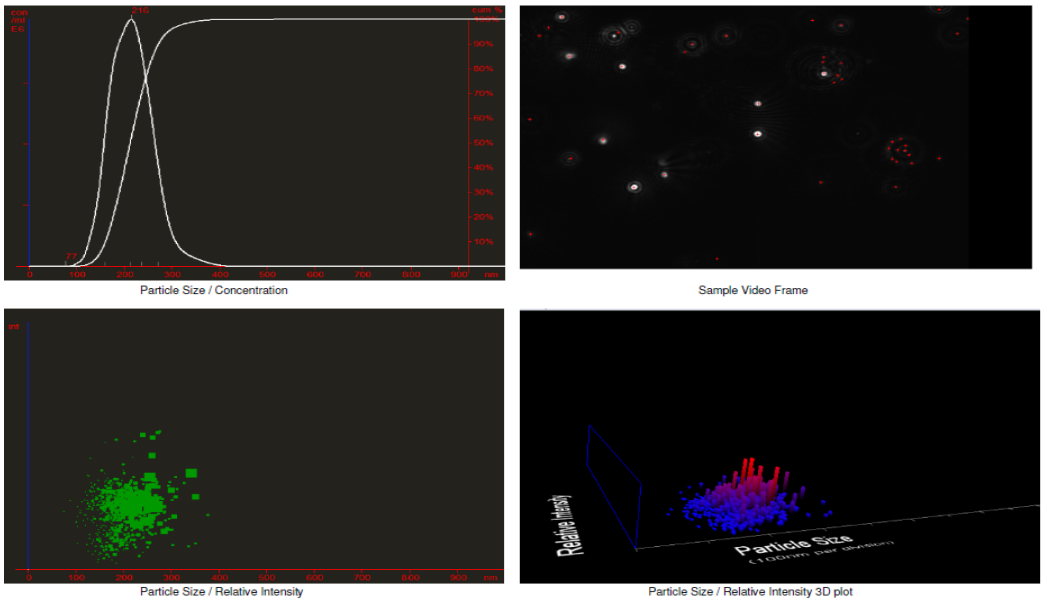

Figure 2.15: A graphical representation of the NTA data as described in table 2.3. NTA was carried out as mentioned in 2.2.1.2. This figure shows the NTA analysis of 280nm Fe_2O_3 showing particle hydrodynamic diameter as a function of concentration and relative intensity. Each panel shows the four typical images produced by NTA. The top left shows the size distribution from NTA measurements of the 280nm Fe_2O_3 particles. The top right panel shows a video frame of the live recording of the patterns made due to scattering of light by these particles. The bottom left panel shows particle size as a function of relative intensity and the bottom left panel shows a 3D representation of the particle size as a function of relative intensity. The monodispersed 280nm Fe_2O_3 sample was found to have a diameter of 256. 67nm.

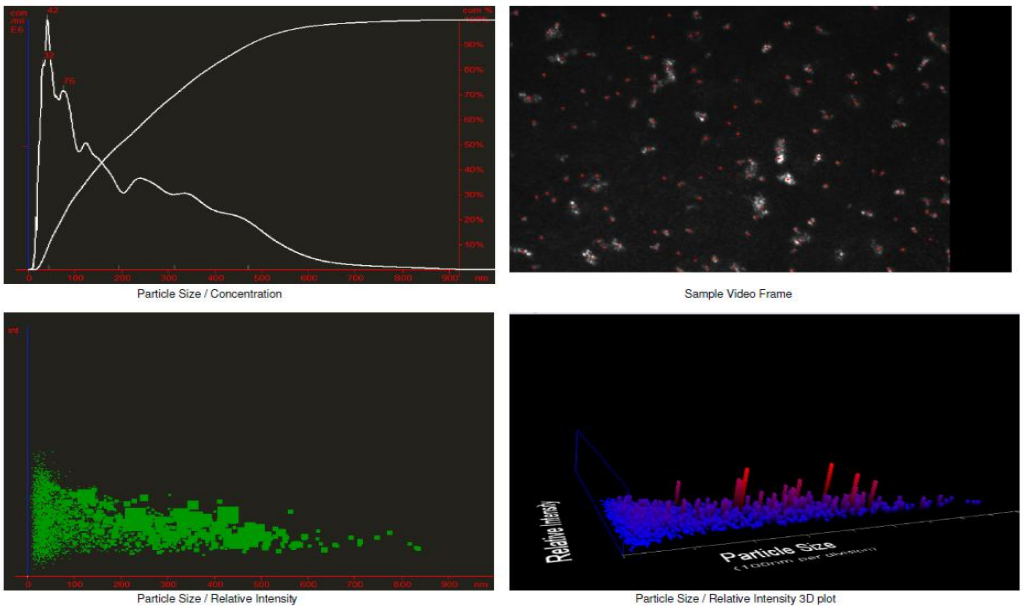

Figure 2.16: A graphical representation of the NTA data shown in table 2.3. This figure shows the NTA analysis of 45nm Fe_3O_4 particles showing the hydrodynamic diameter as a function of concentration and relative intensity. Each panel shows the four typical images produced by NTA. The top left shows the size distribution from NTA measurements of the 45nm Fe_3O_4 particles. The top right panel shows a video frame of the live recording of the patterns made due to scattering of light by these particles. The bottom left panel shows particle size as a function of relative intensity and the bottom left panel shows a 3D representation of the particle size as a function of relative intensity. The mode was found to be 42nm however peaks can also be seen at 76nm and agglomerates were tracked at the 100-700nm range.

2.3.7 Differential Centrifugal Sedimentation

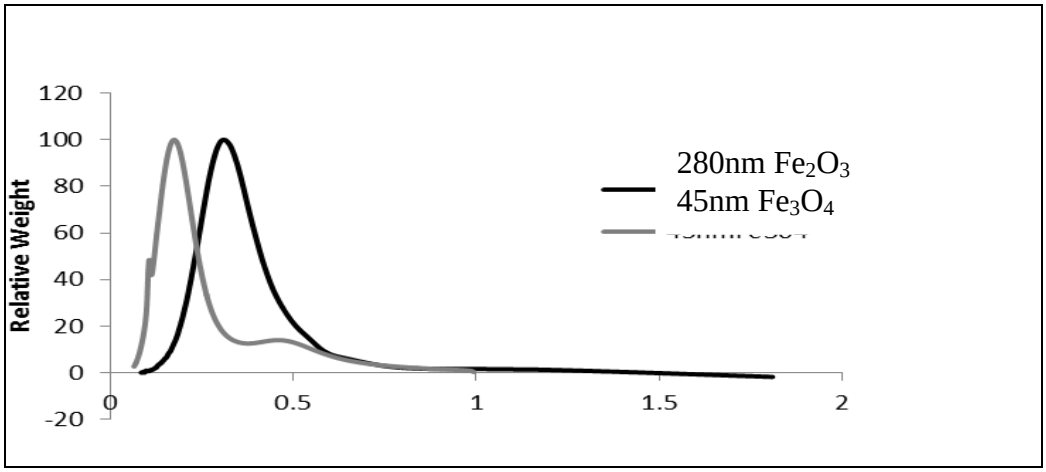

Figure 2.17: Differential centrifugal sedimentation graph showing particle hydrodynamic diameter of the 280nm Fe_2O_3 particles and the 45nm Fe_3O_4 particles as a function of relative weight. DCS was carried out as explained in 2.2.6. The results (n=3) modelled the 280nm particle size at 303.5nm and the 45nm Fe_3O_4 NM gave a size of 174.8nm. The 22nm particles produced an identical peak as that of the 280nm particles data shown in appendix (8.2).

2.3.8 Zeta Potential

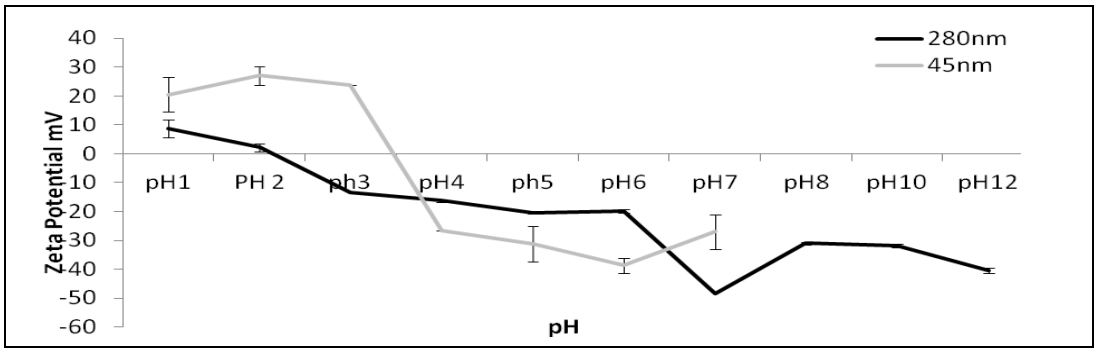

Figure 2.18: Zeta Potential (mV) of iron oxide particles (280nm and 45nm) dispersed in water over pH range showing an IEP of at pH 2.75 for the 280nm particles and at pH 3.5 for the 45nm particles.

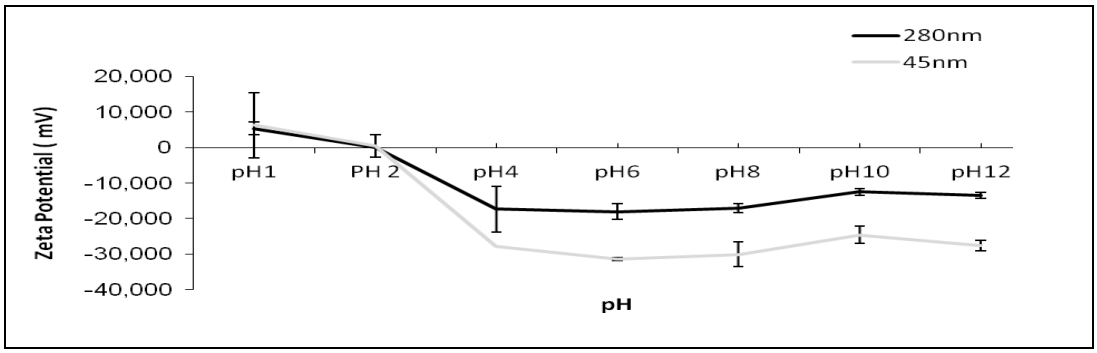

Figure 2.19: Zeta Potential (mV) of iron oxide particles (280nm and 45nm) dispersed in RPMI over pH range showing an IEP of at pH 2 for the 280nm particles and at pH 2.9 for the 45nm particles.

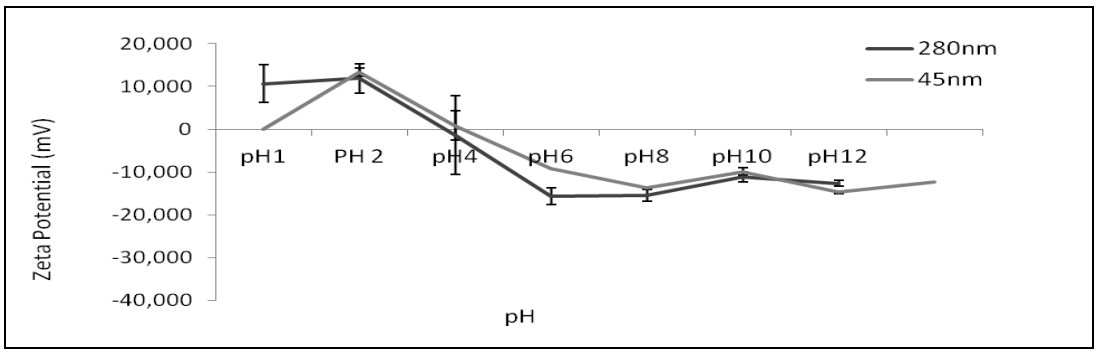

Figure 2.20: Zeta Potential (mV) of iron oxide particles (280nm and 45nm) dispersed in RPMI+0.1% BSA over pH range showing an IEP of at pH 4 for the 280nm particles and at pH 4.1 for the 45nm particles

Figure 2.18 - 2.20 shows the ZP versus pH in three different media types. Samples were prepared as previously described (2.2.5). At every 2pH units (± 0.5 U) the zeta potential was determined and plotted against pH to determine the IEP.

2.3.9 Sonication Study

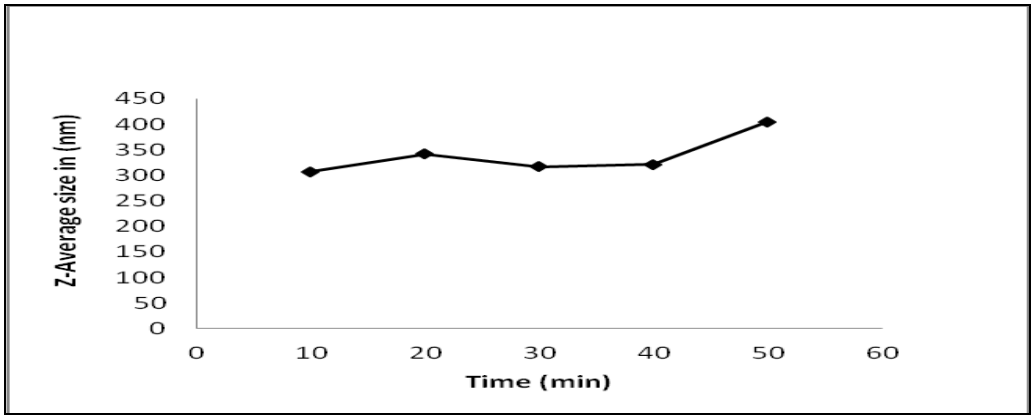

Figure 2.21 The effect of sonication time on hydrodynamic diameter of 280nm Fe_2O_3 particles as determined by DLS performed as detailed in 2.2.2. After 10 minutes sonication the particle had a Z average of 307nm (Pdi 0.24), 20 minutes 342nm(Pdi 0.32), 30 minutes 317nm (Pdi 0.24), 40 minutes 321 nm (Pd1 0.25) and after 50 minutes sonication 407nm (Pdi 0.24)

2.3.10 Metal Analysis by SEM/EDX

(a)

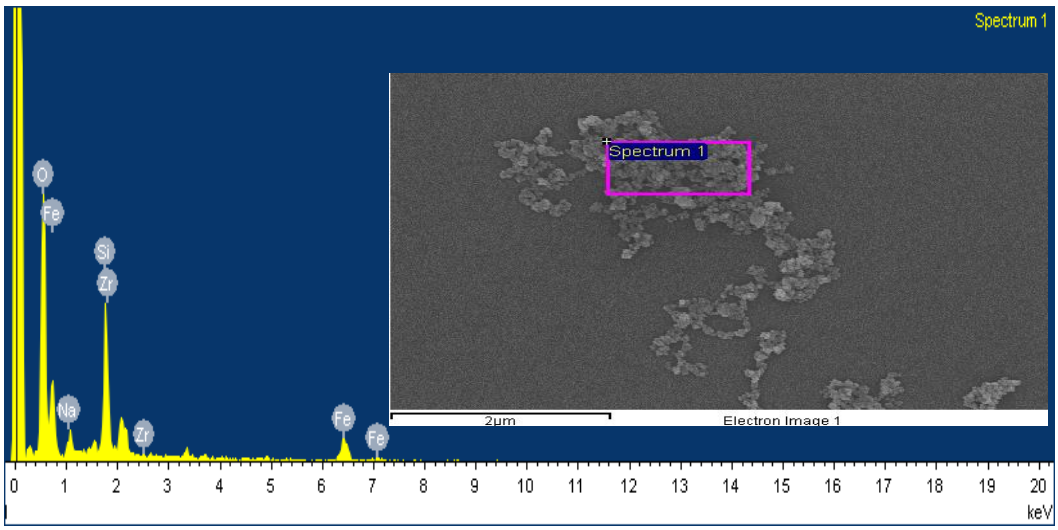

(b)

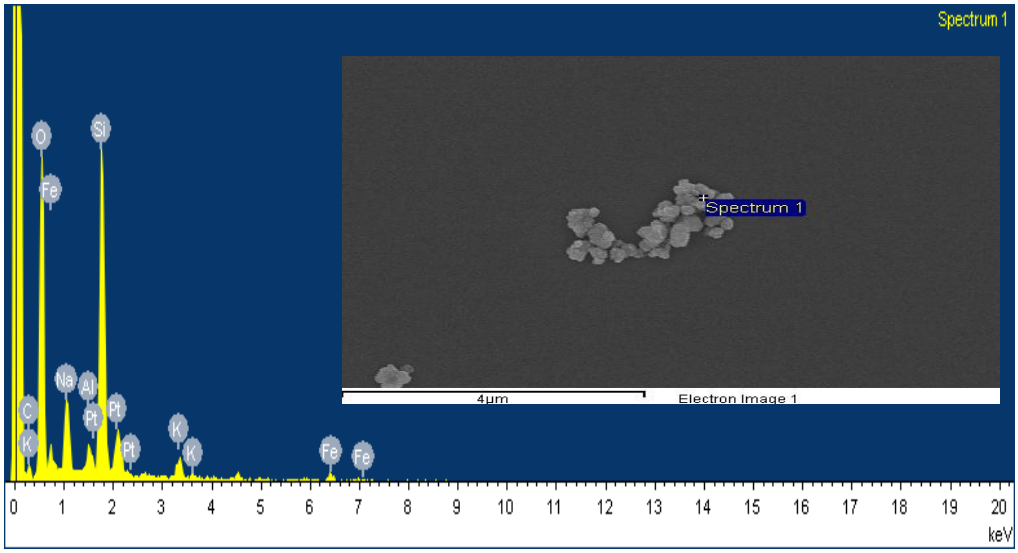

(c)

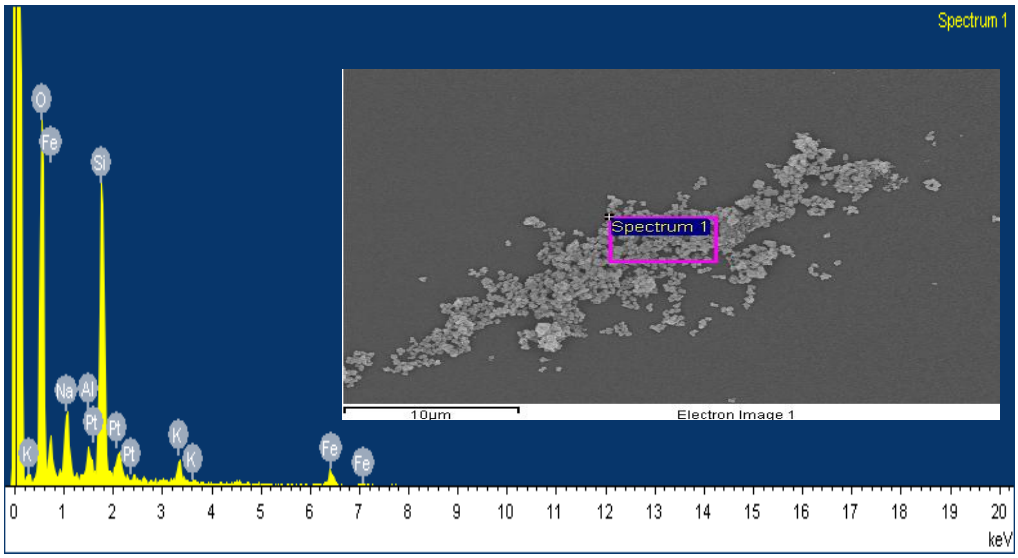

Figure 2.22: SEM/EDX profile for (a) 280nm (b) 45nm and (c) 22nm iron particles (n=1: n=3 in appendix 8.4. Energy Dispersive X-Ray Spectroscopy was carried out on each of the three particle types in order to identify the elemental composition. This non destructive technique analysed three separate sections for each particle type to produce a representative view of the elemental composition of the particles. As can be seen from images Figure 2.22 iron and oxygen is the main component of all the particles ranked by abundance. A large peak was also detected for silica and platinum. As sample preparation involved placing of sample on a glass slide and coating the sample with platinum this can account for presence of these elements.

2.4 Discussion

Iron oxide NMs and particles were examined for the effect of time, sonication, particle concentration, ionic strength, pH, and the presence of FCS on their stability and characteristics. This was accomplished using a range of techniques. Size analysis (DLS and DCS) of the 280nm and the 22nm Fe_2O_3 particles, suggested they were so similar it was not possible to distinguish between them; therefore the remaining study was conducted (after characterisation) with the 280nm Fe_2O_3 and the 45nm Fe_3O_4 particles only.

Physicochemical characterisation of these test particles in a representative dispersant is essential if any comparison to a potential biological effect is to be made. The sizing results alone from the different experimental methods (DLS, NTA, image analysis, etc.) indicate that the effect of cell culture media on agglomeration is significant. This is an important issue as little is known to date about the colloidal stability of iron NMs in cell culture medium.

The images of NM suspension in vials give a good visual comparison of how stable the NMs and particle dispersions were. These sedimentation studies show that the iron oxide particles settle rapidly out of solution when in water but with the addition of proteins they tend to form a more stable dispersion. This can also be clearly seen in the light microscopy images of the cytospin samples. The microscopy studies show the particles are polydispersed in nature and tend to agglomerate. SEM found the diameters of agglomerates for the 280nm ranged from 230nm to 700nm and the 45nm particles ranged from 300nm to greater than 1000nm. SEM and TEM are used frequently to characterise NM size (diameter) and size distribution. Traditionally analysing these characteristics from SEM and TEM images has been achieved manually counting and measuring every particle visually. This is not only subjective but also labour intensive. Using automated particle analysis programmes for nanoparticulate analysis has not always been an option as NM agglomerates tend to confuse the automated software programmes which will recognise agglomerates as one particle giving inaccurate particle size readings. This would therefore overestimate NM size not allowing the difference between the individual and the population to be identified. The user can use tools

in these software programmes to specify each particle size individually however in a large image this is time consuming. Here, open source software called Image J was used for the particle analysis. This software includes functions and algorithms (such as the water shed tool) as add in features of the programme that can be used to break agglomerates (which may occur in specimen preparation) into separate particles before analysis. However this technique requires caution as it cannot be assumed to work for every image and particular attention must be paid to each image to supervise what the software recognises. The results obtained using automated particle counting software gives an indication of particle size but for complete analysis a range of sizing techniques should be employed to gain more insight into the particles under investigation.

DLS size analysis found the agglomeration rate and thus the size increased with particle concentration. If a sample is too concentrated it may not be able to freely diffuse due to particle-particle interactions. Thus the sample concentration is of importance when trying to elicit size. In general these particle-particle interactions will not occur at concentrations below 0.1% by volume [125]. However there is a significant difference in size between the 100µg/ml (.01%), 10µg/ml (0.001%) and the 1µg/ml (0.0001%) dilutions at each particle type, with the 100µg/ml concentration having the greatest effect on the hydrodynamic size of the 280nm and 45nm particles in RPMI. This suggests that there may be some concentration effects at a level below the 0.1% concentration. NM hydrodynamic diameter was also affected by the type of media it was dispersed in. In all cases the particle size was smaller in water and increased in RPMI, also the addition of BSA can be seen to have an effect on the size, in most cases causing a decrease in size, but still significantly higher than in water alone.

Sonication was used as a method of dispersal as the particles did not go easily into solution. To determine if the effect of time had any impact on the size/stability of the iron oxide particles, a sonication study was carried out and the results indicate that up to forty minutes of sonication did not have any adverse effects on size however in comparison after fifty minutes of sonication there was a slight increase in the hydrodynamic diameter. Sonication was required for two main reasons (i) as mentioned above the particles did not easily go into solution (ii) to make sure a

homogeneous sample was always during experimentation. As the size was not significantly impacted by sonication after ten minutes this was taken as the sonication time of particles in water for all future experiments.

The IEP of the NMs was found to be in the range of pH 2 - 4. The largest agglomerate size would be expected to be found at the IEP (i.e. where ZP=0). The further away the ZP deviates from the IEP the smaller the particle agglomerate would be due to increasing repulsive forces. The results indicate that the iron oxide particles are moderately stable at a pH of 7 in water with a ZP of 40mV (±7.59mV). The ZP was also measured in cell culture media and in cell culture media with 0.1% BSA. The ZP readings were much higher in RPMI and ultimately there was a shift to the left with the IEP found to be in the range of pH2. It is important to note that instrument capabilities should be taken into account. The DLS zeta technique is not optimized for cell culture media. The media itself can lead to damage of the instrument cell in which the sample is cased and may lead to uncertainties in the analysis. Consequentially the high value may not represent a true ZP value. However it can also be considered that the higher ZP and low pH at which the IEP value was obtained for the iron particles in RPMI could be due to adsorption of ions onto NM surface. Anions present in RPMI such as phosphates could act as ligands. Therefore, during a titration experiment the more protons (acid) that are required to counteract adsorbed ions will lead to a lower IEP value. This seems like an intuitive explanation of what may be occurring in the system. These types of studies considering the impact of cell culture media on NMs are important at the initial stages of experimentation. NMs with adsorbed species from cell culture media may exhibit novel surface properties which can influence NM behaviour *in vitro* in a way that may not be replicated *in vivo*. For example, Chen *et al.* [148] reports the role of FCS in RPMI in influencing the stability, surface properties and intracellular uptake of magnetic NMs which they attribute to the adsorption of FCS onto the surface of MNPs.

A simple study also investigated the size of the 22nm particles at different pHs (data shown in appendix 8.3). At pH 7 (in water at 10µg/ml) they have a hydrodynamic size of 330nm however this increased significantly to 533nm at a

pH 3 and 1066nm at pH 2, thus supporting the fact that as the ZP reaches its IEP point the NM dispersion becomes less stable and more likely to agglomerate. This simple experiment shows the pH of the dispersants is an important factor to consider in any experimental set up. Although the particles above are stable in RPMI at a pH 7 which is the pH of the cell culture model system it can be seen that at a pH 4 they reach the IEP, suggesting the particles are not stable at this pH. This is an important consideration as the lysosomes of the cell operate at this pH and so NM may be less stable if they enter the cell lysosomes.

Interestingly the NTA and DLS complement each other and each technique makes up for the deficiencies in the other. Using a variety of techniques in this way is not an attempt at method validation but simply a requirement in NM characterisation. The NTA models show an alternative view of the NM size. Upon further investigation of the NTA it can be clearly seen that there are agglomerates present, but as NTA separately tracks each individual particle the size distributions generated reflect the actual number of particles seen or the tracks processed and followed for a longer length of time. As mentioned before, this is an advantage over PCS, a method where a large number of particles are analysed simultaneously and result in a z-average. When using PCS if there are agglomerates present it will lead to a shift in the distribution to the right hiding or obscuring any smaller particles present in the sample, so this combined technique shows that there are agglomerates present and NTA allows us to determine in what range these particles are present and this is verified by SEM/TEM. Care must be taken in interrupting this data, as it is easy to misinterpret data from the NTA as the automatic settings make it easy to analyse only tracks of interest rather than the entire sample leading to a bias in the particle estimation to the size of the stated particle rather than the actual particle size. This is a minor issue that once identified can be easily remedied by adjusting the settings and preparing appropriate dilutions that allow both large and small particles to be identified and tracked, so agglomerates that are present will also be tracked as they move into the field of focus however unlike DLS they will not bias the overall results.

EDX analysis showed output spectra that have characteristic peaks corresponding to the energy levels for iron. As expected iron and oxygen is the most abundant

element present within the sample however a high amount of silica is also present. This can be explained by the sample preparation. In order to analyse a sample on the SEM and thus on EDX, the sample is spun onto a glass slide on which the sample is introduced to the SEM. This glass slide was therefore the source of silica in this instance.

Using a range of characterisation methods can give a more fully rounded indication of the actual nature of the NM. Each technique adds an extra layer and depth of knowledge complementing each other, each will give its own unique model or view of the particles and together this combined approach can help to build an understanding of the complex nature of particles at the nanoscale. For example, some methods are not suited for certain particles. DLS and NTA analysis are based on size calculations for spheres and thus would not be suited as sizing technique for nanorods or nanowires. Taking the 45nm Fe_3O_4 NM as an example; Fe_3O_4 NM was specified to have a nominal primary particle size of 45nm. DLS results find a Z average hydrodynamic value of 450nm at 10µg/ml, the Pdi of 0.3 indicating some degree of polydispersity. NTA shows the sample to have a mode of 42nm but also shows many peaks right up to 500nm. Upon further investigation of the NTA graphs it be clearly seen that there are aggregates present, but as NTA separately tracks each individual particle the size distributions generated reflect the actual number of particles seen whereas the DLS technique analyses particles simultaneously and result in a z-average. When using DLS if there are aggregates present it will lead to a shift in the distribution to the right, hiding or obscuring any smaller particles present in the sample. This combined technique shows that there are aggregates and agglomerates present but NTA shows exactly in what size range and agglomerates or aggregates were found to be present at 76nm and where tracked up to the 700nm size range. SEM adds another level of understanding allowing us to see the individual 45nm primary particles but shows the configuration of these particles together. Using Image J with the watershed tool plug in the individual particle size was found to be 54.07nm. By comparing analytical techniques it can be seen that a range of techniques and not one standard technique is recommended for NM characterisation.

2.5 Conclusion

This study shows it is not sufficient to rely on the manufacturers or suppliers stated physicochemical characteristics for NMs as this may vary from batch to batch. It is important to have a range of techniques in order to elucidate the most important aspects of the particle characteristics. In this newly emerging science of nanotoxicology this should not be mistaken for method validation. Nano specific measuring techniques are constantly evolving from methods employed in the non-nano field. Each technique will give its own unique model or view of the particle. In the absence of a 'gold standard' for nanoparticle characterisation this combined approach can help to build an understanding of the complex nature of particles at the nanoscale. This work found that of the three particles supplied for the study there was no difference between the 280nm and the 22nm Fe_2O_3 particles in terms of size, size distribution and ZP. Given the close similarity in appearance of these two particles it may be a case of mislabelling. It was not possible to confirm this however and the remaining study concentrated on the 280nm Fe_2O_3 and the 45nm Fe_3O_4 particles only.

Chapter 3 Nanomaterial - Protein Interactions Consequences for Nanomaterial Toxicity

3.1 Nanomaterial – Protein Interactions

The molecular environment in which NMs are present influence their properties and potential toxicity. Once NMs enter the body they immediately come into contact with biological fluids and thus will become coated in airway mucus, alveolar lining layer or blood components [78]. These fluids contain amongst other molecules an abundance of proteins and lipids. Proteins can associate with the NMs and form a protein - NM interaction by adsorption. As opposed to absorption, adsorption is the adhesion of molecules (atoms or ions) from a liquid or gaseous state to a surface. Evidence that NMs adsorb proteins onto their surface has been previously described [103, 149, 150] and after initial exposure and throughout their journey in the body NMs will encounter and interact with many different types of proteins depending on the initial exposure and their fate in the body [1]. This is an area of active research in the nanotoxicology community as currently there is limited information on how NMs interact with these biological components or the role of these interactions is influencing NM toxicity. Knowledge of protein interactions not only between the NMs and the protein but also between the NM-protein and the cell interface will allow for a greater understanding of how these materials behave in the body.

3.1.1 The Protein Corona

The specific proteins that adsorbed to the surface of a NM at any given time have been termed the protein 'corona' [151]. Studies investigating protein adsorption suggests that this interaction or this layer of proteins is what the cell 'sees' and thus if we are to understand or elucidate how the body will react to NMs, their cellular location, the pathway and process they undergo in the body, the proteins that associate with the NMs once in the body must be identified [103]. Theoretically, the corona can be classified into what is termed the 'hard' or long lived corona and the 'soft' or short lived corona. The long lived corona being made up of proteins that remain associated with the NM surface for a longer time

due to slow exchange kinetics with the surrounding environment. The soft corona being made up of proteins that associates with the NMs for a short amount of time due to fast exchange kinetics with the surrounding environment [103, 152]. It is becoming increasingly clear that it is the long lived outer layer of adsorbed proteins – the stable hard corona that is of concern in nanotoxicology as the soft corona is transient and being weekly bound to the NM may not be of concern in toxicological terms [1, 103, 153]. It is not just the composition of the protein layer that is significant when elucidating the interaction of NMs with biomolecules and cells but it is important to realize that this is a dynamic association. The factors that may affect the exchange times of proteins adsorption and the kinetics of this association/dissociation, may provide information on the NM's interactions with biological surfaces/receptors and hence its fate in the body. This again points to the importance of NM characterisation as the nature of the NM will influence the protein adsorption kinetics. This includes factors that may not have necessarily been known, such as residues from the manufacturing process and the presence of endotoxin or controllable factors such as dispersants and buffers used in NM preparation and in toxicity testing [25].

3.1.2 The Corona as a Function of the Physicochemical Properties of Nanomaterials

The physicochemical properties (such as size, surface properties, hydrophobicity, surface coatings) of NMs will determine the corona composition in different biological media [102, 154, 155]. For example, Cedervall et al. [102] found the degree of hydrophobicity of NMs influenced the amount and the type of proteins bound to its surface. Lundqvist *et al.* [154] found that the size and surface modifications of polystyrene NMs significantly changes the nature of the bound proteins. Furthermore, as mentioned in 3.1.1 the corona is not static, as different proteins have different affinities and different equilibrium constants to the particle surface. These interactions can change over time [102, 149, 151]. The resident times (which can be from microsecond to days [25]) have been measured using techniques not commonly employed in nanotoxicology (e.g. isothermal titration calorimetry, size exclusion chromatography, surface plasmon resonance spectroscopy, etc.). Considering toxicological investigations, the most abundant

proteins in a solution may not necessarily be of interest as it may be possible that less abundant proteins with a high affinity and/or specificity for a particular receptor may instead be of more relevance [103]. For example, the ability of opsonin proteins to bind (or not bind) to NMs will significantly alter how such a NM is processed in the body for example by promoting receptor mediated phagocytosis. In blood more abundant proteins such as human serum albumin and fibrinogen might bind more favourably to the NM surface, however if proteins of lower abundance but with higher affinities and slower kinetics bind, they can over time displace proteins already present and alter the corona composition.

3.1.3 Impact of Nanomaterial - Protein Interactions on Function of Proteins

The ability of NMs to bind proteins may leave them unavailable for their normal biological functions. Conversely it has also been suggested that binding of proteins to NMs may have an impact on the structure of the proteins [103] and the protein's biological function [154]. Many studies have reported the use on NMs to alter and control signalling and subsequent cellular responses ([156, 157]). Thus the implication of NM - protein binding is not only that the particle toxicity may be driven by their attached proteins but the possibility that NM-protein binding may impact the structure or the biological function of the protein. Investigating this is a challenging task as the protein concentration in body fluids can be up to 35% (0.35g/ml) [103], and plasma (which has 8% proteins) is made up of many different proteins which exist in varying concentrations. Brown *et al.* [118] demonstrated that 14nm CB NPs adsorbed significantly more cytokines (TNF-α) than 260nm CB from solution and went on to find that TNF-α coated 260 CB produced a greater expression of ICAM-1 in epithelial cells than TNF-α 14nm CB. This work supported the hypothesis that one consequence of the NM - protein interactions may be that proteins mask the nanoparticle surface, thereby reducing NM reactivity and protein functionality.

3.1.4 Relevance of the Corona in Toxicological Studies

When considering exposure, translocation and fate of NMs in the body we must consider that NMs have the ability to interact with a variety of different molecules. Thus the protein corona, being a dynamic structure may vary depending on the NM properties but will also evolve depending on the route of exposure (e.g. inhalation, injection, ingestion and dermal adsorption), and on where in the body the NM translocates. This suggests that NM toxicity may be driven by the exposure route due to the specific protein binding and that this is modified as the NMs move around the body. As the biological identity of the NM is a consequence of the outer layer then it is important to investigate this corona to determine how flexible the corona is over time and in various different types and concentrations of proteins as it travels through the body. In this way we can gain an understanding of how the body will react to NMs, their cellular location and the pathway/process they undergo in the body. However the stability or flexibility of the corona over time and during movement between different body compartments remains unclear, including the relationship between proteins of high abundance and proteins of high affinity. Although the long lived or hard corona is important when considering the fate of NMs in the body, there is a limited amount of studies available to demonstrate impacts of corona composition on fate, cellular interactions or toxicity [151]. To date studies have demonstrated the impact of cell culture media on NM toxicity [158]. It has been shown that carboxylated polystyrene NPs, when tested *in vitro* in the absence of FCS have an enhanced response on J774.A1 cell cytotoxicity and uptake than in the presence of FCS [114], suggesting that FCS may impart some protective influence. Indeed cytotoxicity studies have shown the protective effect of serofendic acid (a component of FCS) against oxidative stress in monocytes [159] and neuronal cell types [160, 161]. It could be that this protective FCS effect is cell specific as previous studies have demonstrated that serum enhances the uptake of polystyrene NPs in hepatocytes [17]. With relation to NMs, corona studies have reported that binding of proteins from FCS to graphine oxide NMs [162] and blood proteins to CNTs [163] reduced the cytotoxicity of these NMs in human A549, monocytic leukemia and endothelial cell lines.

In this study the protein corona identity or 'profile' of iron oxide particles in human plasma and cell culture FCS was examined. To simulate exposure of NMs via inhalation followed by translocation to blood a protein corona first in lung lining fluid (LLF) was developed before transferring the NMs into serum or plasma. Also investigated was the role of particle-protein interactions (i.e. the role of adsorbed proteins) in influencing the potential biological reactivity or toxicity of the NMs in macrophages. As serum is present in cell culture media any effect it can have on the toxicity of NMs is essential to understand (especially when considering standardised nanotoxicology protocols). Comparison of serum and plasma corona and its effect in a macrophage cell line can help with future *in vitro* /*in vivo* cytotoxic comparisons.

3.1.5 Plasma

The liquid component of blood is plasma and it contains several thousand different proteins. Table 3.1 highlights the main components of blood plasma. Plasma proteins, most of which are synthesised in the liver, vary in abundance by twelve orders of magnitude [164]. A recent study by Shen *et al.* [164] described a method whereby 2392 proteins were identified from a single plasma sample. They found the relative abundances of these proteins covered a range of over eight orders of magnitude in concentration (< 30pg/ml to ~30mg/ml). Plasma is thus a complex proteome. It has a vast dynamic range, a large abundance of albumin, there is a heterogeneity of glycoproteins [165] and protein compositions and expression varies between individuals. These are just some examples of what makes plasma a very difficult biological sample to investigate. Separation and identification of its components is therefore a difficult task. Plasma functions in maintaining temperature and osmotic pressure, it is also essential in transport, signalling cascades and regulatory mechanisms [165]. For this reason it has a great diagnostic potential and its constituents (or lack thereof) provide biomarkers for disease diagnostics and so much work has been carried out since the 1900's investigating analytical characterisation methods to separate and identify the various fractions of blood plasma.

Table 3.1: The table presents the most abundant components of blood plasma the types and percentage as well as the primary function of these main components (adapted from OpenStax College online source [166]).

Component of blood	Subcomponent	Type and percentage	Primary Physiological Function
Plasma	Water (92%)	Fluid	Transport medium
	Plasma Proteins (7%)	Albumin (66kDa) (54-60%)	Regulates osmotic pressure and pH, transporter, drug delivery.
		Globulins (155-160kDa) (35-38%)	Maintain osmotic pressure. Defence mechanism and role in transport
		Fibrinogen (340kDa) (4-7%)	Blood clotting and haemostasis
	Regulatory Proteins (>1%)	Hormones and Enzymes	Varied/regulation of body function
	Other Solutes (>1%)	nutrients/gases /wastes	Numerous/varied

3.1.6 Foetal Calf Serum

FCS which is the liquid fraction of clotted blood from the fetal calf (minus cells, fibrin and clotting factors) is used in cell culture due to the large number of nutritional factors essential for cell growth and low level of antibodies. Its function in cell culture is in providing essential growth factors for cells such as hormones, attachment and spreading factors, binding proteins, lipids, and minerals

[167]. The major component is BSA (bovine serum albumin) but it also contains amino acids, sugars, lipids and hormones. Just like plasma it is a complex proteome and as such not every component has been identified, however it still remains the most effective growth product for cell culture

3.1.7 Lung Lining Fluid

A major entry route of NMs into the human body is the respiratory tract. Many factors such as the size, shape and surface chemistry of the particles will be a factor in determining the fate of the particles in the lung but it is clear that size is a key parameter that determines if a particle will translocate across the alveolar capillary barrier [24]. In the alveolar region they can come into contact with lung lining fluid (LLF). Although particles <5μm in diameter undergo macrophage phagocytosis and mucocilliary clearance, UFP are not readily phagocytosed and thus can enter the pulmonary interstitium via the epithelium [168].

One line of defence against inhaled particles is LLF. Kendall [168] found that when PM 2.5 is collected into normal lung lining liquid the particles aggregate into larger (>5 um) dense structures compared with samples collected in air or into saline. Such aggregation will allow inhaled particles to become available for phagocytosis by AM where they can then be eliminated from the alveoli to the mucocilliary escalator or across the alveolar epithelium to the interstitium or circulating blood [169]. LLF has been reported to be diverse in its chemistry and composition. This in part may be due to the inherent difficulty in obtaining a representative sample given the complicated sampling procedure (see 3.2.1) but LLF composition will also vary due to its source, local production and mechanisms such as active transport. It is produced and secreted by type II alveolar epithelial cells and Clara cells [169]. As inflammatory cells (e.g. macrophage, lymphocyte, and neutrophils) line the alveolar space they will be found in the LLF. In most cases (from human samples) 80% of these cells found in LLF were alveolar macrophages [170].

The majority of the non cellular components include proteins, such as cytokines and immunoglobulin, surfactant-like lipids and phospholipids, complement

factors and enzymes. The largest component is made up of phospholipids (80%), the most common being phosphatidylcholine. The phospholipids function in reducing surface tension during breathing. The 10% protein fraction is mostly composed of surfactant proteins (SP) A, B, C and D. SP C and B aid the phospholipids in decreasing surface tension during breathing, the SP A and D are large (43 kDa) hydrophilic proteins which are important in allowing particles to be taken up by macrophages [171, 172]. In particular they have carbohydrate recognition domains which allow them to bind to pathogens and set off an immune response [171]. Thus binding or loss of large amounts of this protein (as has been shown to occur upon NM exposure [118]) could lead to ineffective clearance of particles in the lungs.

3.1.8 In Vitro Cytotoxicity of Iron Oxide Nanoparticles

Further to the aims of this work a murine macrophage cell line was the chosen model. The adherent murine macrophage cell line J774A.1 (obtained from the European Collection of Cell Cultures) displays a number of characteristics of primary macrophages, including adhesion and antibody dependent phagocytosis. It has cell – bound receptors for immunoglobulin and complement [173]. It also produces interleukin-1 and lysosome. This cell line has been used as a model system in many nanotoxicity studies (macrophages as described in 1.2.1.3 are part of our innate immune response – they are specialised host defence cells which allows fast recognition and clearance of foreign material). This innate nonspecific response is essential to our immune system protecting us from 98% of pathogens we encounter [67]. Macrophages are commonly used as models in many *in vitro* studies looking at their ability to actively uptake foreign particles and respond with cytokine signalling cascades or production of ROS [81, 83, 95, 174]. Macrophage phagocytosis will be discussed in more detail in Chapter 5.

Iron, as an essential metal, has vital biochemical functions (e.g. electron transfer, oxygen transfer, etc.) and it is regulated in mammals due to its toxic potential upon accumulation. Bioavailability in the body is limited due to its ability to be oxidised to an insoluble form in solution [175]. Iron not bound to protein or stored efficiently will bind non-specifically to many cellular components and can

catalyse production of free radicals which can happen if iron degrades via the Fenton reaction ($H_20_2+Fe_2+\rightarrow Fe_3^+$ and H_o^- + HO(.-) [176]). So iron toxicity can occur if homeostasis is not maintained or if it occurs in excess in the body thereby exceeding the capacity of transferrin to bind it. Non transferrin bound iron will be internalised into tissues (primarily but not exclusively in the liver and heart [175]) and as mentioned previously up to 3500mg (section 2.1.4) can be stored in the body of which 0.2mg/g is in the liver and liver toxicity can occur with iron leaves reach 4mg/g [141] or when iron (bound as serum ferritin) reaches levels greater than 1,000μg/L iron overload occurs [177]. This is a cause for concern, as excess iron in the body has been linked to heart failure, diabetes, arthritis, cirrhosis, liver cancer [177] and more recently has been linked to Alzheimer's and Parkinson's disease [178, 179].

Studies have found iron oxide NMs did enhance human endothelial cell permeability through the production of ROS, for example, Apopa *et al* [180] found that after exposure (50μg/ml iron NMs) to human endothelial cells within 10 minutes uptake into the cells cytoplasm occurred and found cell permeability increased after 10 minutes peaking at 30 minutes after exposure. Brunner *et al.* [64] found MTT conversion and DNA content significantly reduced in human mesothelioma cells after exposure to 3.75 ppm iron oxide but with a rodent fibroblast cell line affected after 30 ppm iron oxide The variability of *in vitro* iron oxide NMs toxicity data may be due to the large variety of iron oxides NMs available (e.g. naked, dextran or citrate stabilised, silica or gold coated) however literature still reports variable findings for naked particles as recently reviewed by Soenen *et al.* [181].

Accumulation of NMs in organs in this way may produce inflammatory as well as cytotoxic effects through oxidative stress ROS [182-192]. The immune system model is particularly important as macrophages are responsible for particle clearance at sites of exposure and the role of ROS has been implicated in J774.A1 mouse macrophage cytotoxicity after exposure to iron oxide nanoparticles [192].

Renwick *et al.* [95] did find that metal oxides (TiO_2) impaired J774.A1.2 macrophage cells in a dose dependant manner and found smaller 29nm particles

were more effective in impairing phagocytosis than a 250nm counterpart. More recently Zhu *et al.* [146] reported iron oxide NM exposed intratracheally in a rat model caused inflammation and increased micro vascular permeability in cells. They went on to study the kinetics of this distribution in a rat model [147] where they saw that the particles were passed through the alveolar-capillary barrier and distributed into organs such as the liver spleen and kidney. Although 'inert' NMs have been reported to produce ROS due to their ability to target mitochondria with iron NMs there is an extra concern as iron oxides being metal NMs can release ions, and so iron NM toxicity can arise from the formation of reactive species as mentioned above via the Fenton reaction. It is unclear if these ions are solely responsible for all toxic effects or if there are separate ion and NM effects as it is difficult to distinguish between these two types of effects *in vitro*. Iron oxide NM toxicity is related to solubility however some studies do find that toxicity cannot be explained by ionic effects alone [64] which does point towards a NM specific cytotoxicity. It is unknown if the NM effects are induced first or in conjunction with the dissolved ion effect, or indeed if there is a synergist or potentiating effect.

3.1.9 Chapter 3 Aims

- To prepare iron oxide NMs with a plasma, FCS and LLF long lived ‘hard corona’ and to use protein characterization techniques to investigate protein binding

- Examine how the NM size, surface area, composition and charge influence the affinity and degree of protein binding.

- Investigate the impact of protein-NM interactions on influencing toxicity of the NMs by investigating the effects of iron oxide particles with their associated corona on exposure on J774.A1 macrophage cells with respect to:

    - Lactate dehydrogenase (LDH) release and mitochondria function
    - IL-1β, TNF-α, IL-10 and MCP-1 release.

3.2 Materials and Methods

3.2.1 Materials

Fe_2O_3 (280nm) and Fe_3O_4 (45nm) were received and prepared as detailed in 2.2.1. Before embarking on this study the particles were examined, looking at the effect of sonication, particle concentration, ionic strength, pH, and the presence of FCS on the stability of Fe NM in media. The particles were extensively characterised as reported in Chapter 2.

Human plasma was obtained from the Irish Blood Transfusion Board, aliquoted into 1ml eppendorfs, and stored at -80^{o}C until required. FCS (Sigma, UK) was aliquoted into 1ml eppendorfs and stored at -80^{o}C until required.

LLF was obtained from male Sprague Dawley rats using the method of Baughman *et al.* [193], briefly; rats of 3 months old were euthanized by intraperitoneal injection of pentobarbitone. The lungs were removed and lavaged with 4 x 8ml volumes of sterile saline. The lavageate was pooled into a single tube which underwent a series of centrifugation steps. After a final centrifugation step at 60000g for 45 minutes the supernatant was discarded and the remaining pellet was resuspended in 10ml sterile PBS. This surfactant-enriched fraction, termed LLF, was aliquoted into 1ml volumes and stored at -80^{o}C until required. The neat plasma, serum or LLF was removed from the freezer and allowed to thaw on ice at room temperature and centrifuged at 16000g for 2 minutes at 4°C and the supernatant was removed. The supernatant was removed into a new low protein binding eppendorf and the pellet was discarded. The protein content of the plasma, serum and LLF was determined using the BCA protein assay, according to the manufacturer's instructions.

3.2.2 Cell Culture

All reagents were obtained from Sigma (UK) unless otherwise stated. Ampoules of J774.A1 were removed from the -170°C liquid nitrogen container and thawed by placing the ampoule into warm water briefly. Cells were then re-suspended in

5 ml of pre-warmed routine culture medium (RPMI 1640 supplemented with 10% heat inactivated FCS; L-glutamine (diluted from 100x stock solution) and 1% penicillin/streptomycin) and centrifuged at 9000g for 5 minutes. The supernatant was removed and the pellet of cells was re-suspended in 3 ml of pre-warmed routine culture medium. The cell suspension was then transferred into 20 ml of pre-warmed routine culture medium in a 75cm^2 tissue culture flask. Cells were incubated for 24 hours in an incubator with a humidified atmosphere (90%) and set at 37^{o}C and 5% CO_2 to allow the cells to adhere to the bottom of the flask. When the cells were observed by a phase contrast microscope to be 70% confluent, they were subcultured into a new 75cm^2 culture flask. To ensure the cells had overcome the lag growth phase they were subcultured at least three times before being used in a bioassay. Cells were sub-cultured via scraping. The cells were scraped from the flask surface, aspirated and dispensed into a new flask in a 1:4 ratio. The final medium volume per culture flask was 25 ml.

3.2.2.1 Cell Counting

Cells were re-suspended with pre-warmed routine culture medium. A volume of cell suspension (100µl) and trypan blue solution (100µl) were added together and mixed thoroughly. A volume of 20µl was pipetted into the cell counting chamber (Bürker-Türk haemocytometer) and the number of cells counted using a phase contrast microscope. Cell concentration was calculated using the formula: Cell concentration (cells/ml) = average number of cells in one large square * the dilution factor * 10^4.

3.2.2.2 Cell Plating

A cell suspension of $5*10^5$ cells/ml in routine culture medium was prepared. A volume of 100µl of the cell suspension was dispensed into each well of a 96 well plate. Peripheral wells of the 96-well tissue culture plate were left blank to be used as negative controls. Cell suspensions were carefully mixed prior to plating to ensure equal numbers of cells in each well. Cells were incubated for 24 hours to achieve 60-70% confluency in each well. This incubation period assures cell recovery, adherence, and progression to exponential growth phase. Each plate

was examined under a phase contrast microscope to assure that cell growth was relatively even across the plate.

3.2.2.3 Cell Preservation

The cells were rinsed in routine culture media freed by scraping from the culture flask and counted. They were then re-suspended in pre-warmed routine culture medium and centrifuged. The supernatant was removed and the pellet was re-suspended in pre-warmed routine culture medium (half the final freezing volume). Routine culture media with 10% DMSO was added slowly to the cells so that the solvent would equilibrate across the cell membranes. Cells were then brought to the final freezing volume (containing 10% dimethyl sulfoxide (DMSO)) and transferred into ampoules at the appropriate density. The ampoules were stored in a -80°C freezer for at least 24 hours. After 24 hours, the tubes were placed in the liquid nitrogen container.

3.2.2.4. Cell Treatments

Particles were received as a dry powder and were weighed using an analytical mass balance in a special ventilated safety cabinet (Sartorius Model: SWC900) and suspended in sterile water at a concentration of 1mg/ml. The NMs were sonicated at 200W for 10 minutes using a bath sonicator (Grattan). J774.A1 macrophages were treated with the NMs in RPMI at concentrations ranging from 3.9µg/ml to 500µg/ml (corresponding to 2.4 and 312µg/cm^2 respectively). A volume of 100µl of each particle suspension was pipetted into triplicate groups of wells on a 96-well plate. Supernatants were removed, centrifuged and stored at -80^{0}C until required. Plates also contained a positive control which was triton x 100 at 0.1% and a negative control of media only. One hundred microlitres of 0.1% triton x 100 in RPMI was added to the remaining adherent cells and the plate was incubated for a further 10 minutes, to obtain a measure of 100% lysis in the LDH assay. Wells containing no cells and particle treatment were also prepared to investigate any interference of the particles in the assay.

3.2.3 Imaging of Macrophages with Particles

A six well plate was seeded with cells at a concentration on $5*10^5$ per well and incubated for 24 hours to allow confluent growth and attachment to the wells. After 48 hours they were exposed to 280nm Fe_2O_3 (500 or 125µg/ml) in a range of BSA (0, 0.1, 0.5 and 1% BSA) and imaged over various time points (4, 18, 24 and 48hrs) under a phase contrast microscope with a Canon camera (40D) attached to capture images.

3.2.4 Preparation of Hard Corona Coated particles

The layer of strongly associated proteins (the hard corona) was created using plasma, serum, or LLF by a series of incubation and washing stages. The particle/protein solutions were prepared in low protein binding eppendorf tubes with the various biological fluids in order to achieve final particle mass concentrations of 100µg/ml and solutions of LLF (10µg/ml), plasma (10 and 55%) or serum (10%). A standard ratio of iron oxide particle dispersion in protein solution was 1:9 as has been reported in similar studies [149, 194]. The particle-protein samples were briefly vortexed (~30 seconds). The particles were then incubated in a shaking heating block for one hour at 37^oC. After incubation the particle suspensions were centrifuged at 12000g for 20 minutes to ensure all NMs were separated from the soft corona. The supernatant was removed after each centrifugation step. This process was repeated until no further protein remained in the supernatant as determined by using both a Pierce® BCA Protein Assay Kit (Thermo Scientific) and a Micro BCA Protein Assay Kit (Thermo scientific) as per the manufacturer's instructions. This produced NM dispersions with a strongly bound layer of associated biomolecules. In addition, particles once coated in LLF were again (using the same procedure) coated in plasma or serum in order to investigate the effects of LLF precoated particles on the protein corona composition. In this way seven different test samples were created as per table 3.2.

Table 3.2: The conditions under which the hard corona was created for each particle.

1	10% P	100µg/ml particles incubated in plasma and PBS (final conc.10% plasma)
2	55% P	100µg/ml particles incubated in plasma and PBS (final conc.55% plasma)
3	10% S	100µg/ml particles incubated in serum and PBS (final conc.10% serum)
4	LLF	100µg/ml NMs incubated in LLF and PBS (final conc.10µg/ml LLF)
5	LLF/ 10%P	Particles incubated as per LLF, after incubation centrifuged and supernatant removed. Then incubated with 10% plasma in PBS.
6	LLF/ 55%P	Particles incubated as per LLF, after incubation centrifuged and supernatant removed. Then incubated with 55% plasma in PBS
7	LLF/ 10%S	Particles incubated as per LLF, after incubation centrifuged and supernatant removed. Then incubated with 10% serum in PBS.

3.2.5 Characterisation of the Particle-Protein Complex

Characterisation of the particles alone included (a) dispersion studies (b) size measurements (DLS and NTA) (c) image analysis (SEM TEM) (d) charge/stability using ZP and (e) metal analysis (EDX). DLS measurements and ZP were used initially to study the hydrodynamic diameter to obtain an indication of size and stability of the particles in water and in PBS. Particles were then remeasured after coating with the biological fluid (10% plasma, 55% plasma, 10% serum, LLF, precoated in LLF and then in 10 and 55% plasma and 10% serum). In this way the DLS (Malvern Zetasizer Nano) was used to give an indication of the thickness of an adsorbed layer on the NM surface. Polydispersity index (Pdi) was obtained to gain an indication of the particle aggregation/flocculation behaviour. An increase in Pdi represents an increase in agglomeration.

Differential Centrifugal Sedimentation (DCS) was employed to investigate the size shift between the coated and uncoated particles. NMs in solution were injected into a spinning disc containing a sucrose gradient. One hundred micrograms per millilitre of either particle or the coated particles were injected into a CPS disc centrifuge. Using specific parameters (disc speed, density and particle absorbance) for each NM tested the sample settled through the gradient according to the size of the particles and the mean size from the resulting peaks indicated the average size of the NM. In order to get an accurate reading of the complex the internal density of the sample and particle absorbance must be known. This was set at 5.24g/cm^3 (Fe_2O_3) and 5.17g/cm^3 (Fe_3O_4) and particle absorbance at 0.5nm. Particles with their corona were also measured using DCS as described above and the resulting shift in the peak was used to calculate the corona or 'shell' layer size using a core - shell two - density model as previously reported by Monopoli et al.[151]. The hard corona shell size (thickness) can be calculated using the core-shell two-density model involving the particle material and the adsorbed protein/biomolecule densities. In practice this was accomplished with the software supplied by CPS instruments after inputting three values these are (i) the assumed coating density (ii) the NM core density (as specified above) and (iii) the NM core diameter. The density of hydrated protein crystals is 1.23g/cm^3 and blood plasma is 1.025g/cm^3 thus the intermediate value of 1.125g/ml was taken as the coating density of our plasma in this model ([151, 195] for this model. The theory behind this model can be found in Pitek et al. [195]. In summary to identify the true size and the corona thickness from this technique a simple core-shell two-density model involving the particle material and adsorbed protein/biomolecule densities as reported in Monopoli et al. [151]. This information supported the DLS data to give a more accurate estimation of the adsorbed layer thickness.

3.2.6 Protein Separation and Identification

To investigate which proteins strongly associated with the particles, one dimensional sodium dodecyl sulphate (SDS) gel electrophoresis and mass spectroscopy (MS) was used.

3.2.6.1 SDS PAGE Reagents

(a) Resolving and Separating Gels

A 10% separating gel and a 4% stacking gel were prepared using the following reagents: 3.095mls Milli Q water, 3.5mls Tris-HCL (pH 8.8) 10% SDS (dissolved in MilliQ water), 3mls acrylamide/bis (29:1) and before pouring 10% (v/v) ammonium sulphate and 5ul TEMED. The stacking gel was prepared using the following reagents 2.82mls MilliQ water 1.575mls Tris-HCL (pH 6.8), 500ul acrylamide (29:1) solution, 50ul 10% SDS, 50ul 10% ammonium sulphate and 5ul TEMED. This was enough for 2 gels, 1.0 mm thick.

(b) Electrophoresis Buffer

Electrophoresis stock buffer was prepared by dissolving 144g glycine, 30g trizma base 10g SDS in 1L dH_2O. Prior to use a 1x buffer was prepared by diluting the stock 1:10 in dH_20.

(c) Preparation of Samples (Removal of Hard Corona)

The NM and the hard corona complexes were separated as previously described [104, 151] as follows: denaturating agent 1.25M dithiothreitol (DTT - Sigma, UK) was added to a loading buffer in a 1:10 dilution. The loading buffer (New England Biolabs) contained 62.5mM Tris-HCl (pH 6.8 at 25°C), 2% (w/v) SDS, 10% glycerol and 0.01% (w/v) bromophenol blue. A 40µl volume of each sample was added to 20µl of the loading buffer/DTT solution in a low binding eppendorf tube and incubated at 100^oC for three minutes. In this way the denatured corona proteins coated in SDS surfactant gain a negative charge. Ten microlitres of each sample was loaded on a 10% resolving gel and a 4% stacking gel.

(d) Electrophoresis

The resolving gel was poured between two glass plates of a Bio-Rad casting apparatus and topped with a layer of isopropanol and left to polymerise (for one hour). After polymerisation the isopropanol was poured off and the stacking gel was dispensed between the casting plates. A 10 well comb was then inserted between the glass plates and left to set for 30 minutes. Once set the comb was removed and the gel and the glass plates containing the gel were washed with

MilliQ water to eliminate bubbles. The gels were immersed in electrophoresis buffer in a Bio-rad electrophoresis tray prior to addition of 10µl of sample to each well. Samples were separated by electrophoresis at 130 mA until the dye had run to the bottom of the gel (one hour) at which time the gel was removed and stored for future reference.

(e) Staining

The resulting gels were stained using either a silver staining kit (Cosmo Bio, Japan) or a mass spectroscopy compatible silver staining kit (GE Healthcare International) according to the manufacturer's instructions.

3.2.6.2 Mass Spectroscopy

After imaging the gel bands (Image Quant LAS 400 Biomolecular Imager - GE), the gel lanes were processed and analyzed with MS to identify the constituent proteins. The lanes were excised from the gel using a scalpel and trypsin digested to the method of Monolopi *et al.* [151] before analysis using a LTQ ESI MS/MS (Thermo Fisher) interfaced with an LTQ Orbitrap (ThermoFinnigan, CA). The resulting spectra were searched using Sequest Uniprot/Swiss-Prot database (www.expasy.org- Accessed October 2012 and February 2013).

3.2.7 Lactate Dehydrogenase Assay

LDH is a soluble enzyme found in the cytosol. As cell membranes are damaged LDH is released from the cell, thus determining LDH content of cell culture media gives an indication of cell membrane integrity and a measure of cytotoxicity. LDH, if present, will catalyse the conversion of pyruvate to lactate with concomitant inter-conversion of NADH and NAD+. Secondly, diaphorase was added which uses the newly formed NADH and H^+ to catalyse the reduction of a tetrazolium salt – formazan. Then formazan can be quantified calorimetrically as it absorbs strongly at 490-520nm. Thus the amount of formazan measured in the cell culture media is proportional to the amount of LDH released into the medium as a result of cytotoxicity. Thus the assay measures LDH release to determine cell death in response to exposure to NMs.

From a confluent flask of cells, the cell culture medium was discarded into a beaker containing Virkon. The cells were harvested using a cell scrapper and the flask was rinsed with 10mls of cell culture medium. The suspension was poured into a 30ml sterile universal container. Under sterile conditions 50-100µl of the cell suspension was removed a cell count was conducted. In a 96 well plate 100 µl of cell suspension was added per well, giving a final cell number of $5*10^5$. After 24 hours the media was removed from the cells the cells were washed twice with 100ul pre warmed PBS buffer. The cells were then exposed to a range of 500-3µg/ml particles in serum free media.

The plate was incubated for 24 hours. Following exposure the culture media was transferred 1.5ml eppendorfs and centrifuge for 30 minutes at 1500g to remove any particles. The supernatants were stored at -80^oC until required. Media with 0.1% triton x 100 was then added to the adherent cells, and the plate was incubated for a further 10 minutes at 37°C, 5% CO_2. The remaining cell suspension was transferred to 1.5ml eppendorfs, centrifuged and stored until required.

A stock solution of 1mg/ml nicotinamide adenine dinucleotide (NADH – Sigma, UK) in 0.75nM sodium pyruvate (Sigma, UK) solution was made fresh and used to create a standard range from 2000-0 LDH activity (units/ml). In a 96 well plate 60µL of each standard was plated to create the standard curve. A volume of 50µl/well of NADH (1mg/ml)/pyruvate (0.75mM) was added to the remaining wells. This was incubated at 37°C, 5% CO_2 for 5 minutes. To this 10µl of each sample was added to the wells containing NADH. This was incubated for a further 30 minutes at 37°C, 5% CO_2. A volume of 50µl 2,4-dinitrophenylhydrazine (Sigma, UK) solution was added to each well. The plate was incubated at room temperature in the dark for 20 minutes. A volume of 50µl 4M NaOH was added to each well, placed on a plate shaker for 5 minutes at room temperature. The absorbance at 550nm was measured using MRX plate reader (Dynatech Labs, UK). The percent total LDH leakage was calculated using the formula = ((sample abs-media control abs)/ (triton X positive control abs – media control abs))*100.

3.2.8 WST-1 Assay

The WST-1 assay is a cell proliferation assay based on the principle that viable cells will reduce the tetrazolium salt (WST-1) to formazan by cellular mitochondrial dehydrogenases. Formazan is a coloured dye (dark yellow) that can then be detected by absorbance at 420-480nm with 440nm being the optimal absorbance range. The absorbance directly correlates to cell number.

Cells were seeded at a density of $5*10^5$ final concentrations in cell culture media inclusive on test particles at 125µg/ml-32µg/ml. Wells were seeded with 100µl cells per well in a 96 well plate. After 24 hours 10µl of WST-1 proliferation agent (Roche, Germany) was added and the plate was incubated for four hours at 37°C and 5% CO_2. After 4 hours the plate was removed from the incubator and placed on a plate shaker for one minute. The absorbance was measured at 440nm. Controls included cells in medium without NMs with WST-1 reagent (negative control) and cells with triton and WST-1 reagent (positive control). Controls also included also included medium without cells with WST-1 reagent, NM in medium without cells and WST-1 reagent and cells with NM only.

3.2.9 Cytokine Estimations using FACS Array Analysis

Supernatants obtained during the LDH assays (see 3.2.7 and 3.2.2.4) were used to estimate the release of the following cytokines from treated cells; IL-1β, TNF-α, IL-10 and MCP-1. Supernatants analysed by FACS include (a) cells exposed to Fe_2O_3 particles (b) cells exposed to Fe_2O_3 particles with LLF corona (c) cells exposed to Fe_2O_3 particles with plasma corona (d) cells exposed to Fe_2O_3 particles with serum corona. Analysis was carried out on a BD FACS Array™ Bioanalyzer, using a BD cytometric bead array mouse/rat soluble protein master buffer kit.

3.2.10 Statistical Analysis

Data from all experiments were analysed using the Minitab 15 statistical package using a general linear model analysis of variance. Significance was set at 5%.

3.3 Results

3.3.1 Imaging of J774.A1 Macrophages Exposed to Fe_2O_3 Particles.

(a) 4 Hours

(i) (ii) (iii) (iv)

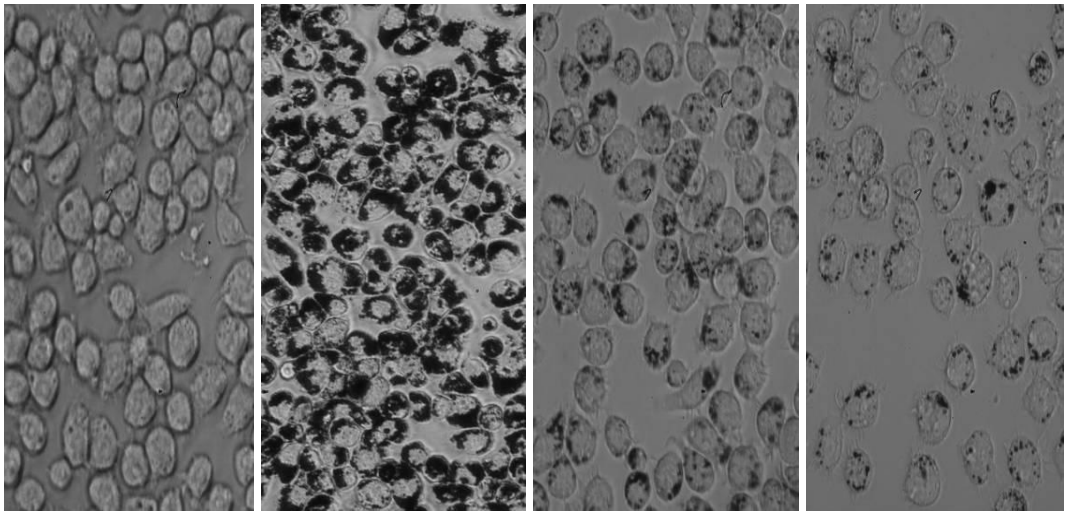

(b) 18 Hours

(i) (ii) (iii) (iv)

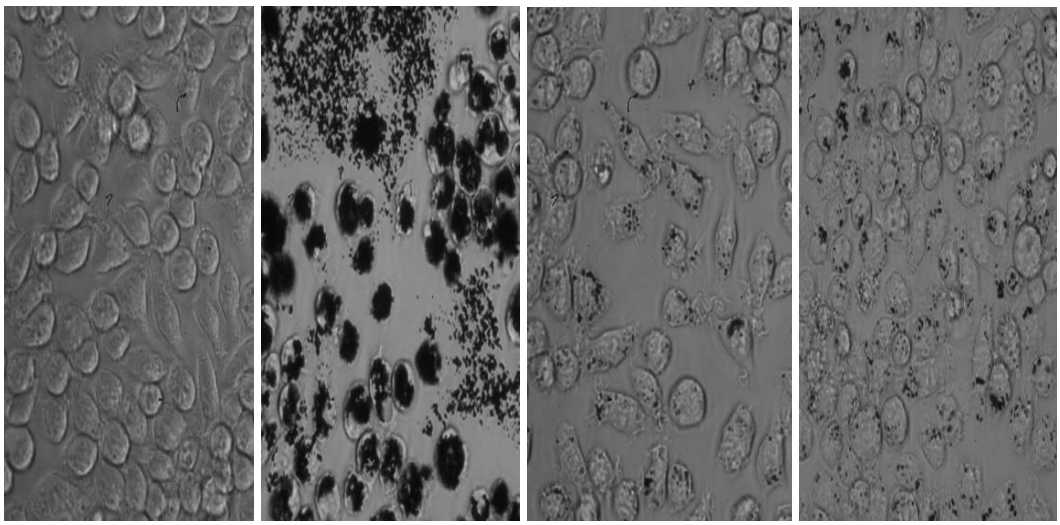

Figure 3.1: Light microscopy (20x) images of J774.A1 macrophages after exposure to Fe_2O_3 particles for (a) 4 hours and (b) 18 hours, where (i) control (ii) exposure to 0.5mg/ml (iii) exposure to 125µg/ml and (iv) exposure to 125µg/ml in RPMI with 1% BSA. These images show how the particles associate with the cells within 4 hours. No very obvious effect on particle uptake can be seen due to the addition of BSA. If there were such an effect this would be difficult to visualize by light microscopy. Images at other time points can be seen in the appendix 8.6.

3.3.2 Hard Corona Analysis

(a) (b)

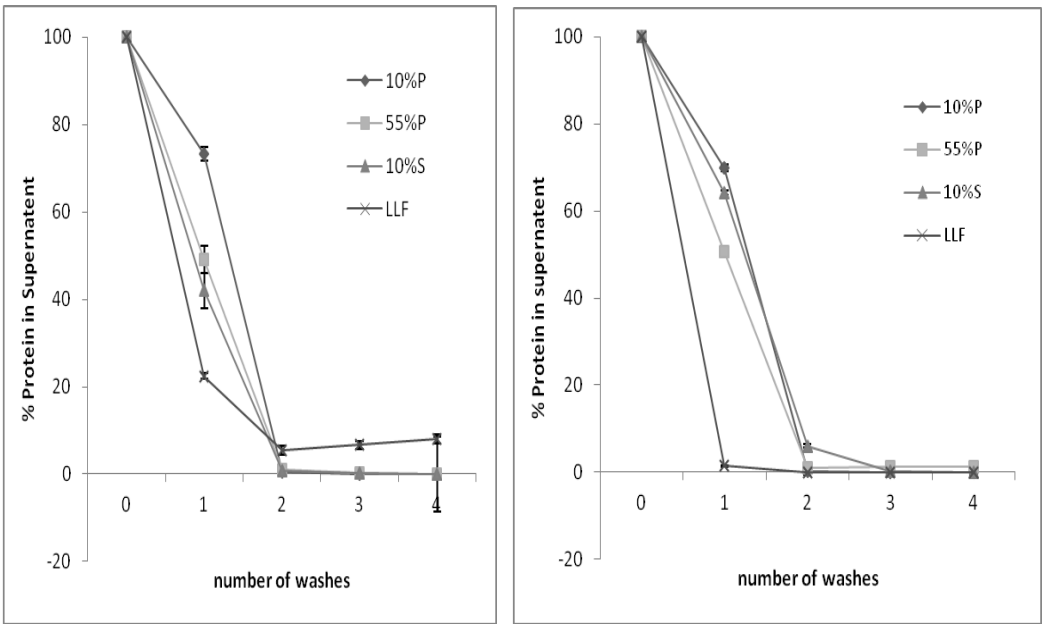

Figure 3.2: The total protein content of the serum (43.286mg/ml), plasma (64.83mg/ml) and LLF (30.52µg/ml) was measured using a BCA protein assay. After hard corona preparation as described in 3.2.4 the protein-NM complexes were studied free of excess protein (i.e. the hard corona). The above graphs show the percentage free protein remaining in (a) Fe_2O_3 particle supernatant and (b) Fe_3O_4 particle supernatant after 1-4 washes as determined by BCA assay, as measured during hard corona preparation. Values represent the mean +/- SD (n=3). After four washes the free protein present in the supernatant diminished to less than 1% of the original protein content for most samples. It was therefore concluded that any proteins remaining in the system were associated with the iron oxide particles and were not free in solution. These remaining proteins attached to the particles were deemed the hard corona. This method of repeatedly centrifuging (washing) the protein-NM complex is a commonly reported method of eliminating the soft corona [151, 195].

3.3.3 DLS Analysis

Table 3.3: Hydrodynamic diameter, polydispersity index (Pdi) and zeta potential for 280nm Fe_2O_3 particles and 45nm Fe_3O_4 particles measured in water, PBS and with their associated long lived or 'hard' protein corona (where P=plasma, and S=serum and LLF= lung lining fluid) as determined by DLS. Values represent the mean +/- SD (n=3).

Fe_2O_3 (280nm)	**Z average (nm)**	**St Dev. (nm)**	**Pdi**	**ZP (pH 7.5) mV**
Water	297.40	1.80	0.28	-21.8mV
PBS	461.00	16.80	0.38	-9.52m
10% P	560.70	13.50	0.35	-12mV
55% P	543.60	5.60	0.39	-12.2mV
10% S	362.30	12.60	0.29	-14.6mV
LLF	822.70	95.40	0.50	-16.2mV
LLF/10%P	1384.00	134.60	0.88	n/a
LLF/55%P	442.40	8.60	0.23	n/a
LLF/10%S	475.20	58.70	0.30	n/a

Fe_3O_4 (45nm)	**Z average (nm)**	**St Dev.(nm)**	**Pdi**	**ZP (pH 7.5) mV**
Water	544.00	9.19	0.44	-24.8mV
PBS	791.00	n/a	0.55	-20mV
10% P	1212.00	n/a	0.65	-0.5mV
55% P	1204.00	n/a	1	-0.2mV
10% S	>1000	n/a	1	.5mV
LLF	>1000	n/a	1	-1.0mV
LLF/10%P	865.90	37.32	0.26	n/a
LLF/55%P	>1000	21.21	0.50	n/a
LLF/10%S	>1000	78.93	0.38	n/a

The DLS measurements show the Fe_2O_3 NM to be 297.4 nm and the Fe_30_4 NM to be 544nm. The ZP measurements, which are an indication of particle charge and suspension stability, find that both particles have a value above 20mV. Both particles showed an increase in hydrodynamic diameter in PBS and after incubations with 10 and 55% plasma compared to deionised water. The largest increase in hydrodynamic diameter was observed for both particles with the LLF

corona. The hydrodynamic diameter for LLF/10%S was similar to 10%S for both particles, with a value of 362.30nm/475.20nm for Fe_2O_3 and over 1000nm/1000nm for Fe_3O_4). LLF pre-treatment followed by incubation in plasma resulted in a Z average that was similar to plasma alone, but smaller than LLF alone. For the 45nm particle in LLF/10% P had a smaller Z average than for 10% P alone, but for 55% P compared to LLF/P55% there was no difference.

The Pdi was generally lower for the 280nm particles than the 45nm particles. PBS and plasma increased the Pdi by a small amount for the 280nm particles, but serum had no major effect on the Pdi. LLF almost doubled the Pdi and this was increased further by the 10% plasma, but reduced by the 55% plasma. LLF/10%S treated 280nm particles had a similar Pdi to the water dispersed particles. Plasma, serum and LLF all increased the Pdi of Fe_3O_4 significantly, but when pretreated with LLF and then serum or plasma the Pdi was reduced, most extensively with 10% plasma.

3.3.4 Corona Characterisation using DCS

Table 3.4: Differential centrifugal sedimentation (DCS) measurements (n=3) showing particle hydrodynamic diameter as a function of relative weight for (a) Fe_2O_3 and (b) Fe_3O_4 particle when dispersed in water and PBS and the particle-corona complexes free from excess plasma, serum and LLF

(a)

280nm Fe_2O_3	**Size (nm)**	**Shell Diameter**
water	303.5	n/a
PBS	323.9	n/a
10%P	311	13nm
LLF/10%P	290.3	38nm
55%P	320.5	3.5nm
LLF/55%P	275.3	59nm
10%S	268.5	69.5
LLF/10%S	309.5	15nm

(b)

45nm Fe_3O_4	**Size (nm)**	**Shell diameter**
water	174.8	n/a
PBS	197.0	n/a
10%P	151.3	63nm
LLF/10%P	154.6	57nm
55%P	151.9	61.5nm
LLF/55%P	186.9	10.5nm
10%S	217.0	n/a
LLF/10%S	174.7	25.5nm

The particle-corona complexes were prepared as described in materials and methods (3.2.5). A volume of 100µg/ml NM was injected into a differential centrifuge. The sample settled according to the size of the particles and the mean size from the resulting peaks was used as the average size of the sample (these are the results displayed above in column a). The hard corona shell size (as seen in column b) was calculated using a core-shell two density model as described in the materials and methods (3.2.5). This method has been used in previous studies [151, 195]. The results show that the particle corona thickness varied according to dispersant/corona and particle type. For Fe_2O_3, the greatest corona depth was 10%S > LLF/P55% > LLF/10%P > LLF/10S% > 10%P > 55%P. For the Fe_3O_4 NM the greatest corona dept was 10%P > 55%P > LLF/10%P > LLF/10%S > LLF/55%P > 10%S.

3.3.5 SDS PAGE Investigation of Protein Corona Profile

(a) SDS-PAGE gel lanes showing binding patterns of proteins associated with the 10% plasma hard corona of iron particles before and after incubation with LLF. For comparison purposes these gels have been cropped. The full gel image from which this lane is cropped can be seen in the appendix (section 8.7 (a) and (b))

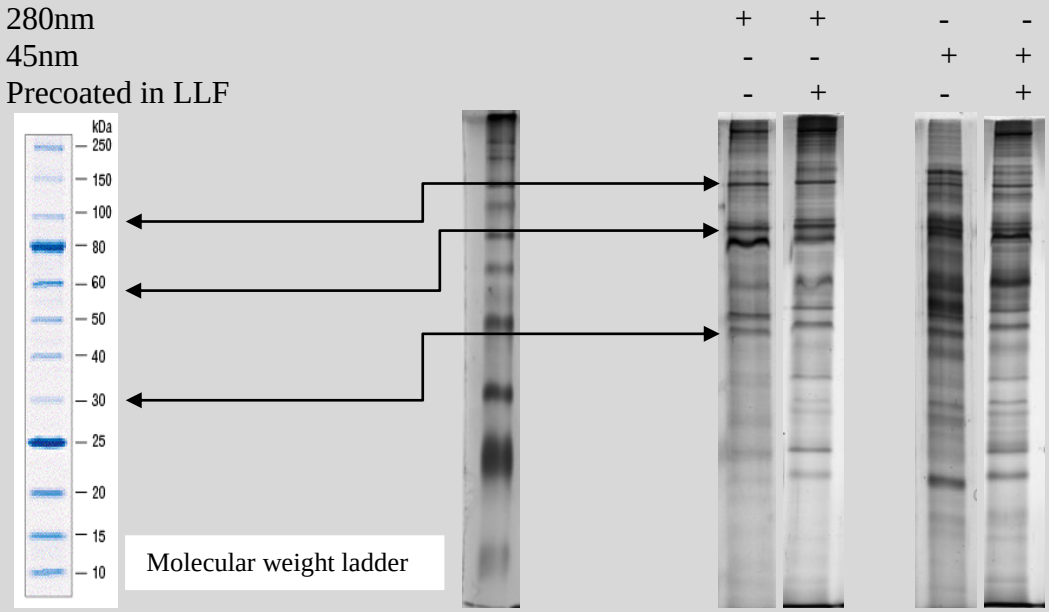

(b) SDS-PAGE gel lanes showing binding patterns of proteins associated with the 55% plasma hard corona of iron particles before and after incubation with LLF. The full gel image from which these lanes are cropped can be seen in the appendix (section 8.7 (d) and (e))

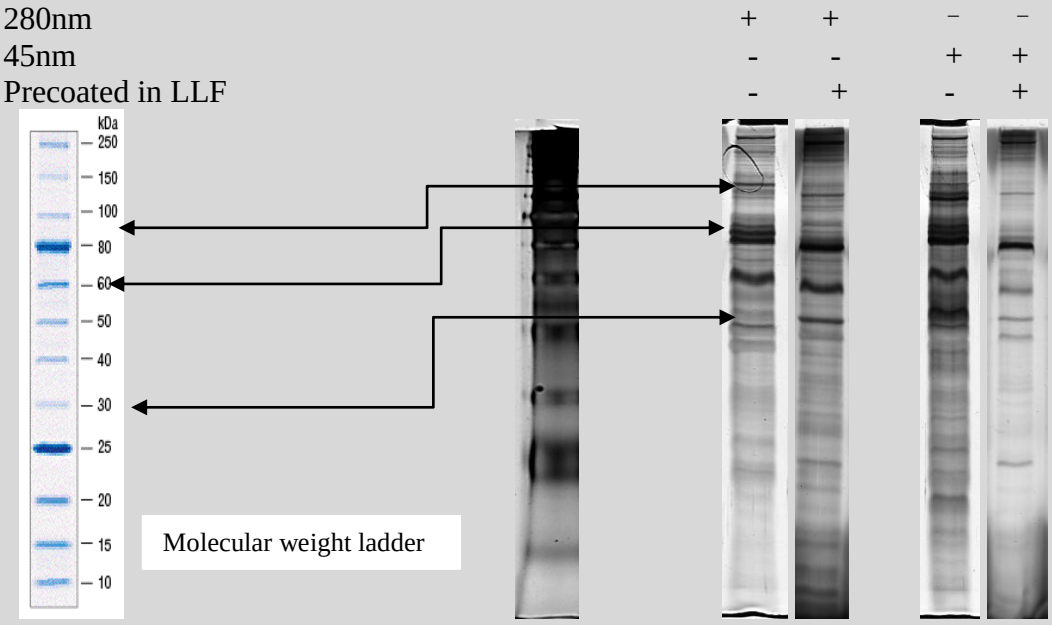

Figure 3.3: SDS-PAGE gels obtained to investigate the binding patterns of iron particle-protein interactions (a) 10%P and LLF/10%P hard corona (b) 55%P and LLF/55%P hard corona.

Table 3.5: Results from Mass Spectroscopy analysis showing the most prevalent proteins in the 280nm iron particle plasma hard corona before (a) and after (b) precoating in LLF. The full list of all proteins identified can be found in the appendix 8.8.

(a)

Fe_2O_3 10% P	**MW**	**Acc No**	**XC Score**	**PEP**	**%C**	**Peptide Ion (hits)**	**Function as defined by Uniprot**
Apolipo-protein B-100	515.28	P04114	350.29	1.11 E-15	12.80	35	Functions as a recognition signal for the cellular binding and internalization of LDL particles by the apoB/E receptor.
Complement C3	187.03	P01024	260.30	2.00 E-13	24.60	27	C3 plays a central role in the activation of the complement system.
Serum albumin	69.32	P02768	110.30	2.40 E-11	20.70	12	good binding capacity for water, Ca^{2+}, Na^{+}, K^{+}, fatty acids, hormones, bilirubin and drugs. Its main function is the regulation of the colloidal osmotic pressure of blood. Major zinc transporter in plasma, typically binds about 80% of all plasma zinc.
Apolipoprotein (a)	500.99	P08519	60.27	2.86 E-09	18.20	6	Apo(a) is the main constituent of lipoprotein(a) (Lp(a))
Complement C4-A	192.65	P0C0L4	50.27	3.07 E-07	3.60	5	C4 plays a central role in the activation of the classical pathway of the complement system

(b)

Fe_2O_3 LLF/10% P	MW	Acc No	XC Score	PEP	%C	Peptide Ion (hits)	Function as defined by Uniprot
Complement C3	187.03	P01024	440.30	1.55 E-14	39.00	48	(see figure 3.4 (a))
Serum albumin	69.32	P02768	230.29	6.91 E-12	45.50	25	(see figure 3.4 (a))
Apolipo protein B-100	515.28	P04114	190.29	9.58 E-11	7.30	19	(see figure 3.4 (a))
Filamin-A	280.56	P21333	170.28	7.63 E-11	12.40	17	Anchors transmembrane proteins to the actin cytoskeleton and serves as a scaffold for a range of cytoplasmic signalling proteins
Myosin-9	226.40	P35579	120.28	1.09 E-09	9.60	12	Cellular myosin that appears to play a role in cytokinesis, cell shape, and specialized functions e.g. secretion and capping.

Table 3.5 reports the protein identified in (a) the Fe_2O_3 10%P corona and (b) the Fe_2O_3 LLF/10%P corona by Mass Spectroscopy (LTQ ESI MS/MS interfaced with an LTQ Orbitrap along with the reported molecular weight (MW-kDa). The Accession number (Acc No) is a unique identifier given to a protein sequence and in this case it refers to entries at the Sequest Uniprot/Swiss-Prot database (http://www.uniprot.org/). The Xcorr value (XC Score) is the cross-correlation value from the search. In other words the scoring method reporting the number of fragmented ions in common between the experimental spectrum and the theoretical spectrum. The PEP or (posterior error probability) is the probability that the observed peptide match is incorrect (a chance event). If the PEP of a peptide spectrum is 1% it means there is a 99% chance that peptide has been correctly identified. Thus the lower the number the higher the probability of a 'true' match. The percentage sequence coverage (%C) and the number of peptides confirmed by mass spec analysis are shown.

SDS-PAGE gel lanes showing binding patterns of proteins associated with a iron particles with a 10% serum hard corona before and after incubation with LLF. The full gel from which these lanes are cropped can be seen in the appendix section 8.7 figure (f) and (g))

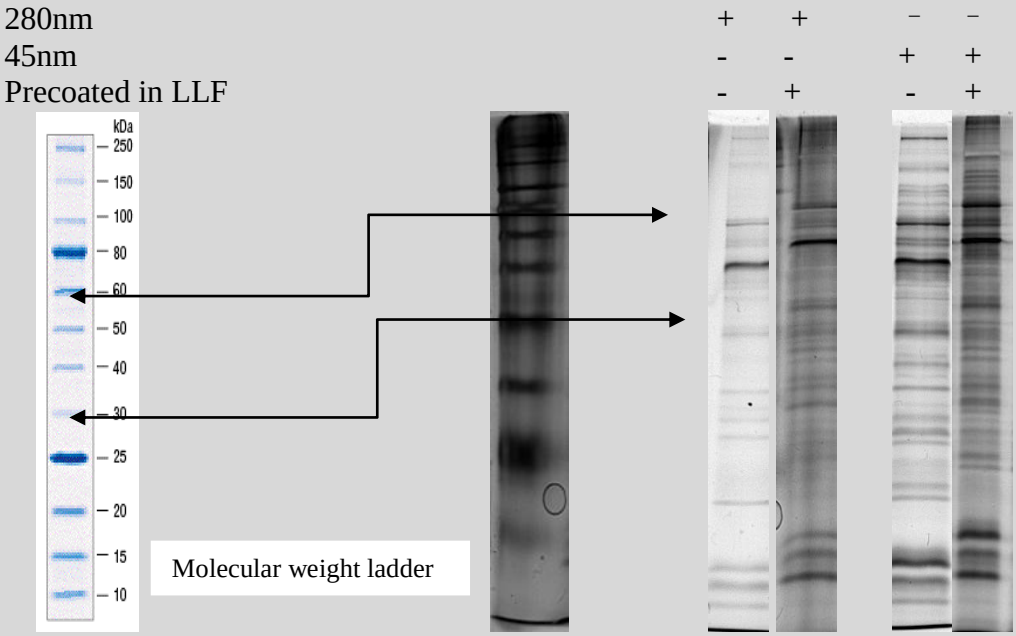

Figure 3.4: SDS-PAGE gels obtained to investigate the binding patterns of iron particle-protein interactions (a) 10%S and LLF/10%S hard corona.

Table 3.6 Results from mass spectroscopy analysis showing the most prevalent proteins identified in the 280nm iron particle serum hard corona profile (before (a) and after (b) incubation with LLF) - the full list of all proteins identified can be found in the supporting information (appendix 8.8)

(a)

Fe_2O_3 10% S	**Acc No.**	**MW**	**XC Score**	**P EP**	**% C**	**Peptide Ion (hits)**	**Function as defined by Uniprot**
Serum albumin	P02768	69.32	60.19	2.71 E-12	10.80	7	(see figure 3.4 (a))
Apo-lipoprotein A-I	P02647	30.76	10.20	4.20 E-10	6.00	1	Participates in the reverse transport of cholesterol from tissues to the liver for excretion
Desmoglein-1	Q02413	113.67	10.20	3.98 E-05	1.50	1	Involved in the interaction of plaque proteins and intermediate filaments mediating cell-cell adhesion.
Cystatin-A	P01040	10.99	10.19	6.70 E-06	18.40	1	This is an intracellular thiol proteinase inhibitor. Has an important role in cell-cell adhesion in the lower levels of the epidermis
Fibronectin	P02751	262.46	10.17	8.90 E-04	.80	1	Fibronectins are involved in cell adhesion, cell motility, opsonization, wound healing, and maintenance of cell shape

(b)

Fe_2O_3 LLF/ 10% S	Acc No	MW	XC Score	P EP	% C	Peptide Ion (hits)	Function as defined by Uniprot
Serum albumin	P02768	69.32	170.28	1.27 E-09	35.80	18	(see figure 3.5 (a))
Apolipoprotein A-I	P02647	30.76	40.20	3.81 E-10	17.60	4	(see figure 3.5 (a))
Ig gamma-1 chain C region	P01857	36.08	30.24	9.62 E-12	17.58	3	None listed
Ig kappa chain C region	P01834	11.60	20.25	4.71 E-12	32.08	2	None listed
Glyceraldehyde-3-phosphate dehydrogenase	P04406	36.03	20.20	4.45 E-09	11.34	2	playing a role in glycolysis and nuclear functions

The SDS-PAGE gels lanes seen in figure 3.3 and 3.4 show proteins of the iron oxide NMs with a 10% plasma hard corona (10%P) before and after incubation with LLF (LLF/10%P); the 55% plasma hard corona (55%P) before and after incubation with LLF (LLF/55%P) (Figure 3.3) and a 10% serum hard corona (10%S) before and after incubation with LLF (LLF/10%S). They were obtained to investigate the binding patterns of 280nm and 45nm Fe particle - protein complexes free from excess proteins. The proteins were separated as described in 3.2.6. The molecular weights of the proteins in the standard ladder are reported on the left for reference.

After staining using a mass spectroscopy compatible staining procedure, selected lanes (280nm Fe_2O_3 in 10% plasma, and after pre incubation in LLF lanes) were trypsin digested to remove the protein and analysed using MS. The above tables (3.3 and 3.4) show the five most abundant proteins identified by MS. All

recorded proteins can be found in the appendix 8.8. The MS findings indicated that the quantity of proteins that make up the hard corona vary, not only in type, but in quantity between plasma and serum. The most abundant protein found in the 10% plasma corona was apolipoprotein B-100, apolipoprotein (a) and complement proteins. After preincubation with LLF the amount of complement and serum albumin that made up the corona doubled. This indicated that the LLF resulted in greater adsorption of proteins onto the NM surface at the 10% plasma concentration. This data is also supported by the DLS /DCS and SDS PAGE binding patterns. This suggests that as NMs and particles translocate to secondary target sites in the body its biological identity is not static but may change over time and recent studies [151] have shown that the protein concentration impacts on the evolution of the protein corona over time, so that the corona evolves as it passes from one biological fluid to another [153]. Bands were also observed at 90kDa (plasminogen), 30kDa (apolipoprotein A) and at 20kDa. The same binding pattern was seen at the higher plasma concentration, but the intensity of the bands varies especially at 50kDa. These bands were different from those observed using 10% serum which was seen to bind many different proteins of a lower molecular weight.

The three most abundant proteins isolated from the Fe_2O_3 in 10% plasma and in LLF/10%P were apolipoprotein B-100, complement C3 and albumin, but the relative order of abundance was different. In the 10% plasma corona the most abundant proteins of the corona also included apolipoprotein (a) and complement C4-A, while in LLF/10%P the most abundant proteins included filamin-A and myosin-9. For the Fe_2O_3 particles in 10% serum or LLF/10%S the most abundant proteins included albumin, which is not surprising since this is the most abundant protein in serum. The remaining composition of the corona was different from the plasma corona in that it included apolipoprotein A-1, desmoglein-1, cystatin-A and fibronectin. While in LLF/10%S the corona included apolipoprotein A-I, alpha-1-antitrypsin, Ig gamma-1chain C region and Ig kappa chain C region.

3.3.6 Cytotoxicity Results

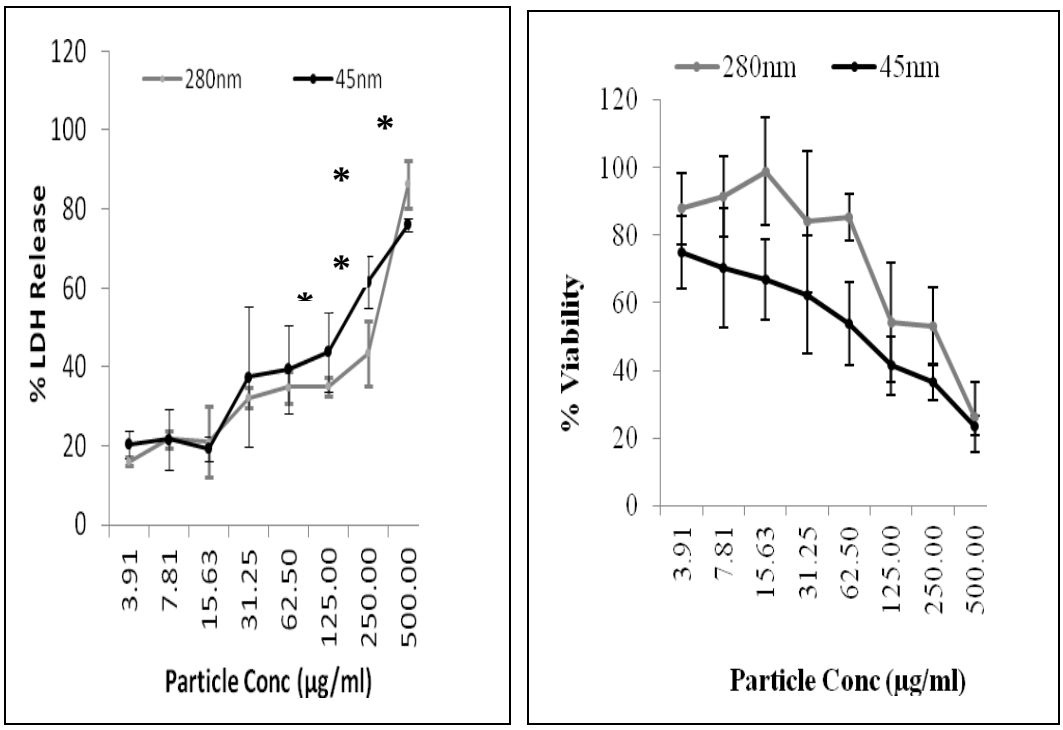

(a) (b)

Figure 3.5: (a) Percentage (of positive control) LDH release and (b) viability assessed by WST-1 of J774.A1 macrophages after exposure to Fe_2O_3 280nm and Fe_3O_4 45nm particles for 24 hours. Values represent the means of 3 experiments ± SEM. The asterisk denotes a significant difference from the negative control ($p < 0.05$).

This work reports that there was no significant release of LDH from the macrophage cell line treated with the 280nm Fe_2O_3 particles after four hours exposure compared to cells in media only (data shown in appendix 8.9). There was also no significant release of LDH for the cells exposed to the 45nm particles after 4 hours compared to media alone, except at the highest concentration of 500µg/ml (data shown in appendix 8.10). Both Fe_2O_3 and Fe_3O_4 induced a dose dependent increase in LDH release after 24 hours (Figure 3.5). The concentration at which the cytotoxicity became significant compared to the control was 62.5 µg/ml for both the Fe_2O_3 280nm and Fe_3O_4 45nm particles (24 hours exposure). ANOVA (95% significance level) indicates there was no significant difference in

percentage LDH release between the 2 particle types (p=0.752). Figure 3.3.6 (b) shows the effect of particle exposure on cell mitochondrial function. Again, the percentage viability of the cells after exposure to Fe_2O_3 280nm and Fe_3O_4 45nm particles after 24 hours exposure showed a dose dependent increase in cytotoxicity. Again there was no difference between the two particle types ($P > 0.05$) and the concentration at which there is a significant difference from untreated cells is at 62.5µg/ml.

3.3.7 Impact of Corona on Cytotoxicity

(a) 280nm

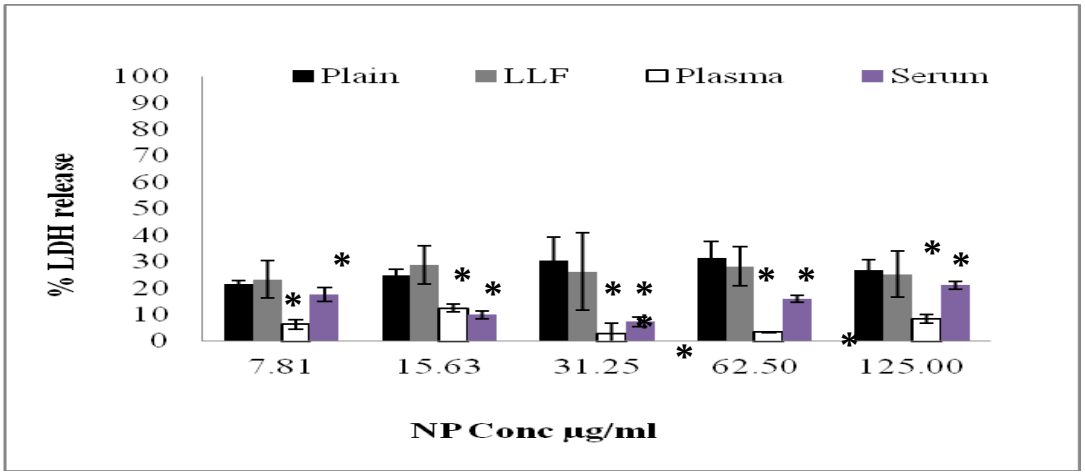

(b)45nm

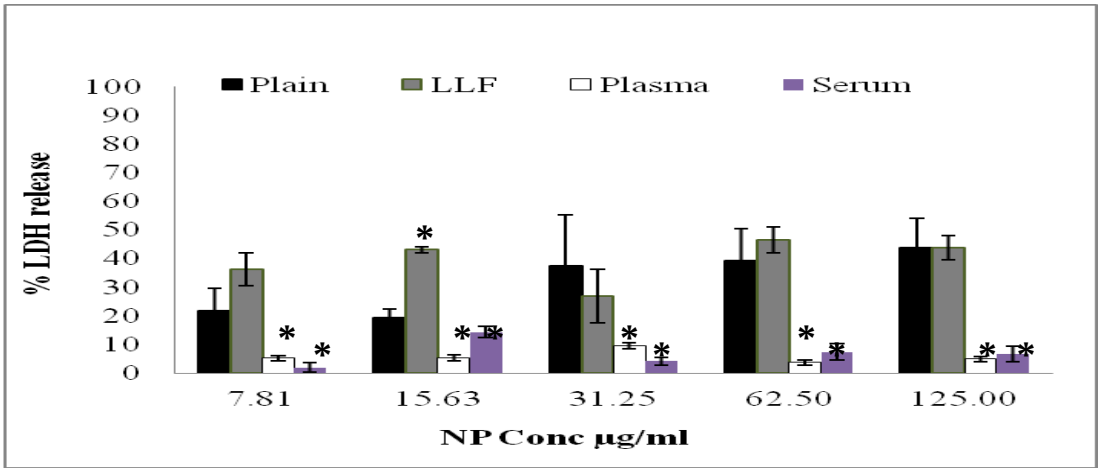

Figure 3.6: Percentage (of positive control) LDH release from J774.A1 macrophages after exposure to (a) Fe_2O_3 280nm particles (b) from

Fe_3O_4 45nm particles with and without its associated 10%P, 10%S and LLF corona after 24 hour exposure. Values represent the means of 3 experiments ± SEM.

The results from figure 3.6 show that following exposure to 280nm Fe_2O_3 there was no significant difference (P=0.123) in the % LDH release between the plain particles (i.e. those without a hard protein corona) and those coated with LLF. There was a significant difference between in the % LDH release from cells exposed to the plain and LLF coated particles than those exposed to serum (P=0.001) and plasma (P=0.001) coated particles as denoted by the asterisks. Indicating that the serum and plasma coated particles mitigate toxicity. There was also a significant difference between the serum and plasma coated particles (P=0.45) with serum coated causing more LDH release than plasma coated particles. The 45nm particles produced similar findings to the 280nm particles, in that there was no significant difference (P=0.197) in the % LDH released from cells exposed to plain uncoated particles and those coated in LLF. As with the 280nm particles the % LDH measured was significantly higher (p=0.001) in cells exposed to plain and LLF coated NMs than those exposed to plasma and serum coated NMs. Unlike the 280nm particles there was no significant difference (p=0.911) between serum and plasma coated particles with respect to % LDH release.

3.3.8 Cytokine Analysis

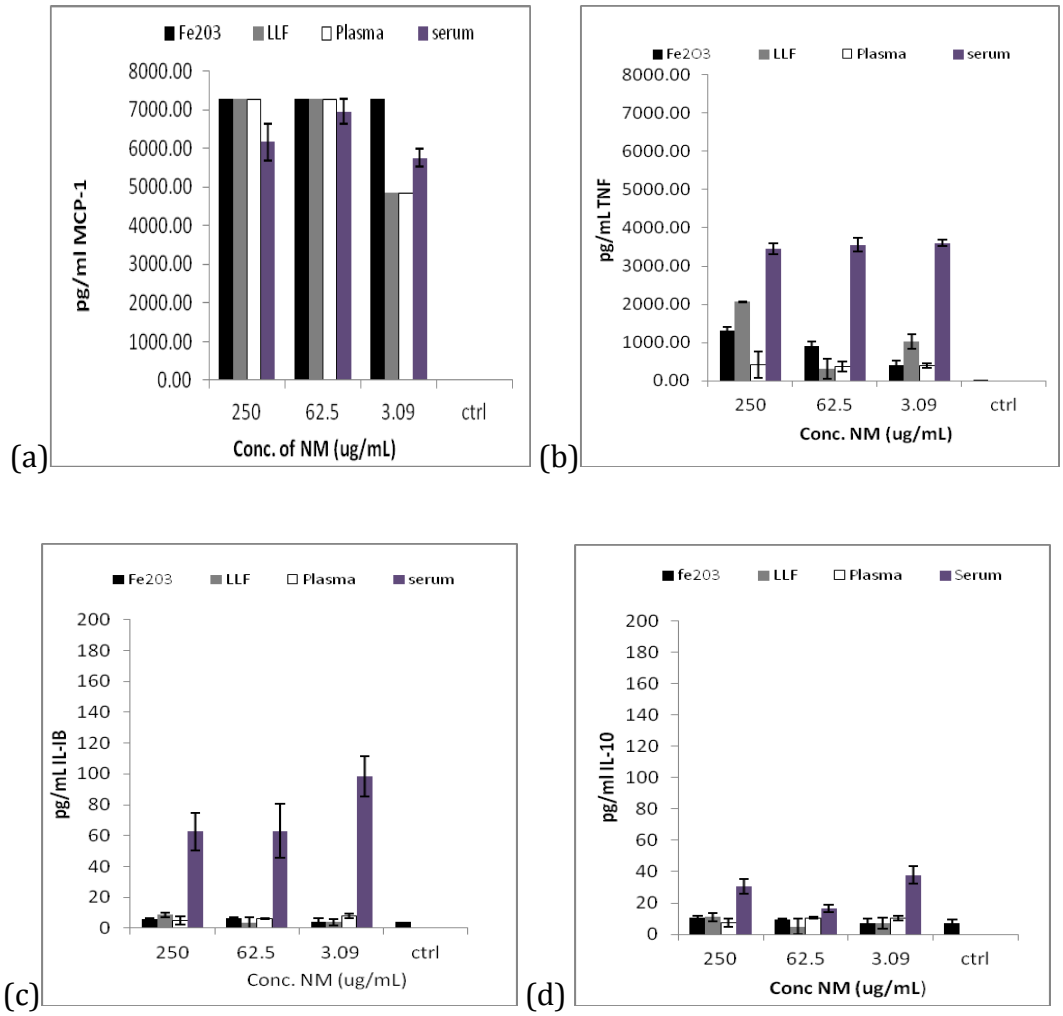

	Fe_2O_3 no corona	Fe_2O_3 LLF	Fe_2O_3 10%P	Fe_2O_3 10%S
MCP-1,	✔	✔	✔	✔
IL-1β,				✔
TNF-α	✔	✔	✔	✔
IL-10				✔

Figure 3.7: Cytokine profile measured from supernatant of J774.A1 cells exposed to Fe_2O_3 with and without associated LLF Plasma and serum corona (a) MCP-1 (b) TNF-α (c) IL-1β and (d) IL-10. Data expressed as a mean ± SEM, n = 3. The effect of the particles with their serum corona has a significant impact (at 95% significant level) on cytokine release with these particles showing increased release compared to the control for MCP-1, TNF-α ,IL-1β and IL-10 at all concentrations tested (250, 62 and 3µg/ml). The table underneath

denotes the treatments were the cytokine levels were significantly greater than the control at the 3 concentrations.

(a)

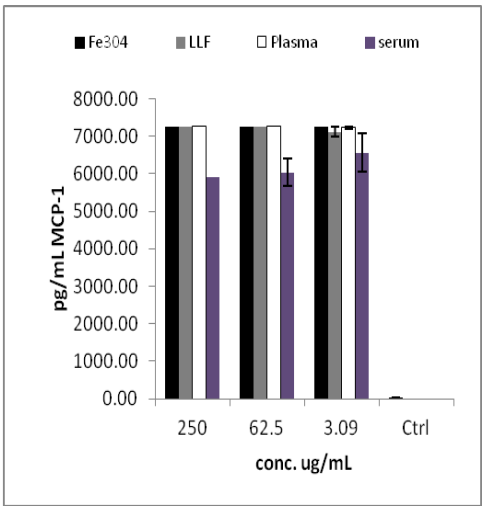

(b)

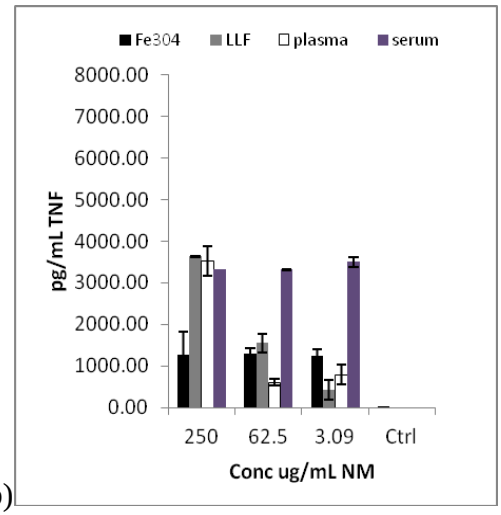

(c)

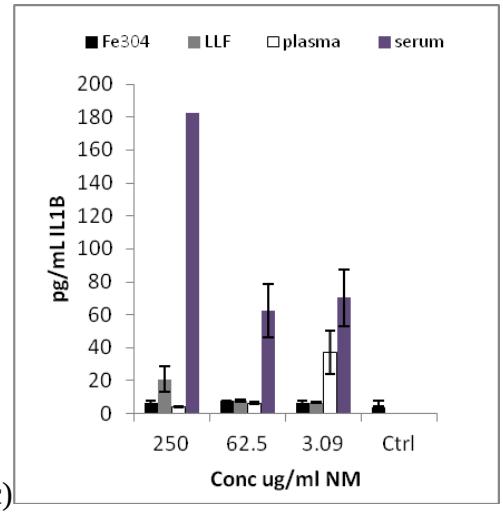

(d)

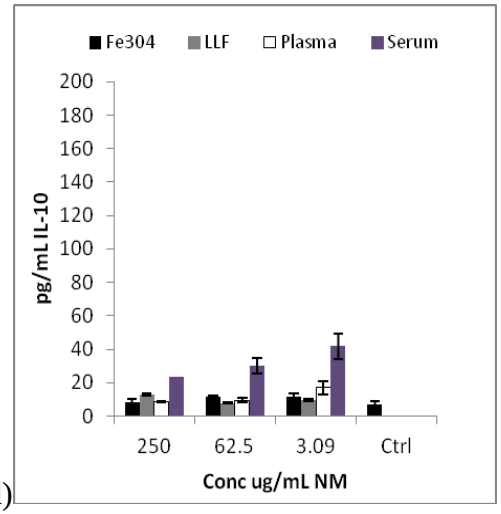

	Fe_3O_4 No corona	Fe_3O_4 LLF	Fe_3O_4 10%P	Fe_3O_4 10%S
MCP-1,	✔	✔	✔	✔
IL-1β,		✔ (only at 250ug/ml)		✔
TNF-α	✔	✔	✔	✔
IL-10			✔	✔

Figure 3.8: Cytokine profile measured from J774.A1 cells exposed to Fe_3O_4 with and without associated LLF, Plasma and serum corona (a) MCP-1 (b) IL-1β (c) TNF-α and (d) IL-10. The table underneath denotes the treatments were the cytokine levels were significantly greater than the control at three concentrations.

3.4 Discussion

This study investigated the effect of the iron oxide particles and iron oxide NMs with a protein hard corona on a J774.A1 'macrophage like' murine cell line in relation to cytotoxicity and ability to stimulate pro-inflammatory cytokine release. The particles were characterised before and after protein coating using differential centrifugal sedimentation, dynamic light scattering and zeta potential measurements. Semi quantification of the hard corona composition was carried out using one dimensional gel electrophoresis and mass spectrometry.

Initially three types of particles were investigated, two Fe_2O_3 particle (280nm and 22nm) and one Fe_3O_4 (45nm) particle which was an ultra superparamagnetic iron oxide (USPIO) NM. The three particle types were examined for the effect of sonication, particle concentration, pH, and the presence of FCS on their stability in media, using a range of techniques. This study on the physical and chemical analysis of the 280nm and the 22nm Fe_2O_3 particles, as well as their cytotoxicity (LDH release see appendix 8.10) suggested that they were so similar that it could not distinguish between them. Therefore the remaining studies continued with the 280nm Fe_2O_3 and the 45nm Fe_3O_4 particles only.

The images of the cells after particle expose (Figure 3.1 and those found in the appendix 8.6) show that within four hours particles appear to associate with the cells and after 48 hours cell death appears to occur. Cell death can clearly be seen to occur after exposure to the higher concentration (500µg/ml) of particles. The light microscopy imaging, the LDH release data and the WST-1 assay all indicated that the 280nm Fe_2O_3 and the 45nm Fe_3O_4 particles were of relatively low toxicity to the macrophage cell line at 4 hours. By 24 hours both particles induced toxicity to a similar extent despite their difference in chemistry and size.

Naked particles induced a dose dependent increase in LDH release for both particle sizes These results concur with published literature on naked iron oxide NM toxicity (example review by Soenen *et al.* [181]) which indicate that these types of NMs are tolerated at high levels [47, 144]. The data presented in this thesis does show this using two separate endpoints. However given the large

variety of testing methods/endpoints and the types/sources of naked iron oxide NMs published in the existing literature it is difficult to develop an overall consensus on iron oxide NM toxicity in macrophage cell lines. This work adds to the published literature and overall suggests that the hard corona of particles has an effect on cytotoxicity as assessed by LDH released in a J774.A1 cell line. LLF had no significant impact on this toxicity, while serum and plasma reduced the toxicity significantly, perhaps this may be because the plasma and serum coat the particles surface in a way that LLF does not. The low protein content of LLF may be a crucial factor here. Indeed SDS gels of the LLF coated particles (appendix 8.11) shows only one major band was obtained. This is an interesting result indicating that exposure via inhalation is an important route to consider for future toxicological studies and that the addition of serum into pulmonary cell culture models may, firstly not be relevant and secondly might lead to an underestimation of the potential toxicity of the particles.

The applications and current uses of these particles are discussed in Chapter 2. For these particles to be useful in the biomedical field they need to be stabilised or functionalised by the application of a coating [181]. In this study the particles were used in their non-functionalised form in order to investigate the 'naked' particles, in this way the study was not complicated with the issue of coating or coating degradation on toxicity. The coating effect on iron oxide NM cytotoxicity and cellular uptake in different cell media has been previously described [158, 181] and such issues may be responsible for many inconsistencies in the published literature on iron oxide NM toxicity. The large variety of iron oxide particles, cells types used in cytotoxicity studies and the variety of cytotoxicity protocols available, is also no doubt an issue of concern when elucidating iron oxide NM toxicity.

Due to the nature of the iron oxide particles used in this study, care had to be taken when optimising the cytotoxicity assays. Contamination of samples by particles before spectroscopic analysis can lead to an increase in the absorbance readings. Particles have been shown to interact with colour generating dyes in colorimetric assays for example, as has been found when employing the MTT assay when examining CNT cytotoxicity [196, 197]. After a preliminary

examination of the particles this was found to be true for the particles employed in this study (data shown in appendix 8.5), therefore before analysis the supernatant was removed from each test well in the 96 well plates and centrifuged to remove any particles. Failure to take such precautions may result in a higher estimation of cell viability or LDH release. It was also considered that particles may adsorb LDH; such binding can of course confound endpoint measurements leading to an underestimation of cytoxicity as it will not be present in the supernatant for detection. For this reason it is important to use a variety of endpoints.

This study's focus was on the long lived protein corona, those proteins that remain strongly bound to the NMs. During preparation of the long lived corona samples, a BCA protein assay was carried out on each wash to investigate the concentration of remaining protein and it was seen that after 3-4 washes less than 1% of the total protein was detectable in the washes. It must be considered that this method however has limitations in that the complexes must be heavier than any unbound proteins in order to be separated successfully. Given that iron oxide has a density of 5.24g/cm^3 (blood serum=1.025g/cm3) in this case the complex does suit this method of separation.

Immediately after preparation of the particles or NM corona, the particle – protein complex was characterised using DLS, ZP and DSC. According to DLS measurements all the particle types showed an increase in hydrodynamic diameter in PBS compared to deionised water. This has been reported previously for other particle types [198-200] and for iron oxide particles [137]. For both particles there was a further increase in the hydrodynamic diameter after incubation in plasma (10% and 55%). It is interesting to note that DLS measurements also show that incubation in 55% plasma contributed to a smaller increase in the hydrodynamic diameter than after incubation in the 10% plasma. This was observed for both particle types and was also confirmed by DCS data. The largest increase in Z average was seen in the LLF corona.

These DLS characterisation results find that NMs with their associated long lived hard corona showed an increase in the hydrodynamic diameter compared to the

particles dispersed in water; however the Pdi measurements remained similar, suggesting that this increase was not due to agglomeration, but due to the additional adsorbed layer. However the LLF coated and precoated particles had a high Pdi and very low ZP indicating they were not stable in solution and tended to be highly agglomerated. LLF has been previously reported to have this effect on particulate matter [168].

The ZP measurements, which are an indication of particle charge and suspension stability, showed that the particles were stable in water. The ZP value of the particles decreased by up to 50% measured with their associated proteins. A decrease in the zeta potential may be explained in one of two ways: (i) the 'slipping plane' (the point at where the ZP is obtained) being moved further away from the particles and hence reducing the zeta potential, or (ii) the drag caused by the presence of the coating on the particles reducing the mobility of the particles (and hence also reducing the ZP).

By examining the difference in peak shift between the naked NMs and NMs with a protein corona in the DCS data, information on the external protein coating was obtained. Using the core-shell two density model the shell thickness (i.e. that of the protein coating) was reported. This information supported the DLS data to give a more accurate estimation of the adsorbed layer thickness. For the 280nm iron oxide NMs, there was an increase in shell size after treatment using every coating and after precoating in LLF followed by serum or plasma. For the 280nm particles the 10% plasma corona shell was determined to be 13nm. It is interesting that this dropped to 3.5nm for the 55% plasma corona. After preincubation in LLF the corona, for both 10 and 55% plasma and 10% serum, increased to 38nm, 59nm and 69.5nm respectively, suggesting that the LLF in some way adds to the hard corona. It was seen that the shell size varied according to dispersant/corona and particle type. For Fe_2O_3, the greatest corona depth was LLF/S10% > LLF/P55% > LLF/P10% > 10%P > 10%S > 55%P.

For the 45nm particles a slightly different trend was observed compared to the 280nm Fe_2O_3 particle where the protein shell coating in plasma (both 10 and 55%) appeared to be larger before precoating with LLF. This interesting

observation was confirmed by DLS results and visually by the SDS PAGE gels, where it can be observed that after precoating the 45nm particles with LLF and then plasma there appeared to be less protein in the gel lane than with the 55% plasma coating alone. The 10% serum corona did not produce a measurable shell corona thickness. However, after precoating with LLF there was a 25.5nm coating observed. The protein shell thickness was not calculated for the LLF coated particles as the protein density was unknown. For the Fe_3O_4 NM the greatest corona dept was 10%P > 55%P > LLF/10%P > LLF/10%S > LLF/55%P > 10%S.

Each sample (280nm Fe_2O_3, 45nm Fe_3O_4, NMs with a plasma and serum corona, and NMs preincubation with LLF) was further investigated using SDS PAGE so as to examine the hard corona protein profile. The SDS gels revealed that there was no obvious alteration in the binding patterns of the 280nm plasma and serum corona after preincubation with LLF. The binding patterns were almost identical to the non-preincubated particles however they did show higher band intensity after preincubation. The observation for the 45nm iron oxide particles was similar to that of the 280nm however the 45nm iron oxide NMs with its associated 55% plasma hard corona did show there was more protein binding compared with the same particles which was first precoated using LLF followed by a 55% associated corona. This was not observed for the 10% plasma corona suggesting that the LLF in some way hindered protein adsorption at higher concentrations.

The observation that the hard corona can significantly vary in composition depending on the concentration of protein and the coating (plasma, serum or preincubated in LLF) is an interesting observation which potentially has implications for interpretation of *in vitro* experimental data. The different coating protocols also provide an opportunity to prepare the particles for in vitro studies that better model the exposure scenario *in vivo*. The ability to track the evolution of a protein corona in a real life scenario (lungs to blood) is an important element of this study. It is interesting to note that both opsonic proteins (i.e. proteins that enhance phagocytosis such as complement proteins and immunoglobulins) and dysopsonic proteins (i.e. proteins that are less recognisable to macrophages such

as apolipoproteins and albumin) were detected by MS in the corona adding yet another layer of complexity in elucidating how particles are processed once in the body (i.e. the retention time in the blood/clearance by macrophages).

NMs studied *in vitro* in cells lines with FCS concentrations may not correlate to actual real life exposure scenarios where the NMs are in a high plasma concentration and come into contact with many types of biological fluids. Considering this, the macrophage response to iron oxide particles and NMs in a plasma, serum and LLF corona was investigated. The plasma concentration at 10% and 55% and serum concentration at 10% corona as chosen in order to compare the *in vivo* and *in vitro* situation. As inhalation is a likely route of exposure to NMs, the corona of NMs first preincubated in LLF and then incubated in either plasma or serum was also investigated further as it has previously been shown that NMs can translocate from the lungs to the blood [201].

This study also examined the ability of the iron oxide particles (with and without their corona) to stimulate the release of the acute phase cytokines IL-1β, TNF-α, the cytokine IL-10 and chemotactic protein MCP-1 from J774.A1 macrophages. This was a study made in connection to the LDH assay and so the cytokine profile was measured from the supernatant saved from the LDH assay. Both the 280nm and the 45nm iron oxide particles with their associated serum corona showed a significant difference from the negative control (at all 3 concentrations tested) in terms of cytokine release with an increase in release for MCP-1, TNF-α, IL-8 and IL-10. In general it would be expected that the amount of proteins (cytokine) produced is an indicator of the number of viable cells present and that an increase in protein production occurs in correlation to the increasing particle dose until a point (LC_{50}) at which point the protein production would decrease. The results from the LDH assay revealed that the serum coated particles produced a lower LDH response; this means there are more intact cells available to produce measurable quantities of cytokines. In the absence of normalised data these results should be viewed not as a separate experiment but taken together with the LDH data. Higher quantities of viable cells may explain the higher cytokine levels not only in the proinflammatory cytokines but also in the anti-inflammatory cytokine inhibitor IL-10. Thus it may not so much be an indication of an

inflammatory response (which is heavily dependent on cytokine and chemokine release) but validates the LDH assay. As both particles with their associated serum corona showed a significant difference from the control in terms of cytokine release, with an increase in release for MCP-1, TNF-α, IL-8 and IL-10, it was expected then that this may also be the case for particles with a plasma corona however a higher cytokine release was not seen consistently for this treatment at all concentrations. However it should be noted that at 250μg/ml both 45nm Fe_3O_4 and the 280nm Fe_2O_3 particles with a plasma corona did produce a significant increase in MCP-1 and TNF-α.

This work ultimately shows that the biological identity of particles is a result of their attached proteins. Bound proteins may aid binding to receptors expressed in cells thus facilitating endocytosis into cells. Although this was not examined within the scope of this thesis it is possible to hypothesise that greater interaction with receptors would lead to a greater intracellular dose that might enhance toxicity. However, studies have also demonstrated ([114, 158]) an ability of NMs, when tested *in vitro* in the absence of FCS, to have an enhanced response on cell cytotoxic response and uptake over NMs in presence of FCS and more recent studies emerging have linked the protein corona to reduced cytoxicity [162, 163]. This study shows the ability of the protein corona to reduce the cytotoxicity of iron oxide particles to the J774.A1 cell line. The more proteins making up the corona, (as identified by MS) the less % LDH release was found *in vitro*. It can be speculated that NMs and particles with their associated corona, do not interact as much with the cells as NMs and particles in the absence of a corona. It may be that the naked iron oxide NMs which caused the higher LDH release are more prone to associating with cells in order to bind biomolecules to their plain surface in a bid to lower their surface reactivity.

3.5 Conclusion

Although it is difficult to correlate the impact of any individual protein identified in the protein corona to cytoxicity this study has shown that binding of serum and blood plasma proteins to iron oxide particles reduces cytoxicity to macrophages. It was found that the particle - protein interactions vary according to protein type (serum or plasma or LLF) the concentration and on precoating in LLF. It is interesting to note that not only the type of biological material, but the concentration of that material impacts on the protein binding profile of the corona.

There is a clear difference in the biological identity of the iron oxide particles in plasma, serum and in LLF and this illustrates the implications for interpretation of data from *in vivo* cell culture tests that do not take the protein corona into consideration. Clearly the protein corona is an important element to consider in experimental design so that a better insight into particle/protein interactions can be obtained in a biological system. Thus this work implies that the biological consequences of NM-cell interactions cannot be examined without considering the biological environment and may explain the contradictory toxicity results proposed thus far observed for iron oxide NMs. Such studies provide an opportunity to devise particle preparation protocols that mimic the corona composition *in vivo* to better study cellular responses *in vitro*.

Why NMs appear to have an affinity for one protein compared with another and why these affinities vary according to the protein concentration is unknown. This is a worthwhile opportunity for future studies, particularly focusing on FCS, as this may lead to standardised experimental conditions that can advance the nanotoxicological field, leading to a more harmonised approach to NM and particle toxicity investigations. This work has been repeated using other particle types as a comparison.

Chapter 4 The Effect of the Silica Particles and Nanomaterial Protein Corona on Macrophage Cytotoxicity

4.1 Introduction

NMs exhibit a relatively high surface area to volume ratio compared to larger particles. The small size of NMs restricts the space available for intermolecular bonds causing them to become strained and more reactive, hence leading to a relatively higher surface reactivity. Consequences of the high surface reactivity include a tendency to adopt spherical shapes where possible, to agglomerate and in biological fluids NMs to associate with proteins and other biomolecules [202]. This behaviour that not only lowers their high free energy state but can also determine their potential fate (organ distribution) in the body. In 3.1.1 the term protein corona was introduced to describe the specific set of proteins in a biological media which associate with NMs. These protein interactions, the type, degree and amount are essential to investigate in nanotoxicology, as the presence of proteins on the NM surface will determine their *in vivo* response [25]. For example the presence of opsonins in the NM corona will promote phagocytosis whereas the presence of dysopsonins will inhibit phagocytosis and promote circulation of NMs in the body [151]. Recently emerging research shows that NMs adsorb proteins from a biological matrix in a manner that is correlated with the specific NM physicochemical properties [154, 203]. Although this is a growing area of interest in nanotoxicology recent studies focus more on the corona characterisation [25, 104, 204] and adsorption kinetics [149, 204] and less on the toxicological significance of the protein corona. The emerging studies looking at the toxicological impact of the protein corona [150, 162, 163] have reported that binding of proteins to NMs does tend to reduce the cytotoxic potential of NMs. Previous work in this thesis (Chapter 3) does find that iron oxide particles with a plasma and serum protein hard corona were less cytotoxic than naked particles, as determined by the LDH release. These types of findings have important consequences for nanotoxicity studies again highlighting the need for well characterised NMs and standardised experimental conditions.

In Chapter 2 it was discovered, after extensive characterisation, that there was no difference in the physicochemical characteristics of the 22nm and 280nm iron oxide particles that were used to examine if particle size can influence the affinity and degree of protein-particle binding. Therefore in order to re-examine this hypothesis of the thesis the work expanded to incorporate silica NMs. Four silica particles and NMs (200nm and 50nm neutral silica and 200nm and 50nm amino modified silica) were examined to determine their responses in the same macrophage cell line (J774.A1). Their ability to bind proteins from plasma serum and LLF were investigated in the same manner as that carried out for iron oxide particles in Chapter 3. These particles have previously been used in corona and toxicity studies [151, 205] and were characterised as part this work.

4.1.2 Silica Nanomaterials

Owing to the relative ease with which stable monodisperse silica NM can be made they are one of the most widely available NMs in the marketplace today (as can be seen in table 1.1). In the order of 1.5 million tonnes of silica NMs are produced annually and this represents a market value of around €2.7 billion [14]. A study commissioned by the European Commission on the types and uses of NMs (which shall be summarised briefly herein with regards to silica) reports that silica NMs find uses as function fillers in polymers, electronics and the cosmetic industry and to a lesser extent in paints and coatings and food additives [14]. The function of silica NMs depends on the form it is manufactured in. For example colloidal silica are generally spherical particles and are mainly used in the paper industry as coatings for ink jet paper, the electronics industry for polishing computer chips and in the food and textile industry. Silica NM manufactured as 'precipitated silica' (5-100nm) are used primarily in the manufacture of rubber and as anti-caking agents in the food and healthcare industries (e.g. toothpastes, detergents and cosmetics). Fumed silica is a type of silica that is in the size range of 5 and 100 nm and is used in the rubber and plastic industry, as an antifoaming agent in the food industry (e.g. in the manufacture of decaffeinated coffee and tea) [14].

It is important to emphasise synthetic amorphous silica should be distinguished from crystalline silica. Crystalline silica (or quartz) has been classified as a class 1 carcinogen by IARC [206]. Amorphous silica has been in use since the 1920's and some studies report amorphous silica to be relatively inert or benign.

Animal (mouse model) data shows treatment with low doses (20-80mg/kg) produces no observed effects on animal health and with the LD_{50} in this model reported to be greater than 1000mg/kg [207]. High doses have been reported to induce inflammation, cytotoxicity and tissue damage in the lungs [208]. However other *in vivo* data shows a dose and time dependent inflammatory response (neutrophilic inflammation and macrophage accumulation) to intratracheally instilled 14nm silica NM at concentrations of 0.3-100µg/mouse measured 3 days after exposure. A recent *in vitro* study reports that amorphous silica NMs (15 and 46nm) have a greater effect on A549 cells (measured as ROS generation) than a 5µm crystalline silica particle [208]. Overall in vivo studies show SNP cause reversible lung inflammation, (granuloma formation) that does not progress to cause lung fibrosis and most of the *in vitro* studies report results of size and dose-dependent cytotoxicity as well as increased reactive oxygen species levels [209].

Given the quantities in which silica NMs are produced, the limited (or incomplete) data available on the adverse health effects, coupled with the growing number of applications in the healthcare and food industries more scrutiny and critical analysis of the existing data is warranted. Ideally all toxicological data/publications should also include detailed characterisation of the physical chemical properties of the material [210].

Although uptake mechanisms were not under investigation in this study it is important to note that a range of uptake behaviours have been reported for NMs (including silica NMs (SiO_2 NMs)) as mentioned in 1.2.1. SiO_2 NMs (which agglomerated to size of 5 µm in diameter in cell culture media) have been shown to enter the cytoplasm of cells (A549 cells) [19]. Silica NMs less than 100 nm in size have been found to induce endocytosis-dependent ROS (HaCaT cells), while conversely the affinity of silica NMs for the cells lipid bilayer allows the potential for passive uptake in vesicles [211]. Of course the corona that forms on their

surface once in contact with biological fluids is one factor that can effect these interactions and Lesniak *et al.* [150] found that silica NMs exposed to cells (HeLa; hCMEC/D3 and A549) in the absence of serum have a stronger adhesion to the cell membrane than those in medium with serum. These different exposure conditions were found to affect both the rate of uptake and the intracellular location of the silica NMs.

The same experimental design used previously for iron oxide NMs (outlined in Chapter 3) was employed in order to investigate the corona composition of SiO_2 NMs in FCS (as used for *in vitro* cell culture) and in human blood plasma. Inhalation as a route of exposure was again of particular interest in this study and so in order to simulate exposure via inhalation followed by translocation to blood a protein corona first in LLF then in serum or plasma was prepared. This study therefore expands on the previous work with iron oxides not only by allowing direct comparison of two NM types but also by investigating the effect of size and surface modification on the corona development. Comparison of serum and plasma corona in this way and investigation of its cytoxicity can help with *in vitro*/*in vivo* cytotoxic comparisons.

4.1.3 Chapter 4 Aims

- To prepare silica NMs with a hard plasma, serum and LLF corona, and to use protein characterization techniques to investigate protein binding.

- Examine how particle size, composition and charge influence the affinity and degree of protein binding.

- Investigate the role the protein-particle interaction has in influencing toxicity of the NMs by investigating the effects of NM-protein exposure on J774.A1 macrophage cell line with respect to LDH release and cytokine release and compare these results to those results already obtained for Fe_2O_3 and Fe_3O_4 particles and nanoparticles.

4.2 Materials and Methods:

4.2.1 Materials

Silica nonporous particles (Kisker, Germany) were obtained in two sizes (200nm, 50nm) and had either an unmodified surface (neutral) or animated (positive) surface and a density of 2.6g/$cm^{3.}$ They were provided dispersed in deionised water. The NH_2 modified particles were further NH_2 modified after zeta potential experiments revealed the particles were not strongly positive. Surface modification of silica NMs involved the addition of aminopropyltrimethoxysilane (APTMS) to a concentration of 10mg/ml NMs. The pH was adjusted to pH5 with acetic acid and the mixture was stirred for 4 hours at 400rpm. Finally the particles were purified from excess APTMS by centrifugation and re-suspension in ethanol and water. The particles were then diluted in filtered sterile MilliQ water to 1mg/ml. Silica NMs were diluted as required in either sterile deionised water or filtered sterile PBS or RPMI before analysis. Before exposure each sample was sonicated at 200W for five minutes using a bath sonicator (Grattan).

4.2.2 Cell Culture and Treatments

The adherent mouse macrophage cell line J774.A1 was used as a model system and was routinely cultured as described in 3.2.2. J774.A1 macrophages were treated with the NMs in RPMI at concentrations ranging from 0.9µg/ml to 200µg/ml (corresponding to 2.4 and 125µg/cm^2 respectively). The LDH and WST-1 assay were carried out as described in 3.2.7. Briefly for the WST-1 assay, after incubation the supernatant from each well was removed and replaced with culture medium containing WST-1 in a 1:10 ratio. The plates were incubated for 4 hours at 37°C. Before reading, the plates were centrifuged at 250g for 3 minutes, the supernatants were removed and transferred to a new 96 well plate and read using a multiwall plate reader at a wavelength of 450nm. Data was expressed as the percentage viability of treated cells compared with the medium only control.

For the LDH assay 0.75 mM aqueous sodium pyruvate (containing NADH 1mg/ml) was pipetted into each well of a 96 well plate and incubated at 37°C for 5 minutes. A volume of 10µl of cell supernatants were added to the wells in triplicate and mixed on a plate shaker. The plates were incubated for 30 minutes at 37°C. Fifty microlitres of 2,4-dinitrophenylhydrazine (dissolved in 1M HCL) was added to each well and incubated at room temperature for 20 minutes. Fifty microlitres of 4 M NaOH was added to each well, mixed and allowed to stand for 5 minutes. The absorbance was read at 540nm as described in 3.2.7. The LDH content of the supernatants was expressed as a percentage of the 100% lysis.

4.2.3 Preparation of Hard Corona Coated Nanomaterial

The NMs were mixed in low protein binding eppendorf tubes with plasma, serum or LLF as described in order to prepare the hard corona as described in 3.2.4.

4.2.4 Characterisation of Nanomaterial-Protein Complex

Characterisation of the particles alone included (as described in 3.2.5) size analysis measurements (DLS) and charge/stability using ZP. Image analysis (SEM) was also carried out and previously reported by Brown et al (in publication). DLS measurements were used initially to study the hydrodynamic diameter and zeta potential to get an indication of size and stability of the particles in water and in PBS. Particles were then remeasured once coated (see 3.2.4) in proteins (10% plasma, 55% plasma, 10% serum, LLF, precoated in LLF and then in 10% plasma, 55% plasma or 10% serum). The difference between the results gives information on corona layer thickness and in this way the DLS was used to determine the thickness of an adsorbed layer. Pdi was also measured to access particle aggregation/flocculation behaviour. An increase in Pdi represents an increase in agglomeration. The NM stability and charge in water and PBS was determined using ZP measurements (Malvern Zetasizer Nano) as described previously in 2.2.4. Protein separation and identification of the hard corona was carried out using SDS-PAGE and MS as described in 3.2.6.

4.2.5 Cytokine Estimations using FACS Array Analysis

Supernatants obtained during LDH assays were used to estimate the release of the following cytokines from treated cells; IL-1β, TNF-α, IL-10 and MCP-1. Analysis was carried out on a BD FACS Array™ Bioanalyzer, using a BD cytometric Bead array mouse/rat soluble protein master buffer kit as per manufactures instructions.

4.2.6 Statistical Analysis

Data from all experiments were analysed using the Minitab 15 statistical package using a general linear model analysis of variance. Significance was set at 5%.

4.3 Results

4.3.1 DLS Characterisation

Table 4.1 Hydrodynamic diameter, polydispersity index (Pdi) and zeta potential for SiO_2 200nm and 50nm particles measured in water, PBS and with their associated long lived protein corona (where P=plasma, and S=serum and LLF= lung lining fluid) as determined by DLS. Values represent the mean ± SEM (n=3).

SiO_2 200nm	Z average (nm)	St Dev.(nm)	Pdi	ZP (pH 7.5) mV
Water	174.40	1.58	0.06	(-)25.0
PBS	186.60	2.73	0.08	(-)23.2
10%P	211.60	3.23	0.24	(-)12.0
55%P	272.80	7.37	0.31	(-)9.8
10%S	207.70	4.30	0.12	(-)10.4
LLF	>1302.00	93.80	0.50	(-)13.4
LLF/10%P	267.40	5.77	0.28	n/a
LLF/55%P	236.10	8.84	0.22	n/a
LLF/10%S	261.40	8.58	0.46	n/a

SiO_2 50nm	Z average (nm)	St Dev. (nm)	Pdi	ZP (pH7.5) mV
Water	54.16	0.06	0.12	(-)21.00
PBS	64.08	0.99	0.16	(-)23.90
10%P	109.80	3.55	0.27	(-)11.10
55%P	116.40	1.75	0.42	(-)11.20
10%S	122.70	0.08	0.29	-12.40
LLF	1142.00	101.00	0.32	-8.02
LLF/10%P	209.50	5.16	0.41	n/a
LLF/55%P	203.60	2.92	0.36	n/a
LLF/10%S	464.70	38.80	0.43	n/a

Table 4.2 Hydrodynamic diameter, Pdi and zeta potential for NH_2 modified SiO_2 200nm and 50nm particles measured in water, PBS and with their associated long lived protein corona as determined (where P=plasma, and S=serum and LLF= lung lining fluid) by DLS Values represent the mean ± SEM (n=3).

SiO_2 NH_2 200nm	**Z average (nm)**	**St Dev. (nm)**	**Pdi**	**ZP (pH 7.5) mV**
Water	239.20	4.05	0.04	38.20
PBS	262.40	3.16	0.07	(-)1.20
10%P	313.40	5.30	0.25	(-)10.70
55%P	396.90	7.54	0.31	(-)10.30
10S%	241.10	5.60	0.19	(-)12.30
LLF	2256.00	55.15	1.00	(-)23.80
LLF/10%P	270.00	2.19	0.34	n/a
LLF/55%P	278.30	17.38	0.36	n/a
LLF/10%S	306.40	5.60	0.31	n/a

SiO_2 NH_2 50nm	**Z average (nm)**	**St Dev.**	**Pdi**	**ZP (pH 7.5) mV**
Water	145.50	1.71	0.20	30.00
PBS	159.00	0.10	0.23	0.04
10%P	302.10	1.78	0.35	(-)8.13
55%P	223.00	7.60	0.24	(-)8.66
10%S	362.60	12.20	0.30	(-)9.67
LLF	546.90	11.11	0.45	2.71
LLF/10%P	935.00	17.88	0.31	n/a
LLF/55%P	646.00	19.46	0.40	n/a
LLF/10%S	>1000	58.50	0.31	n/.a

The particles were characterised before and after addition of their protein corona. The hydrodynamic diameter measurements were determined by DLS and are listed in table 4.1. It can be seen that both the 200nm and the 50nm particles dispersed in water had a size similar to that reported by the manufacturers. The SiO_2 200nm and 50nm and the SiO_2 NH_2 200nm **w**ere all found to have a very low Pdi value in both water and PBS suggesting they were not agglomerated or

stable. However the SiO_2 NH_2 50nm particles appeared to agglomerate more than the non amino modified particles and when dispersed in water were found to be 145.5nm. They were also found to agglomerate in PBS with a hydrodynamic diameter of 159nm. The DLS results show that all particles with their associated hard corona show an increase in the hydrodynamic diameter. For all particles this was seen most markedly in the LLF corona where the hydrodynamic diameter was the largest. For all the particles (expect the 200nm NH_2 silica particles) the hydrodynamic diameter of the particles were smaller than those pre-incubated in LLF and then in plasma or serum. The ZP measurements show all particles are more stable or less agglomerated in water and PBS without their corona. The measured ZP values showed the difference in surface chemistry between the two types of particles. The ZP of both the 200 and 50nm NH_2 modified particles were positive but it is interesting to note that the ZP of the amino modified NMs in PBS or with their associated corona was lower than that of the particles in water alone.

4.3.2 Hard Corona Analysis

(a)

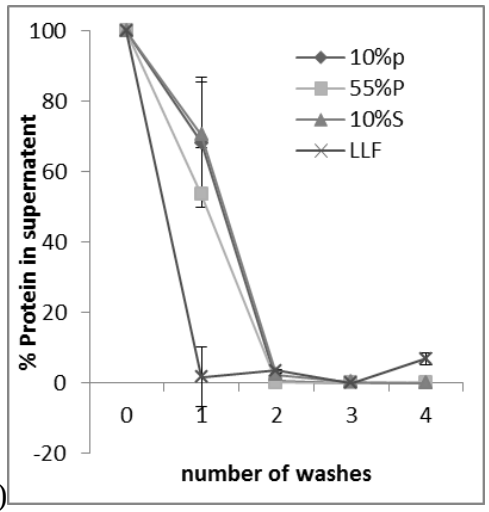

(b)

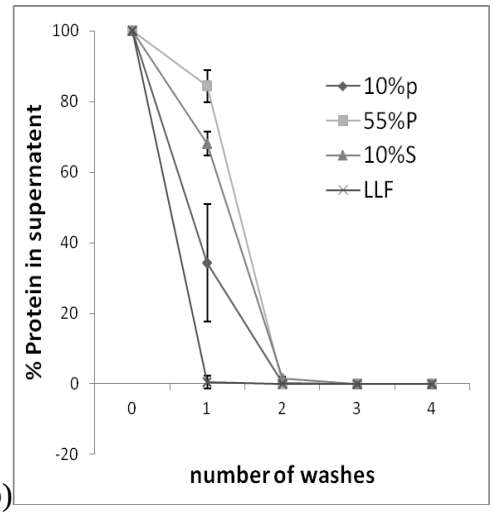

(c) 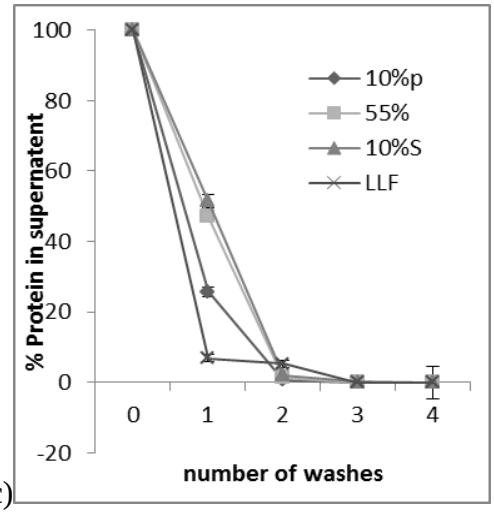

(d) 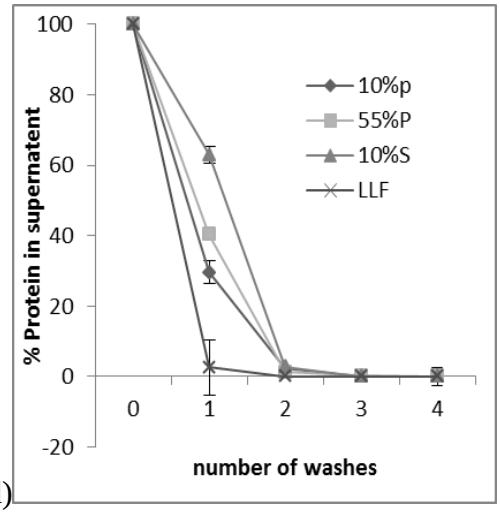

Figure 4.1: The above graphs show the percentage of free protein remaining in the (a) SiO_2 200nm particle supernatant, (b) SiO_2 50nm NM supernatant, (c) SiO_2-NH_2 200nm particles and (d) SiO_2-NH_2 50nm particle supernatant after 1-4 washes. Protein was determined by the BCA assay in each wash step, as measured during hard corona preparation. Values represent the mean +/- SD (n=3). As can be seen after 4 washes no free protein was detectable in the supernatant for most samples. It was therefore concluded that any proteins remaining in the system were associated with the iron particles and not free in solution. These remaining proteins attached to the particles were what formed the hard corona

4.3.3 SDS PAGE Investigation of Protein Corona Profile

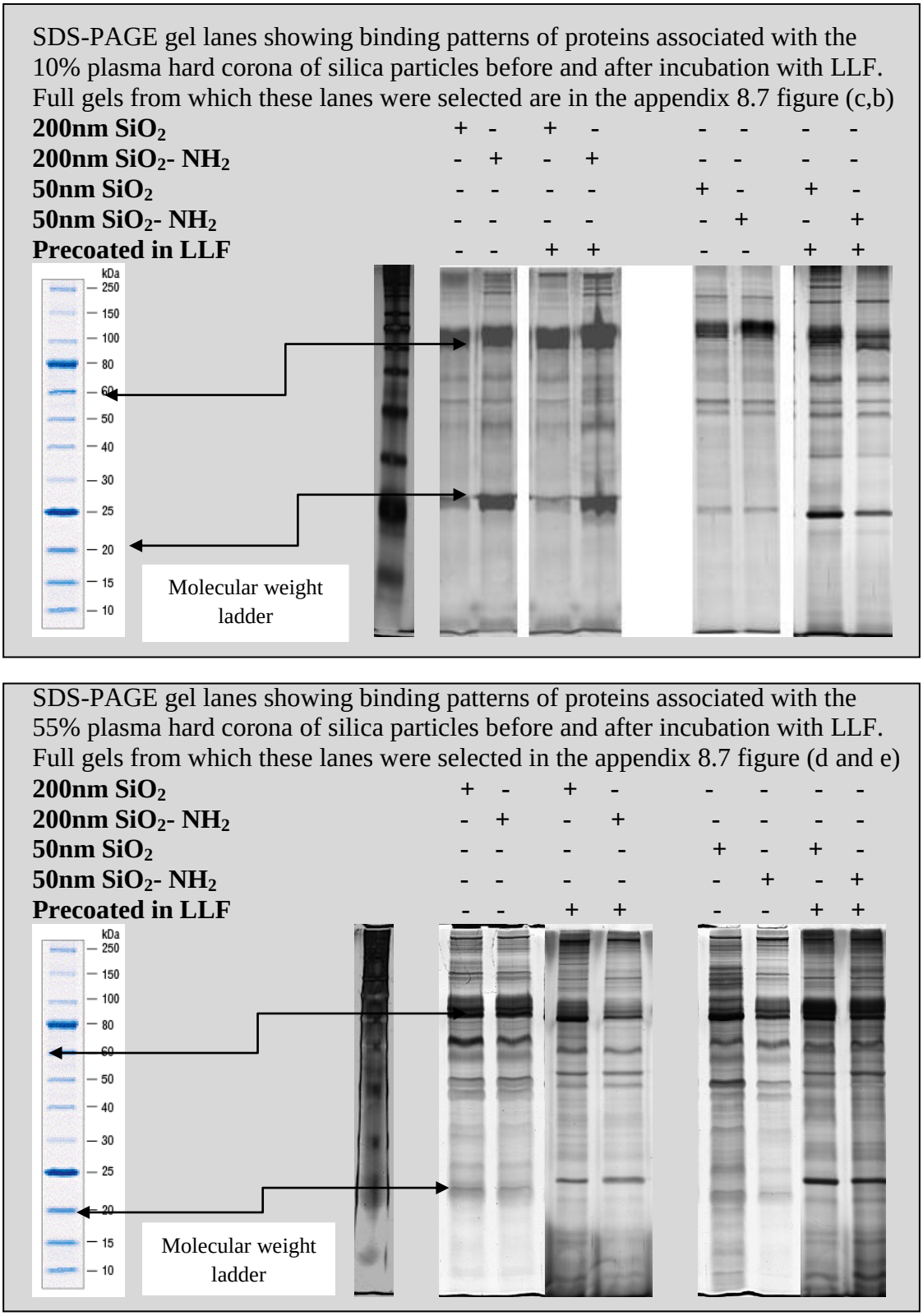

Figure 4.2: SDS-PAGE gels obtained to investigate the binding patterns of silica particle-protein interactions (a) 10%P and LLF/10%P hard corona (b) 55%P and LLF/55%P hard corona.

SDS gel lanes showing binding patterns of proteins associated with the 10% serum hard corona of silica particles before and after incubation with LLF. The full gels from which these lane images were taken can be seen in the appendix(8.7 (f) and (g))

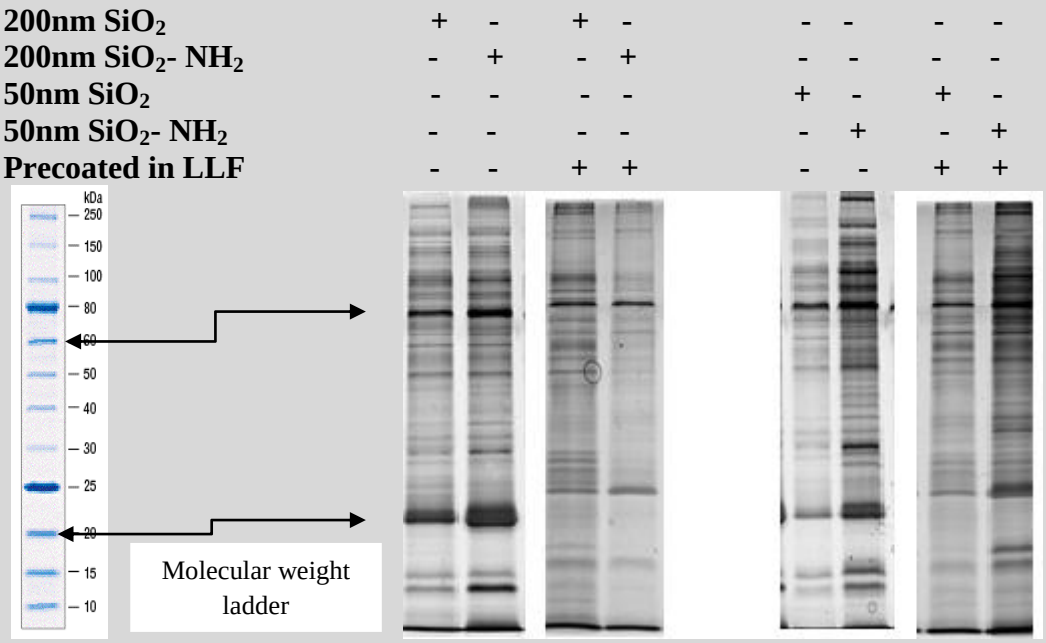

Figure 4.3: SD-PAGE gel lanes obtained to investigate the binding patterns of silica particle-protein interactions associated with the 10% serum hard corona and before and after pre coating in LLF (10%S and LLF/10%S).

Figure 4.2 and 4.3 show the SDS-Page protein profile of each corona and demonstrates interesting differences in the protein binding patterns not only in different concentrations of the same biological fluid (i.e. 10% and 55% plasma) but also between plasma and serum. The most common bands across all silica particle types and biological fluids were observed at 60kDa and 20kDa. The charge of the particle charge did not appear to affect the protein profile of the plasma corona however the SDS-PAGE gels do reveal a difference in the binding patterns of the 50nm plain and amino modified particles in the serum corona. The binding patterns do seem to alter depending on particle size (200nm or 50nm) most notably with the 10% plasma corona and to a lesser degree for the 55% plasma corona and the 10% serum corona. When the particles were pre-coated with LLF and then in plasma the binding pattern remained similar in that both

concentrations, however the intensity of these binding patterns are higher. In particular there is a 20kDa band which shows a stronger intensity after preincubation with LLF. This was seen predominately for the 10% and 55% plasma corona.

Table 4.3: Proteins of the 200nm silica plasma hard corona (before (a) and after (b) precoating in LLF) as identified by MS- the full list of all proteins identified can be found in the supporting information (appendix 8.8)

Table 4.3 **(a)**

SiO_2 (200nm1 10%P)	**MW**	**Acc No**	**XC Score**	**% C**	**PEP**	**Pep. Ion (Hit)**	**Function as defined by Uniprot**
Apolipoprotein B-100	515.28	P04114	480.32	16.31	2.55 E-14	48	Recognition signal for the cellular binding and internalization of LDL particles by the apoB/E receptor.
Complement C3	187.03	P01024	398.30	35.30	9.99 E-15	43	C3 plays a central role in the activation of the complement system.
Histidine-rich glycoprotein	59.54	P04196	160.31	37.71	6.66 E-11	58	Binds a number of ligands (heme, heparin, heparin and plasminogen). Implicated in regulating immune complex, pathogen clearance, cell adhesion, angiogenesis, coagulation and fibrinolysis. Mediates clearance of necrotic cells through enhancing the phagocytosis of necrotic cells.
Complement C4-A	192.65	P0C0L4	130.29	12.44	8.61 E-12	13	C4 plays a central role in the activation of the classical pathway of the complement system..
Serum albumin	69.32	P02768	110.28	21.51	6.44E-09	12	Good binding capacity for water, Ca^{2+}, Na^{+}, K^{+}, fatty acids, hormones, bilirubin and drugs. Main function is regulation of osmotic pressure of blood. Major zinc transporter in plasma, typically binds about 80% of all plasma zinc.

Table 4.3 (b)

SiO_2 (200nm) LLF/10%P	**MW**	**Acc No**	**XC Score**	**% C**	**PEP**	**Pep Ion (Hits)**	**Function as defined by Uniprot**
Apolipoprote-in B-100	515.28	P04114	590.31	21.60	1.00E-30	59	As above (table 4.3(a))
Complement C3	187.03	P01024	300.31	28.40	5.55E-15	30	As above (table 4.3(a))
Serum albumin	69.32	P02768	200.32	46.10	8.88E-15	21	As above (table 4.3(a))
Histidine-rich glycoprotein	59.54	P04196	100.28	26.30	1.69E-11	11	As above (table 4.3(a))
Hemoglobin subunit beta	15.99	P68871	70.21	44.90	7.97E-12	7	Involved in oxygen transport from the lung to the various peripheral tissues.

Table 4.3 reports the protein identified in (a) SiO_2 200nm10%P corona and (b) *the SiO_2 200nm LLF/10%P* corona *by Mass Spectroscopy (LTQ ESI MS/MS along with the reported molecular weight (MW-kDa). The table reports the Accession number (Acc No) is a unique identifier given to a protein sequence (refers to entries at the Sequest Uniprot/Swiss-Prot database* (http://www.uniprot.org/*)). The Xcorr value (XC Score) is the cross-correlation value from the search. The posterior error probability (PEP) or is the probability that the observed peptide match is incorrect (a chance event). The percentage sequence coverage (%C) and the number of peptides confirmed by mass spec analysis are shown.*

Table 4.4: Tables show the most prevalent proteins in the 200nm silica particle serum hard corona profile (before (a) and after (b) incubation with LLF), as identified by MS. The full list of all proteins identified can be found in the supporting information (appendix 8.8).

Table 4.4(a)

SiO_2 (200nm) 10%S Corona	**MW**	**Acc No**	**XC Score**	**PEP**	**%C**	**Pep Ion (Hits)**	**Function as defined by Uniprot**
Serum albumin	69.32	P02768	60.21	8.79 E-10	12.32	8	As above (table 4.3(a))
Apolipoprotein B-100	515.28	P04114	30.18	2.29 E-06	0.88	3	As above (table 4.3(a))
Apolipoprotein A-I	30.76	P02647	30.17	2.45 E-08	11.24	3	As above (table 4.3(a))
Heat shock protein HSP 90-alpha	84.60	P07900	28.25	3.12 E-10	5.74	3	Molecular chaperone that promotes the maturation, structural maintenance and proper regulation of specific target proteins involved for instance in cell cycle control and signal transduction.
Thrombospondin-4	105.80	P35443	20.25	1.29 E-07	3.54	2	Adhesive glycoprotein that mediates cell-to-cell and cell-to-matrix interactions.

Table 4.4(b)

SiO_2 (200nm) LLF/10%S Corona	MW	Acc No	XC Score	PEP	%C	Pep Ion (Hits)	Function as defined by Uniprot
Serum albumin	69.32	P02768	90.29	1.14 E-10	22.20	12	As above (table 4.3(a))
Thrombospondin-1	129.30	P07996	20.25	6.00 E-14	3.10	2	Adhesive glycoprotein that mediates cell-to-cell and cell-to-matrix interactions.
Hemoglobin subunit alpha	15.245	P69905	20.22	4.70 E-11	21.80	2	As Above (table 4.3(a))
Apolipoprotein A-I	30.76	P02647	20.19	4.77 E-06	11.20	2	As Above (table 4.3(a))
Complement C3	187.03	P01024	20.17	2.78 E-08	2.50	2	As Above ((table 4.3(a))

Table 4.4 reports the protein identified in (a) the SiO_2 200nm 10%S corona and (b) the SiO_2 200nm LLF/10%S corona by Mass Spectroscopy (LTQ ESI MS/MS along with the reported molecular weight (MW-kDa). The table reports the Accession number (Acc No). The Xcorr value (XC Score) (PEP) the probability that the observed peptide match is incorrect (a chance event). The percentage sequence coverage (%C) and the number of peptide Ions as previously described.

For all particles there were five main bands derived from the 10% plasma corona. The strongest band was seen in the 60kDa range. MS results suggest these are serum albumin and histidine rich glycoprotein. For the two weaker bands at 50-40kDa range, MS suggests these are apolipoprotein A4, actin and Ig mu chain proteins., A band at 30kDa also exists which MS suggests is apolipoprotein A-1 and a strong band at 20kDa which was not identified by Mass Spectroscopy. As can be seen from figure 4.2 the 10% plasma corona for all particle types varies a lot from the 55% plasma corona where there is stronger band intensity at the 50kDa range and more bands in the higher kDa (100-250) range, in particular the 20kDa band for all particle types is not as strong as with the 10% plasma corona

suggesting less proteins are bound to the particles in this region at this plasma concentration. For all particles this 20kDa band is much stronger in all particle types after pre-incubation in LLF.

Observation of the binding patterns of the serum corona for the 4 particle types shows there are far lower molecular weight proteins compared to the plasma corona. The 50nm SiO_2 (both plain and amino modified) particles in their serum corona both bind far more proteins (as indicated by quantity of bands) than their 200nm counterparts. This intensity is stronger still after precoating in LLF. However the intensity of the bands in the serum corona overall are not as strong as those obtained for the plasma corona gels and MS results identified far less proteins in the serum corona of the 200nm SiO_2 plain NM than the plasma corona as can be seen in table 4.3 and 4.4)

Mass spectroscopy results of the 10% plasma corona and the precoated in LLF 10% plasma corona of the 200nm SiO_2 particles show that both coronas have similar profiles made up of four main proteins. These proteins were apolipoprotein B-100, complement C3 and C4-A, histidine rich glycoprotein and serum albumin. The abundance of these proteins varies before and after precoating in LLF. The 10% plasma corona found an order of: apolipoprotein B-100 > complement C3 > histidine rich glycoprotein > complement C4-A > serum albumin. Whereas the 10% plasma corona after precoating in LLF showed a slightly different order; apolipoprotein B-100 > complement > serum albumin> histidine rich glycoprotein, complement 4-A was not observed in this protein corona make up. There was a larger diversity of proteins identified by MS in the hard corona of the precoated SiO_2 200nm particles (both serum and plasma) than the uncoated particles. The differences in the corona profile based on particle characteristics have also been reported in our previous study for iron oxide NMs.

4.3.4. Cytotoxicity Results

4.3.4.1 WST-1

(a) (b)

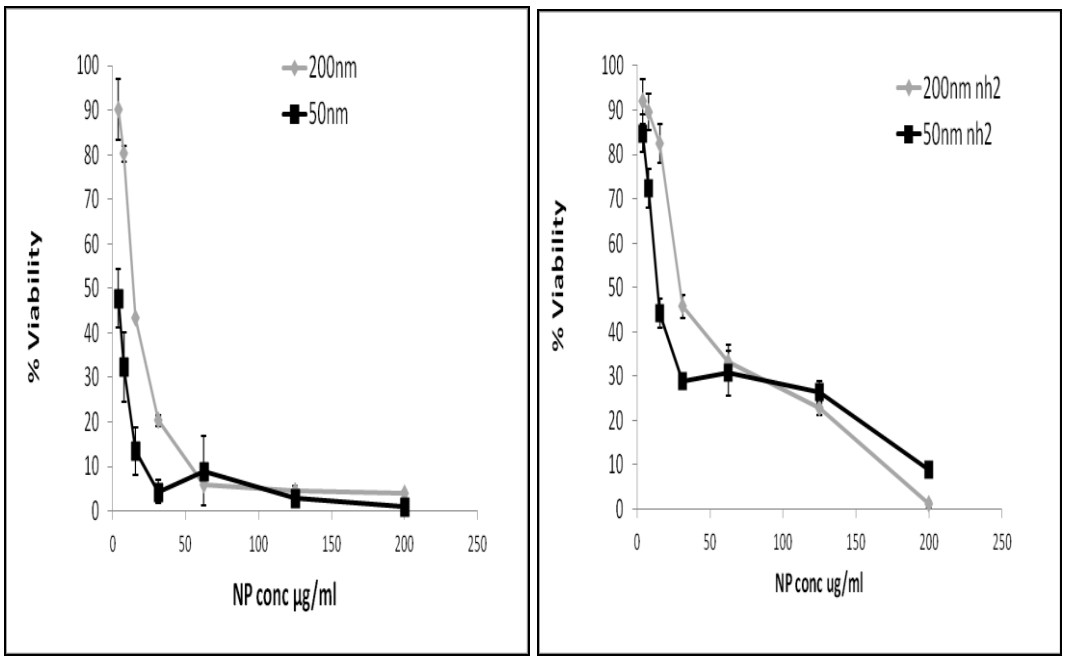

Figure 4.4: WST-1 assay. Percent viability of J774.A1 cells after exposure to silica NM (a 200 and 50nm and (b) NH_2 modified 200nm and 50nm, after 24 hours exposure (n=3). Data is expressed as the % mean ± SEM. The WST-1 assay revealed no significant difference between the 200nm $Si0_2NH_2$ and the 50nm $Si0_2NH_2$ NMs to impact mitochondrial function. The 200nm and 50nm SiO_2 particles were significantly different only at the lowest concentrations of 3.9µg/ml and 7.8µg/ml ($P<0.001$).

4.3.4.2 LDH Assay

(a) (b)

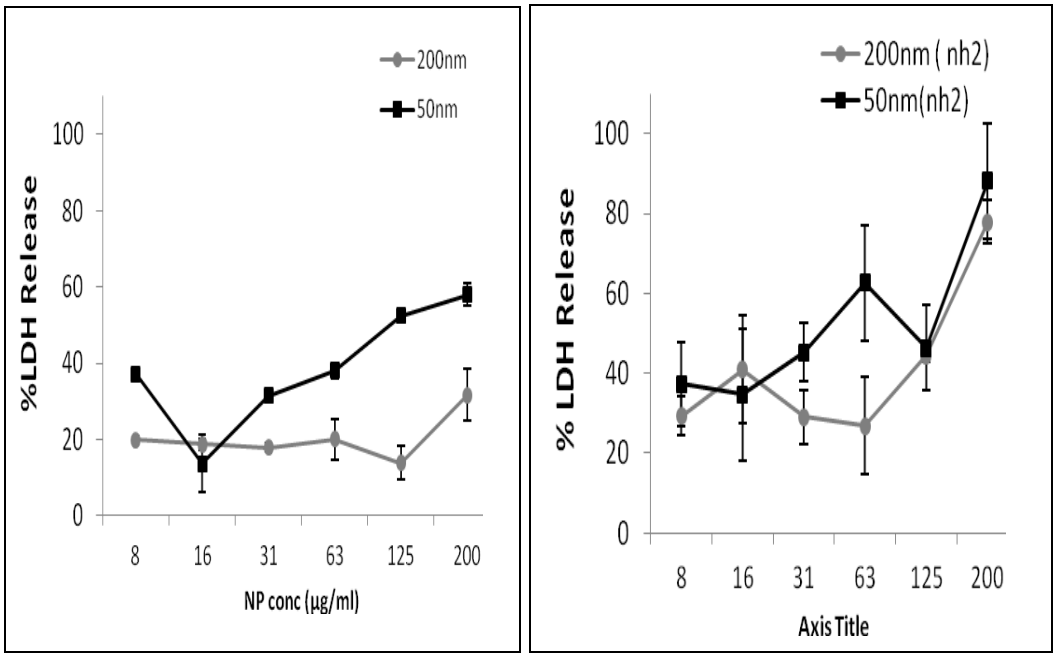

Figure 4.5: Percentage LDH release (expressed as % of positive control) in J774.A1 cells after exposure to (a) 200 and 50 nm SiO_2 particles and (b) $Si0_2NH_2$ after 24 hours exposure. (n=3, data is expressed as the % mean ±SEM).

The LDH assay shows all particles at all concentrations a significant increase in LDH release from J774.A1 cells compared to control cells with no treatment after 24 hour exposure. No dose response effect was found (general linear model ANOVA) for the 200nm SiO_2 or for the 50nm SiO_2-NH_2 particles. LDH release from cells treated with the 50nm SiO_2 at 200µg/ml was significantly greater compared to lower concentrations (31.25µg/ml ($P<0.05$), 15.62µg/ml ($P<0.001$) and 7.8µg/ml ($P<0.05$)). Analysis of LDH release following exposure to the 200nm SiO_2 NH_2 particles found a significantly greater LDH release for the 200µg/ml compared to the cells treated with 125µg/ml-7.8µg/ml ($P<0.001$). No other dose dependent effects were found.

4.3.5 Impact of Corona on Cytotoxicity

(a) 200nm SiO_2 (b) 50nm SiO_2

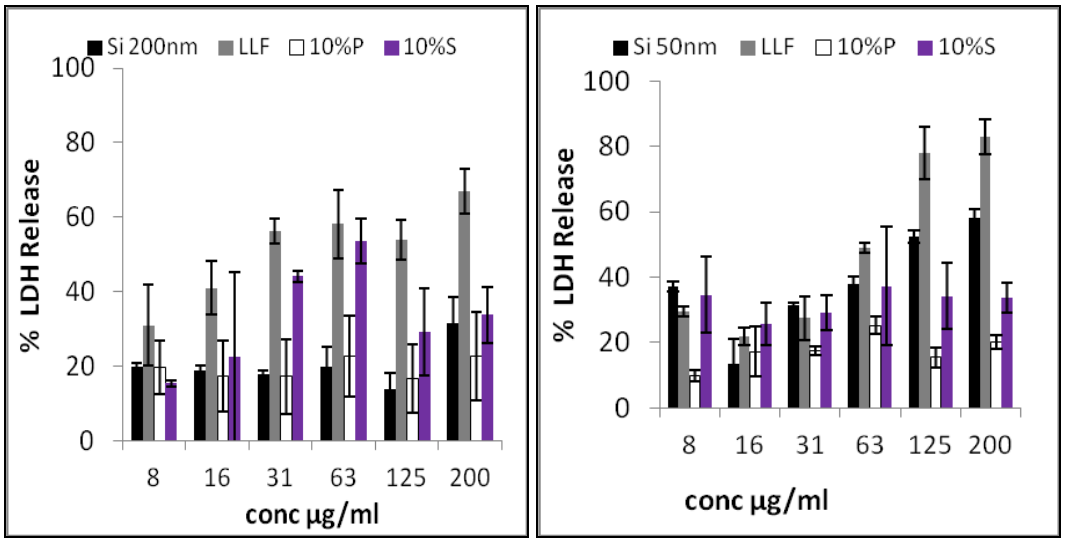

(c) 200nm SiO_2 (NH_2) (d) 50nm SiO_2 (NH_2)

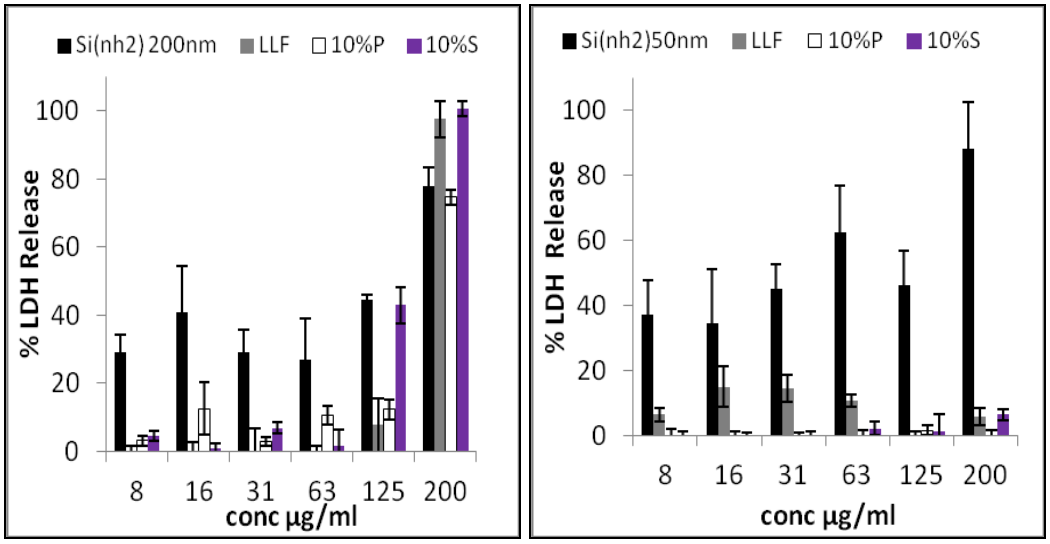

Figure 4.6: Percentage (of positive control) of LDH release from J774.A1 cells after exposure to SMN with associated corona in (a) 200nm and (b) 50nm. (c) 200nm amino modified and (d) 50nm amino modified (n=3, data is expressed as the % mean ±SEM).

ANOVA (general linear model) indicates there was no significant difference in the percentage LDH release after exposure of J774.A1 cells to 200nm SiO_2 particles and the percentage LDH release from exposure to the SiO_2 particles with a plasma (P=0.215) and serum (p=0.7780) corona after 24 hours. However there was a significant difference between the 200nm SiO_2 particles and the 200nm SiO_2 particles with a LLF corona (P<0.01) suggesting these particles with their LLF corona are more toxic than the naked particles. The 200nm SiO_2 particles with a plasma corona appear to be less cytotoxic than the particles with a serum (P<0.05) or LLF (P<0.001) corona.

There was a significant difference between the LDH release after exposure to 50nm SiO_2 particles and those with a plasma corona (P<0.001) indicating the 50nm particles were more cytotoxic. There was also a significant difference between LDH release seen after exposure to the 50nm SiO_2 particles in a plasma and a LLF corona (P<0.001) indicating the particles in a LLF corona was more cytotoxic than the particles in a plasma corona. There was no significant difference in the LDH release from the 50nm SiO_2 particles in a LLF corona (P=0.3107) and a serum corona (P=0.695).

Statistical analysis of the data also shows the only significant difference observed after exposure to 200nm SiO_2 NH_2 was between the naked particles and the particles in a LLF corona (P<0.01) the naked particles being the more toxic in the J774.A1 cell line. However after exposure to the 50nm SiO_2NH_2 NMs the naked particles were significantly more toxic to the J774.A1 cells than any other treatment (10%P, 10%S and LLF) (P<0.001). A significant difference was also found between these particles in a plasma and LLF corona (P<.001) and these particles with a serum and LLF corona (P<0.001).in both cases the particles in their LLF being more cytotoxic than the particles in their serum or plasma corona.

4.3.6 Cytokine Analysis

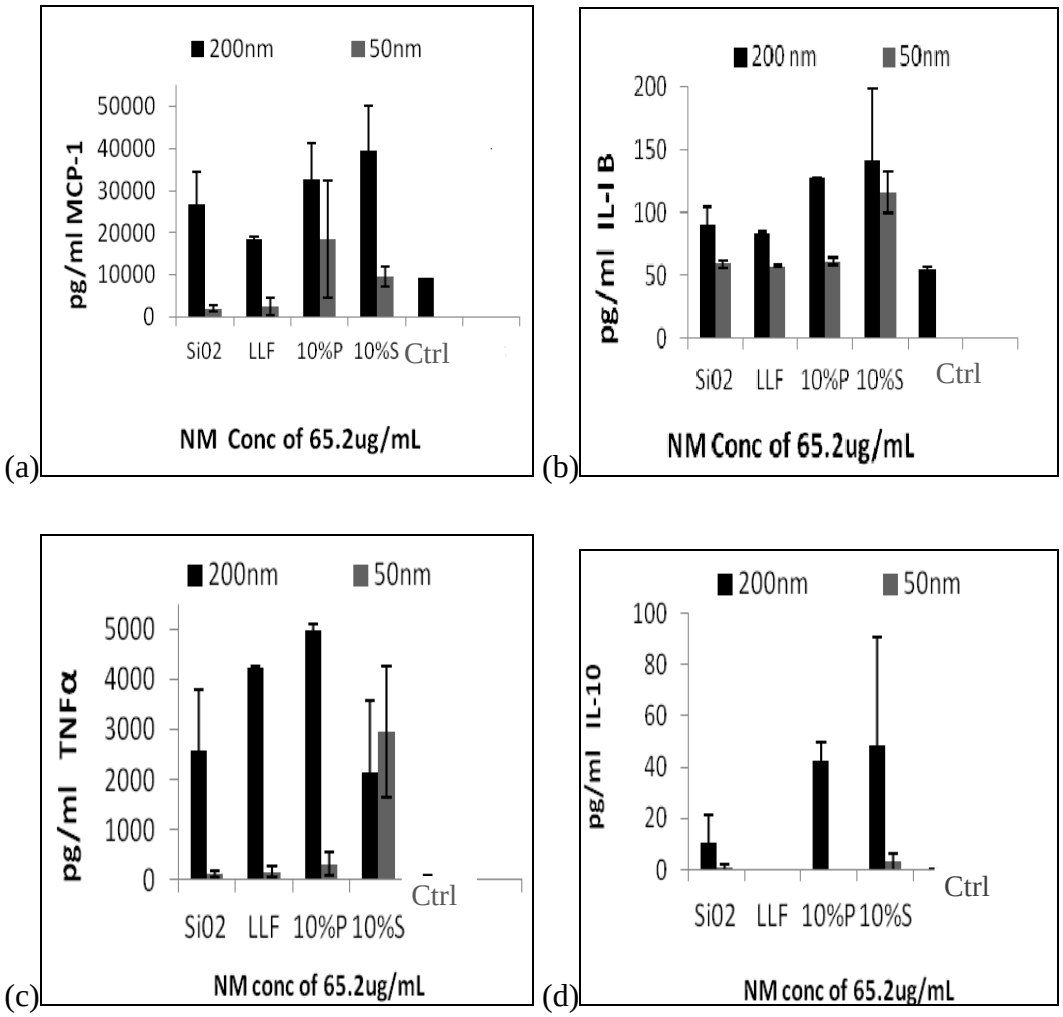

	Silica 200nm no corona	Silica 200nm LLF	Silica 200nm 10%P	Silica 200nm 10%S	Silica 50nm no corona	Silica 50nm LLF	Silica 50nm 10%P	Silica 50nm 10%S
MCP-1,	✔	✔	✔	✔				
IL-1β,	✔	✔	✔	✔				✔
TNF-α	✔	✔	✔	✔				✔
IL-10	✔		✔					

Figure 4.7: Cytokine profile measured from J774.A1 cells exposed to silica NMs with and without associated LLF, plasma and serum corona at 65.2µg/ml (a) MCP-1 (b) IL-1β (c) TNF-α and (d) IL-10. Data expressed as a mean ± SEM, n = 3. The table underneath denotes the treatments were the cytokine levels were greater than the negative control.

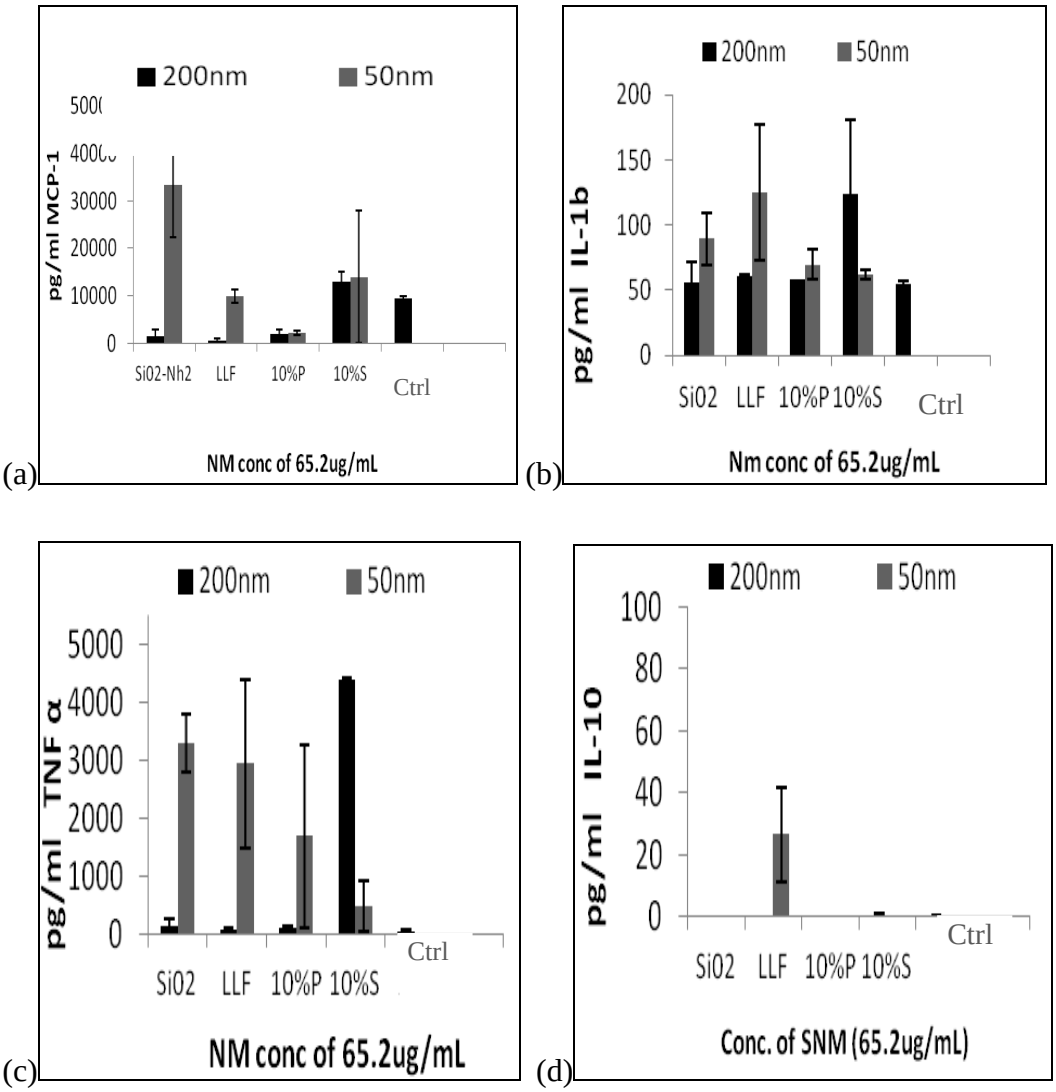

	SiO_2NH_2 200nm no corona	SiO_2NH_2 200nm LLF	SiO_2NH_2 200nm 10%P	SiO_2NH_2 200nm 10%S	SiO_2NH_2 50nm no corona	SiO_2NH_2 50nm LLF	SiO_2NH_2 50nm 10%P	SiO_2NH_2 50nm 10%S
MCP-1,					✔			
IL-1β,								
TNF-α				✔	✔	✔	✔	✔
IL-10						✔		

Figure 4.8: Cytokine profile measured from J774.A1 cells exposed to amino modified silica NMs with and without their associated LLF, plasma and serum corona where (a) MCP-1 (b) IL-1β (c) TNF-α and (d) IL-10. Data expressed as mean ± SEM, n = 3. The table underneath denotes the treatments were the cytokine levels were significantly greater than the control.

4.4 Discussion

This study investigated the effects of silica particles and NMs and their associated protein corona on a macrophage murine cell line in relation to their cytotoxicity. It was reported in Chapter 3 that the cytotoxicity of iron oxide particles was influenced by the presence of a protein corona. That study did not address if the charge or size of the NM influenced the profile of the protein corona and thus this study expands further to investigating silica NMs of two sizes (200nm and 50nm) which were either neutral or positively charged by amino modification. Following the same experimental set up as in Chapter 3 (to investigate the particles with plasma, serum and LLF) a 10% and 55% plasma and a 10% serum concentration was used to prepare the corona. This was chosen to best compare an *in vivo* and *in vitro* exposure. Just as in Chapter 3 the corona of NMs first preincubated in LLF and then incubated in either plasma or serum was also prepared and investigated.

In order to investigate the impact of the protein corona on the particles properties, the particles were characterised before and after protein coating. The hydrodynamic diameter measurements as determined by DLS found that both the 200nm and the 50nm particles dispersed in water had a size similar to that reported by the manufacturers. There was a slight increase in hydrodynamic size in PBS (of 12 and 10nm respectively for the plain particles; 23nm and14nm for the amino modified silica particles). This was different from what was observed with the iron oxide particles where DLS data suggests the iron oxide particles agglomerated more in PBS than was seen for the silica particles. The silica particles were found to have a very low Pdi value in both water and PBS. The amino modified 50nm silica NMs appeared to agglomerate more than the non amino modified particles and when dispersed in water were found to be 145.5nm with a Pdi of 0.2. They were also found to agglomerate in PBS with a hydrodynamic diameter of 159nm, the Pdi was 0.23. Once the particles were analysed with their associated hard corona a large increase in the hydrodynamic diameter was observed. The particles appeared to agglomerate when incubated with LLF, as indicated by the high Pdi value. Previous studies [168] have shown that LLF modifies the surface chemistry of particles promoting enhanced

agglomeration and this work appears to support this. The hydrodynamic diameter of the particles in a plasma and serum corona are smaller than those pre-incubated in LLF and then in plasma and serum corona. It may be the case that the LLF caused particle agglomeration which results in a larger hydrodynamic diameters however the Pdi of the particles dispersed with a plasma and serum corona before and after LLF coating remained somewhat stable (0.1 - 0.4). This suggests that the particles with their associated LLF corona in some way allows for more biological molecules from serum and plasma to bind to the NM. The SDS-PAGE gels showing the plain silica NM with their associated hard corona appear to verify this, showing that there is more protein bands present in the samples after preincubation with LLF. This increase in particles size observed in LLF and in LLF with serum or plasma corona which was observed for all but one particle treatment. The 200nm NH_2 silica particles with its 10% P coating was 313.4nm and after LLF preincubation was 270nm.

The NH_2 modified particles had a low or neutral value when initially characterised and so they were further NH_2 modified as for this study the charge was a key variable to investigate. Again as was found for the previous work with iron oxide particles this shows that relying on manufacturers specifications for NM characteristics without independent characterisation may lead to an erroneous conclusion. The measured ZP values showed the difference in surface chemistry between the two types of particles. It should be noted that although ZP is not a direct measure of the surface charge of the particles, it can be used to indicate stability and tendency to agglomerate. All particles appear to be more stable in water and PBS without a corona as the NM with a corona resulted in a decrease in ZP. The ZP of the non modified particles was, as expected, positive but it is interesting to note that the ZP of the amino modified NMs in PBS or with their associated corona was reduced, indicating the surface was extensively covered with the protein thereby masking the positive NH_2 groups. It could also mean the protein/lipid coating somehow moved the shear plane (i.e. the point where the ZP is measured) away from the particle surface.

As mentioned previously the observations of the particles with their LLF corona show the hydrodynamic diameter increased compared to all other measurements

(i.e. in water, PBS and with their serum and plasma corona). This increase was associated with a large increase in Pdi and a relatively low ZP indicating that the particles were agglomerating and/or obtaining a layer of molecules to their surface. However, results from triplicate experiments with LLF were not reproducible as there were very low count levels (i.e. low levels of scattered light) leading to poor quality data, thus this DLS data alone does not clarify if the LLF prevents/allows for further protein adsorption to the surface of the silica NMs or if the sample is agglomerating.

This study demonstrates that the protein profile of the corona (as seen on the SDS-PAGE binding patterns) shows interesting differences in the protein binding patterns not only in different concentrations of the same biological fluid (i.e. 10% and 55% plasma) but also between plasma and serum. The most common bands across all silica particle types and biological fluids were observed at 60kDa and 20kDa. This 20kDa band was not observed with the SDS PAGE gel analysis of the iron oxide corona. For all particles the 55% plasma corona does show more bands in the protein profile than the 10% plasma corona and the serum corona shows a very different binding pattern from the plasma corona. This was also observed for the iron oxide particles. Overall the effect of particle charge did not appear to affect the protein profile of the plasma corona however the SDS-PAGE gels do reveal a difference in the binding patterns of the 50nm plain and amino modified particles in the serum corona. The binding patterns do seem to alter depending on particle size (200nm or 50nm) most notably with the 10% plasma corona and to a lesser degree for the 55% plasma corona and the 10% serum corona. When the particles were pre-coated with LLF and then in plasma the binding pattern remained similar in that both concentrations of plasma (10 and 55%) seemed to bind the same type of protein regardless of NM size or type (neutral or positive). This may be due to LLF causing agglomeration with the particles and thus any size specific effects could be mitigated. However, the intensity of these binding patterns are higher, in particular there is a 20kDa band which shows a stronger intensity after preincubation with LLF. This was seen predominately for the 10% and 55% plasma corona. No obvious difference was observed in the 10% or 55% plasma corona binding patterns for the 200nm SiO_2 and SiO_2-NH_2 particles either before or after incubation in LLF in the types of

proteins identified although the intensity of the bands do suggest the particles precoated in LLF do bind more protein. The 50nm (both neutral and positive) also appeared to have stronger bands after pre-coating in LLF indicating more protein adsorption after incubation in LLF. This was also indicated by the DLS results where it can be seen that the hydrodynamic diameter increased after pre-incubation with LLF.

This work was concerned with the protein profile of the corona and does not address how the corona is formed as the mechanisms of protein adsorption are beyond the scope of this thesis. There are many mechanisms by which proteins may adsorb to the particle surface and of course it will depend on the biological environment and the nature of the NM in question. For example, it has been reported that proteins containing amino acids with thiol, sulfide, and disulfide groups may interact strongly forming covalent bonds with metallic NMs [103]. Perhaps a similar mechanism is occurring here and it may in some way explain the strong preferential binding of proteins such as complement and immunoglobulin which have thiol groups in their native confirmation, although non covalent bonds may also occur. In particular this study finds the most common protein in the corona (besides serum albumin) were apolipoproteins. Other studies also show a high abundance of apolipoproteins in the corona (see review [212]). These proteins do have accessible free thiol groups in their structure [213].

The WST-1 assay revealed there was a significant difference in viability between the 200nm and 50nm SiO_2 particles but only at the 2 lowest concentrations (at 3.9 and 7.8µg/ml). At these two concentrations the viability of the cells after exposure to 200nm silica was not significant from the negative control suggesting the 50nm plain particles were more cytotoxic than the 200nm particles at this low concentration. There was no significant difference between the 200nm $Si0_2NH_2$ and the 50nm $Si0_2NH_2$ NMs to impact mitochondrial function.

The LDH assay shows all particles at all concentrations had a significant increase in LDH compared to cells with no treatment. It is interesting to note that the corona associated with the silica particles had a different effect on the LDH

release in J774.A1 macrophages compared to the iron oxide particles. It was still the case that the plasma and serum corona reduced cytoxicity, however there were some exceptions: there was no significant difference in the percentage LDH release after exposure to 200nm SiO_2 particles and those with their plasma and serum corona but there was a significant difference between the plain and the LLF coated particles suggesting the particles with their LLF corona are more toxic than the plain non coated particles. There was a significant difference between the LDH release after exposure to 50nm SiO_2 particles and those with a plasma corona but no significant difference in the LLF particles and those with a serum corona. Upon exposure to the animated particles this work also reports that a significance difference in LDH release upon exposure to 200nm SiO_2 NH_2 and those in with a LLF corona and exposure to the 50nm SiO_2NH_2 were more cytotoxic to the J774.A1 than the same particles with a plasma serum and LLF corona. The findings demonstrate the nature of the corona can influence the subsequent toxicity of the particles, the most pronounced effect can be seen for the 50nm NH_2 modified silica NM where the serum and plasma and LLF corona significantly reduced the particle toxicity to macrophages. This work again points to recommendations for future *in vitro* assays to consider the corona profile when developing assays that are relevant for comparison to cellular responses *in vivo.*

The suggestion that different dispersants can enhance or reduce toxicity is not a novel observation and a recent study with these same particles (Brown *et al.*, 2013, in publication) reports that the use of different dispersants can influence particle toxicity. This study builds on this premise and addresses the corona proteins (i.e. those proteins that are strongly associated with the particles and likely to be the proteins (*in vitro* or *in vivo*) recognised by cells). This adds a new layer of understanding to the previously demonstrated ability of NMs, when tested *in vitro* in the absence of FCS, to have an enhanced response on cell cytotoxic response and uptake that NMs in presence of FCS [114, 158]. A simplistic approach of relating specific proteins in the protein corona to an effect *in vitro/in vivo* may lead to erroneous comparisons but this work does ultimately indicates that for both types of silica at two sizes the particles with their associated plasma corona masked the cytotoxicity in a J774.A1 cell line. This seems counterintuitive as the particles were found to bind many proteins that serve to

mark the particles as opsonins (complement C3 and C4A for example). It can be hypothesised that binding of these proteins to the NM surface may lead to a conformational change in their structure causing them to become inactive. In the previous study (Chapter 3) it was speculated that NMs with their associated corona having a lower surface energy are not likely to interact as much with cells as NMs in the absence of a corona. It could be possible that particles without their corona (i.e. those which caused the higher LDH release) are more prone to associating with cells in order to bind biomolecules to their plain uncoated surface in a bid to lower their free energy state. However this work indicates a more complex situation as particles with a LLF corona do appeared to increase LDH release in some treatments (cells exposed to 200nm silica but not 50nm silica). This was not previously found for iron oxide particles. This is an interesting result indicating that exposure via inhalation is an important route to consider for future toxicological studies and that the addition of serum into pulmonary cell culture models may not be relevant and might lead to an underestimation of the potential toxicity of the particles.

To further investigate the effect of the corona on silica particles cytotoxicity, cytokine stimulation after exposure to J774.A1 macrophages was examined. MCP-1, IL-1β, TNF-α and IL-10 levels were determined by multiparametric FACS analysis. This is a common tool used to assess the number of cytokines release by single cells. As in Chapter 3 where iron oxide particles were investigated this study was also made in connection with the LDH assay and so the cytokine profile was measured from the supernatant saved from the LDH assay. Cytokine release within the cell is a highly regulated process and thus it is difficult to make a simple correlation between cytokine levels and potential cytoxicity. The results here show that all particles with all treatments stimulated secretion of MCP-1, Il-1β and TNF-α. The 200nm silica particles with and without their corona, produced quantities of MCP-1, Il-1β , TNF-α and IL-10 at quantities significantly higher than the control. This was in direct contrast to the smaller size 50nm particles where only the particles with a serum corona caused a significant increase in TNF-α and IL-1β and was also dissimilar to the 200nm amino modified silica particles ,where only the serum corona particles caused an increase in TNF-α production. The 50nm amino modified particles also produce

significant quantities of TNF-α and Il-1β without any hard corona and with a LLF corona produced more quantities of TNF-α , Il-1β and IL-10 compared to the control. It is difficult to compare the magnitude of the measured cytokine release directly amongst all these samples as each cytokine will not act in a similar manner (for example, the rate of diffusion of different cytokines from cells may vary [214]). Also in the absence of normalised data these results should be viewed not as a separate experiment but taken together with the LDH data. It is possible to gain information by looking at the trends and seen and it can be seen that there are high MCP-1 and TNF-α levels and low IL-10 anti inflammatory release this was also seen for iron oxide NM exposure to J774.A1 cells.

4.5 Conclusion

Previous work detailed in Chapter 3 found that that proteins such as albumin, immunoglobulin and complement make up the hard corona profile of iron oxides in biological fluids. The research also demonstrated the effect of LLF to alter this hard corona. This study shows that silica particles behave in a similar manner and after investigation of the serum and plasma hard corona it was found that albumin, apolipoproteins and complement (just as with iron oxide particles) make up their hard corona. The presence of LLF also altered the protein profile corona of silica NMs. Although the serum and plasma coronas of both particle types (iron and silica) had proteins in their corona in common this work also demonstrate that each particle type and size has a unique protein corona profile. The ability of NMs to bind these types of proteins is important as complement and immunoglobulin binding can lead to particle opsonization which in particular for J774.A1 macrophages can promote receptor mediated phagocytosis *in vivo*. Although this work did not find that binding of these proteins caused an enhanced cytotoxic response, it did find that the toxicity (LDH release in J77 4.A1 cells) is altered by the specific corona in particular the plasma and serum corona of the 50nm amino modified silica particles had the most profound effect in mitigating toxicity.

Chapter 5 Chemotactic Response in Macrophages after Exposure to Serum Activated with Nanomaterials.

5.1 Chemotaxis

The movement of any cell that is directed by extracellular gradients of diffusible chemicals (chemoattractants) is known as chemotaxis [215]. In the absence of a gradient chemoattractants can increase the non directional migration of cells and this is known as chemokinesis. Chemotactic cell migration was first described by Leber in 1888, in 1936 Clarke *et al.*, demonstrated the phenomenon *in vivo* and by 1962 Boyden *et al.*, discovered it was the mechanism that allowed for leukocyte recruitment describing an *in vitro* technique for assessing the chemotactic activity of 'soluble substances on motile cells'[216, 217]. Chemotaxis is involved in many fundamental physiological processes such as immunity, embryogenesis and migration of neurons. When chemotaxis is impaired, it can cause diverse diseases such as cancer metastasis, angiogenesis and inflammatory diseases [215]. Although most cells in tissues are stationary, leukocytes are motile and migrate actively through the walls of blood vessels into surrounding tissues (see figure 5.1) [67]. The recruitment of leukocytes from blood vessels into tissues by chemotaxis plays a fundamental role in the *in vivo* response to infection [67] and any impaired ability of leukocytes to move in this manner could impair the inflammatory response [218]. Conversely any activation of the chemotactic response could lead to non specific inflammation causing an autoimmune response.

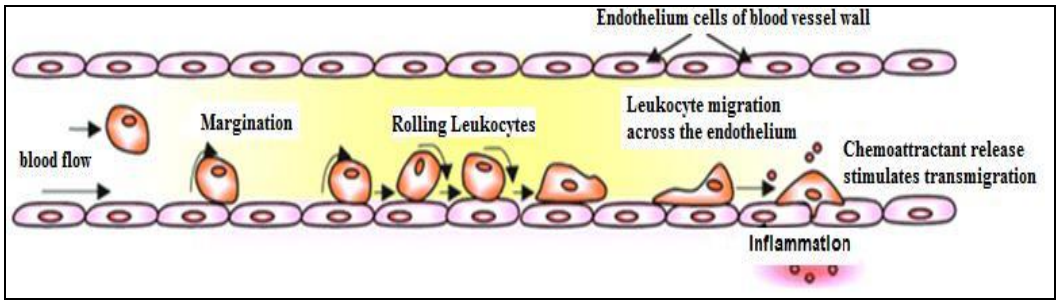

Figure 5.1: Transendothelial migration of cells. Image adapted from Toetsch et al. [218] showing the leukocyte adhesion cascade; rolling (mediated by selectins), activation (mediated by chemokines) and migration as directed by chemotaxis.

5.1.2 Complement Activation Cascade

There is a large and diverse group of chemoattractants that can guide chemotactic transendothelial migration of macrophages such as lipids, peptides, complement proteins and chemotactic cytokines (chemokines). Most chemoattractants operate via the guanine nucleotide-binding protein (G protein) coupled seven-transmembrane-spanning receptor (see figure 5.3) [217]. Complement proteins (or more specifically the proteolytic fragments of complement proteins) are chemoattractants that consist of over 30 proteins. They are produced primarily by hepatocytes (but can also be produced by macrophages and intestinal epithelial cells) and circulate in the body in an inactive form [219]. These proteins are connected as part of a biochemical cascade. Once the first protein in the pathway is activated it initiates a complement proteolytic cascade. There are three main activating pathways in the complement cascade; the classical, lectin and alternative pathways (see figure 5.2). Activation of the cascade leads to multiple interconnections among complement proteins, immune cells and mediators which go on to initiate inflammatory and opsonization responses. Thus in this way the complement activation cascade forms part of the body's non specific innate immune response, providing the mechanism to protect against infections and support the repair of damaged tissues [220].

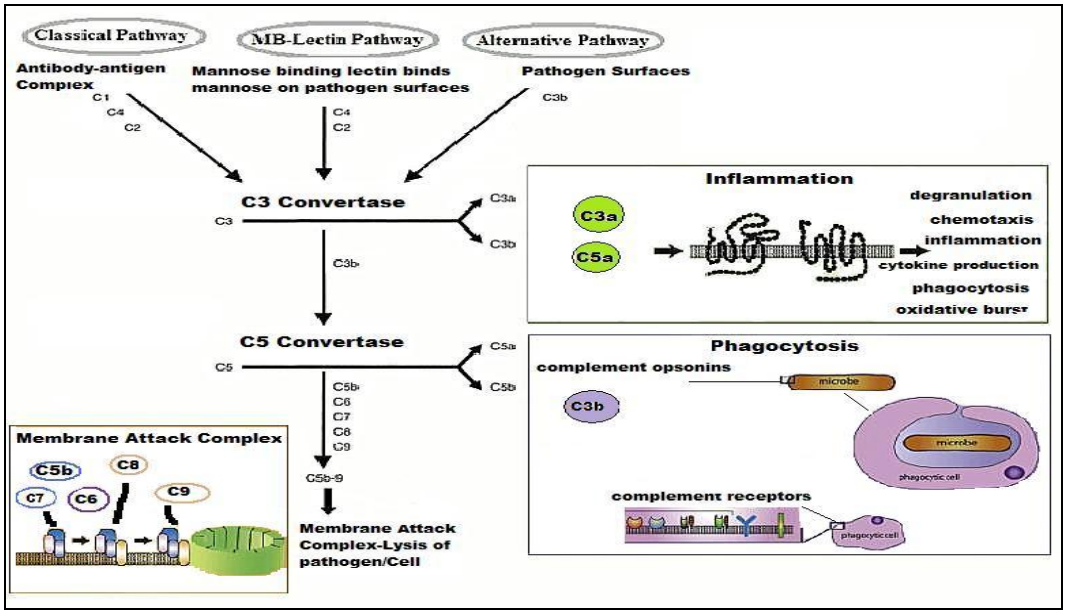

Figure 5.2 Adapted from [219] and [221] showing the classical, lectin and alternative pathways of the complement activation cascade. The

proteins upstream of C5 are essential for opsonization and immune complex clearance. All pathways of complement activation converge at the cleavage of C3 and C5 to ultimately trigger the assembly of the membrane attack complex (MAC), which forms pores in lipid bilayer membranes resulting in cell lysis.

As can be seen in figure 5.2 the classical pathway is activated when antibody/antigen complexes interact with the first complement component (C1). C1 is cleaved and the cascade is initiated ultimately leading to the formation of C3 protein. It is at this point that the classical, lectin and alternative pathway converge. Native C3 is not a functional molecule however it becomes biologically active once cleaved (by C3 convertase) into C3a, C3b, and C5. C5 is subsequently cleaved (by C5 convertase) to form C5a and C5b. This proteolysis of C3, C5 as well as C4 gives rise to N-terminal positively charged fragments C3a, C4a and C5a, collectively known as anaphylatoxins [217]. Anaphylatoxins cause smooth muscle contraction, histamine release from mast cells, enhanced vascular permeability and they also mediate chemotaxis and inflammation [222]. The most potent of these is C5a which at the nanomolar level permits chemotaxis of neutrophils, eosinophils, basophils, monocytes and macrophages [217].

Further downstream of the cascade the addition of C6, C7, C8 and C9 components to the C5b results in the formation of the membrane attack complex (MAC). This C5b-9 MAC molecule can create transmembrane channels that lead to cell lysis [223]. The C3b protein can be covalently attached to target surfaces leading to opsonization once receptors on the surface of phagocytes recognize and bind to the C3b molecule on the surface of the pathogen (i.e. phagocytosis). So, it can be seen how the complement system 'complements' the innate and adaptive immune system and why its regulation is essential for prevention of disease.

NM mediated complement activation is important in the clearance mechanism of particles by macrophages. Complement activation allows for surface opsonization allowing for phagocytosis and MAC assembly. The process is facilitated by chemotactic attraction, i.e. the production of chemoattractant C activation products (such as C5a in serum proteins present in the alveolar surface) results in

chemotactic migration of alveolar macrophages [224]. There are a wide range of studies which look at the ability of particles and fibres to activate the production of chemotactic factors and the alternative complement pathway [225-228]. Warheit *et al.* [229] found that asbestos fibers could activate complement *in vitro* in rat serum and cell free rat lung lavage and in a follow up study by the same author (1988) showed that complement was activated *in vitro* (rat serum and lavaged proteins) by many other fibers and particles including iron-coated chrysotile asbestos, fiberglass, wollastonite fibers, carbonyl iron and zymosan [224]. These early studies showed that complement activation facilitates macrophage recruitment to sites of fibre/particle deposition.

The ability of NMs to activate the immune system is of interest not only in nanotoxicology but also in the complementary field of nanomedicine. The interaction between NMs and their ability to activate the complement system is regulated by many factors and pathways (figure 5.2) and although regulatory proteins can inhibit convertase activity their protective effects can be overcome by uncontrolled complement activation which may lead to hypersensitivity reactions or anaphylaxis. Indeed this has already been reported with regulatory approved nanomedicine (for example Dioxil^{TM}) [230]. However complement activation can also be used to the advantage of nanomedicine and NMs which are used for internal administration. A study in 2007 by Reddy *et al.* [231] exploits the ability of NMs to cause complement activation to facilitate the delivery of vaccines, reporting that the uptake of the NM by dendritic cells, activation of T-cells and generation of the antigen-specific immune response was dependent on complement activation by the NM. Thus it can be seen that the ability of NMs to activate complement may be either beneficial or adverse depending on its application.

Governa et al. demonstrated that crystalline silica can induce the generation of a C5a-like protein when exposed to human plasma, which is chemoattractant for leucocytes [232]. Renwick *et al.* compared the ability of ultrafine and fine CB and TiO_2 particles to affect alveolar macrophage chemotaxis by examining the ability of isolated macrophages obtained from rats instilled with 125ug and 500µg/ml particles to migrate towards a C5a gradient (serum activated with

zymosan) [174]. They found that at 500µg/ml both the ultrafine TiO_2 and CB (but not the fine TiO_2 or CB) caused a significant increase in macrophage chemotaxis compared with a saline control suggesting that this increased sensitivity to a C5a chemotactic gradient could make the ultrafine particles exposed macrophages more likely to be retained in the lungs, hindering their clearance by the normal mucocilliary route.

More recently Barlow *et al.* demonstrated high doses of CB NMs did have the capacity to cause chemotactic factor generation in foetal calf serum after incubation with the serum for 2 hours at 37°C [228]. This was reported as a 1.8-fold increase in macrophage migration towards the treated serum compared with untreated serum. It was also reported that this effect was partially inhibited by antioxidant intervention. The same author also reports [233] that exposure of epithelial type II cells to CB nanoparticles resulted in significant release of macrophage chemoattractant (compared to the negative control, fine carbon black and TiO_2 and TiO_2 NM) as measured by macrophage migration towards cell conditioned medium.

CNTs have also been found to activate the human serum complement system via the classical pathway, for example, Salvador-Morales *et al.* found that human serum exposed to CNTs at 37°C for one hour activated serum to the same extend as a positive control of serum exposed to Zymosan [225]. Interestingly surface modification of these CNTs altered their interactions with complement proteins and Anderson et al. [234] demonstrated that modified CNTs (resulting in CNTs with linear poly(ethylene glycol) amphiphiles) trigger the lectin complement activation pathway as opposed to the classical pathway. Besides the surface modification of NMs other factors such as polymer coating and surface charge are important factor for complement activation.

A review by Dobrovolskaia et al. [235] suggested that NMs with a charged or reactive surface group (polypropylene sulphide nanoparticles, lipid nanocapsules, polycation-based nanoparticles and polystyrene nanospheres) are more able to activate complement than neutral particles. In addition, it was demonstrated that NM coatings affected the ability of NM to activate complement with poly

ethylene glycol (PEG). Poloxamine coatings reduced complement activation, but dextran coatings were associated with an increase in nanoparticle-mediated complement activation [235].

The findings detailed in Chapter 3 and Chapter 4 suggest that complement proteins (C3, C4 C4a and C5) are present in the protein plasma and serum corona profile of both iron and silica particles. This was an interesting finding as complement proteins in this C3 and C4 form can lead to particle opsonization and in particular for J774.A1 macrophages can promote receptor mediated phagocytosis *in vivo*. Cleavage of these C proteins can generate N-terminal positively charged fragments, C3a, C4a and C5a (anaphylatoxins) mediating chemotaxis and inflammation. However, the research in this thesis indicates that the protein corona reduced or mitigated toxicity

5.1.3 Macrophage Migration

Migrating macrophages can be identified *in vitro* by filopodia which are extensions of about 0.1– 0.2μm in diameter and up to 20μm in length [67]. *In vitro*, migrating macrophages can be observed to move in a cyclic form starting with an extension of the leading edge of the cell (protrusion of filopodia), adhesion of this leading edge to the matrix, contraction of the cytoplasm and finally release from contact sites at the tail end [236]. Filopodia support membrane-enclosed cytoplasm termed lamellipodia. Migration occurs by modification of the extracellular matrix and in macrophages this cytoskeletal rearrangement is driven by the actin cytoskeleton. Thus in this way the actin within the lamellipodia of macrophages, in association with structural and regulatory proteins, allows for cell locomotion. This controlled cell locomotion allows cell movement and the shape changes required for chemotaxis. Therefore it has a key role in locomotion, phagocytosis, and the regulation of cell shape [67]. Although the exact regulatory intracellular signalling mechanism of macrophage migration is beyond the scope of this thesis, in recent years there has been an increase in the understanding regarding the signalling pathways from outside the cell and the actin rearrangement in the cell as well as the roles of the many individual proteins in each step of the cell migration process.

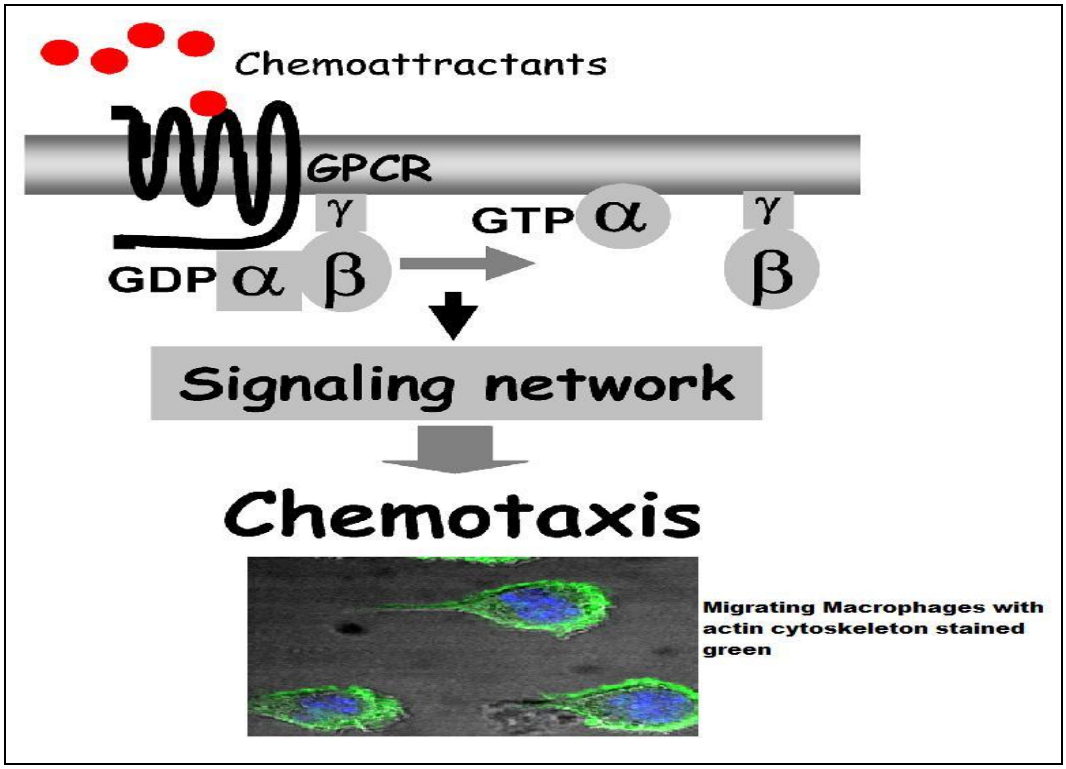

Figure 5.3 The G-protein-coupled receptor mediated signalling network showing, binding of chemoattractant to the G- protein receptor leading to chemotaxis and J774.A1 macrophages stained for actin (assembly of actin at the leading edge drives the cell forward) adapted from Jin et al. [215].

Chemotactic factors (such as complement) regulate cell migration via a family of G protein coupled receptors (GPCRs) and tyrosine kinase receptors. The binding of chemoattractant to GPCR induces the dissociation of the G-protein into Ga and Gbc subunits [215]. Gbc activates proteins in the Ras family, which regulate the formation of lamellipodia and filopodia and ultimately lead to actin polarization (see figure 5.4)

5.1.4 Chemotactic Assays

There are many chemotactic models that can be employed to measure chemotaxis *in vitro* (this subject has been reviewed by many authors, (e.g. Toetsch et al. [218], Li et al. [237] and Kramer et al.[238]). The transwell or static model (see

figure 5.4) has historically been a widely used and is a popular tool to quantify migration of cells exposed to different chemoattractant concentrations. As it was first introduced by Boyden it is often referred to as the Boyden chamber assay [216]. The chamber contains two compartments that are separated by a porous filter membrane. The size of the cells being examined determines the required pore size of the membranes. Cells are seeded in the medium in the upper part of the chamber and can migrate in the vertical direction through the pores of the membrane into the lower compartment. Chemoattractants diffuse from the bottom compartment to the upper compartment through the membrane generating a gradient. The cells on the upper filter can then be removed with a cotton swab and the cells that migrate to the bottom of the filter can be stained and quantified. Since the introduction of this method in the 1960's by Boyden there have been continual improvements of this technique (becoming simplified or the introduction of disposable 96 plate formats, etc.) and other similar versions of this static method have been introduced (such as the micropipette based assay, Zigmond chamber and Dunn chamber) that work in a similar manner to produce chemical concentration gradients by free diffusion.

These types of static assay have limitations in that they require large amounts of reagents and cells. The transwell migration kits that are now commercially available for examining a large amount of samples can be expensive and the optimal time of migration for the cell type needs to be pre-determined. The practice of using a cotton swab to remove non migrated cells on the filter can be difficult and prone to error in that it heavily relies on the technique used by the individual. Thus this technique may not be quantifiable and if it is can vary in outcome. The chemokinetic (speed at which cells migrate) and chemotactic effects (direction in which cells migrate) may not be distinguishable. There is no way to incorporate the effects of shear stress on the cells under investigation and there is no reliable way to sustain and control the chemoattractant gradient.

More recently microfluidic models/techniques have been employed in chemotaxis assays. These models involve the use of micro fabricated chips consisting of channels of fixed dimensions. Cells are seeded in these channels and the treatment can be applied under a control flow. As such these models are designed

to better mimic the body's microvasculature. These types of models allow for stable chemical concentration gradients and as they are miniaturised allow the use of small amounts of reagents and cells. These microfluidic models also allow for the control of shear stress making them a valuable physiologically relevant model for this work. The chips can also be visualised in real time allowing the cells to be visualised and chemotaxis to be analysed over time. In this work the transwell system was used to investigate macrophage response to NM treated serum, some experimental work with the microfluidic system was also carried out to see how this system might add more to the knowledge base.

5.1.5 Chapter 5 Aims

- To determine whether activation of chemoattractant factors in serum can occur following NM exposure.

- To determine if NMs differ in their ability to activate chemoattractants in serum as indicated by increased macrophage migration towards the particle-treated serum *in vitro* using a transwell assay and experimentally using a microfluidic assay.

- To investigate the ability of NMs coated in various physiological relevant protein coatings (plasma, serum and LLF) to activate chemoattractants in serum, using both a transwell and experimentally using a microfluidic assay.

5.2 Materials and Methods

5.2.1 Serum Activation

Non heat inactivated FCS was treated in a manner similar to that described by Barlow *et al.* [228] and Renwick et al. [174]. Serum was exposed to 62.5µg/ml NM and to NM with associated corona (prepared fresh as described in 3.2.4). Barlow *et al.*, reports the use of 10mg/ml carbon black for serum activation (followed by a 6 hour incubation with macrophages) however here we choose a more relevant exposure dose of 62.5µg/ml. Previous work (Chapter 3) indicated that NMs exposed to macrophages at this concentration were cytotoxic (significant release of LDH compared to control) and thus this was the concentration chosen for activating the serum. The serum was incubated with the NM at 37°C for two hours to promote activation of complement. After two hours the serum was incubated for further thirty minutes at 56°C to ensure that no further complement activation occurred. Following incubation, the samples were centrifuged at 12,000 g for fifteen minutes to remove the particles. The supernatants and particles were stored at -80°C until required. A positive control of C5a-rich serum was prepared using the same conditions by incubating the FCS with 10mg/ml Zymosan (Sigma, UK). A negative control of FCS incubated with PBS was also prepared. All samples were diluted to 10% in serum free RPMI for use in the chemotactic assay, 10% zymosan activated serum has been routinely used in other chemotaxis studies [174, 228]

5.2.2 Chemotactic Model/Assay

The particles used in these experiments were iron oxide NM (280nm Fe_2O_3 and 45nm Fe_3O_4 and silica NMs (200nm and 50nm). These particles have been previously characterised and described as detailed in Chapter 3 and Chapter 4.

The transwell system (as described in 5.2.3) was used first in order to investigate cell migration of J774.A1 cells in response to NM activated serum. This high throughput method allowed for multiple sample screening. The microfluidic system was also used to further investigate the chemotactic response under more

physiologically relevant conditions. This method (as described in 5.2.4) employed the use of cells grown in channels on a substrate chip. Using such a method therefore allows the cells in this channel to be temperature controlled and subject to a constant controllable sheer force. Such an experimental set up therefore better resembles the body's vasculature making these experiments more physiologically relevant [218]. Due to the complexity and cost inherent with microfluidic investigation a triplicate sample size was not possible for this experiment as such this was more of an experimental/investigative research. Nonetheless it is relevant as this assay complements the transwell model allowing real time investigation of cell migration under sheer stress conditions. In addition cells from each experiment were fixed and stained for further microscopic analysis as described in 5.2.3

5.2.3 Transwell Chemotactic Assay

J774.A1 cells were cultured until 80-90% confluent and serum starved (this increases the sensitivity of the cells and enhances migration response) overnight at $37^{o}C$, 5% $CO_{2.}$ Cells were washed multiple times with PBS to remove any bound serum, counted and adjusted to a concentration of $1*10^{6}$ in serum free RPMI cell culture medium. Transwell plates (Corning, USA) were obtained in a 24 well plate format with inserts containing a 5µm polycarbonate filter (see figure 5.4). Prior to the experiment the transwell plates were incubated for one hour with serum free media (600µl per well and 100µl per insert) prior to cell addition in order to improve cell attachment. This was carried out according to the manufacturer's protocol which suggested an initial equilibrium period may improve cell attachment [239]. The serum free medium was removed before the addition of cells.

Each well of the plate was seeded with 600µl of chemoattractant (i.e. particle treated serum prepared as described in 5.2.1). The inserts were aseptically placed into each well of the receiver plate making sure no air was trapped between the bottom of the insert and the solution in the well. The inserts were seeded with 100µl of cells in serum free media. The plates were incubated for thirty minutes at $37^{o}C$ in 5% CO_2. After thirty minutes the plate was removed and the sides

were gently tapped to ensure no bubbles were present and replaced in the incubator. The cells were incubated for a further five and half hours. A six hour time point was chosen based on previous published research using the same method [228] and based on the transwell protocol recommended by the transwell plate manufacturer [240]. After a six hour total incubation, the media was removed from the inserts and the front facing top side of the filters were swabbed using a sterile cotton swab in order to remove any remaining attached cells on the filter that did not migrated through the inserts. The cell viability of the cells that did migrate was determined using a cell proliferation assay (Celltiter 96, Promega, UK). This proliferation assay was a colorimetric assay used to determine the number of viable cells. MTS reagent (120µl) was added to the bottom of each well and the plates were incubated for a further 2 hours (37^{o}C in 5% CO_2). The absorbance of the formed formazan product (which is soluble in tissue culture media) was measured at 490nm (Epoch Bio-Tek, UK). The results were reported as percentage of negative control.

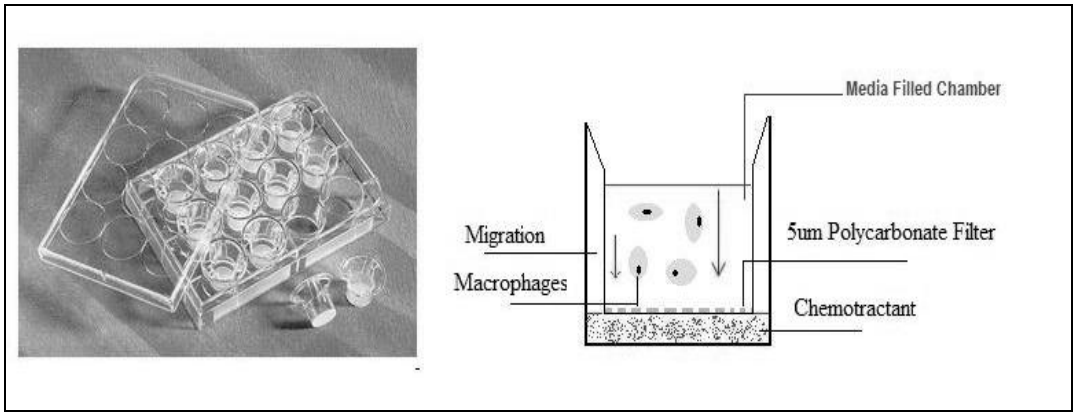

Figure 5.4 Transwell plate used in chemotaxis assay image (adapted from [239]) with line diagram showing set up of the chemotaxis chamber.

5.2.4 Microfluidic Experimental Assay

A Vena ECTM platform (Cellix, Ireland) was used to mimic the situation observed in the body's blood vessels. The substrate tissue culture treated chip (see figure 5.5 insert) was UV sterilised for 30 minutes prior to cell seeding.

J774.A1 cells were cultured on the substrate chip in a 35mm Petri dish at a concentration of $1*10^6$ cells per ml for 24 hours at 37^oC at 5% CO_2. The substrate was removed from the media and with the aid of sterile tweezers clamped to a custom microscope frame (figure 5.5). A VenaEC biochip (see figure 5.5 insert) was place on top of the substrate to create two parallel channels which mimic microcapillaries (figure 5.5).

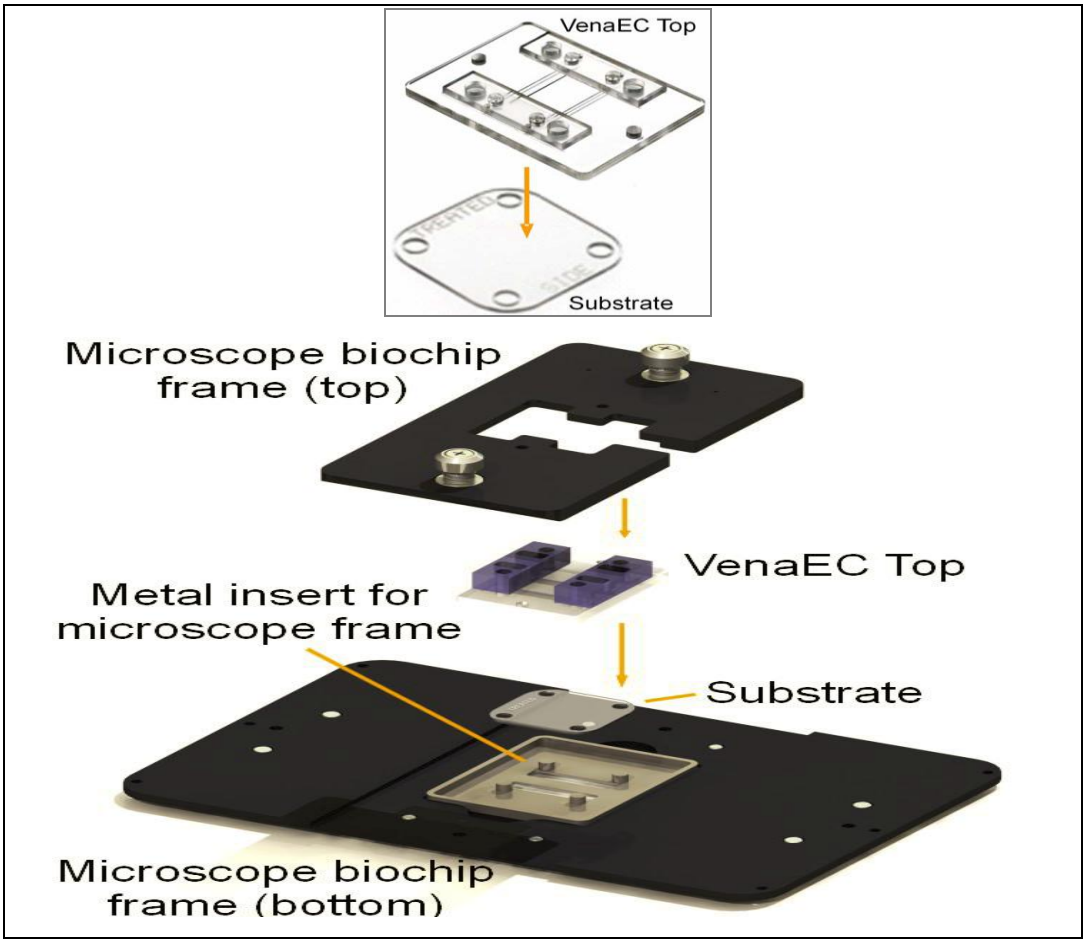

Figure 5.5: Substrate chip and EC Vena biochip assembly on microscope frame (source www.cellix.com accessed November 2012) insert showing how substrate and biochip are assembled to create two cell lined channels.

The customised microfluidic system consisted of an epifluorescent microscope (Zeiss/Axivovert) with a mercury lamp light source, which was enclosed in a temperature controlled chamber. The microscope frame was placed on the stage of the microscope and in order to circulate the sample through the channels each

port on the bio chip was connected via inlet and outlet cables (Cellix, Ireland) through which the activated serum samples suspended in RPMI were pumped. The samples were circulated using the Mirus™ Nanopump (Cellix, Ireland). In this way the cells within the microfluidic channels were exposed to the activated serum in a controlled flow, from static flow to shear stress rates of 0.5Pa. The microscope was coupled to an AxioCam digital camera which allowed live imaging of the channels on the biochip. For each activated serum sample (and controls) a new chip was set up in this manner. After a maximum of 5 minutes the chip was removed and the cells were fixed and stained. The media from each exposure was saved and stored at -80^{o}C for further cytokine analysis. This assay therefore mimics the condition of the cells in the blood vessels in that they are maintained, treated and imaged under flow conditions. The assay provides an indication of cell activation and motility. However as the cells are treated under constant flow of medium and so there is no gradient established. Thus this microfluidic experiment builds upon the previous transwell assay allowing more information on activation and motility to be gathered in real time rather than directly comparing chemotactic techniques.

5.2.4.1 Cell Staining / Confocal Imaging- Experimental Assay

The substrate was removed from the chip, washed 3 times in PBS and fixed with 3.7% paraformaldehyde in PBS at room temperature for 30 minutes. They were washed in PBS and permeabilized with 0.1% triton for 3 minutes at room temperature. The substrate with the fixed cells was then washed three times with PBS before staining. The cells on the substrate chip were stained with Alexa Fluor Phalloidin (448 Excitation/Emission: 495/518nm) (1:200 dilution) to visualise the actin cytoskeleton morphology and Hoechst (1:800 of 1µg/ml stock) to visualise the nuclei, for 1.5 hours at room temperature in the dark. The cells were then washed three times with PBS before being mounted on glass slides using a drop of mounting medium (Darko, USA). The cells were examined using a Zeiss Laser Scanning Microscope (LSM) 510 system (Carl Zeiss Jena, Germany) with a 63× oil immersion objective. The LSM was equipped with 4 laser sources. The samples were excited at 488nm laser wavelengths and imaged with emission with band pass filter of 450 – 560nm

5.2.4.2 Cytokine Analysis- Transwell and Experimental Chemotactic Assay

Supernatants of cell culture media saved from the microfluidic chemotaxis assay were investigated to estimate the release of the following cytokines from macrophages; IL-1β, TNF-α, IL-10 and MCP-1. Analysis was carried out on a BD FACS Array™ Bioanalyzer, using a BD cytometric Bead array mouse/rat soluble protein master buffer kit as per manufactures instructions.

5.2.5 Data Analysis

Statistical analysis on the transwell data was carried out using the Minitab 15 statistical package using a 2 way ANOVA. Significance was set at 5%. For the experimental microfluidic data images were obtained from each recording at specific regular time points. Non Migrated cells in one field were counted and a graph of percentage cell migration was generated.

5.3 Results

5.3.1 Transwell Chemotactic Assay

(a)

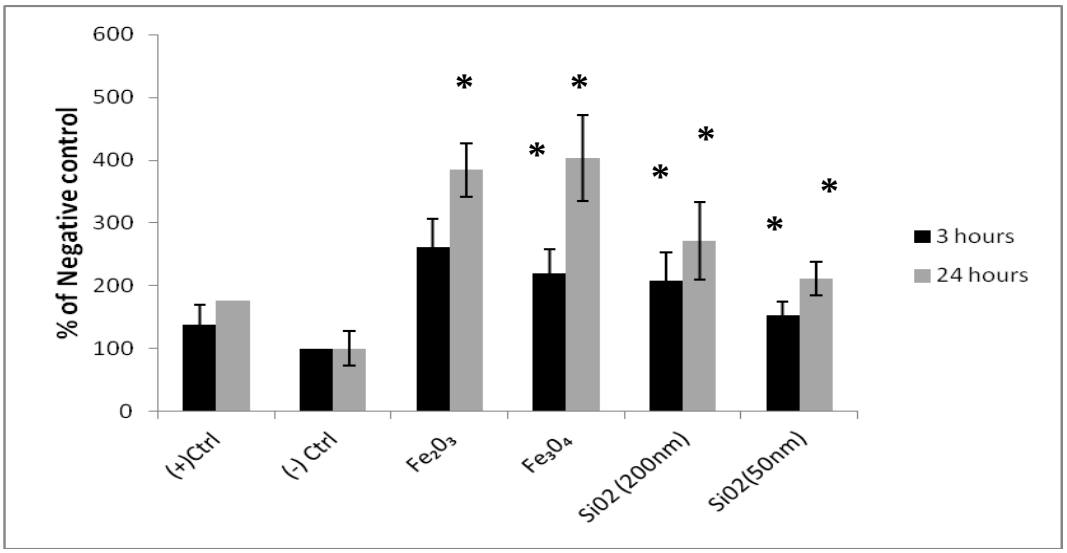

Figure 5.6: (a) Macrophage migration after 3 and 24 hours in the transwell chemotaxis assay (as described in 5.2.2) towards NM treated serum. All results are reported as percentage of negative control. The negative control was serum treated with PBS and the positive control was serum treated with zymosan (or zymosan activated serum (ZAS), as described in 5.2.1. Data expressed as mean ± SEM, n = 3. Asterisks denote a significant increase compared to the negative control ($p < 0.05$).*

Study of the ratio of migrating cells compared to the total number of cells or a negative control is a common method of determining chemotactic signaling. Here we observed that serum which was activated with particles (62.5µg/ml for 2 hours) (Fe_2O_3, Fe_3O_4, 200nm silica and 50nm silica) caused a significant increase in cell migration compared to both the negative and positive control. Previous studies (e.g. [228, 241]) use high concentrations of particles for serum activation, here however a more relevant dose of 62.5µg/ml was used as discussed in 5.2.1. The findings show that NMs when exposed to serum at 62.5µg/ml induced the generation of a complement factors or complement like factors which produce a

significant increase in macrophage chemotaxis *in vitro* compared to unactivated control of serum. There was no difference between the ability of the iron oxide and silica particle activated serum to induce macrophage migration at a 3 hour time point.

5.3.2 Impact of Corona on Chemotaxis as Determined by Transwell Assay

(a)

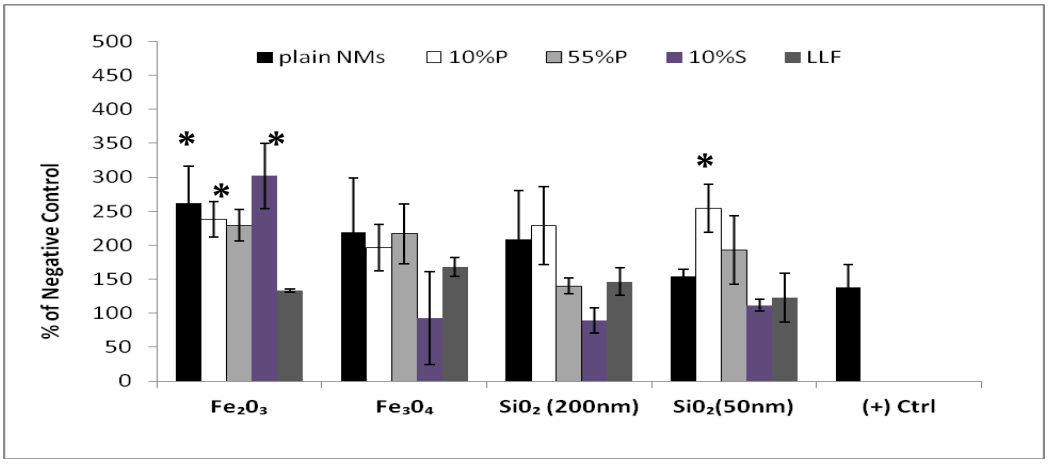

(b)

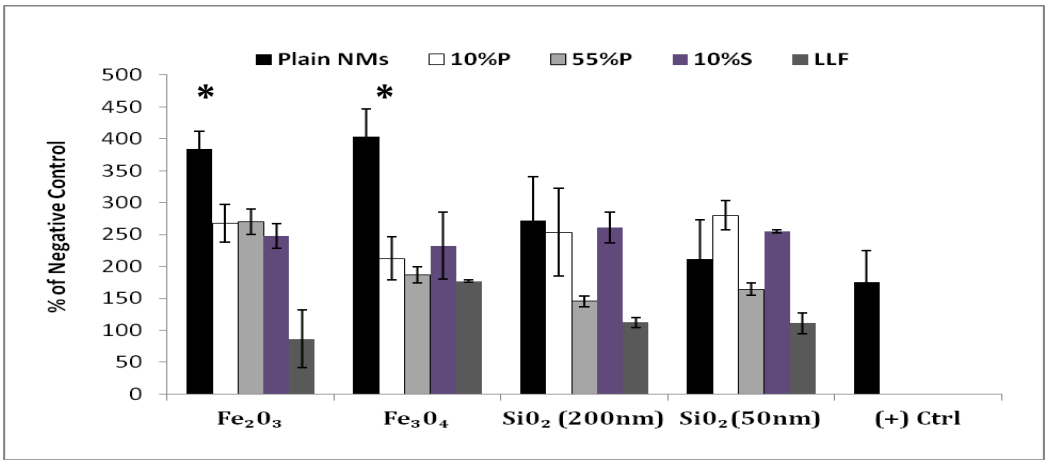

Figure 5.7: Macrophage migration towards particle treated serum as determined by transwell assay. Measurements were taken at (a) 3 hours and (b) 24 hours. The negative control consisted of serum incubated with PBS. Results are reported as percentage of negative control. The positive control included serum exposed to zymosan. Data expressed as mean ± SEM, n = 3. Asterisks denote a significant increase compared to the positive control ($p < 0.05$).*

The results shown in figure 5.7 indicate that serum activated with Fe_2O_3 and Fe_3O_4 caused the highest amount of migration. This was even significantly higher than the amount of migration measured by zymosan activated serum samples. Overall both the iron oxide and the silica NMs (with and without their corona) activated serum sample had a significant increase in migration compared to the negative control. A second aim of this study was to investigate the ability of NMs coated in various physiological relevant protein coatings (plasma, serum and LLF) to activate chemoattractants in serum. The transwell experiments show that the particles with their associated corona varied in their ability to cause chemotaxis and interestingly, there is a significant difference between the ability of the silica particles with their plasma hard corona and particles with the serum hard corona to induce chemotaxis after 3 hours (but not 24 hours). Serum activated with silica (200 and 50nm) particles in their plasma corona caused a higher amount of migration than the serum activated with silica particles in their serum corona. After 24 hours, the serum activated with Fe_2O_3 and silica (200nm and 50nm) particles in LLF caused a decreased amount of cell displacement than the plain particles without their LLF corona.

5.3.3 Experimental Microfluidic Assay Analysis

Figure 5.8 (a-e) shows the analysis of microfluidic data obtained from microfluidic chemotaxis assay as described in 5.3.4 (a) after exposure to Fe_2O_3 particle activated serum (b) Fe_3O_4 particle activated serum (c) silica (200nm) particle activated serum and (d) after exposure to silica (50nm) particle activated serum and (e) the negative control of cells exposed to serum activated with PBS.

Figure 5.8(a)

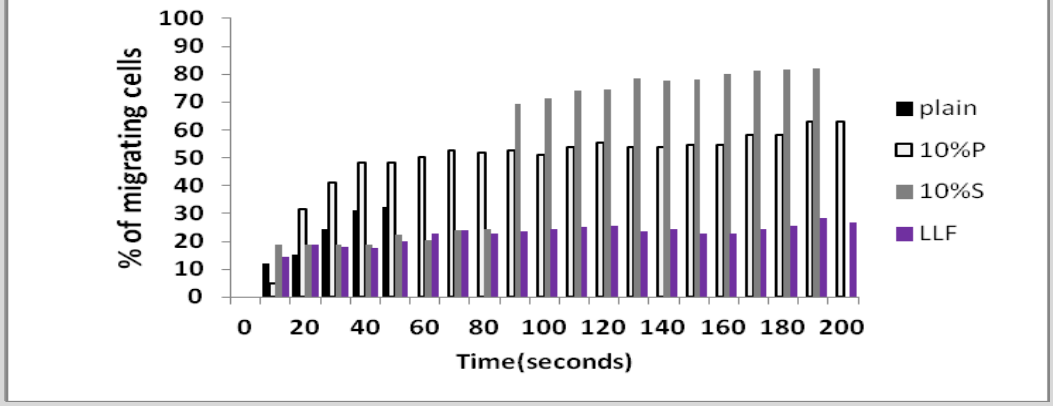

Sample	% migration 10 seconds	% migration 100 seconds	% migration 200 seconds
Control (serum activated with PBS)	0	1.3	3.3
Serum activated with Fe_2O_3	11.88	n/a	n/a
Serum activated with Fe_2O_3 (10%P)	4.89	51.05	62.93
Serum activated with Fe_2O_3 (10%S)	18.87	71.42	82.14
Serum activated with Fe_2O_3 (LLF)	14.51	24.35	26.69

Figure 5.8(a) Microfluidic analysis of cells exposed to Fe_2O_3 particle activated serum Graph showing percentage of migrating cells after exposure to serum activated with Fe_2O_3 with and without their plasma, serum and LLF corona with table showing percentage loss at 10 seconds, 100 seconds and 200 seconds.

The microfluidic data was obtained from the experimental microfluidic chemotaxis assay as described in 5.3.4 after exposure to Fe_2O_3, Fe_2O_3 in its plasma corona, Fe_2O_3 in its serum corona and Fe_2O_3 in its LLF corona. The figure represents the percentage of migrating cells after exposure to the serum activated by the particles with and without their plasma, serum and LLF corona. Live imaging of the cells in the microfluidic channel allowed for observation of cell behaviour upon exposure to the activated serum. From these videos,

micrographs were acquired at 10 second intervals. The images can be seen in appendix (8.13). Exposure was generally up to 200 seconds but for the serum activated with Fe_2O_3 NM it was after 50 seconds as the cells were seen to migrate quickly. Leaving the experiment to run for 200 seconds would have resulted in no remaining cells in the channel to examine. The number of cells on each micrograph was counted and graphs generated thus figure 5.8(a)) show the percentage of remaining cells as a function of time.

The nature of this study and the expense of the micro fabricated chips limited the amount of replicates (n=1), however this technique complements the static transwell assay (n=3) by allowing the cell behaviour in real time to be observed. These observational results indicated that cell migration (which was in the direction of the flow) was more pronounced when cells were exposed to the serum activated by the Fe_2O_3 NM without a plasma, serum or LLF corona. Conformational changes were observed immediately upon exposure of the activated serum as the cells began to migrate in the direction of the flow. Similar results were noted when the cells were exposed to the serum activated by Fe_2O_3 in the serum and plasma corona where the cells were seen to migrate and the cell conformational changes were apparent. In direct comparison it can be seen that when the cells were exposed to serum activated by Fe_2O_3 in the LLF corona there seems to be much less migration and the cell shape does not alter. Figure 5.8 (a) shows that the cells exposed to serum activated with NM in their serum and plasma corona caused the most cell migration over 200 second time point with a 82% and 63% loss respectively. The control had a 3% loss of cells due to migration in 200 seconds. However it should be noted that the cells exposed to serum activated with the plain Fe_2O_3 were observed to move faster and the experiment could not be run for 200 seconds.

Figure 5.8(b)

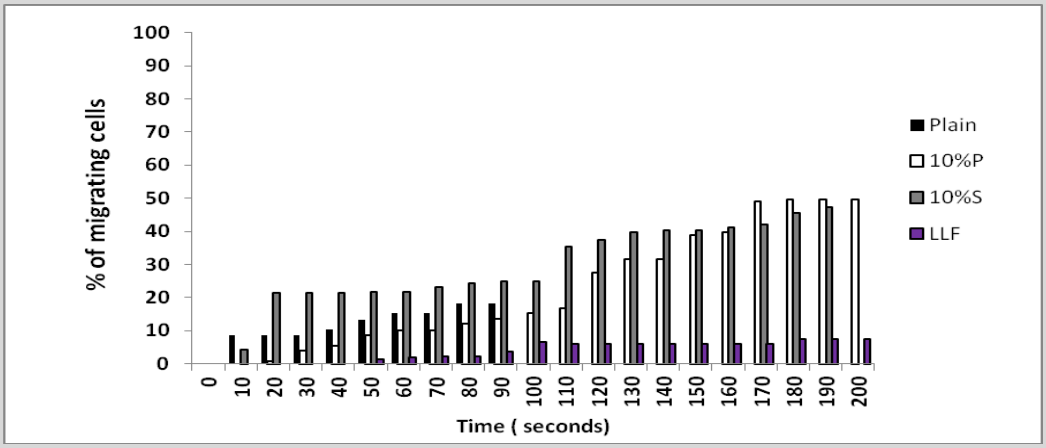

Sample	% migration 10 seconds	% migration 100 seconds	% migration 200 seconds
Control (serum activated with PBS)	0	1.3	3.3
Serum activated with Fe_3O_4	8.57	n/n	n/a
Serum activated with Fe_3O_4 (10%P)	0	15.43	49.66
Serum activated with Fe_3O_4(10%S)	0	24.95	47.18
Serum activated with Fe_3O_4 (LLF)	0	6.54	7.47

Figure 5.8 (b) Microfluidic analyses of cells exposed to Fe_3O_4 particle activated serum. The graph shows the percentage of cells that migrated over 200 seconds after exposure to serum activated by Fe_3O_4, and serum activated by in Fe_3O_4 with its associated plasma, serum and LLF corona with table showing percentage loss at 10 seconds, 100 seconds and 200 seconds.

The microfluidic data was obtained from the experimental microfluidic chemotaxis assay as described in 5.3.4 As with figure 5.8 (a) this figure also represents the percentage of migrating cells after exposure to the serum activated by the particles with and without its plasma, serum and LLF corona. Images of migrating cells can be seen in the appendix (8.13). The least amount of cell migration was observed in the cells exposed to serum activated by the NM in the LLF corona, 7.47% after 200 seconds, compared to serum activated with serum

and plasma (49.66 and 47.18% respectively). Although these results are experimental (n=1) and should be treated with caution it is interesting to note the difference between the two iron oxide particles (Fe_2O_3 and Fe_3O_4) and their effects on macrophage migration. Both activated serum samples had a similar pattern in that more cell migration was observed with the serum activated with the particles in their serum and plasma corona compared to the serum activated with the particles in their LLF corona. However it can be seen that the serum activated with Fe_2O_3 caused more migration initially (i.e. after 10 seconds) compared to the Fe_3O_4 activated serum samples. There was a 0% migration of macrophages exposed to serum activated with Fe_3O_4 in their plasma, serum and LLF corona comapred to a 18.87% (plasma), 4.89% (serum) and 14.51% (LLF) migration in the cells exposed to Fe_2O_3 activated serum samples.

Figure 5.8(c)

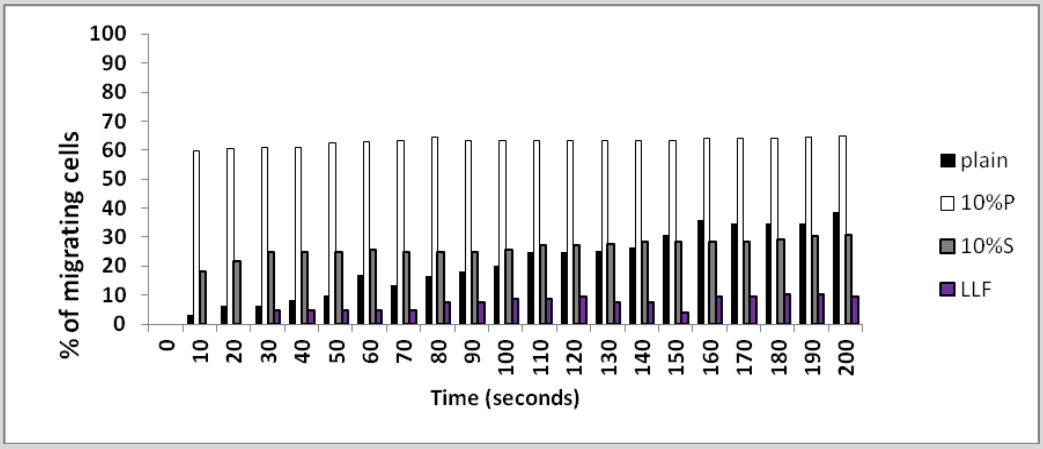

Sample	% migration 10 seconds	% migration 100 seconds	% migration 200 seconds
Control (serum activated with PBS)	0	1.3	3.3
Serum activated with 200nm SiO_2	3.06	9.97	38.56
Serum activated with 200nm SiO_2(10%P)	59.61	62.6	65
Serum activated with 200nm SiO_2(10%S)	18.18	24.7	30.35
Serum activated with 200nm SiO_2 (LLF)	0	4.7	9.43

Figure 5.8(c): Microfluidic analysis of cells exposed to 200nm silica activated serum. The graph shows the percentage of cells that migrate over time after exposure to serum activated with 200nm silica particles and 200nm silica particles in a plasma, serum and LLF corona.

Figure 5.8 (c) represents the percentage of migrating macrophages after exposure to the serum activated with 200nm silica particles and 200nm silica particles in a plasma, serum or LLF corona. Compared to the control cells exposed to serum activated with PBS, it can be seen that there was an increase in migration of cells for all samples tested. The cells exposed to serum activated with the 200nm Silica NM in their plasma corona showing the most amount of cell displacement (65% after 200 seconds). As was seen with the previous results (Figure 5.8 a and b) the macrophages which were exposed to serum activated by silica particles in their LLF corona showed the least amount of cell migration.

Figure 5.8(d)

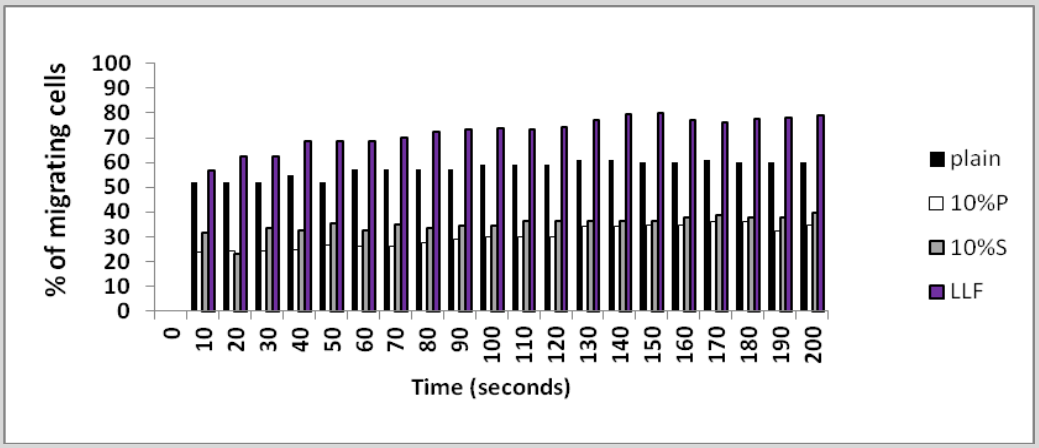

Sample	% migration 10 seconds	% migration 100 seconds	% migration 200 seconds
Control (serum activated with PBS)	0	1.3	3.3
Serum activated with 50nm SiO_2	52.00	57.00	66.00
Serum activated with 50nm SiO_2 (10%P)	23.77	28.90	34.80
Serum activated with 50nm SiO_2(10%S)	31.57	34.32	39.59
Serum activated with 50nm SiO_2 (LLF)	56.79	73.37	79.08

Figure 5.8(d): Microfluidic analysis of cells exposed to 50nm silica activated serum. The graph represent the percentage of cells which migrate over time after exposure to serum activated by 500nm silica particles and 50nm silica particles with its associated plasma, serum and LLF corona with table showing percentage migration at 10 seconds, 100 seconds and 200 seconds.

Figure 5.8(d) shows analysis of microfluidic data obtained from microfluidic chemotaxis assay as described in 5.3.4. As with the preceding graphs (figure 5.8 a , b and c) this graph represents the migration of macrophages upon exposure to serum activated with 50nm silica particles with and without a protein corona. Observation results show that upon exposure to the serum in the microfluidic channel the cell morphology was seen to change as the cells moved creating a clear leading edge and a tail or trailing end. It is interesting to note that the cells exposed to serum activated with the silica NM in the LLF corona showed the largest amount of migration. This is in direct comparison to that observed for all other samples tested in their LLF corona.

Figure 5.8(e)

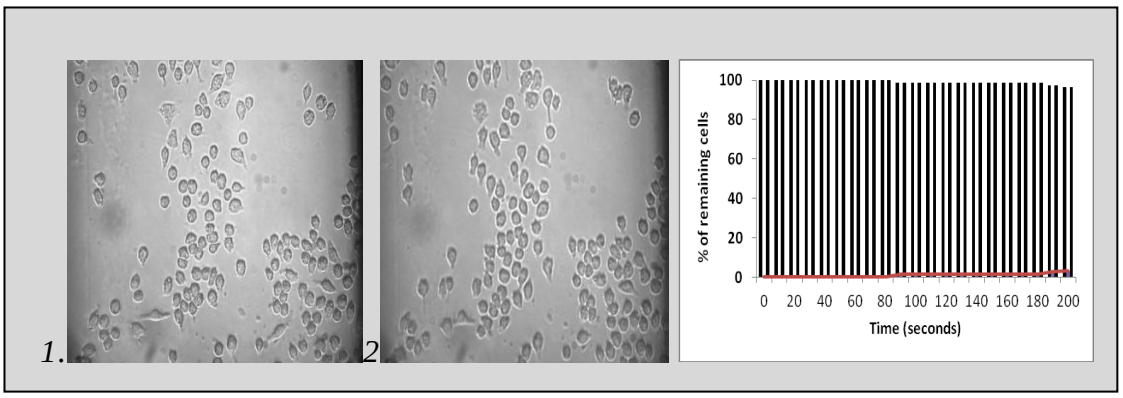

Figure 5.8(e) Microfluidic analysis of cells exposed to serum activated with PBS. Image 1 at 0 seconds and image 2 at 200 seconds. The red line in the graph represents the % migrating cells.

The microfluidic assay allowed for direct observation of cells behaviour in real time as they were exposed to the activated serum. Conformational changes were observed immediately upon exposure of the activated serum and they began to migrate in the direction of the flow. Cell polarization and migration was observed

in response to all treatments. As can be seen in the control 5.8 (e) the cells did not appear to migrate after exposure to serum treated with PBS. With a 3% loss of cells after 200 seconds noted and after 6 hours a 44% loss was recorded (6 hour data shown). This was in direct comparison to the migration pattern of the cells observed after exposure to serum activated by Fe_2O_3 NM where the experiment was stopped after 50 seconds due to rapid cell migration with 32% cell loss after 50 seconds. Furthermore, the macrophages exposed to the non-coated iron and silica were observed to display an increased number of filopodia and protrusions along the leading edge. The cells treated with serum activated with particles in their LLF corona exhibited a low rate of migration for all samples except the serum activated with 50nm Silica in the LLF corona.

5.3.4 Confocal Microscopy

(a) Control

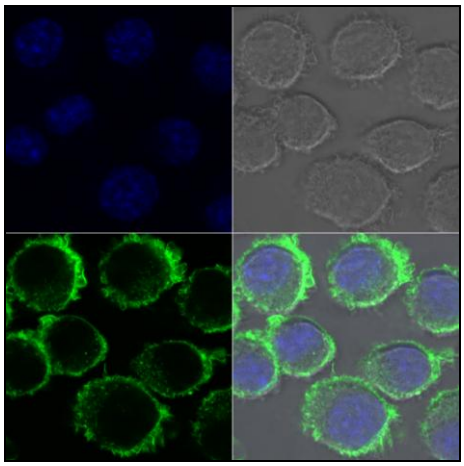

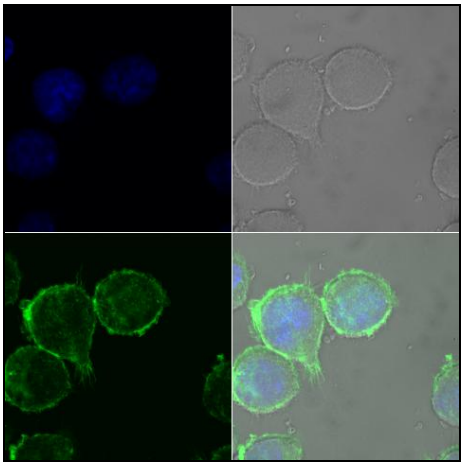

(b) Fe_2O_3

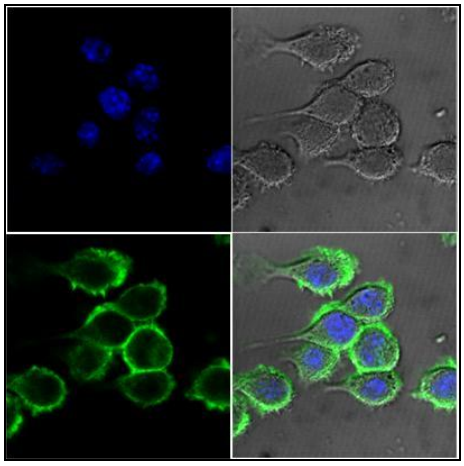

(c) Fe_3O_4

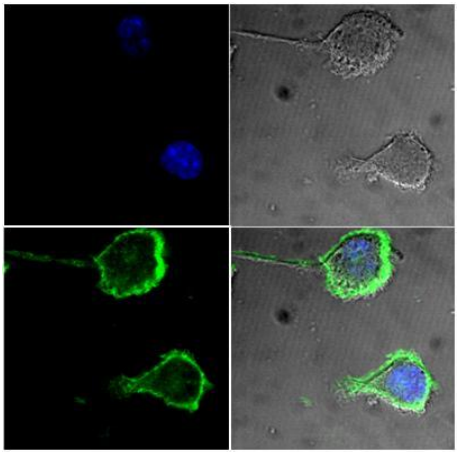

(d) Silica 200nm

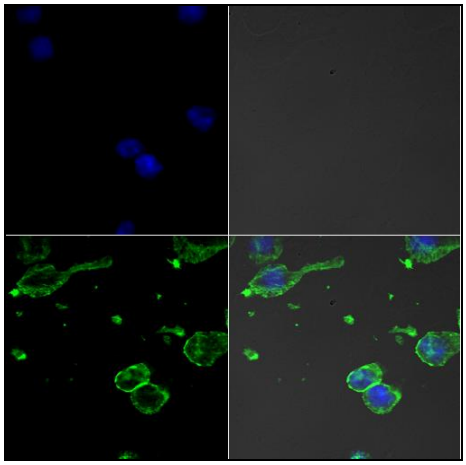

(e) Silica 50nm

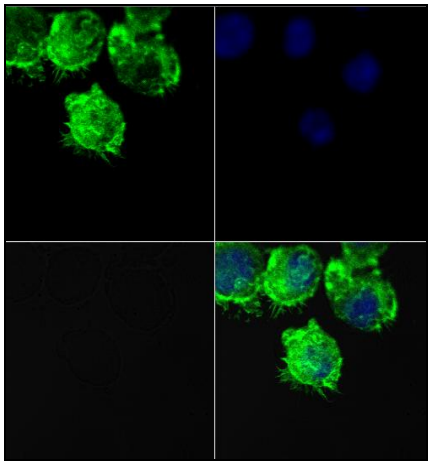

Figure 5.9: Confocal Imaging taken using 63X oil immersion lens showing (a) control (i.e. J774A1 cells exposed to media only) (b) cells exposed to serum activated with Fe_2O_3 particles (b) cells exposed to serum activated with Fe_3O_4 (d) cells exposed to serum activated with 200nm silica particles and (e) cells exposed to serum activated with 50nm silica particles. The cells imaged were those remaining on the microfluidic Cellix substrate chip from microfluidic analysis. Cells were fixed in 3.7% paraformaldehyde and stained with Phalloidin-FITC and Hoechst. Images were obtained on a Zeiss Laser Scanning Microscope (LSM 510 META from Zeiss, Germany).

After the microfluidic chemotaxis assay was completed the remaining cells on the biochips were fixed and stained (one chip per sample). Observation of the cell morphology revealed long tail like protrusions displayed during cell migration. It can be seen that these tails, filopodia and other protrusions include actin and that they were prevalent in the cells exposed to serum activated with the plain uncoated particles, plasma corona particles and serum corona particles. This was not seen for the negative control (serum activated with PBS) and these structures were less evident when the serum was treated with particles with their LLF corona. It was also interesting to see that that as the cells migrated they left behind some actin 'debris' which was clearly seen to remain along the microfluidic channels. More images of these protrusions and the remaining actin can be seen in the appendix (8.14).

5.3.5 Cytokine Analysis

(a) Fe_2O_3 (b) Fe_3O_4

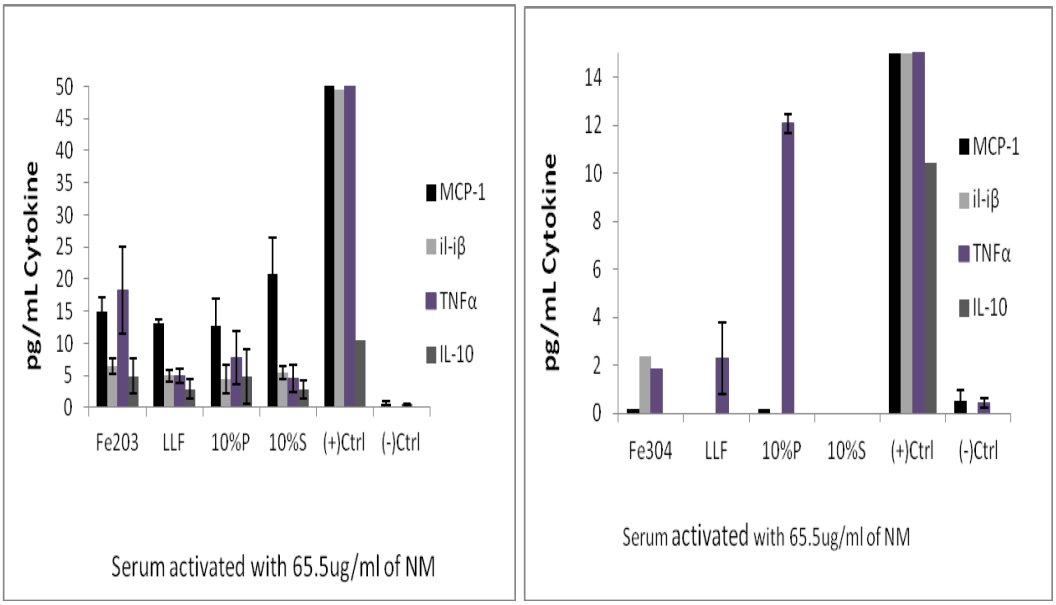

Figure 5.10: Cytokine analysis of J774.A1 cells exposed to activated serum. After the microfluidic chemotactic experiment (as described in 5.2.4) the supernatant was saved and used to investigate cytokine release. (a)Serum activated with Fe_2O_3 particles with and without corona as described in 5.1.1. (b)Serum activated with Fe_3O_4 particles with and without corona as described in 5.1.1. The positive control was media obtained during the microfluidic chemotaxis investigation of cells exposed to Zymosan activated serum. The negative control was the media obtained during the microfluidic investigation of cells exposed to serum activated with PBS.

All the Fe_20_3 activated serum samples release of cytokine (IL-1β, TNF-α, IL-10 and MCP-1) were below the levels measured in the positive control (the positive control was statically significant from all other measured samples ($p < 0.05$)). All the activated serum samples did have measureable cytokine levels greater than the negative control p ($p< 0.05$) however this was not the case for the cytokine levels measured after exposure to Fe_30_4 activated serum. In particular FACS array analysis indicated that cells exposed to the serum activated with Fe_30_4

10% serum did not have any detectable levels of cytokine. This was also the case in cells after exposure to serum activated with silica particles (data not shown). Overall the Fe_20_3 had the highest levels of measurable cytokine levels, which was significantly ($p < 0.05$) different from those measured in Fe_30_4 samples. The exception was TNF-α release measured after exposure to serum activated with Fe_30_4 particles in their 10% plasma corona and in their LLF corona. This was not significant.

5.4 Discussion

The presence of complement enhances NM recognition by macrophages and in its activated form can lead to particle opsonization promoting receptor mediated phagocytosis. Mass spectroscopy analysis (see Chapter 3 and 4) of the plasma and serum protein hard coronas formed on iron oxide and silica particles, suggested that complement proteins C3 and C4-A are present in both the plasma and serum corona profile of iron and silica particles. These proteins play a central role in the complement system. The ability of NMs to activate complement factors in serum was therefore investigated. This was examined as the ability of NMs to activate complement in serum as indicated by increased macrophage migration towards this chemoattractant. Both a standard transwell assay and an experimental microfluidic assay were used to investigate the ability of NMs to activate macrophage migration with an emphasis on the role of the protein corona.

The transwell migration assay was used in order to confirm the presence of a chemotactic response. This is a standard method used frequently in toxicology or migration assays [218]. Its advantage in this study was that the 24 well plate technique allowed for multiple screening of all samples simultaneously under the same conditions. A positive control consisting of zymosan activated serum (ZAS) which is a rich source of C5a (a known macrophage chemoattractant) [233] was used.

A 3 hour incubation time was first investigated as such time points have been previously reported for other studies investigating macrophage chemotaxis [229, 233, 241]. After 3 hours a microscopic analysis indicated that the cells did not migrate to the bottom of the chamber but migrated through the filter and remained attached to the bottom of the filter. Thus the technique to swab the top of each filter to remove cells that did not migrate was developed. The cell viability of the remaining cells was determined using a cell proliferation assay. The NM, when exposed to serum at 62.5µg/ml induced the generation of a complement factors which produced a significant increase in macrophage chemotaxis *in vitro* compared to the control (serum) and there was no difference between the ability of the iron oxide and silica particle activated serum to induce macrophage migration. To investigate the possibility of slower migrating cells, a 24 hour time

point was also examined and it was found that there was a significant increase in the migration of macrophages towards iron oxide NM treated serum after 24 hours exposure compared to 3 hours. This was not observed for the silica treated serum. Overall it can be seen from figure 5.6 that all treatments at both time points were significant compared to the negative control for increased macrophage migration J774.A1 macrophages have a doubling time of 17 hours thus the 24 hour time point may not be a reliable indication of chemotaxis compared to the 3 hour time point. It could be that any additional signal detected after 17 hours is due to either increased cell number or it may be an indication of chemokinetic migration rather than directed or pointed chemotactic directional movement. Thus it may be a case that for this assay the 3 hour time point is more relevant to chemotaxis as it can be speculated that the increase cell migration at 24 hours may be due to (a) cell proliferation or (b) chemokinesis as opposed to chemotaxis (i.e. non directional cell migration).

The ability of the NM protein corona to alter the chemotactic factor generation in serum was also investigated and it was found that all the particles (with and without a corona)~~,~~ resulted in a significant increase in macrophage chemotaxis in the transwell assay compared to the control. More interesting it was noted that compared to the positive zymosan control, the Fe_2O_3 NM (naked and with a plasma and serum corona) and the silica (50nm) particles with a plasma corona had a significant effect in macrophage chemotaxis.

Complement proteins are also normally found in lung lining fluid [242] and our previous work (conducted in Chapter 3 and 4) suggested that coating the NM in LLF promoted binding of complement proteins (in particular complement C3 and complement C4-A) to the surface of the NM when further coated in plasma or serum. We proposed that these complement proteins could be activated via the alternative pathway to produce chemotactic factors. Such an *in vivo* response in LLF of complement activation (for example to particle exposed lungs) may lead to macrophage migration and inflammation. However, it was interesting to note that cells exposed to serum activated with NM in a LLF corona showed a decrease in cell migration compared to the plain particles with no corona although the difference was only significant when compared to the ability of Fe_2O_3 NM

activated serum after 3 hours it was significant compared to all other samples tested after 24 hours.

Previous authors have demonstrated the ability of particles and fibres [174, 224, 225, 228, 234] to activate the alternative complement pathway. Although the exact chemoattractant component was not identified in this study the ability to activate serum complement *in vitro* is important to investigate as *in vivo* chemoattractants are regulators of cellular trafficking. Their activation is not only essential to the immune system but also central to the pathogenesis of many inflammatory diseases. The ability of NM to cause complement activation in serum *in vitro* suggests that *in vivo* they may contribute to rapid recruitment of macrophages to sites of particle deposition and to clearance of NMs from the circulation via complement receptor mediated phagocytosis. This could be considered a positive mechanism allowing for clearance of particles from the body however it should be considered that *in vivo* the situation may be more complicated [174, 241]. Thus although the complement system allows for recruitment of macrophages, and our data suggests that NMs do generate these complement factors *in vitro* further investigation would be necessary *in vivo* to test the ability of recruited macrophages to clear particles. It may be the case that any sustained chemotactic signal could retain macrophages at the sites of recruitment which in the case of the lung may hinder clearance by the normal mucocilliary route as suggested by Renwick *et al.* [95].

A limitation of the transwell assay is the inability to maintain the serum activated complement gradient. This assay thus may lead to an underestimation of any quantified chemotactic response due to the loss or diffusion of the gradient and so in order to observe the cells and their behaviour in response to activated serum a microfluidic system was prepared. This experimental system did not have a maintained chemotactic gradient however the technique offers more observational information and compared to traditional static models the microfluidic assay provides much greater control over the cell microenvironment because the microfluidic system is run under physiologically relevant conditions. Cells are subject to a constant controlled sheer stress in a way that resembles the body's vasculature (i.e. blood vessels *in vivo* are subjected to differing shear stresses).

Shear stress is defined as 'the force per unit area (measured as dyne/cm^2) exerted by a fluid on the surface of the tube' [218]. In this study the cells within the microfluidic channels were exposed to activated serum under a sheer stress rate of 0.5Pa (or 5dyn/cm^2). This was chosen as the physiological range of shear stresses is 1 to 5dyn/cm^2 in venules and the physiological range of shear stresses for leukocyte recruitment is 1 to 6dyn/cm^2 [243, 244].

The microfluidic technique also allowed the cells to be observed as they responded in real time. Immediately upon exposure to the serum activated RPMI samples (prepared as described in 5.2.1) cell migration was observed. The migration was immediate in the case of the Fe_2O_3 and Fe_3O_4 activated serum samples the effect was rapid and the experiment was stopped within 100 seconds in order to retain cells on the chip for confocal analysis. After 10 seconds it was calculated that there was an 8.57% migration of cells after exposure to the serum activated with Fe_2O_3 particles compared to no migration observed for the cells exposed to the serum activated with the same Fe_2O_3 particles in a serum, plasma and LLF corona. It was interesting to note that after 200 seconds the rate of cell migration was lowest (7.47%) in the cells exposed to serum activated with Fe_2O_3 in a LLF corona compared to the same particles in a plasma (9.66%) and serum (47.18%) corona. This trend was also observed for the Fe_3O_4 particles. A similar effect was seen in the transwell assay (i.e. that the LLF inhibited migration) although in the transwell assay it was not found to be a significant effect. Observation of these cells exposed to RPMI diluted with serum activated with particles (iron and silica) in a LLF corona during the experiment revealed the cell morphology did not change noticeably and the cell shape remained rounded in a similar manner to the control cells. However, conformational changes were observed immediately in the cells that were exposed to serum activated with the naked particles or those in their serum and plasma corona. Long tails were observed during cell movement. Similar trends were observed for the cells treated with RPMI diluted in serum activated with silica particles (with and without their associated hard corona) although the overall the percentage of migration was lower than that observed for the iron treated cells. There was one exception; cells exposed to serum activated with 50nm SiO_2 in its LLF corona produced 79% migration.

Confocal analysis of the cells after exposure to the activated serum samples was carried out in order to further examine the cell morphology. The cells were stained for actin which was present in the long tails of the cells. These cell protrusions were very clear in the migrating macrophages. However those cells that were exposed to RPMI diluted with serum activated with the plain particles did not behave in a similar manner. Also these long protrusions were not so apparent in the cells after exposure to RPMI containing serum activated with silica NM or in any of the serum cells imaged after exposure to serum activated with particles in their LLF corona.

The cytokines IL-1β, TNF-α, IL-10 and MCP-1 release were examined in the media saved after microfluidic chemotactic analysis by FACS array. Serum activated with both the 200nm and the 50nm silica particles did not produce any measurable cytokine release. In comparison, the media from the Fe_2O_3 treated serum experiments did produce detectable levels of all cytokines investigated and the levels were significantly lower than those produced by cells after exposure to the positive activated serum control. It was interesting to note that the MCP-1 levels were highest in the Fe_2O_3 treated sample. This monocyte chemotactic protein (which is produced primarily by macrophages and endothelial cells) is a potent chemotactic factor for macrophages. It was observed from the microfluidic chemotactic data that the Fe_2O_3 treated serum did result in enhanced migration compared to all other samples and the confocal images of these cells revealed long actin tails. The transwell chemotactic data also shows that migration of the cells treated with Fe_2O_3 treated serum was higher than most other samples tested. It did not cause a greater amount of migration when compared to the Fe_3O_4 serum activated sample. In all cases the cells exposed to Fe_3O_4 treated serum produced lower quantities of cytokine. This is particularly evident in the cells exposed to the serum activated with Fe_3O_4 in a serum corona which did not have any detectable levels of cytokine release. Overall the Fe_2O_3 treated cells had the highest levels of measurable cytokine production. This was found to be statistically significant from those detected in Fe_3O_4 treated cells. Although there was a release of TNF-α observed (another product of activated macrophages) measured after exposure to serum activated with Fe_3O_4 particles in their 10%

plasma corona and in their LLF corona it was found not significant. The presence (or absence) of cytokines in a sample reflects a complex relationship between activation/production and inhibitory signals acting on the J774.A1 macrophage and thus care should be given to data that associates the presence or absence of detectable cytokine levels to their activity or their absence

As described previously, it was concluded that the protein corona of the NMs changed the particle biological identity activity and impacted on their *in vitro* cytoxicity. For example, Chapter 3 describes how binding of serum and blood plasma proteins to iron oxide nanoparticles reduces cytoxicity to macrophages, there was a significant difference between the percentage LDH release from cells exposed to the untreated and LLF coated particles than those exposed to serum or plasma coated particles. In Chapter 4 we also describe how the corona altered the toxicity of silica particles in the case of the plasma corona reduced toxicity. There have also been published reports that the corona mitigates toxicity as mentioned in Chapter 3 and 4 (see [162, 163]). As complement proteins are part of the innate and/or adaptive immune responses [245], the ability of iron and silica particles to activate complement in serum was investigated and it is interesting to note that the corona also had an impact on the cell migration as indicated by the chemotactic assays.

Although the main aim of this thesis was not to correlate the ability of NMs to generate chemotactic factors in serum to their toxicity some trends were seen. For example, naked Fe_2O_3 particles were more toxic (as measured by LDH release) than the same particles in its serum and plasma corona using a macrophage cell line. We can see from both the microfluidic chemotactic assay and transwell chemotactic assay that the plain Fe_2O_3 particles did generate chemotactic factors in serum and had the ability to cause macrophage migration at a higher rate than the same particles with a serum or plasma corona and the cells exposed to media in serum activated with plain Fe_2O_3 NMs released a greater amount of MCP-1. However this trend was not observed for all treatments and the same particles with a LLF corona was seen to be as toxic as the plain particles (LDH release in J774.A1 cell line) and these particles did generate chemotactic factors in serum, however it did not have a significant impact on cell migration compared to the

plain particles. This same trend was observed for the Fe_3O_4 particles, in that the naked and LLF corona particles were more toxic than the particles in its plasma and serum corona. The microfluidic chemotactic assay and the 24 hour transwell chemotactic assay show that these plain particles caused a high rate of cellular migration, again however it was seen that the cells exposed to media containing serum activated by Fe_3O_4 with a LLF corona was not observed to cause a high rate of cellular migration.

5.5 Conclusion

The aim of this study was to determine if serum exposed to NMs can cause the generation of chemoattractant factors, to determine if NMs differed in their ability to activate chemoattractants in serum and to investigate the ability of NMs with their associated plasma, serum and LLF corona to activate complement factors in serum as seen by the ability of the activated serum to induce macrophage migration. The results suggest serum when exposed to iron oxide and silica NMs at 62.5µg/ml induces the generation of a component which can induce significant increases in macrophage chemotaxis *in vitro* compared to serum exposed to PBS. There was no difference between the ability of the iron oxide and silica NM activated serum to induce macrophage migration.

This study also suggests that the corona can impact on cell migration. In particular, the Fe_2O_3 NM with its associated plasma and serum corona and the silica (50nm) particles in a plasma corona produced an increased response in macrophage migration compared with the ZAS.

The use of a more physiologically relevant microfluidic model allowed a more in-depth view of how J774.A1 cells responded to the activated serum samples. It was shown that the cells migrated immediately after exposure to the RPMI with the activated serum. In particular the serum activated with plain iron oxide particles produced the greatest response in terms of the number of migrating cells. Confocal microscopy revealed long actin tails formed by these cells as they migrated. The LLF corona inhibited the cell migration and these cells did not appear to alter in their confirmation or become polarised. Morphologically, they remained rounded and did not migrate at the similar rate to all the other samples apart from 50nm silica. There were no detectable levels of MCP-1, IL-8, TNF-α and IL-10 in the media from silica treated cells, the greatest levels where detected in after exposure serum activated with Fe_2O_3 particles. Overall, the study suggests that the iron particles without their plasma, serum and LLF corona are more active in producing chemoattractant products in serum than the same particles in their serum or plasma LLF corona.

Chapter 6 Discussion and Summary

The introduction to this thesis described the increase in the number of studies investigating nanotoxicology over the last decades. Despite numerous *in vivo* and *in vitro* studies examining the cytotoxic effects of NMs there is no conclusive position regarding their safety or toxicity and although the knowledge base continually increases, we are still only beginning to understand how NMs interact with biological systems. There are various reasons for this, including the fact that NMs represents a diverse range of materials. NMs of the same materials can be created or functionalised in a variety of methods which confers unique physical and chemical properties. For example, the cytotoxicity of iron oxide NMs can be mediated by the presence or absence of polymer coatings [246, 247]. Another layer of complexity is introduced when it is considered that given the large variety of testing methods and endpoints the same type of NM (i.e. naked, coated or functionalised) can produce variable *in vitro* toxicity data making it difficult to come to a consensus regarding their toxicity. These challenges encountered when using classical toxicological assays can to some extent be overcome with extensive NM characterisation. Such extensive characterisation allows not only for better experimental design, such as modification of standard assays to suit the test NMs but also allows for critical analysis of results obtained from standard toxicological assays that are not designed specifically for NMs. This results in a stronger correlation between biological endpoints and particle properties [210]. The first conclusion of this thesis suggests that NMs demand comprehensive characterisation and the successful interpretation of any nanotoxicological assay relies on such characterisation.

6.1 Characterisation

Initially this study extensively characterised a set of iron oxide NMs. The lack of nano specific characterisation tools available, the use of characterisation methods which have evolved from techniques employed in the non-nano field (such as the study of colloids and ultrafine particles) and the diversity of information required for full characterisation leads to a conclusion that a range of techniques are required for useful characterisation. A range of techniques is therefore required to

make up for the lack of a gold standard. Such a combined approach can help to build an understanding of the complex nature of particles at the nanoscale and how their physicochemical characteristics relate to their biological behaviour or toxicity. The interpretation of this data is of course also important as many techniques employed in NM characterisation are difficult to analyse. For example, DLS, which is a fast and effective way of evaluating the hydrodynamic size of NMs under conditions that resemble the *in vivo* situation, produces size results that can be represented in a variety of ways such as intensity, volume and number distributions. The characterisation studies used in this work, to examine the size of NMs, produced different results depending on the technique used. Each technique adds an extra layer of information which complements each other. For example, DLS and NTA analysis effectively measure the same property, hydrodynamic diameter. However, each technique operates in a unique way. Where DLS can give information on the NM behaviour over time and can also investigate the zeta potential, it does tend to give results bias towards the larger particles in the sample, as the technique works by calculating the intensity of scattered light. As large particles scatter more light than smaller particles, masking of the presence of the small particles may occur. However, NTA analysis does not measure the intensity of scattered light like DLS, but allows NMs to be analysed individually thus avoiding any bias towards the larger particles in the sample. It is important to note the limitations of each technique. For example, DLS can only be used with spherical particles and although TEM may produce visual data, the technique itself may cause particle agglomeration. NTA analysis is not accurate for concentrated samples requiring dilutions to be made for accurate analysis. It is at this point that interpretation of data and experience in sample characterisation is vital. This study concludes that it is not sufficient to rely on the manufacturers specifications of particle characteristics and particles should be characterised extensively by more than one technique.

6.2 Nanomaterial Cytotoxicity in a J774.A1.AI cell line

This thesis aimed to investigate if the properties of the NMs affect their cytotoxicity using a macrophage (J774.A1) cell line. Initially this hypothesis was explored with iron oxide particles. However extensive characterisation of the iron

oxide NMs revealed that of the three particle types used in the study, there was no difference between the 280nm and the 22nm Fe_2O_3 particles in terms of size, size distribution and ZP. Thus the work progressed with 280nm Fe_2O_3 and the 45nm Fe_3O_4 particles only. As these are two separate types of iron oxide particle (Fe_2O_3 and Fe_3O_4) it was not possible to directly compare their cytotoxicity in a way that revealed any correlation between their physical chemical properties and their cytoxicity. However, it was interesting to note that there was no difference between the two particle types in their cytotoxicity (as assessed by LDH release or mitochondrial function). The study indicates that relatively large concentrations (62.5µg/ml) of iron oxide particles were required to induce a cytotoxic effect. It is difficult to compare these results with the published literature as there is a large volume of data on iron oxide toxicity. The literature reports results for different types of iron oxide particles, *in vitro* using several cell lines and *in vivo* with different models or testing many endpoints, using different methods to determine toxicity, such as cytotoxicity, viability and oxidative stress, etc. Many studies (for example as reviewed by Mahmoudi *et al.* [144]) do show that these types of NMs are tolerated at high levels and therefore this data, using two separate endpoints, does seem to support this.

The cytotoxicity investigation of four different types of silica NMs in the J774.A1 macrophage cell line suggests that that the physical properties (size and charge) did have an impact the cytoxicity (LDH release and cell viability). At low concentrations (3.9 and 7.8µg/ml) the WST-1 assay revealed that the 50nm plain particles were more cytotoxic than the 200nm particles. It was also seen that the 50nm particles released more measurable LDH than the 200nm. There was no significant difference between the 200nm $Si0_2NH_2$ and the 50nm $Si0_2NH_2$ NMs in terms of their impact on cell viability. This work does correlate well with published literature which suggests that anamorphous silica NMs can have acute *in vitro* and *in vivo* effects as discussed in Chapter 4 and in particular studies have reported that these in acute toxicity to be a size dependant response (*in vitro* [248-251] and *in vivo* (mouse model) [252, 253]).

6.3 Nanomaterial - Protein Interactions and the Hard Corona

This thesis investigated the hypothesis that the protein corona of NMs can determine their biological identity *in vitro.* In order to achieve this, the protein 'profile' or identity of the corona was examined. The protein corona of iron oxide and silica NMs in plasma, serum and LLF was examined to investigate whether or not the size, composition and charge influenced the affinity and degree of protein binding. The plasma and serum corona were chosen to best compare the *in vivo* and *in vitro* situation and in order to model inhalation exposure followed by translocation, a corona of LLF followed by creation of a plasma and serum corona was also investigated using each particle type. The particles in a plasma, serum and LLF corona were analysed using SDS-PAGE and mass spectroscopy.

This thesis shows that the protein profile of the NM coronas vary depending on the NM type, size and charge. The amount of protein bound to the iron oxide particle surface was measured by DCS and it was found that the corona shell dept varied according to the type of particle (Fe_20_3 or Fe_30_4). Further to this the SDS-PAGE results reveal the corona can significantly vary in composition depending on the concentration of protein the particles are suspended in and also on the type of biological fluid they are suspended in (plasma, serum or LLF). Investigation of the silica corona found that the binding patterns had some similarities to those observed with iron particles in that the silica particle corona varied according to the particle size (50nm or 200nm) and just as was discovered with the iron particles the protein binding patterns differed not only when in different concentrations of the same biological fluid (i.e. 10% and 55% plasma) but also between plasma and serum and LLF. Overall the effect of particle charge did not appear to affect the protein profile of the corona however the SDS-PAGE gels do reveal a difference in the binding patterns of the 50nm plain and amino modified silica particles in the serum corona. Thus this thesis shows that particle - protein interactions vary according to (i) the type of nanomaterial (silica or iron) used (ii) the biological fluid used to create the corona (serum or plasma or LLF), (iii) the concentration of the biological fluid used and also on (iv) on precoating in LLF. It is interesting to note that not only the type of biological material, but the concentration of that material impacts on the protein binding profile of the corona.

Although this has not been extensively researched in the published literature to the extent undertaken here, recent published literature does reveal that the composition of the protein corona does depends on the size, shape, and composition of the nanomaterial and the type of physiological environment in which it is exposed as discussed in Chapter 3 and 4 (see [102, 154, 212]. In particular a recent publication has shown that NMs (silica NMs) surface in bovine serum and in human serum varies (as this thesis finds) and recommends that human serum, rather than the animal serum, should be used while conducting *in vitro* research [254]. This study also reports that the most abundant protein in the serum and plasma corona of silica particles to be albumin, but they also found (as this thesis work shows) apolipoproteins and complement proteins to be part of the corona profile of silica NMs. Although there is a limited amount of published work in this filed to date those that have investigated the corona in this way do show that particles bind these proteins (e.g. [151] for polystyrene and silica NMs; [153] for silica and polystyrene particles [154] for polystyrene particles; and [212] review of 63 different types of NMs).

The quantities of proteins that make up the hard corona vary, not only in type, but in quantity between plasma and serum. The work presented in this thesis suggests that the most abundant proteins isolated from the Fe_2O_3 plasma corona and in the LLF/10%P corona were the same although their relative order of abundance was different. These proteins in common were apolipoprotein B-100, complement C3 and albumin. The Fe_2O_3 plasma corona was also found to contain apolipoprotein (a) and complement C4-A. For the Fe_2O_3 particles in its associated serum or LLF/10%S corona the most abundant proteins included albumin, apolipoprotein A-1 and proteins involved in cell adhesion (desmoglein-1, cystatin-A and fibronectin). The LLF/10%S the corona included apolipoprotein A-I, alpha-1-antitrypsin, Ig gamma-1chain C region and Ig kappa chain C region.

Similar to Fe_2O_3 particle the most abundant proteins in the 200nm silica NM plasma hard corona included apolipoprotein B-100 complement C3 complement C4-A and albumin. In addition, it also included histidine rich glycoprotein. The abundance of these proteins varied before and after precoating in LLF. Again the corona of the 200nm silica particle in the serum corona was similar to the Fe_2O_3

particle and the most abundant proteins were again found to include serum albumin and apolipoporotein B-100 with the addition of apolipoprotein A-1, again after preincubation with LLF the relative abundance of these proteins varies slightly.

It is interesting to see how the protein profile differs between particles in their serum corona and particles in their plasma corona suggesting the biological identity of these particles will be different *in vivo* and *in vitro*. Also the protein profile of the particles first preincubated in LLF and then in plasma or serum are different again implying that the biological identity of these particles can be different upon inhalation as opposed to injection. It is also interesting to note that both the iron and silica particles bind common proteins (in particular apolipoproteins and complement proteins as well as albumin). The ability to investigate the protein corona and quantify the protein profile in this manner may offer scope in relating the toxicity of particles to a particular route of exposure. If we take into account the physiological relevance of these proteins it may be possible to hypothesise what effect such binding may have. Take for example the finding that both the silica and iron particles coronas (in serum and plasma) contained apolipoproteins- these proteins are involved in lipid transportation in the bloodstream and thus if they are present in the active form (i.e. if they have not be altered due to binding to the NP surface) it may affect the intracellular trafficking and transport of NMs in the body. Another protein found to be present in both the silica and iron serum and plasma coronas were complement proteins. Complement proteins (as discussed in Chapter 5) play a central role in the activation of the complement system and thus are part of the body's non specific innate immune response, providing the mechanism to protect against infections and support the repair of damaged tissues. The ability of the particles to bind these types of proteins is very relevant in toxicological investigations. Complement binding therefore could lead to particle opsonization promoting receptor mediated phagocytosis *in vivo.*

6.4 The Hard Corona and Cytotoxicity

Following exposure of the macrophage cell line to the iron oxide particles(both the 280nm and the 45nm particles) there no difference in cytoxicity in terms of the percentage LDH release) between plain particles and those with a LLF corona. However, cytotoxicity was lower after exposure (for the 280nm and the 45nm particles) in both their serum and protein corona suggesting that the presence of the plasma and serum corona somehow mitigated cytotoxicity. Furthermore the particles in their plasma corona caused less LDH release than serum coated particles suggesting that these two media were not identical in terms of altering the cytotoxic response to the particles. Overall, this shows that the biological identity of the NM changes *in vitro* depending on their corona.

The silica particles did not produce the same results as the iron oxide NMs in that there was no significant difference in the percentage LDH release after exposure to 200nm SiO_2 particles and those with either a plasma or a serum corona. Therefore, it was not the case that this serum and plasma corona reduced the toxicity of the 200 nm SiO_2 as was seen for the iron oxide particles. However, despite this difference, the silica particles in their plasma corona were found to be significantly less cytotoxic than the serum and LLF coated particles. The results also suggested that the particles with a LLF corona were more toxic than the naked non coated particles, an observation that was not made for the iron oxides.

The effects of positively charged SiO_2 (200nm) on cytotoxicity were also investigated. Statistical analysis found that the only significant difference observed after exposure to 200nm SiO_2 NH_2 was between the particles dispersed in media only and the LLF coated particles where, in contrast to the uncharged 200nm SiO_2, the LLF reduced toxicity. Plasma and serum derived corona did not alter the cytotoxicity of these particles. In contrast, for the 50nm SiO_2NH_2 particles, plasma, serum of LLF corona all significantly reduced toxicity to the J774.A1 cells. It is unclear why the NH_2 200nm SiO_2 should be so different to the NH_2 50nm $Si0_2$ particles with respect to the lack of protection against their cytotoxicity in the presence of serum or plasma in particular when it was found that there was no difference in their cytoxicity when compared without the corona.

The literature available on the hard corona of particles has tended in the past to be more descriptive, examining ways to investigate the corona or characterise it rather than relate it to its toxicity. However, recent papers are emerging which correlate the corona to toxicity, finding that serum proteins bound to particles (carbon nanoparticles and graphine) mitigates cytotoxicity *in vitro.* This study shows a similar trend for iron oxide particles but indicates that the LLF corona may increase the toxic potential of silica particles.

The work presented here also suggests that the particles with and without a plasma, serum and LLF corona may affect the cell migration or chemotaxis of macrophages *in vivo,* as the *in vitro* findings from the chemotactic assay report that both iron oxide and silica particles when exposed to serum at 62.5µg/ml can induce significant increases in macrophage attraction. This thesis finds the corona also plays a role in impacting this ability as the results show that particles without a protein corona allowed for an increased response in the ability to effect macrophage migration

6.5 Implications for *in vivo* interpretations

This study suggests that the cytoxicity of the NMs is dependent on the medium in which they are suspended, more specifically, that the cytoxicity is dependent upon the protein profile of the hard corona of the particles. Thus it is the hard corona profile that is important in toxicological terms. However, the nature of the hard corona is dependent upon the physical and chemical characteristics of the particles. When developing *in vitro* assays it is important to keep this in mind, that *in vitro,* particles will associate with serum proteins and so the biological identity of the particles will be different from the same particles *in vivo,* where the particles associated with biological fluids such as LLF or blood plasma proteins. If *in vitro* tools are to be relevant in reflecting the *in vivo* toxicity of particles, this must be considered and all the advantages of *in vitro* cytotoxicity testing (speed, cost and elimination of testing on animals) will only be realised if the protein corona is taken into account. As such this research suggests a role for designing particles preparation protocols that mimic the corona composition *in vivo* to better study cellular responses *in vitro*.

6.6 Future work

Research on the protein corona is in its infancy and as much as this thesis has answered the research questions posed regarding the biological identity of the NMs it has also provided additional research questions. This thesis focused on identifying proteins of the corona and investigating how the corona affects the cytotoxicity however it would be interesting to examine the nature of the protein binding to determine if adsorption of proteins incurs any conformational change in the protein tertiary structure. Given that NMs adsorb specific proteins it would be interesting to investigate further how different NMs may affect the levels of certain proteins in the body, i.e. would protein adsorption to NMs lead to a depletion of critical proteins in the body or could protein adsorption allow for the delivery of large amounts of proteins to a target organ. Having found that it is possible to characterise the protein corona future work could also investigate if any possible correlation between the proteins profile of a specific particle corona and a cytotoxic effect *in vitro.*

Ultimately as NM toxicological effects are complex and involve a variety of factors, future work could always investigate the different modes of action, if/how particles are taken up by cells and to what extent the corona plays in uptake in various models. This work shows that solely relying on the physicochemical effects of NMs without consideration of their physical environment or characterisation will lead to erroneous results and to date the published literature does find conflicting toxicity results for identical NMs. Thus future work to investigate modes of action or uptake in various models as mentioned above will need to consider two main points (i) characterisation of the particles in a pertinent environment (ii) characterisation of the particles may result in having to alter standard *in vitro* assays to take into account the new information on particle characteristics (such as particle adsorption, sedimentation or biological identity in different cell culture media). Indeed this last point on the need to quality control or custom designed *in vitro* cytoxicity assays represents a large body of work (given the diversity of NMs in the market) and although it is not the most exciting of laboratory work it would be the first step in advancing this field into a more harmonious future. It would allow comparison of toxicological results from

laboratories across the world and could help in delivering a consensus or a new paradigm on NM toxicity. At the very least such a project would decrease the conflicting published literature and aid in comparison of toxicological reports.

6.7 Concluding Remarks

- NM characterisation is paramount in any nanotoxicological investigation.

- It is not sufficient to rely on the NM manufacturers/suppliers physicochemical specifications instead characterisation experiments should be conducted before the investigation in an environment that best represents *in vivo* behaviour of NMs.

- Given the absence of nano-specific characterisation methods and the number of measurable NM parameters (size, morphology, composition, charge, etc.) a range of characterisation tools is recommended when characterising NMs.

- Toxicity (LDH release) of 45nm iron oxide in a macrophage lines after 4 hours was only seen at high concentrations (500µg/ml). Toxicity (LDH release) was seen for both the 280nm and 45nm iron oxide particle. After twenty four hours exposure toxicity as seen (LDH release) for both particle types at 62.5µg/ml. There was no significant difference between the 2 particles. The percentage viability of the macrophages after exposure to Fe_2O_3 280nm and Fe_3O_4 45nm particles after 24 hours exposure showed a dose dependent increase in cytotoxicity as assessed by WST-1.

- The cytotoxicity results obtained from the studies with silica particles found that the physical properties (size and charge) did have an impact the cytoxicity (LDH release and cell viability).

- This thesis shows that the protein profile of the NMs vary depending on the NM type size and charge. The quantities of proteins that make up the

hard corona vary, not only in type, but in quantity between plasma and serum.

- There is a clear difference but also similarities in the biological identity of the particles in plasma, serum and in LLF.

- Iron oxide and silica NMs exposed to serum induces the generation of a component which can induce significant increases in macrophage attraction *in vitro* compared to serum exposed to PBS and the presence of a protein corona can impact this migration.

References

1. Johnston, H., et al., *Investigating the Relationship Between Nanomaterial Hazard and Physicochemical Properties: Informing the Exploitation of Nanomaterials within Therapeutic and Diagnostic Applications.* Journal of Controlled Release, 2012. **164**(3): p. 307-313
2. Feynman, R.P., *There's Plenty of Room at the Bottom- An Invitation to Enter a New Field of Physics.* Resonance: Journal of Science Education, 1960. **16** (9): p. 890-905.
3. European-Commission2011, *Commission Recommendation on the Definition of Nanomaterial.* 2011/696/EU [online]. Available from:http://eurlex.europa.eu/LexUriServ/LexUriServ.do?uri=OJ:L:2011 :275:0038:0040:EN:PDF [Accessed Nov 2012].
4. JRC-Reference-Report2010, *Considerations on a Definition of Nanomaterial for Regulatory Purposes.* EUR 24403 EN [online] Available from:http://ec.europa.eu/dgs/jrc/downloads/jrcreferencereport201007 nanomaterials .pdf [Accessed Nov 2012].
5. Laurent, S., et al., *Magnetic Fluid Hyperthermia: Focus on Superparamagnetic Iron Oxide Nanoparticles.* Advanced Colloid Interface Science, 2011. **166**(1-2): p. 8-23.
6. Rahman, I.A. and V. Padavettan, *Synthesis of Silica Nanoparticles by Sol-gel: Size-dependent Properties, Surface Modification, and Applications Insilica-Polymer Nanocomposites - A review.* Journal of Nanomaterials, 2012. **2012**: p. 15.
7. Gao, H., Xu, B., *Applications of Nanomaterials Inside Cells.* Nano Today, 2009. **4** (3): p. 281.
8. Green-Technology-Forum-Report2007, *Nanotechnology for Green Building.* [online] Accessed from: http://esonn.fr/esonn2010/xlectures /mangematin/Nano_Green_Building55ex.pdf [Accessed Oct 2011].
9. Chaudhry, Q., et al., *Applications and Implications of nNanotechnologies for the Food Sector.* Food Additives and Contaminants, 2008. **25**(3): p. 241-258.
10. Khin, M.M., et al., *A Review on Nanomaterials for Environmental Remediation.* Energy & Environmental Science, 2012. **5**(8): p. 8075-8109.

11. Roadmap-Report-Concerning-the-Use-of-Nanomaterials-in-the-Energy-Sector2006, [Online] Accessed from: http://www.scribd.com/doc /102129338/Roadmap-Report-Concerning-the-Use-of-Nanomaterials-in-the-Energy-Sector [Accessed Nov 2012].
12. The-Royal-Society-and-Royal-Academy-of-Engineering2004, *Nanoscience and Nanotechnologies: Opportunities and Uncertainties [Online] Accessed from:http://www.raeng.org.uk/news/publications/list /reports /nanoscience_nanotechnologies.pdf [Accessed Nov 2012]*.
13. Tsuzuki., T., *Commercial Scale Production of Inorganic Nanoparticles.* International Journal of Nanotechnology, 2009. **6** (5/6): p. 567 - 578.
14. Types-and-Uses-of-Nanomaterials-Including-safety-Aspects-Accompanying-the-Communication-from-the-Commission-to-the-European-Parliament-the-Council-and-the- and European-Economic-and-Social-Committee-on-the-Second-Regulatory-Review-on-Nanomaterials2012, *[Online] Accessed from: http://ec.europa.eu/nanotechnology/pdf/second_regulatory_review_on_nanomaterials_-_staff_working_paper_accompanying_com(2012)_572.pdf [Accessed Feb 2013]*.
15. The-Project-on-Emerging-Nanotechnologies, [Online] Available from: http://www.nanotechproject.org/investories/consumer [Accessed Dec 2012].
16. Aitken, R.J., et al., *Manufacture and Use of Nanomaterials: Current Status in the UK and Global Trends.* Occupational Medicine-Oxford, 2006. **56**(5): p. 300-306.
17. Johnston, H.J., et al., *Evaluating the Uptake and Intracellular Fate of Polystyrene Nanoparticles by Primary and Hepatocyte Cell Lines in vitro.* Toxicology and Applied Pharmacology, 2010. **242**(1): p. 66-78.
18. Sohaebuddin, S., et al., *Nanomaterial Cytotoxicity is Composition, Size, and Cell Type Dependent.* Particle and Fibre Toxicology, 2010. **7**(1): p. 22.
19. Wang, T., et al., *Cellular Uptake of Nanoparticles by Membrane Penetration: A Study Combining Confocal Microscopy with FTIR Spectroelectrochemistry.* ACS Nano, 2012. **6**(2): p. 1251-9.

20. Mu, Q., et al., *Mechanism of Cellular Uptake of Genotoxic Silica Nanoparticles.* Particle and Fibre Toxicology, 2012. **9**: p. 29.
21. Jani, P., et al., *The Uptake and Translocation of Latex Nanospheres and Microspheres after Oral-Administration to Rats.* Journal of Pharmacy and Pharmacology, 1989. **41**(12): p. 809-&.
22. Oberdorster, G., E. Oberdorster, and J. Oberdorster, *Nanotoxicology: An Emerging Discipline Evolving from Studies of Ultrafine Particles.* Environmental Health Perspectives, 2005. **113**(7): p. 823-839.
23. Oberdorster, G., et al., *Extrapulmonary Translocation of Ultrafine Carbon Particles Following Whole-Body Inhalation Exposure of Rats.* Journal of Toxicology and Environmental Health, 2002. **65**(20): p. 1531-1543.
24. Oberdorster, G., V. Stone, and K. Donaldson, *Toxicology of Nanoparticles: A Historical Perspective.* Nanotoxicology, 2007. **1**(1): p. 2 - 25.
25. Nel, A.E., et al., *Understanding Biophysicochemical Interactions at the Nano-Bio Interface.* Nature Materials, 2009. **8**(7): p. 543-557.
26. Donaldson, K.S., A., *A Short History of the Toxicology of Inhaled Particles.* Particle and Fibre Toxicology, 2012. **May**(9): p. 13.
27. Dockery, D.W., et al., *An Association Between Air-Pollution and Mortality in 6 United-States Cities.* New England Journal of Medicine, 1993. **329**(24): p. 1753-1759.
28. Kappos, A.D., et al., *Health Effects of Particles in Ambient Air.* International Journal of Hygiene and Environmental Health, 2004. **207**(4): p. 399-407.
29. Peters, A., et al., *Increased Particulate Air Pollution and the Triggering of Myocardial Infarction.* Circulation, 2001. **103**(23): p. 2810-2815.
30. Pope, C.A., et al., *Lung Cancer, Cardiopulmonary Mortality, and Long-Term Exposure to Fine Particulate Air Pollution.* Journal of the American Medical Association, 2002. **287**(9): p. 1132-1141.
31. Pope, C.A., et al., *Cardiovascular Mortality and Long-Term Exposure to Particulate Air Pollution - Epidemiological Evidence of General Pathophysiological Pathways of Disease.* Circulation, 2004. **109**(1): p. 71-77.

32. Donaldson, K.S., V., *Current Hypotheses on the Mechanisms of Toxicity of Ultrafine Particles.* Annali dell'Istituto superiore di sanità, 2003. **39**(3): p. 405-410.
33. Monteiller, C., et al., *The Pro-Inflammatory Effects of Low-Toxicity Low-Solubility Particles, Nanoparticles and Fine Particles, on Epithelial Cells in vitro: The role of Surface Area.* Occupational and Environmental Medicine, 2007. **64**(9): p. 609-615.
34. Oberdorster, G., *Pulmonary Effects of Inhaled Ultrafine Particles.* International Archives of Occupational and Environmental Health, 2001. **74**(1): p. 1-8.
35. Mossman, B., W. Light, and E. Wei, *Asbestos - Mechanisms of Toxicity and Carcinogenicity in the Respiratory-Tract.* Annual Review of Pharmacology and Toxicology, 1983. **23**: p. 595-615.
36. Mossman, B.T. and A. Churg, *Mechanisms in the Pathogenesis ofAsbestosis and Silicosis.* American Journal of Respiratory and Critical Care Medicine, 1998. **157**(5): p. 1666-1680.
37. Verma, A. and F. Stellacci, *Effect of Surface Properties on Nanoparticle-Cell Interactions.* Small, 2010. **6**(1): p. 12-21.
38. Zhao, F., et al., *Cellular uptake, intracellular trafficking, and cytotoxicity of nanomaterials.* Small, 2011. **7**(10): p. 1322-37.
39. Hubbell, J.A. and A. Chilkoti, *Nanomaterials for Drug Delivery.* Science, 2012. **337**(6092): p. 303-5.
40. Kunzmann, A., et al., *Efficient Internalization of Silica-Coated Iron Oxide Nanoparticles of Different Sizes by Primary Human Macrophages and Dendritic Cells.* Toxicology Applied Pharmacology, 2011. **253**(2): p. 81-93.
41. Doherty, G.J. and H.T. McMahon, *Mechanisms of Endocytosis.* Annual Review of Biochemistry, 2009. **78**: p. 857-902.
42. Rejman, J., et al., *Size-Dependent Internalization of Particles Via the Pathways of Clathrin- and Caveolae-Mediated Endocytosis.* Biochemistry Journal, 2004. **377**: p. 159-69.
43. Kim, J.S., et al., *Cellular Uptake of Magnetic Nanoparticle is Mediated Through Energy-Dependent Endocytosis in A549 Cells.* Journal of Veterinary Science, 2006. **7**(4): p. 321-6.

44. Fernando, L.P., et al., *Mechanism of Cellular Uptake of Highly Fluorescent Conjugated Polymer Nanoparticles.* Biomacromolecules, 2010. **11**(10): p. 2675-82.
45. Nam, H.Y., et al., *Cellular Uptake Mechanism and IntracellularFate of Hydrophobically Modified Glycol Chitosan Nanoparticles.* Journal of Controled Release, 2009. **135**(3): p. 259-67.
46. Dausend, J., et al., *Uptake Mechanism of Oppositely Charged Fluorescent Nanoparticles in HeLa Cells.* Macromolecular Bioscience, 2008. **8**(12): p. 1135-43.
47. Liu, S.Y., et al., *Effect and Intracellular Uptake of PureMagnetic Fe3O4 Nanoparticles in the Cells and Organs of Lung and Liver.* Chinese Medical Journal, 2009. **122**(15): p. 1821-5.
48. Geiser, M., et al., *Ultrafine Particles Cross Cellular Membranes by Nonphagocytic Mechanisms in Lungs and in Cultured Cells.* Environmental Health Perspectives, 2005. **113**(11): p. 1555.
49. Wang T , et al., *Cellular Uptake of Nanoparticles by Membrane Penetration: A Study Combining Confocal Microscopy with FTIR Spectroelectrochemistry.* ACS Nano, 2012 **6**(2): p. 1251-1259.
50. Dos Santos, T., et al., *Effects of Transport Inhibitors on the Cellular Uptake of Carboxylated Polystyrene Nanoparticles in Different Cell Lines.* PLoS One, 2011. **6**(9): p. 24438.
51. Chithrani, B.D., A.A. Ghazani, and W.C. Chan, *Determining the Size and Shape Dependence of Gold Nanoparticle Uptake into Mammalian Cells.* Nano Letters, 2006. **6**(4): p. 662-8.
52. Marano, F., et al., *Nanoparticles: Molecular Targets and Cell Signalling.* Archives of Toxicology, 2011. **85**(7): p. 733-41.
53. Donaldson, K., Borm,P., *Particle Toxicology*. 2007, New York: Taylor and Francis Group. 7.
54. Orient, A., et al., *Novel Sources of Reactive Oxygen Species in the Human Body.* Nephrology Dialysis Transplantation, 2007. **22**(5): p. 1281-1288.
55. Hensley, K., et al., *Reactive Oxygen Species, Cell Signaling, and Cell Injury.* Free Radical Biology Medicine, 2000. **28**(10): p. 1456-62.

56. Thannickal, V.J. and B.L. Fanburg, *Reactive Oxygen Species in Cell Signaling.* American Journal of Physiology - Lung Cellular and Molecular Physiology, 2000. **279**(6): p. L1005-28.
57. Tetley, T.D., *Health Effects of nNanomaterials.* Biochemical Society Transactions, 2007. **35**: p. 527-531.
58. Nel, A., et al., *Toxic Potential of Materials at the Nanolevel.* Science, 2006. **311**(5761): p. 622-7.
59. Galli, F., et al., *Oxidative Stress and Reactive Oxygen Species.* Contributions to Nephrology 2005. **149**: p. 240-60.
60. Oberdorster, G., et al., *Role of the Alveolar Macrophage in Lung Injury: Studies with Ultrafine Particles.* Environmental Health Perspectives, 1992. **97**: p. 193-9.
61. Stone, V., et al., *The Role of Oxidative Stress in the Prolonged Inhibitory Effect of Ultrafine Carbon Black on Epithelial Cell Function.* Toxicology in Vitro, 1998. **12**(6): p. 649.
62. Duffin, R., et al., *Proinflammogenic Effects of Low-Toxicity and Metal Nanoparticles in vivo and in vitro: Highlighting the Role of Particle Surface Area and Surface Reactivity.* Inhalation Toxicology, 2007. **19**(10): p. 849-56.
63. Duffin, R.T., C.L., Clouter, A., Brown, D.M., MacNee, W., Satone, s., Donaldson, k., *The Importance of Surface Area and Specific Reactivity in the Actue Pulmonary Inflamation Responce to Particles.* Annals of Occupational Hygiene, 2002. **46**: p. 242-254.
64. Brunner, T.J., et al., *In vitro Cytotoxicity of Oxide Nanoparticles: Comparison to Asbestos, Silica, and the Effect of Particle Solubility.* Environmental Science & Technology, 2006. **40**(14): p. 4374-4381.
65. du Bois, R.M., *The Alveolar Macrophage.* Thorax, 1985. **40**(5): p. 321-7.
66. Ravetch, J.V., *Fc Receptors.* Current Opinion in Immunology, 1997. **9**(1): p. 121-125.
67. Jones, G.E., *Cellular Signaling in Macrophage Migration and Chemotaxis.* Journal of Leukocyte Biology, 2000. **68**(5): p. 593-602.
68. Takemura, R. and Z. Werb, *Secretory Products of Macrophages and their Physiological Functions.* American Journal of Physiology, 1984. **246**(1 Pt 1): p. C1-9.

69. Cavaillon, J.M., *Cytokines and Macrophages.* Biomedicine and Pharmacotherapy 1994. **48**(10): p. 445-53.
70. Cavaillon, J.M., et al., *Circulating Cytokines: the Tip of the Iceberg?* Circulatory Shock, 1992. **38**(2): p. 145-52.
71. Aitken, R., et al., *Nanoparticles - One Word: A Multiplicity of Different Hazards.* Nanotoxicology, 2009. **3**(4): p. 263-264.
72. Nanorisk-Framework-Environmental-Defense-DuPont-Nano-Partnership-Report2007, [online] Accessed from: http://apps.edf.org/documents/6496_nano%20risk%20framework.pdf [Accessed Oct 2011].
73. Oberdorster, G., et al., *Principles for Characterizing the Potential Human Health Effects from Exposure to Nanomaterials: Elements of a Screening Strategy.* Particle and Fibre Toxicology, 2005. **2**: p. 8.
74. Borm, P., et al., *The Potential Risks of Nanomaterials: a Review Carried out for ECETOC.* Particle and Fibre Toxicology, 2006. **3**(1): p. 11.
75. Geiser, M. and W.G. Kreyling, *Deposition and Biokinetics of Inhaled Nanoparticles.* Particle and Fibre Toxicology, 2010. **7**: p. 2.
76. Oberdorster, G., J. Ferin, and B.E. Lehnert, *Correlation Between Particle Size, in vivo Particle Persistence, and Lung Injury.* Environmental Health Perspectives, 1994. **102**(5): p. 173-9.
77. Moller, W., et al., *Deposition, Retention, and tTranslocation of Ultrafine Particles from the Central Airways and Lung Periphery.* American Journal of Respiratory and Critical Care Medicine, 2008. **177**(4): p. 426-32.
78. Brain, J.D., et al., *Biologic Responses to Nanomaterials Depend on Exposure, Clearance, and Material Characteristics.* Nanotoxicology, 2009. **3**(3): p. 174-180.
79. Montes-Burgos, I., et al., *Characterisation of Nanoparticle Size and State Prior to Nanotoxicological Studies.* Journal of Nanoparticle Research, 2010. **12**(1): p. 47-53.
80. Elder, A., et al., *Translocation of Inhaled Ultrafine Manganese Oxide Particles to the Central Nervous System.* Environmental Health Perspective, 2006. **114**(8): p. 1172-8.
81. Brown, D.M., et al., *Calcium and ROS-Mediated Activation of Transcription Factors and TNF-alpha Cytokine Gene Expression in*

Macrophages Exposed to Ultrafine Particles. American Journal of Physiology-Lung Cellular and Molecular Physiology, 2004. **286**(2): p. 344-L353.

82. Hosokawa, M., K. Nohgi, and T. Tokoyama, *Nanoparticle Technology Handbook*. 1st ed. 2007, Amsterdam. 644.
83. Brown, D.M., et al., *Size-Dependent Proinflammatory Effects of Ultrafine Polystyrene Particles: a Role for Surface Area and Oxidative Stress in the Enhanced Activity of Ultrafines.* Toxicology Applied Pharmacology, 2001. **175**(3): p. 191-9.
84. Donaldson, K., X.Y. Li, and W. MacNee, *Ultrafine (Nanometre) Particle Mediated Lung Injury.* Journal of Aerosol Science, 1998. **29**(5–6): p. 553-560.
85. Donaldson, K., et al., *Ultrafine Particles.* Occupational and Environmental Medicine, 2001. **58**(3): p. 211.
86. Donaldson, K. and P. Borm, *Particle Paradigms.* Inhalation Toxicology, 2000. **12**: p. 1-6.
87. Brown, D.M., et al., *An in vitro Study of the Potential of Carbon Nanotubes and Nanofibres to Induce Inflammatory Mediators and Frustrated Phagocytosis.* Carbon, 2007. **45**(9): p. 1743-1756.
88. Poland, C.A., et al., *Carbon Nanotubes Introduced into the Abdominal Cavity of Mice Show Asbestos-Like Pathogenicity in a Pilot Study.* Nature Nanotechnology, 2008. **3**(7): p. 423-428.
89. Hamilton, R.F., et al., *Particle Length-Dependent Titanium Dioxide Nanomaterials Toxicity and Bioactivity.* Particle and Fibre Toxicology, 2009. **6**: p. 35.
90. Porter, D.W., et al., *Mouse Pulmonary Dose and Time Course-Responses Induced by Exposure to Multi-Walled Carbon Nanotubes.* Toxicology, 2010. **269**(2-3): p. 136-47.
91. Ryman-Rasmussen, J.P., et al., *Inhaled Carbon Nanotubes Reach the Subpleural Tissue in Mice.* Nature Nanotechnolgy, 2009. **4**(11): p. 747-51.
92. Silva, F.C., et al., *Surface-Charge of Resident, Elicited, and Activated Mouse Peritoneal-Macrophages.* Journal of Leukocyte Biology, 1987. **41**(2): p. 143-149.

93. Goodman, C.M., et al., *Toxicity of Gold Nanoparticles Functionalized with Cationic and Anionic Side Chains.* Bioconjugate Chemistry, 2004. **15**(4): p. 897-900.
94. Lockman, P.R., et al., *Nanoparticle Surface Charges alter Blood-Brain Barrier Integrity and Permeability.* Journal of Drug Targeting, 2004. **12**(9-10): p. 635-641.
95. Renwick, L.C., K. Donaldson, and A. Clouter, *Impairment of Alveolar Macrophage Phagocytosis by Ultrafine Particles.* Toxicology and Applied Pharmacology, 2001. **172**(2): p. 119-127.
96. Wilson, M.R., et al., *Nanoparticle Interactions with Zinc and Iron: Implications for Toxicology and Inflammation.* Toxicology and Applied Pharmacology, 2007. **225**(1): p. 80-89.
97. Borm, P., et al., *Research Strategies for Safety Evaluation of Nanomaterials: Role of Dissolution in Biological Fate and Effects of Nanoscale Particles.* Toxicological Sciences, 2006. **90**(1): p. 23-32.
98. Murphy, F.A., et al., *The Mechanism of Pleural Inflammation by Long Carbon Nanotubes: Interaction of Long Fibres with Macrophages Stimulates them to Amplify Pro-Inflammatory Responses in Mesothelial Cells.* Particle and Fibre Toxicology, 2012. **9**: p. 8.
99. Walczyk, D., et al., *What the Cell "Sees" in Bionanoscience.* Journal of the American Chemical Society, 2010. **132**(16): p. 5761-5768.
100. Hussain, S.M., et al., *In vitro Toxicity of Nanoparticles in BRL 3A Rat Liver Cells.* Toxicology in Vitro, 2005. **19**(7): p. 975-983.
101. Soto, K.F., et al., *Comparative in vitro Cytotoxicity Assessment of Some Manufactured Nanoparticulate Materials Characterized by Transmission Electron Microscopy.* Journal of Nanoparticle Research, 2005. **7**(2-3): p. 145-169.
102. Cedervall, T., et al., *Understanding the Nanoparticle-Protein Corona Using Methods to Quantify Exchange Rates and Affinities of Proteins for Nanoparticles.* Proceedings of the National Academy of Sciences of the United States of America, 2007. **104**(7): p. 2050-2055.
103. Lynch, I. and K.A. Dawson, *Protein-Nanoparticle Interactions.* Nano Today, 2008. **3**(1-2): p. 40-47.

104. Monopoli, M., F. Baldelli, and K. Dawson, *Nanobiotechnology: Nanoparticle Coronas Take Shape.* Nature Nanotechnology, 2011. **6**(1): p. 11-2.

105. Hara, H., et al., *Role of Stent Design and Coatings on Restenosis and Thrombosis.* Advanced Drug Delivery Review 2006. **58**(3): p. 377-86.

106. Navarro, M., et al., *Biomaterials in Orthopaedics.* J R Soc Interface, 2008. **5**(27): p. 1137-58.

107. Williams, D.F., *On the Mechanisms of Biocompatibility.* Biomaterials, 2008. **29**(20): p. 2941-53.

108. Parashar, U.K., P.S. Saxena, and A. Srivastava, *Role of Nanomaterials in Biotechnology.* Digest Journal of Nanomaterials and Biostructures, 2008. **3**(2): p. 81-87.

109. Salata, O., *Applications of Nanoparticles in Biology and Medicine.* J Nanobiotechnology, 2004. **2**(1): p. 3.

110. Powers, K.W., et al., *Characterization of the Size, Shape, and State of Dispersion of Nanoparticles for Toxicological Studies.* Nanotoxicology, 2007. **1**(1): p. 42-51.

111. Warheit, D.B., *How Meaningful are the Results of Nanotoxicity Studies in the Absence of Adequate Material Characterization?* Toxicological Sciences, 2008. **101**(2): p. 183-185.

112. Park, H. and V.H. Grassian, *Commercially Manufactured Engineered Nanomaterials for Environmental and Health Studies: Important Insights Provided by Independent Characterization.* Environmental Toxicology and Chemistry, 2010. **29**(3): p. 715-721.

113. Murdock, R.C., et al., *Characterization of Nanomaterial Dispersion in Solution Prior to in vitro Exposure Using Dynamic Light Scattering Technique.* Toxicological Sciences, 2008. **101**(2): p. 239-253.

114. Clift, M.J., et al., *The Effects of Serum on the Toxicity of Manufactured Nanoparticles.* Toxicological Letters, 2010. **198**(3): p. 358-65.

115. Compagnin, C., et al., *The Cellular Uptake of Meta-tetra (hydroxyphenyl)chlorin Entrapped in Organically Modified Silica Nanoparticles is Mediated by Serum Proteins.* Nanotechnology, 2009. **20**(34).

116. Drescher, D., et al., *Toxicity of Amorphous Silica Nanoparticles on Eukaryotic Cell Model is Determined by Particle Agglomeration and Serum Protein Adsorption Effects.* Analytical and Bioanalytical Chemistry, 2011. **400**(5): p. 1367-1373.
117. Zhu, Y., et al., *Effects of Serum Proteins on Intracellular Uptake and Cytotoxicity of Carbon Nanoparticles.* Carbon, 2009. **47**(5): p. 1351-1358.
118. Brown, D.M., et al., *Interaction Between Nanoparticles and Cytokine Proteins: Impact on Protein and Particle Functionality.* Nanotechnology, 2010. **21**(21).
119. Frazier, J., Bradlaw, JA.,, *Technical Problems Associated with In Vitro Toxicity Testing Systems*. 1989, Johns Hopkins Bloomberg School of Public Health: Maryland.
120. Wang, R., et al., *Generation of Toxic Degradation Products by Sonication of Pluronic(R) Dispersants: Implications for Nanotoxicity Testing.* Nanotoxicology, 2012.
121. Kroll, A., et al., *Current in vitro Methods in Nanoparticle Risk Assessment: Limitations and Challenges.* European Journal of Pharmaceutics and Biopharmaceutics, 2009. **72**(2): p. 370-377.
122. Stone, V., H. Johnston, and R.P.F. Schins, *Development of in vitro Systems for Nanotoxicology: Methodological Considerations.* Critical Reviews in Toxicology, 2009. **39**(7): p. 613-626.
123. Teeguarden, J.G., et al., *Particokinetics in vitro: Dosimetry Considerations for in vitro Nanoparticle Toxicity Assessments.* Toxicology Science, 2007. **95**(2): p. 300-12.
124. Xu, R., *ISO International Standards for Particle Sizing.* China Particuology, 2004. **2**(4): p. 164-167.
125. Malvern-Zetasizer-Nano-User-Manual-(MAN0317)2008, *[online] Accessed from: http://www.nbtc.cornell.edu/facilities/downloads/Zetasizer%20Manual.pdf [Accessed Dec 2010]*.
126. NanoSight-Analytical-Software-Operating-Manual(NTA2.1)2010, [online] Accessed from http://nanobio.physics .ucsb.edu/pdfs/equipment /Nanosight%20NTA2.1%20software%20manual.pdf [Accessed Sept 2012].

127. Nanoparticle-Tracking-Analysis-and-Dynamic-Light-Scattering-A-Comparison2010 *[online] Accessed from www.nanosight.com [accesed on Sept 2012]*.

128. Filipe, V., A. Hawe, and W. Jiskoot, *Critical Evaluation of Nanoparticle Tracking Analysis (NTA) by NanoSight for the Measurement of Nanoparticles and Protein Aggregates.* Pharmaceutical Research, 2010. **27**(5): p. 796-810.

129. CPSInstruments-Disc-Centrifuge-Nanoparticle-Size-Analysis-Manual2007, *[online] Accessed from http://www.cpsinstruments.eu /pdf/General%20Brochure.pdf [Sept 2012]*.

130. Nadlera, M., et al., *Preparation of Colloidal Carbon Nanotube Dispersions and their Characterisation Using a Disc Centrifuge.* Carbon, 2008. **11**(46): p. 1384-1392.

131. Laskin, A. and J.P. Cowin, *Automated single particle SEM/EDX analysis of submicrometer particles down to 0.1 mu m.* Analytical Chemistry, 2001. **73**(5): p. 1023-1029.

132. OrganisationforEconomicCo-operationandDevelopment2010, *List of Manufactured Nanomaterials and List of Endpoints for Phase one of the Sponsorship Programme for the Testing of Manufactured Nanomaterials (Revision) ENV/JM/MONO(2010)46 [online] Accessed From: http://search.oecd.org/officialdocuments/displaydocumentpdf/?cote=env/jm/mono(2010)46&doclanguage=en [Accessed Dec 2011]*.

133. Laurent, S. and M. Mahmoudi, *Superparamagnetic Iron Oxide Nanoparticles: Promises for Diagnosis and Treatment of Cancer.* International Journal of Molecular Epidemiology and Genetics, 2011. **2**(4): p. 367-90.

134. Boyer, C., et al., *The Design and Utility of Polymer-Stabilized Iron-Oxide Nanoparticles for Nanomedicine Applications.* NPG Asia Materials, 2010. **2**: p. 23-30.

135. Pisanic, T.R., 2nd, et al., *Nanotoxicity of Iron Oxide Nanoparticle Internalization in Growing Neurons.* Biomaterials, 2007. **28**(16): p. 2572-81.

136. Teja, A.S. and P.Y. Koh, *Synthesis, Properties and Applications of Magnetic Iron Oxide Nanoparticles.* Progress in Crystal Growth and Characterization of Materials, 2009. **55**(1-2): p. 22-45.
137. Neuberger, T., et al., *Superparamagnetic Nanoparticles for Biomedical Applications: Possibilities and Limitations of a New Drug Delivery System.* Journal of Magnetism and Magnetic Materials, 2005. **293**(1): p. 483-496.
138. Shubayev, V., T. Pisanic, and S. Jin, *Magnetic Nanoparticles for Theragnostics.* Advanced Drug Delivery Reviews, 2009. **61**(6): p. 467-77.
139. MagForce-Nanotechnologies-European-Regulatory-Approval-for-its-Nano-Cancer®Therapy2010, *[online] Accessed from: http://www.magforce.de/en/presse-investoren/news-events/select_category/2.html [Accessed Nov 2010]*.
140. Maier-Hauff, K., et al., *Efficacy and Safety of Intratumoral Thermotherapy Using Magnetic Iron Oxide Nanoparticles Combined with External Beam Radiotherapy on Patients with Recurrent Glioblastoma Multiforme.* The Journal of Neuro-Oncology 2011. **103**(2): p. 317-24.
141. Mandarano, G., et al., *Development and Use of Iron Oxide Nanoparticles (Part 2): The Application of Iron Oxide Contrast Agents in MRI.* Biomedical Imaging and Intervention Journal 2010. **6**(2): p. e12.
142. Lacava, Z.G.M., et al., *Biological Effects of Magnetic Fluids: Toxicity Studies.* Journal of Magnetism and Magnetic Materials, 1999. **201**(1–3): p. 431-434.
143. Hafeli, U.O., et al., *Cell Uptake and in vitro Toxicity of Magnetic Nanoparticles Suitable for Drug Delivery.* Molecular Pharmacology, 2009. **6**(5): p. 1417-28.
144. Mahmoudi, M., et al., *Cell Toxicity of Superparamagnetic Iron Oxide Nanoparticles.* Journal of Colloid and Interface Science, 2009. **336**(2): p. 510-518.
145. Siglienti, I., et al., *Cytokine Profile of Iron-Laden Macrophages: Implications for Cellular Magnetic Resonance Imaging.* Journal of Neuroimmunology, 2006. **173**(1-2): p. 166-73.

146. Zhu, M.T., et al., *Comparative Study of Pulmonary Responses to Nano and Submicron Sized Ferric Oxide in Rats.* Toxicology, 2008. **247**(2-3): p. 102-111.

147. Zhu, M.T., et al., *Particokinetics and Extrapulmonary Translocation of Intratracheally Instilled Ferric Oxide Nanoparticles in Rats and the Potential Health Risk Assessment.* Toxicological Sciences, 2009. **107**(2): p. 342-351.

148. Chen, Z., et al., *Effects of Proteins from Culture Medium on Surface Property of Silanes- Functionalized Magnetic Nanoparticles.* Nanoscale Research Letters, 2008. **4**(3): p. 204-9.

149. Jansch, M., et al., *Adsorption Kinetics of Plasma Proteins on Ultrasmall Superparamagnetic Iron Oxide (USPIO) Nanoparticles.* International Journal of Pharmaceutics, 2012. **428**(1-2): p. 125-133.

150. Lesniak, A., et al., *Effects of the presence or Absence of a Proteincorona on Silica Nanoparticle Uptake and Impact on Cells.* Acs Nano, 2012.

151. Monopoli, M., et al., *Physical-Chemical Aspects of Protein Corona: Relevance to in Vitro and in Vivo Biological Impacts of Nanoparticles.* Journal of American Chemical Society, 2010. **133** (8): p. 2525–2534.

152. Giri, J., et al., *Interactions of Poly(amidoamine) Dendrimers with Human Serum Albumin: Binding Constants and Mechanisms.* Acs Nano, 2011. **5**(5): p. 3456-68.

153. Lundqvist, M., et al., *The Evolution of the Protein Corona around Nanoparticles: A Test Study.* Acs Nano, 2011. **5**(9): p. 7503-9.

154. Lundqvist, M., et al., *Nanoparticle Size and Surface Properties Determine the Protein Corona with Possible Implications for Biological Impacts.* Proceedings of the National Academy of Sciences of the United States of America, 2008. **105**(38): p. 14265-14270.

155. Treuel, L., et al., *The Influence of Surface Composition of Nanoparticles on their Interactions with Serum Albumin.* ChemPhysChem, 2010. **11**(14): p. 3093-9.

156. Huang, Y.F., et al., *Nanoparticle-mMediated IgE-Receptor Aggregation and Signaling in RBL Mast Cells.* Journal of American Chemical Society, 2009. **131**(47): p. 17328-34.

157. Sniadecki, N.J., *A Tiny Touch: Activation of Cell Signaling Pathways with Magnetic Nanoparticles.* Endocrinology, 2010. **151**(2): p. 451-7.
158. Petri-Fink, A., et al., *Effect of Cell Media on Polymer Coated Superparamagnetic Iron Oxide Nanoparticles (SPIONs): Colloidal Stability, Cytotoxicity, and Cellular Uptake Studies.* European Journal of Pharmaceutics and Biopharmaceutics 2008. **68**(1): p. 129-37.
159. Takeda, T., et al., *Serofendic Acid, a Novel Substance Extracted from Fetal Calf Serum, Protects Against Oxidative Stress in Neonatal Rat Cardiac Myocytes.* Journal of the American College of Cardiology, 2006. **47**(9): p. 1882-90.
160. Akaike, A., H. Katsuki, and T. Kume, *Pharmacological and Physiological Properties of Serofendic Acid, a Novel Neuroprotective Substance Isolated from Fetal Calf Serum.* Life Sciences, 2003. **74**(2-3): p. 263-9.
161. Osakada, F., et al., *Serofendic Acid, a Sulfur-Containing Diterpenoid Derived from Fetal Calf Serum, Attenuates Reactive Oxygen Species-Induced Oxidative Stress in Cultured Striatal Neurons.* Journal of Pharmacology and Experimental Therapeutics 2004. **311**(1): p. 51-9.
162. Hu, W.B., et al., *Protein Corona-Mediated Mitigation of Cytotoxicity of Graphene Oxide.* Acs Nano, 2011. **5**(5): p. 3693-3700.
163. Ge, C.C., et al., *Binding of Blood Proteins to Carbon Nanotubes Reduces Cytotoxicity.* Proceedings of the National Academy of Sciences of the United States of America, 2011. **108**(41): p. 16968-16973.
164. Shen, Y.F., et al., *Characterization of the Human Blood Plasma Proteome.* Proteomics, 2005. **5**(15): p. 4034-4045.
165. Anderson, N.L. and N.G. Anderson, *The Human Plasma Proteome - History, Character, and Diagnostic Prospects.* Molecular & Cellular Proteomics, 2002. **1**(11): p. 845-867.
166. OpenStaxCollege-An-Overview-of-Blood, *[online] Accessed from: http://cnx.org/content/m46710/1.4/ [Accessed Aug 2013]*.
167. Freshney, R.I., *Culture of Animal Cells: A Manual of Basic Technique*. 3 ed, ed. I. John Wiley & Sons. 1994.
168. Kendall, M., et al., *Lung Lining Liquid Modifies PM2.5 in Favor of Particle Aggregation: A Protective Mechanism.* American Journal of

Physiology-Lung Cellular and Molecular Physiology, 2002. **282**(1): p. L109-L114.

169. Ng, A.W., A. Bidani, and T.A. Heming, *Innate Host Defense of the Lung: Effects of Lung-Lining Fluid pH.* Lung, 2004. **182**(5): p. 297-317.
170. Interpretation-of-Bronchoalveolar-Lavage-Fluid-Cytology-Interpretation-of-BALF-Cytology-2001, *[online] Accessed from: http://www.ildcare.eu/downloads/informatie/bal_cd.pdf [Accessed Oct 2010]*. 2004.
171. Schleh, C. and J. Hohlfeld, *Interaction of Nanoparticles with the Pulmonary Surfactant System.* Inhalation Toxicology, 2009. **21**(s1): p. 97-103.
172. Bakshi, M.S., et al., *Metal Nanoparticle Pollutants Interfere with Pulmonary Surfactant Function in vitro.* Biophysical Journal, 2008. **94**(3): p. 855-868.
173. European-Collection-of-Cell-Cultures, *[online] Accessed from http://www.hpacultures.org.uk/products/celllines [accesed on Sept 2011]*.
174. Renwick, L.C., et al., *Increased Inflammation and Altered Macrophage Chemotactic Responses Caused by Two Ultrafine Particle Types.* Occupational and Environmental Medicine, 2004. **61**(5): p. 442-447.
175. Papanikolaou, G. and K. Pantopoulos, *Iron Metabolism and Toxicity.* Toxicology and Applied Pharmacology, 2005. **202**(2): p. 199-211.
176. Galey, J.B., *Potential Use of Iron Chelators Against Oxidative Damage.* Advances in Pharmacology, 1997. **38**: p. 167-203.
177. Shander, A., et al., *Iron Overload and Toxicity: Implications for Anesthesiologists.* Journal of Clinical Anesthesia, 2012. **24**(5): p. 419-425.
178. Berg, D., et al., *Brain Iron Pathways and their Relevance to Parkinsons Disease.* Journal of Neurochemistry, 2001. **79**(2): p. 225-36.
179. Altamura, C., et al., *Ceruloplasmin/Transferrin System is Related to Clinical Status in Acute Stroke.* Stroke, 2009. **40**(4): p. 1282-8.
180. Apopa, P.L., et al., *Iron Oxide Nanoparticles Induce Human Microvascular Endothelial Cell Permeability Through Reactive Oxygen Species Production and Microtubule Remodeling.* Particle and Fibre Toxicology, 2009. **6**(1): p. 1.

181. Soenen, S.J. and M. De Cuyper, *Assessing Iron Oxide Nanoparticle Toxicity in vitro: Current Status and Future Prospects.* Nanomedicine 2010. **5**(8): p. 1261-75.

182. Autrup, H., et al., *Ag and TiO2 Nanoparticles Induce Oxidative Stress in A549 Cells.* Toxicology Letters, 2009. **189**(1): p. 181-181.

183. Crosby, M.E., T.R. Downs, and S. Pfuhler, *Silica Nanoparticles Administered at the Maximum Tolerated Dose Induce Oxidative Stress Response Pathway Regulation, Indirectly Causing Genotoxicity.* Environmental and Molecular Mutagenesis, 2011. **52**(1): p. 81-81.

184. Sharma, V., D. Anderson, and A. Dhawan, *Zinc Oxide Nanoparticles Induce Oxidative Stress and Genotoxicity in Human Liver Cells (HepG2).* Journal of Biomedical Nanotechnology, 2011. **7**(1): p. 98-99.

185. Dinischiotu, A., et al., *Magnetite Nanoparticles Induce Oxidative Stress in MRC5 Cell Line.* Free Radical Research, 2009. **43**: p. 62-62.

186. Fahmy, B., Cormier, S., *Copper Oxide Nanoparticles Induce Oxidative Stress and Cytotoxicity in Airway Epithelial Cells.* Toxicology in Vitro, 2009. **23**(7): p. 1365-1371.

187. Huang, C.C., et al., *Zinc Oxide Nanoparticles Induce Oxidative Stress and Alter Calcium Homeostasis in Human Bronchial Epithelial Cells (BEAS-2B).* Free Radical Biology and Medicine, 2008. **45**: p. S31-S31.

188. Kumar, A., et al., *Engineered ZnO and TiO2 Nanoparticles Induce Oxidative Stress and DNA Damage Leading to Reduced Viability of Escherichia coli.* Free Radical Biology and Medicine, 2011. **51**(10): p. 1872-1881.

189. Siddiqui, M.A., et al., *Nickel Oxide Nanoparticles Induce Cytotoxicity, Oxidative Stress and Apoptosis in Cultured Human Cells that is Abrogated by the Dietary Antioxidant Curcumin.* Food and Chemical Toxicology, 2012. **50**(3-4): p. 641-647.

190. Shukla, R.K., et al., *Titanium Dioxide Nanoparticles Induce Oxidative Stress-Mediated Apoptosis in Human Keratinocyte Cells.* Journal of Biomedical Nanotechnology, 2011. **7**(1): p. 100-101.

191. Muresanu, D.F., et al., *Engineered Nanoparticles From Metals Ag, Cu, and Al (50-60 nm) Induce Oxidative Stress, Blood-Brain Barrier Disruption, Neuronal Nitric Oxide Synthase Upregulation, and Cell Injury*

in the Rat Brain. Neuroprotective Effects of Insulin Like Growth Factor-1. Cell Transplantation, 2011. **20**(4): p. 576-576.

192. Naqvi, S., et al., *Concentration-Dependent Toxicity of Iron Oxide Nanoparticles Mediated by Increased Oxidative Stress.* International Journal of Nanomedicine, 2010. **5**: p. 983-989.
193. Baughman, R.P., et al., *Enhancement of Macrophage and Monocyte Cytotoxicity by the Surface Active Material of Lung Lining Fluid.* Journal of Laboratory and Clinical Medicine 1987. **109**(6): p. 692-7.
194. Thode, K., et al., *Determination of Plasma Protein Adsorption on Magnetic Iron Oxides: Sample Preparation.* Pharmaceutical Research, 1997. **14**(7): p. 905-10.
195. Pitek, A.S., et al., *Transferrin coated nanoparticles: study of the bionano interface in human plasma.* PLoS One, 2012. **7**(7): p. e40685.
196. Worle-Knirsch, J.M., K. Pulskamp, and H.F. Krug, *Oops They Did it Again! Carbon Nanotubes Hoax Scientists in Viability Assays.* Nano Letters, 2006. **6**(6): p. 1261-8.
197. Monteiro-Riviere, N.A., A.O. Inman, and L.W. Zhang, *Limitations and Relative Utility of Screening Assays to Assess Engineered Nanoparticle Toxicity in a Human Cell Line.* Toxicology and Applied Pharmacology, 2009. **234**(2): p. 222-35.
198. Sager, T.M., et al., *Improved Method to Disperse Nanoparticles for in vitro and in vivo Investigation of Toxicity.* Nanotoxicology, 2007. **1**(2): p. 118-129.
199. Gosens, I., et al., *Impact of Agglomeration Atate of Nano and Submicron Sized Gold Particles on Pulmonary Inflammation.* Particle and Fibre Toxicology, 2010. **7**(1): p. 37.
200. Bihari, P., et al., *Optimized Dispersion of Nanoparticles for Biological in vitro and in vivo Studies.* Particle and Fibre Toxicology, 2008. **5**: p. 14.
201. Choi, H.S., et al., *Rapid Translocation of Nanoparticles from the Lung Airspaces to the Body.* Nature Biotechnology, 2010. **28**(12): p. 1300-U113.
202. Wang, X., et al., *Engineering Nanomaterial Surfaces for Biomedical Applications.* Experimental Medicine and Biology, 2009. **234**(10): p. 1128-39.

203. Maiorano, G., et al., *Effects of Cell Culture Media on the Dynamic Formation of Protein-Nanoparticle Complexes and Influence on the Cellular Response.* Acs Nano, 2010. **4**(12): p. 7481-7491.
204. Sund, J., et al., *Proteomic Characterization of Engineered Nanomaterial-Protein Interactions in Relation to Surface Reactivity.* Acs Nano, 2011. **5**(6): p. 4300-9.
205. Sandberg, W.J., *Comparison of non-crystalline silica nanoparticles in IL-1beta release from macrophages.* . Particle and Fibre Toxicology, 2012(9): p. 32.
206. Donaldson, K. and P.J. Borm, *The quartz hazard: a variable entity.* Annals of Occupational Hygiene, 1998. **42**(5): p. 287-94.
207. Liu, T., et al., *Single and repeated dose toxicity of mesoporous hollow silica nanoparticles in intravenously exposed mice.* Biomaterials, 2011. **32**(6): p. 1657-68.
208. Stone, V., et al., *Engineered Nanoparticles - Review of Health and Environmental Safety (ENRHES).* 2009(Accessed November 2012 : http://ihcp.jrc.ec.europa.eu/whats-new/enhres-final-report).
209. Napierska, D., et al., *The nanosilica hazard: another variable entity.* Particle and Fibre Toxicology, 2010. **7**(1): p. 39.
210. Dhawan, A. and V. Sharma, *Toxicity Assessment of Nanomaterials: Methods and Challenges.* Analytical and Bioanalytical Chemistry, 2010. **398**(2): p. 589-605.
211. Nabeshi, H., et al., *Amorphous Nanosilica Induce Endocytosis-Dependent ROS Generation and DNA Damage in Human Keratinocytes.* Particle and Fibre Toxicology, 2011. **8**: p. 1.
212. Walkey, C.D. and W.C. Chan, *Understanding and Controlling the Interaction of Nanomaterials with Proteins in a Physiological Environment.* Chemical Society Reviews, 2012. **41**(7): p. 2780-99.
213. Kveder, M., et al., *The Study of Structural Accessibility of Free Thiol Groups in Human Low-Density Lipoproteins.* Biochimica et Biophysica, 2003. **1631**(3): p. 239-45.
214. Han, Q., et al., *Multidimensional Analysis of the Frequencies and Rates of Cytokine Secretion from Single Cells by Quantitative Microengraving.* Lab on a Chip, 2010. **10**(11): p. 1391-400.

215. Jin, T., X. Xu, and D. Hereld, *Chemotaxis, Chemokine Receptors and Human Disease.* Cytokine, 2008. **44**(1): p. 1-8.

216. Boyden, S., *The Chemotactic Effect of Mixtures of Antibody and Antigen on Polymorphonuclear Leucocytes.* The Journal of Experimental Medicine, 1962. **115**: p. 453-66.

217. Luster, A., *Chemotaxis: Role in Immune Response 2001*. [online] Accessed from: http://www.els.net [Accessed Dec 2012].

218. Toetsch, S., et al., *The Evolution of Chemotaxis Assays from Static Models to Physiologically Relevant Platforms.* Integrative Biology, 2009. **1**(2): p. 170-81.

219. Zhou, W., J.E. Marsh, and S.H. Sacks, *Intrarenal Synthesis of Complement.* Kidney International, 2001. **59**(4): p. 1227-35.

220. Markiewski, M., Lambris, J., *The Role of Complement in Inflammatory Diseases from Behind the Scenes into the Spotlight.* American Journal of Pathology, 2007. **171**(3): p. 715-27.

221. Dunkelberger, J., Song, W., *Role and Mechanism of Action of Complement in Regulating T Cell Immunity*. Molecular Immunology, 2010. **47**(13): p. 2176-86.

222. Gennaro, R., et al., *C5a Fragment of Bovine Complement. Purification, Bioassays, Amino-Acid Sequence and Other Structural Studies.* European Journal of Biochemistry, 1986. **155**(1): p. 77-86.

223. Sunyer, J.O. and J.D. Lambris, *Complement*, in *Encyclopedia of Life Sciences* 2001, John Wiley & Sons, Ltd.

224. Warheit, D.B., et al., *Pulmonary Macrophages are Attracted to Inhaled Particles Through Complement Activation.* Experimental Lung Research, 1988. **14**(1): p. 51-66.

225. Salvador-Morales, C., et al., *Complement Activation and Protein Adsorption by Carbon Nanotubes.* Molecular Immunology, 2006. **43**(3): p. 193-201.

226. Rybak-Smith, M.J., et al., *Effect of Functionalization of Carbon Nanotubes with Psychosine on Complement Activation and Protein Adsorption.* Journal of Biomedical Nanotechnology, 2011. **7**(6): p. 830-9.

227. Neun, B.W. and M.A. Dobrovolskaia, *Qualitative Analysis of Total Complement Activation by Nanoparticles.* Characterization of Nanoparticles Intended for Drug Delivery, 2011. **697**: p. 237-45.
228. Barlow, P.G., et al., *Serum Exposed to Nanoparticle Carbon Black Displays Increased Potential to Induce Macrophage Migration.* Toxicological Letters, 2005. **155**(3): p. 397-401.
229. Warheit, D.B., et al., *Inhaled Asbestos Activates a Complement-Dependent Chemoattractant for Macrophages.* Laboratory Investigation, 1985. **52**(5): p. 505-14.
230. Pham, C.T., et al., *Variable antibody-dependent activation of complement by functionalized phospholipid nanoparticle surfaces.* Journal of Biological Chemistry, 2011. **286**(1): p. 123-30.
231. Reddy, S.T., et al., *Exploiting Lymphatic Transport and Complement Activation in Nanoparticle Vaccines.* Nature Biotechnology, 2007. **25**(10): p. 1159-64.
232. Governa, M., et al., *Cleavage of the Fifth Component of Human Complement and Release of a Split Product with C5a-like Activity by Crystalline Silica Through Free Radical Generation and Kallikrein Activation.* Toxicology and Applied Pharmacology, 2002. **179**(3): p. 129-36.
233. Barlow, P.G., et al., *Carbon black nanoparticles induce type II epithelial cells to release chemotaxins for alveolar macrophages.* Particle and Fibre Toxicology, 2005. **2**: p. 11.
234. Andersen, A.J., et al., *Single-Walled Carbon Nanotube Surface Control of Complement Recognition and Activation.* Acs Nano, 2013. **7**(2): p. 1108-19.
235. Dobrovolskaia, M.A., et al., *Preclinical Studies to Understand Nanoparticle Interaction with the Immune System and its Potential Effects on Nanoparticle Biodistribution.* Molecular Pharmacology, 2008. **5**(4): p. 487-95.
236. Sheetz, M.P., et al., *Cell Migration as a Five-Step Cycle.* Biochemical Society Symposia, 1999. **65**: p. 233-43.
237. Li, J. and F. Lin, *Microfluidic Devices for Studying Chemotaxis and Electrotaxis.* Trends in Cell Biology, 2011. **21**(8): p. 489-97.

238. Kramer, N., et al., *In Vitro Cell Migration and Invasion Assays.* Mutation Research, 2013. **752**(1): p. 10-24.
239. Corning Ltd., *Transwell® Permeable Supports Including Snapwell™ and Netwell™ Inserts Instructions for Use [online] available from http://catalog2.corning.com/Lifesciences/media/pdf/Transwell_Instruction Manual.pdf] Accessed October 2012*. 2010.
240. Corning Ltd., *Cell Migration, Chemotaxis and Invasion Assay Using Staining Protocol [online] available from [http://catalog2.corning.com/Lifesciences/media/pdf/protocol_CLS_AN_211_CellMigration_Chemotaxis_InvasionAssay_Using_Staining.pdf] Accessed October 2012*. 2010.
241. Donaldson, K., et al., *Impaired Chemotactic Responses of Bronchoalveolar Leukocytes in Experimental Pneumoconiosis.* The Journal of Pathology, 1990. **160**(1): p. 63-9.
242. Warheit, D.B. and A.R. Brody, *Chemotactic Enhancement by Lavaged Proteins.* American Review of Respiratory Disease, 1988. **137**(1): p. 243-4.
243. Papaioannou, T.G. and C. Stefanadis, *Vascular Wall Shear Stress: Basic Principles and Methods.* Hellenic Journal of Cardiology, 2005. **46**(1): p. 9-15.
244. Samuel, S., P., et al., , *Multifactorial Determinants that Govern Nanoparticle Uptake by Human Endothelial Cells Under Flow*. International Journal of Nanomedicine, 2012(7): p. 2943–2956.
245. Hussain, S., J.A. Vanoirbeek, and P.H. Hoet, *Interactions of Nanomaterials with the Immune System.* Nanomedicine and Nanobiotechnology, 2012. **4**(2): p. 169-83.
246. Singh, N., et al., *Potential Toxicity of Superparamagnetic Iron Oxide Nanoparticles (SPION).* Nano Review, 2010. **1**.
247. Yu, M., et al., *Dextran and Polymer Polyethylene Glycol (PEG) Coating Reduce Both 5 and 30 nm Iron Oxide Nanoparticle Cytotoxicity in 2D and 3D Cell Culture.* International Journal of Molecular Sciences, 2012. **13**(5): p. 5554-70.

248. Ariano, P., et al., *Interaction of Spherical Silica Nanoparticles with Neuronal Cells: Size-Dependent Toxicity and Perturbation of Calcium Homeostasis.* Small, 2011. **7**(6): p. 766-774.
249. Yu, K.O., et al., *Toxicity of amorphous silica nanoparticles in mouse keratinocytes.* Journal of Nanoparticle Research, 2009. **11**(1): p. 15-24.
250. Napierska, D., et al., *Size-dependent cytotoxicity of monodisperse silica nanoparticles in human endothelial cells.* Small, 2009. **5**(7): p. 846-53.
251. McCarthy, J., et al., *Mechanisms of toxicity of amorphous silica nanoparticles on human lung submucosal cells in vitro: protective effects of fisetin.* Chemical Research in Toxicology, 2012. **25**(10): p. 2227-35.
252. Du, Z., et al., *Cardiovascular toxicity of different sizes amorphous silica nanoparticles in rats after intratracheal instillation.* Cardiovascular Toxicology, 2013. **13**(3): p. 194-207.
253. Kaewamatawong, T., et al., *Acute pulmonary toxicity caused by exposure to colloidal silica: particle size dependent pathological changes in mice.* Toxicologic Pathology, 2005. **33**(7): p. 743-9.
254. Izak-Nau, E., et al., *Altered characteristics of silica nanoparticles in bovine and human serum: the importance of nanomaterial characterization prior to its toxicological evaluation.* Particle and Fibre Toxicology, 2013. **10**(1): p. 56.

Chapter 8 Appendix

8.1. DLS Measurements

Table 8.1 Data (averages of n=3) obtained from Malvern zetasizer analysis. Replicate DLS measurements were carried out on 280, 22 and 45nm particles at 100, 10 and 1µg/ml in water, RPMI and in RPMI with 0.1% BSA. Results show Z average, Standard error of all three measurements. Measurements were carried out as described in 2.2.2.3.

Sample ID	Average	SE	Sample ID	Average	SE	Sample ID	Average	SE
280nm in water 100 µg/ml	318.70	9.77	280nm RPMI 100 µg/ml	1029.60	151.40	280nm 100 µg/ml RPMI + 0.1% BSA	507.98	57.93
280nm in water 10 µg/ml	292.73	3.73	280nm RPMI 10 µg/ml	565.10	4.60	280nm 10 µg/ml RPMI + 0.1% BSA	419.4	27.43
280 nm in water 1 µg/ml	573.91	104.32	280nm RPMI 1 µg/ml	512.88	0.00	280nm 1 µg/ml RPMI +0.1% BSA	439.75	52.85
22nm in water 100 µg/ml	401.40	39.24	22nm RPMI 100 µg/ml	489.55	97.15	22nm 100 µg/ml RPMI + 0.1% BSA	518.6	63.53
22nm in water 10 µg/ml	309.17	23.33	22nm RPMI 10 µg/ml	627.65	32.75	22nm 10 µg/ml RPMI + 0.1% BSA	449	48.48
22nm in water 1 µg/ml	493.44	64.56	22nm RPMI 1 µg/ml	605.30	93.51	22nm 1 µg/ml RPMI + 0.1% BSA	511.4	59.19
45nm in water 100 µg/ml	1613.50	80.50	45nm RPMI 100 µg/ml	1725.50	34.50	45 nm 100 µg/ml in RPMI +0.1% BSA	1648.33	68.42
45nm in water 10 µg/ml	450.35	86.65	45nm RPMI 10 µg/ml	1040.03	69.25	45 nm 10 µg/ml in RPMI +0.1% BSA	791.87	91.20
45nm in water 1 µg/ml	308.65	15.35	45nm RPMI 1 µg/ml	714.54	82.11	45nm 1 µg/ml in RPMI + 0.1% BSA	324.32	80.07

8.2 Differential Centrifugal Sedimentation Analysis

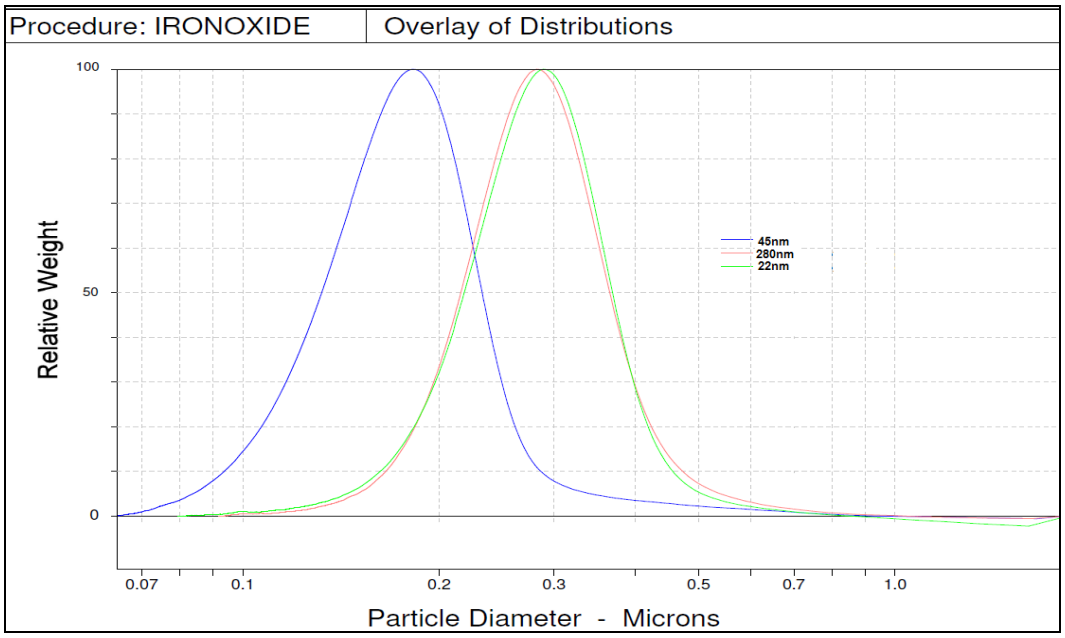

Figure 8.1 Differential centrifugal sedimentation analysis of 22nm and 280nm Fe_2O_3 and 45 nm Fe_3O_4 particles as described in 2.3.7. Here we can see the 22nm and 280nm data are similar peaking at 289nm and 282.2 nm respectively.

8.3 DLS Study- Effect of pH on Hydrodynamic Diameter.

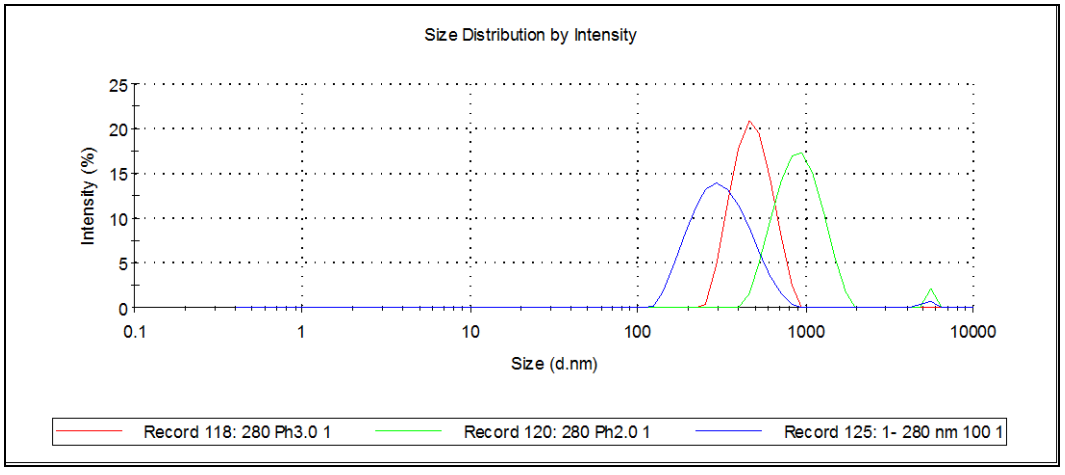

Figure 8.2: As described in 2.4 image showing increasing hydrodynamic diameter of 280nm iron particles at decreasing pH. ___280 nm at pH7____280 nm at pH3_____280nm at pH2.

8.4 EDX Measurements Replicates

8.4.1. EDX Measurements- 280nm Fe_2O_3

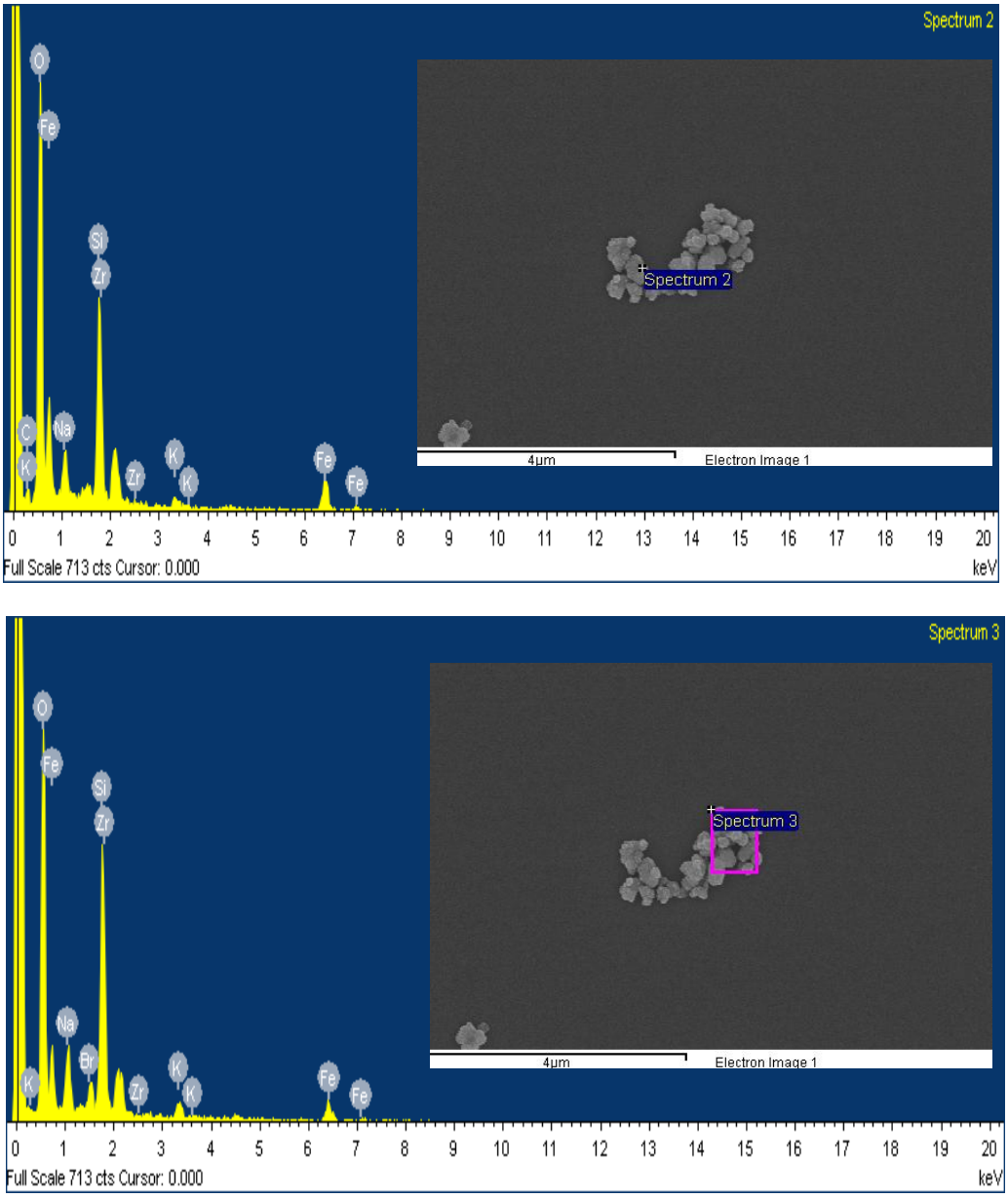

Figure 8.3 Replicates of EDX mesurments of 280nm Fe_2O_3 particles as described in 2.23.

8.4.2. EDX Measurements- 22nm Fe_2O_3

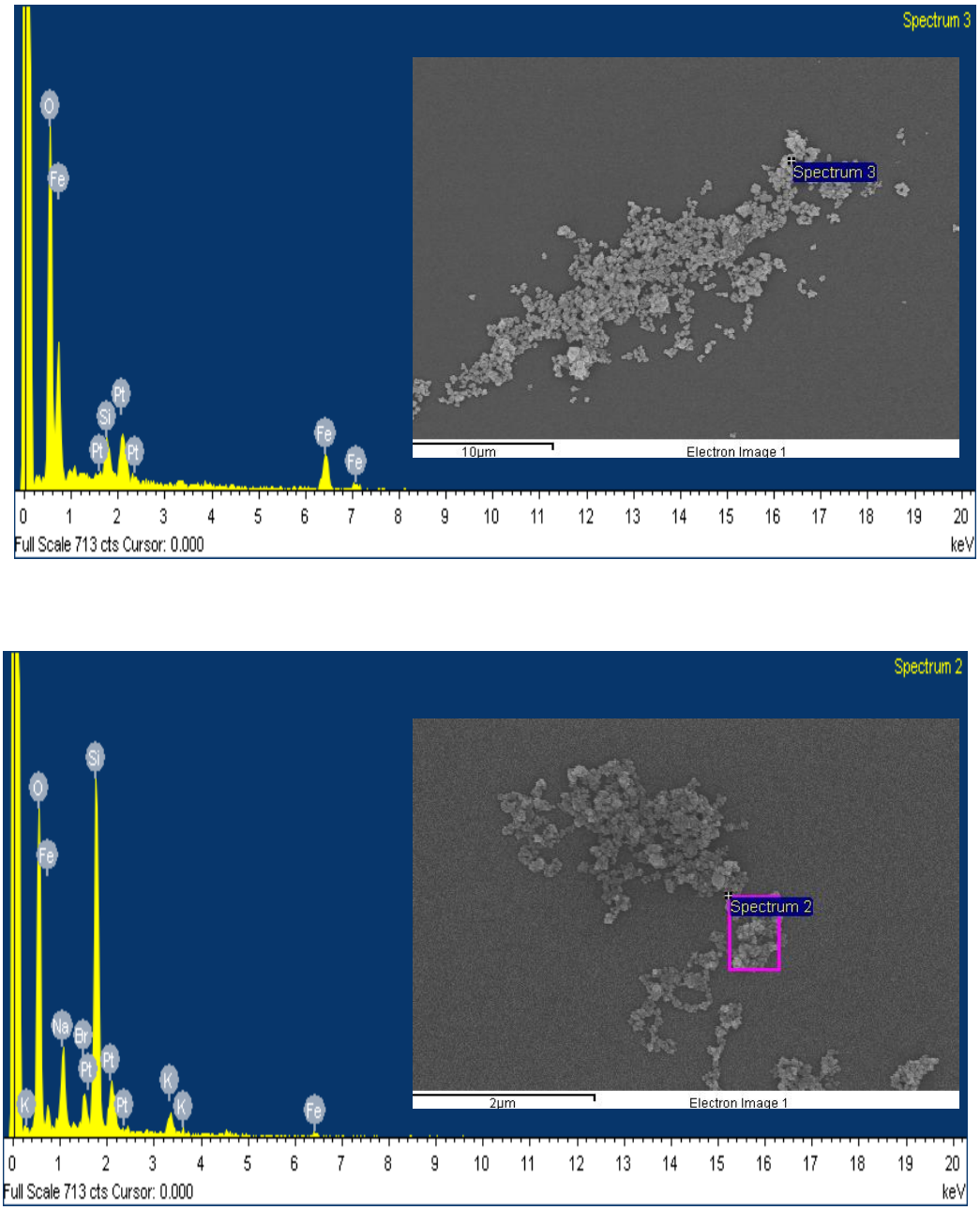

Figure 8.4 Replicates of EDX mesurments of 22nm Fe_2O_3 particles as described in 2.23.

8.4.3. EDX Measurements- 45nm Fe_3O_4

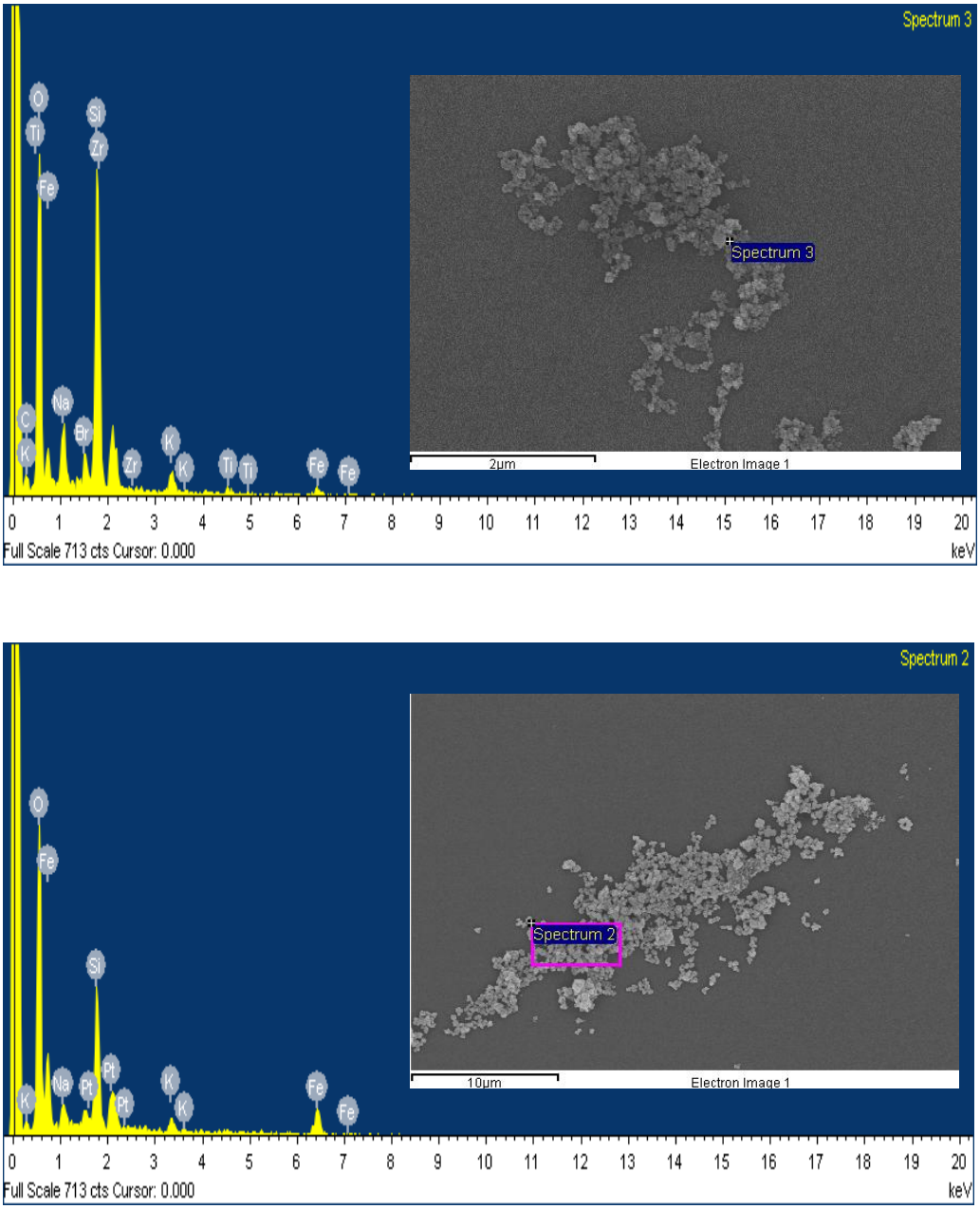

Figure 8.5 Replicates of EDX mesurments of 45nm Fe_3O_4 particles as described in 2.23.

8.5 Interference of 280nm Fe_2O_3 Particles on Absorbance Readings as Seen During WST-1 Assay (n=1)

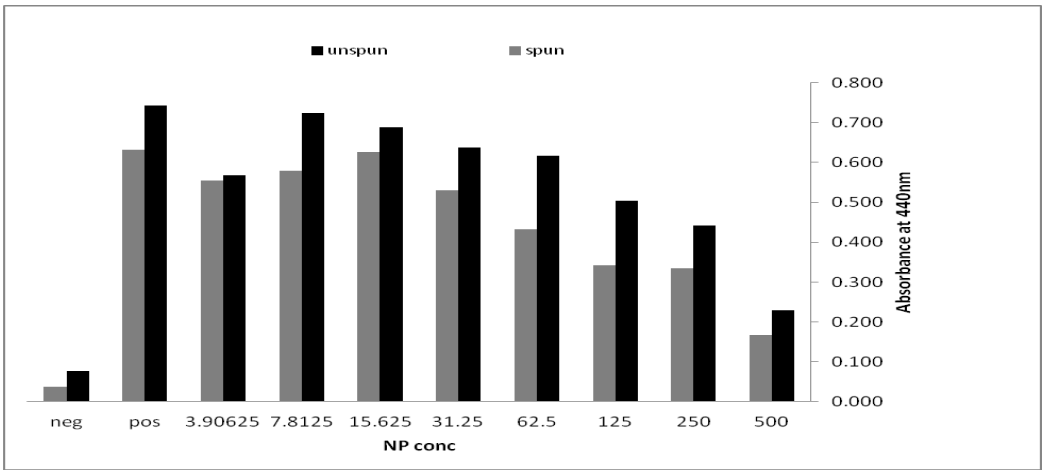

Figure 8.6 showing absorbance readings on a MRX plate reader at 440nm for WST-1 assay samples before and after removal of NM (by centrifugation) as described in 3.4. Particle interference in in vitro assays is an issue that needs to be addressed in the experimental design. For both the LDH and the WST-1 assay it was decided to centrifuge each sample to remove NM before measuring absorbance in order to avoid and overestimation of viability. The graph show the difference in absorbance readings between samples where NM have and have not been removed.

8.6 Light Microscopy Images of J774.A1 Cells after Exposure to 280nm Fe_2O_3 Particles.

A 96 well plate was seeded with $5*10^4$ J774.A1 cells and incubated for 48 hours, after which time there were exposed to a 500µg/ml r 125µg/ml 280nm iron oxide particles in RPMI imaged over various time points.

A

(i) (ii) (iii) (iv)

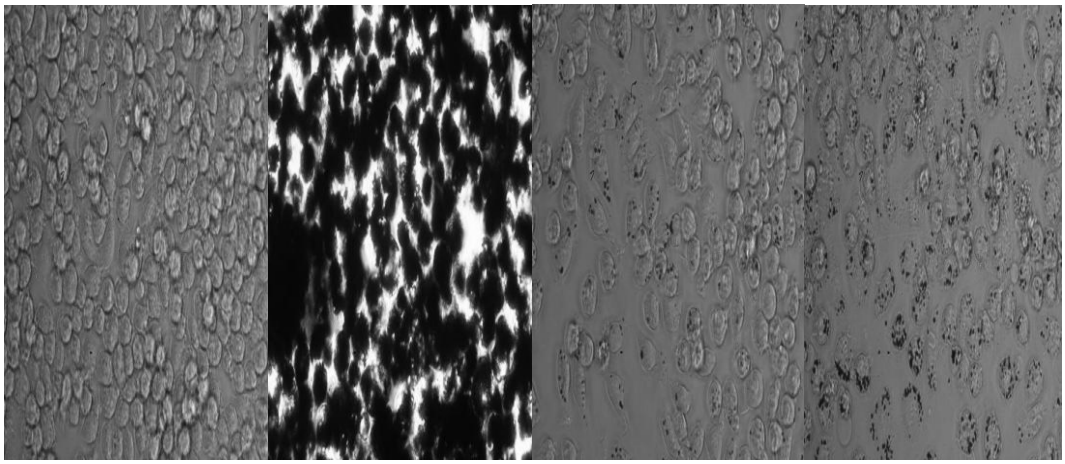

B

(i) (ii) (iii) (iv)

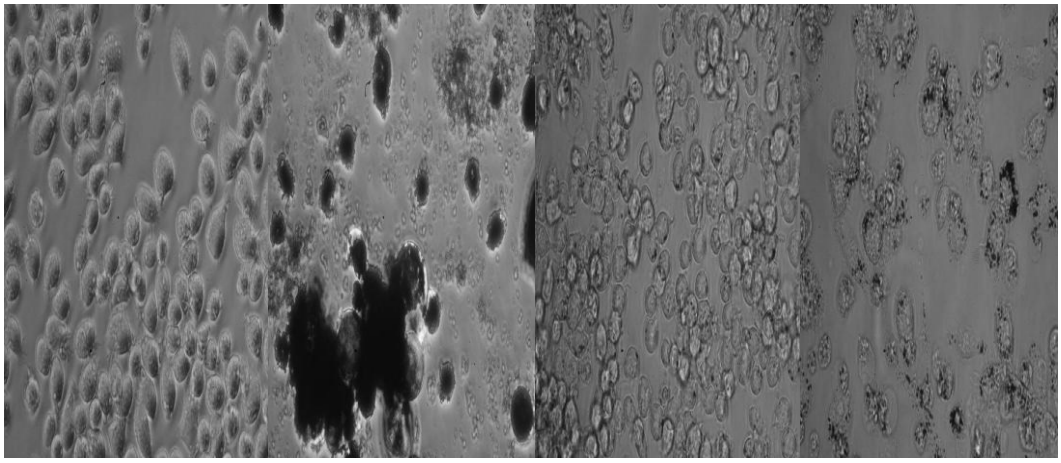

Figure 8.7 Light microscopy (20x) images of J774.A1 macrophages after exposure to Fe_2O_3 particles for (a) 24 hours and (b) 48 hours, where (i) control (ii) exposure to 0.5mg/ml (iii) exposure to 125µg/ml and (iv) exposure to 125µg/ml in RPMI with 1% BSA , as described in 3.3.1

8.7 SDS-PAGE Gels

(a) *Analysis of the protein corona by SDS-PAGE after incubation in 10% plasma as described in 3.2.6. The first two lanes show the proteins of the Fe_2O_3 and Fe_3O_4 10% plasma corona. Lane 6 and 7 show 50nm $Si0_2$-Nh_2 with 10% plasma corona. Lane 2 and 3 are found in figure 3.3 and lanes 6 and 7 in figure 4.2.*

1. Ladder	2. Fe_20_3 (280nm)	3. Fe_30_4 (45nm)	4. SiO_2 (50nm)	5. SiO_2 (50nm)	6. SiO_2 (50nm)	7. SiO_2-Nh_2 (50nm)

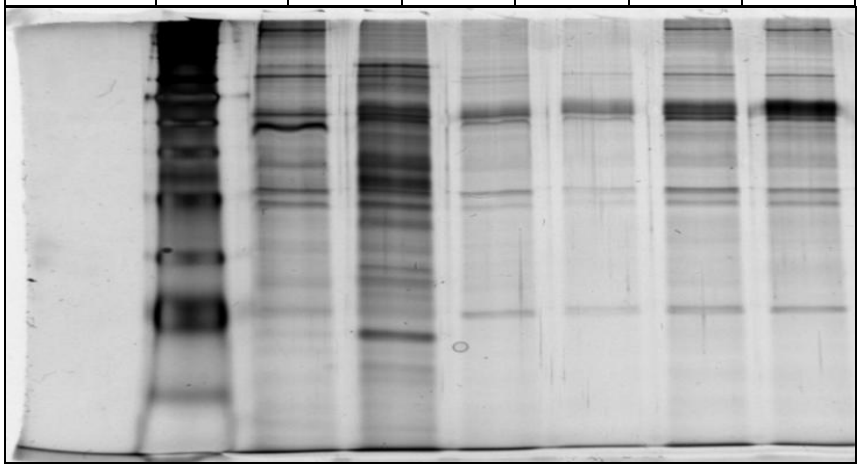

(b) *Analysis of the protein corona by SDS-PAGE after incubation with LLF and then in 10% plasma as described in 3.2.6.*

1. ladder	2. Fe_20_3 280nm	3. Fe_30_4 45nm	4. SiO_2 200nm	5. SiO_2-Nh_2 200nm	6. SiO_2-Nh_2 50nm	7. SiO_2-Nh_2 50nm

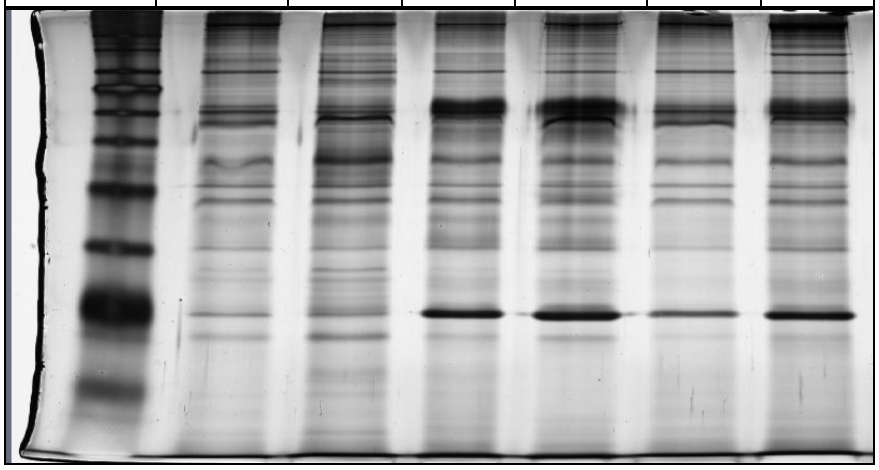

(c) *Analysis of the protein corona by SDS-PAGE after incubation with 10% plasma as described in 3.2.6.*

1. ladder	2. Fe_2O_3 280nm	3. Fe_3O_4 45nm	4. SiO_2 200nm	5. SiO_2-Nh_2 200nm	6. SiO_2-Nh_2/LLF 200nm	7. SiO_2-Nh_2/LLF 200nm

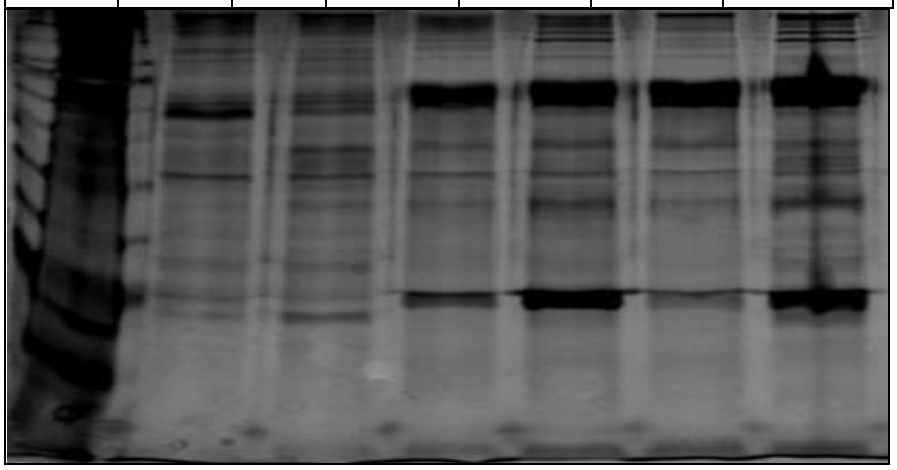

(d) *Analysis of the protein corona by SDS-PAGE after incubation with 55% plasma as described in 3.2.6.*

1. ladder	2. Fe_2O_3 280nm	3. Fe_3O_4 45nm	4. SiO_2 200nm	5. SiO_2 50nm	6. SiO_2-Nh_2 200nm	7. 6. SiO_2-Nh_2/ 50nm

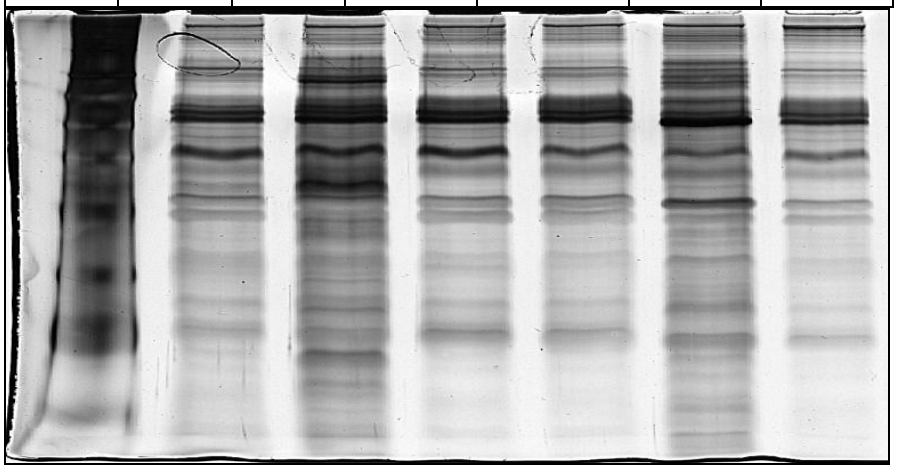

(e) *Analysis of the protein corona by SDS-PAGE after incubation with LLF and then in 55% plasma as described in 3.2.6.*

ladder	2. Fe_2O_3 280nm	3. Fe_3O_4 45nm	4. SiO_2 200nm	5. SiO_2 50nm	6. SiO_2-Nh_2 200nm	7. 6. SiO_2-Nh_2/ 50nm)

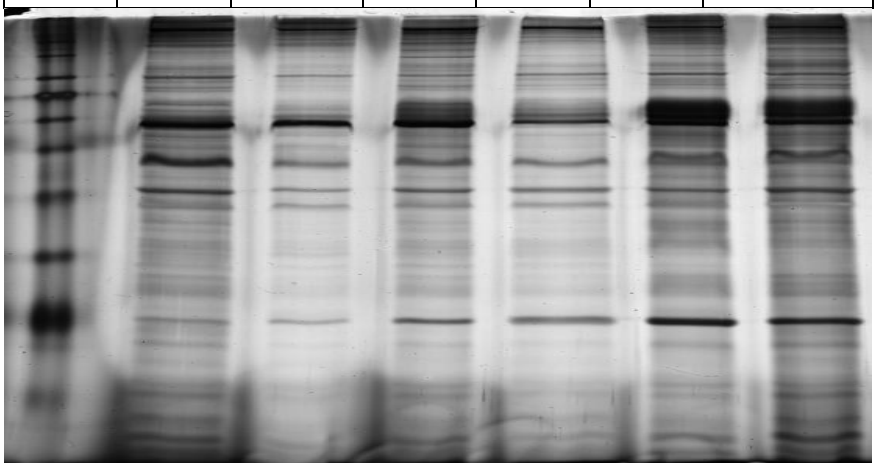

(f) *Analysis of the protein corona by SDS-PAGE after incubation 10% serum as described in 3.2.6.*

ladder	2. Fe_2O_3 280nm	3. Fe_3O_4 45nm	4. SiO_2 200nm	5. SiO_2 50nm	6. SiO_2-Nh_2 200nm	7. 6. SiO_2-Nh_2/ 50nm)

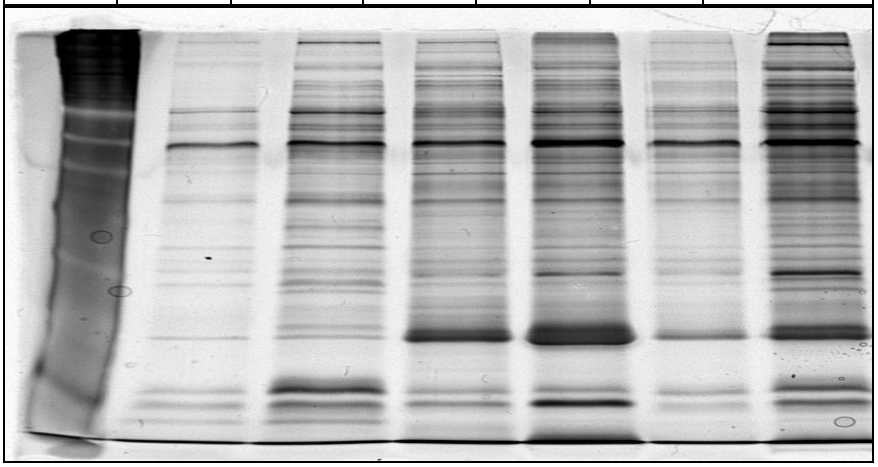

(g) *Analysis of the protein corona by SDS-PAGE after incubation with LLF and then in 10% serum as described in 3.2.6.*

ladder	2. Fe_2O_3 280nm	3. Fe_3O_4 45nm	4. SiO_2 200nm	5. SiO_2 50nm	6. SiO_2-Nh_2 200nm	7. 6. SiO_2-Nh_2/ 50nm)

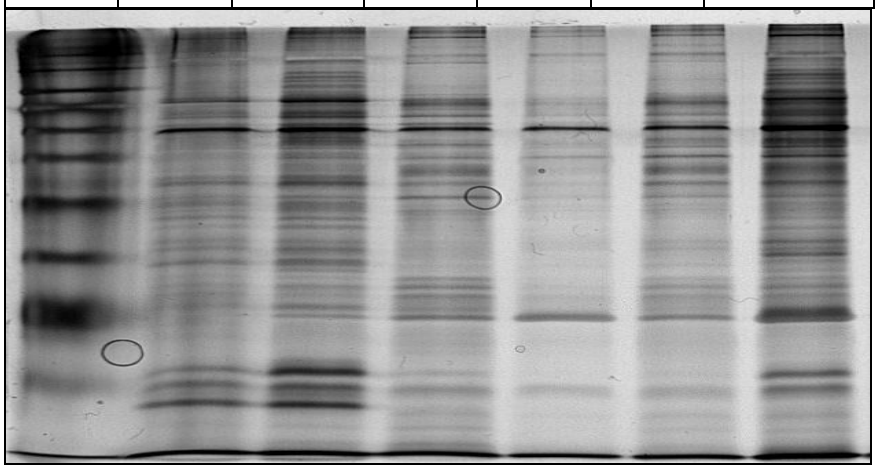

Figure 8.8 (a-f) SDS-PAGE gels prepared as described in Chapter 3 and Chapter 4 methods and materials (3.2.6; 4.4.2). These above images are supplementary to the information and graphs found in 3.3.5 and 4.3.3.

8.8 Proteins Identified by Mass Spectroscopy after SDS-PAGE Analysis of the Nanomaterial Corona. Samples Prepared as Described in 3.2.4.

Briefly after staining using a mass spectroscopy compatible staining procedure, selected lanes (280nm Fe_2O_3 in 10% plasma, 10% serum corona, and after pre incubation in LLF lanes) were trypsin digested and analysed using MS. The tables below show the results from Mass Spececctroscopy

280nm Fe_2O_3 with Associated Plasma Hard Corona (10%P)	**MW**	**Acc No.**	**XC Score**	**P EP**	**% C**	**Peptide Hit**
Apolipoprotein B-100	515.28	P04114	350.29	1.11E-15	12.80	35
Complement C3	187.03	P01024	260.30	2.00E-13	24.60	27
Serum albumin	69.32	P02768	110.30	2.40E-11	20.70	12
Apolipoprotein(a)	500.99	P08519	60.27	2.86E-09	18.20	6
Complement C4-A	192.65	P0C0L4	50.27	3.07E-07	3.60	5
Plasma protease	55.12	P05155	50.22	8.03E-07	11.60	5
Histidine-rich glycoprotein	59.54	P04196	50.20	2.28E-10	14.10	5
Ig mu chain	49.27	P01871	40.19	8.28E-07	13.50	4
Coagulation factor XI	70.063	P03951	30.23	7.02E-09	8.50	3
Coagulation factor XII	67.77	P00748	20.29	1.25E-13	5.90	2
Actin, cytoplasmic	41.71	P60709	20.28	5.42E-13	12.80	2
Hemoglobin subunit beta	15.989	P68871	20.22	7.22E-07	23.80	2
Hemoglobin subunit alpha	15.25	P69905	20.20	2.06E-07	21.80	2
Ig kappa chain C region	11.60	P01834	20.16	1.19E-06	17.00	2
Plasminogen	90.51	P00747	10.26	4.60E-13	2.70	1
Trypsin-3	32.50	P35030	10.25	1.49E-06	6.60	1
Complement C1q subcomponent subunit C	25.76	P02747	10.23	7.06E-07	7.30	1
Apolipoprotein C-II	11.28	P02655	10.22	1.36E-09	20.80	1
Actin, aortic smooth muscle	41.98	P62736	10.20	5.62E-09	4.20	1
Ig heavy chain V-III region BRO	13.22	P01766	10.20	5.71E-09	15.80	1
Ig gamma-1 chain C region	36.08	P01857	10.20	4.22E-11	4.80	1

Hornerin	282.22	Q86YZ3	10.18	2.02E-07	1.70	1
Apolipoprotein A-I	30.76	P02647	10.17	4.45E-07	5.20	1
Apolipoprotein C-III	10.84	P02656	10.17	1.76E-06	16.20	1
Vitronectin	54.27	P04004	10.16	1.71E-08	3.10	1
Platelet factor 4 variant	11.54	P10720	10.15	2.13E-04	14.40	1
Alpha-1-antitrypsin	46.71	P01009	10.13	4.76E-07	3.30	1

280nm Fe_2O_3 LLF/10% Plasma	**MW**	**Acc. No.**	**XC Score**	**PEP**	**%C**	**Peptide Hit**
Complement C3	187.03	P01024	440.30	1.55E-14	39.00	48
Serum albumin	69.32	P02768	230.29	6.91E-12	45.50	25
Apolipoprotein B-100	515.283.	P04114	190.29	9.58E-11	7.30	19
Filamin-A	280.56	P21333	170.28	7.63E-11	12.40	17
Myosin-9	226.39	P35579	120.28	1.09E-09	9.60	12
Talin-1	269.59	Q9Y490	80.34	2.45E-12	6.10	8
Apolipoprotein(a)	500.99	P08519	50.20	5.33E-09	25.60	5
Ig kappa chain C region	11.60	P01834	40.25	5.24E-10	67.00	5
Fibrinogen alpha chain	94.91	P02671	40.23	6.84E-07	6.60	4
Actin, cytoplasmic 1	41.70	P60709	30.31	1.43E-10	16.30	3
Hemoglobin subunit beta	15.98	P68871	30.23	1.49E-08	33.30	3
Alpha-actinin-1	102.99	P12814	30.23	2.90E-11	5.20	3
Integrin beta-3	87.00	P05106	30.22	6.62E-10	6.50	3
Actin, aortic smooth muscle	41.98	P62736	30.21	5.77E-11	8.50	4
Ig lambda-1 chain C regions	11.34	P0CG04	30.20	6.75E-06	46.20	3
Thrombospondin-1	129.29	P07996	30.19	1.23E-04	4.30	3
Apolipoprotein A-I	30.75	P02647	30.16	1.83E-06	10.10	3
Apolipoprotein A-IV	45.37	P06727	20.26	1.10E-08	7.10	2
Ig gamma-1 chain C region	36.08	P01857	20.26	2.91E-11	10.60	2
Apolipoprotein C-II	11.27	P02655	20.25	4.55E-14	20.80	2
Band 3 anion transport protein	101.72	P02730	20.21	1.25E-09	3.70	2
Integrin alpha-IIb	113.30	P08514	20.20	1.76E-07	3.30	2
Hemoglobin subunit alpha	15.24	P69905	20.19	2.00E-10	31.00	2
Complement C4-A	192.64	P0C0L4	20.17	9.94E-05	1.10	2

Ig mu chain C region	49.27	P01871	20.17	1.35E-06	6.90	2
Histone H2B type 1-B	13.94	P33778	20.17	9.28E-08	11.90	2
Alpha-2-macroglobulin	163.18	P01023	20.17	8.02E-07	1.80	2

280nm Fe_2O_3 with Associated Serum Hard Corona (10%S)	**Acc No.**	**MW**	**Score**	**PEP**	**%C**	**Peptide Hits**
Serum albumin	P02768	69.32	60.19	2.71E-12	10.80	7
Trypsin-3	P35030	32.50	10.25	1.19E-06	6.60	2
Apolipoprotein A-I	P02647	30.75	10.20	4.20E-10	6.00	1
Desmoglein-1	Q02413	113.67	10.20	3.98E-05	1.50	1
Cystatin-A	P01040	10.99	10.19	6.70E-06	18.40	1
Protein S100-A9	P06702	13.23	10.18	7.74E-04	13.20	1
Fibronectin	P02751	262.45	10.17	8.90E-04	0.80	1
Dermcidin	P81605	11.27	10.15	3.06E-05	12.70	1
Ubiquitin-60S ribosomal protein L40	P62987	14.71	10.14	2.40E-04	12.50	1
Hemoglobin subunit alpha	P69905	15.24	10.14	3.62E-04	10.60	1
Desmoplakin	P15924	331.56	10.13	8.10E-05	0.30	1
Lysozyme C	P61626	16.52	10.13	1.84E-06	8.10	1
Glial fibrillary acidic protein	P14136	49.84	8.15	1.81E-05	2.50	1

280nm Fe_2O_3 LLF/10% Serum	**Acc No**	**MW**	**Score**	**P EP**	**%C**	**Peptide Hits**
Serum albumin	P02768	69.32	170.28	1.27E-09	35.80	18
Apolipoprotein A-I	P02647	30.76	40.20	3.81E-10	17.60	4
Alpha-1-antitrypsin	P01009	46.71	30.25	3.92E-12	12.20	3
Ig gamma-1 chain C region	P01857	36.08	30.24	9.62E-12	17.58	3
Ig kappa chain C region	P01834	11.60	20.25	4.71E-12	32.08	2
Glyceraldehyde-3-phosphate dehydrogenase	P04406	36.030.4	20.20	4.45E-09	11.34	2
Hemoglobin subunit alpha	P69905	15247.9	20.20	7.68E-10	21.83	3
Desmoglein-1	Q02413	113676.0	20.19	8.22E-10	3.24	2
Thrombospondin-1	P07996	129299.2	20.18	2.21E-07	2.22	2
Complement C3	P01024	187029.3	20.18	2.49E-05	2.16	2
Alpha-1-acid	P02763	23496.8	10.25	2.44E-07	7.46	1

glycoprotein 1						
Hornerin	Q86YZ3	282225.7	10.24	2.27E-07	1.68	1
Trypsin-3	P35030	32508.0	10.24	1.06E-07	6.58	2
Fibronectin	P02751	262457.6	10.21	3.17E-06	0.80	1
Ig gamma-2 chain C region	P01859	35877.8	10.18	3.80E-10	4.91	1
Transthyretin	P02766	15877.1	10.17	1.11E-08	8.84	1
Antithrombin-III	P01008	52569.0	10.16	6.03E-05	2.37	1
Hemoglobin subunit beta	P68871	15988.3	10.16	3.74E-04	12.93	1
Dermcidin	P81605	11276.8	10.16	1.65E-05	12.73	1
Apolipoprotein C-III	P02656	10845.5	10.16	3.37E-06	16.16	1
Alpha-2-macroglobulin	P01023	163187.4	10.15	3.96E-05	0.95	1
Tetranectin	P05452	22552.3	10.14	8.16E-05	5.94	1
Apolipoprotein B-100	P04114	515283.6	10.14	6.51E-05	0.33	1
Serotransferrin	P02787	77013.7	10.13	2.01E-05	2.01	1
Glial fibrillary acidic protein	P14136	49849.7	8.15	1.97E-05	2.55	1

SiO_2 (200nm) with 10% P Corona	**Acc No**	**MW**	**XC Score**	**%C**	**PEP**	**Peptide Hits**
Apolipoprotein B-100	P04114	515.28	480.32	16.31	2.55E-14	48
Complement C3	P01024	187.03	398.30	35.30	9.99E-15	43
Histidine-rich glycoprotein	P04196	59.54	160.31	37.71	6.66E-11	58
Complement C4-A	P0C0L4	192.65	130.29	12.44	8.61E-12	13
Serum albumin	P02768	69.32	110.28	21.51	6.44E-09	12
Apolipoprotein A-I	P02647	30.76	80.23	31.46	2.98E-09	10
C4b-binding protein alpha chain	P04003	66.99	60.24	14.07	5.74E-07	6
Apolipoprotein(a)	P08519	500.99	40.23	10.95	9.15E-07	4
Apolipoprotein A-IV	P06727	45.37	30.22	12.12	3.51E-11	3
Complement component C9	P02748	63.13	30.16	6.80	2.58E-06	3
Apolipoprotein C-II	P02655	11.27	20.26	20.79	1.76E-10	2
Actin, aortic smooth muscle	P62736	41.98	20.20	8.49	9.93E-09	2
Ig mu chain C region	P01871	49.27	20.19	6.86	1.61E-06	2

Hemoglobin subunit beta	P68871	15.98	20.18	23.81	1.99E-08	2
Ig kappa chain C region	P01834	11.60	20.17	32.08	9.41E-09	3
Actin, cytoplasmic 1	P60709	41.70	10.28	8.00	4.87E-10	1
Complement C4-B	P0C0L5	192.67	10.27	1.55	6.01E-11	1
Ig heavy chain V-III region BRO	P01766	13.21	10.21	15.83	4.42E-05	1
Apolipoprotein C-III	P02656	10.84	10.20	16.16	2.10E-05	1
Band 3 anion transport protein	P02730	101.72	10.20	1.87	5.26E-04	1
Ig gamma-1 chain C region	P01857	36.08	10.20	4.85	4.37E-09	1
Trypsin-3	P35030	32.50	10.20	6.58	4.50E-06	2
Ig gamma-2 chain C region	P01859	35.87	10.19	4.91	7.93E-06	1
Protein S100-A9	P06702	13.23	10.18	13.16	2.35E-04	1
Fibrinogen alpha chain	P02671	94.91	10.17	1.62	2.54E-08	1
Uromodulin-like 1	Q5DID0	144.20	10.17	2.43	2.49E-04	1
Desmoplakin	P15924	331.56	10.16	0.49	7.10E-04	1
Ubiquitin-60S ribosomal protein L40	P62987	14.71	10.16	12.50	2.35E-04	1
Complement C5	P01031	188.18	10.15	0.66	6.57E-04	1
Putative beta-actin-like protein 3	Q9BYX7	41.98	10.15	2.93	2.04E-04	1
Coagulation factor XI	P03951	70.06	10.14	1.92	2.53E-04	1
Ig lambda-2 chain C regions	P0CG05	11.28	10.14	17.92	7.30E-05	1

SiO_2 (200nm) PC and 10% P Corona	**Acc No**	**MW**	**XC Score**	**% C**	**PEP**	**Peptide Hits**
Apolipoprotein B-100	P04114	515.28	590.31	21.60	1.00E-30	59
Complement C3	P01024	187.03	300.31	28.40	5.55E-15	30
Serum albumin	P02768	69.32	200.32	46.10	8.88E-15	21
Histidine-rich glycoprotein	P04196	59.54	100.28	26.30	1.69E-11	11
Hemoglobin subunit beta	P68871	15.99	70.21	44.90	7.97E-12	7
Apolipoprotein(a)	P08519	500.99	40.28	19.00	3.33E-15	4
Myosin-9	P35579	226.39	40.26	3.50	5.24E-11	4
Serotransferrin	P02787	77.01	40.26	9.30	4.71E-10	4
Filamin-A	P21333	280.56	40.25	2.70	2.08E-10	4
Alpha-2-macroglobulin	P01023	163.18	40.20	4.60	1.27E-11	4
Actin, cytoplasmic 1	P60709	41.70	30.31	18.40	1.00E-30	3
Ig kappa chain C region	P01834	11.60	20.28	33.00	3.34E-09	2
Platelet basic protein	P02775	13.88	20.26	22.70	1.25E-09	2
Apolipoprotein C-II	P02655	11.27	20.25	20.80	5.08E-09	2
Actin, aortic smooth muscle	P62736	41.98	20.22	4.20	1.49E-05	2
Ig gamma-1 chain C region	P01857	36.08	20.22	10.90	7.45E-10	2
Integrin beta-3	P05106	87.00	20.22	4.20	2.83E-06	2
Integrin alpha-IIb	P08514	113.30	20.20	3.80	1.14E-06	2
Complement C5	P01031	188.18	20.20	2.10	9.91E-08	2
Apolipoprotein A-I	P02647	30.75	20.19	10.50	4.97E-08	2
Hemoglobin subunit alpha	P69905	15.24	20.18	21.80	4.91E-08	2
Ig mu chain C region	P01871	49.27	20.18	6.90	8.37E-09	2
Vinculin	P18206	123.72	10.26	1.90	7.33E-14	1
Prothrombin	P00734	69.99	10.25	2.60	6.68E-09	1
Alpha-1-acid glycoprotein 1	P02763	23.49	10.23	7.50	1.10E-09	1

Thrombospondin-1	P07996	129.29	10.22	1.80	4.30E-13	1
Myosin-11	P35749	227.19	10.19	0.80	1.75E-06	1
Fibrinogen alpha chain	P02671	94.91	10.19	1.60	2.36E-10	1
Ig kappa chain V-III region SIE	P01620	11.76	10.19	16.50	4.23E-04	1
Plasminogen	P00747	90.51	10.19	2.70	2.37E-05	1
Alpha-actinin-1	P12814	102.99	10.18	1.80	5.65E-06	1
Myosin-10	P35580	228.85	10.18	0.90	2.76E-04	1
Trypsin-3	P35030	32.50	10.18	6.60	5.19E-04	2
Haptoglobin	P00738	45.17	10.18	3.40	1.35E-07	1
Tubulin alpha-1B chain	P68363	50.11	10.17	3.10	1.16E-04	1
Putative beta-actin-like protein 3	Q9BYX7	41.98	10.16	2.90	1.29E-06	1
Histone H2A type 1-B/E	P04908	14.12	10.15	14.60	6.76E-05	1
Protein S100-A9	P06702	13.23	10.14	13.20	9.56E-04	1
Apolipoprotein A-IV	P06727	45.37	10.14	3.50	2.03E-04	1
Complement component C9	P02748	63.13	10.14	2.30	3.46E-04	1
Talin-1	Q9Y490	269.59	10.14	0.40	1.59E-04	1
Apolipoprotein C-III	P02656	10.84	10.13	16.20	1.02E-05	1
U5 small nuclear ribonucleoprotein 200 kDa helicase	O75643	244.35	10.13	0.80	2.64E-04	1
Beta-actin-like protein 2	Q562R1	41.97	8.13	4.80	8.69E-05	1

SiO_2 (200nm) 10% s Corona	**Acc No**	**MW**	**XScore**	**%C**	**PEP**	**Peptide Hits**
Serum albumin	P02768	69.32	60.21	12.32	8.79E-10	8
Apolipoprotein B-100	P04114	515.28	30.18	0.88	2.29E-06	3
Apolipoprotein A-I	P02647	30.75	30.17	11.24	2.45E-08	3
Heat shock protein HSP 90-alpha	P07900	84.60	28.25	5.74	3.12E-10	3
Thrombospondin-4	P35443	105.80	20.25	3.54	1.29E-07	2
Fibronectin	P02751	262.45	20.18	1.38	2.44E-05	2

Complement C3	P01024	187.02	20.15	2.53	1.50E-06	2
Trypsin-3	P35030	32.50	10.25	6.58	3.35E-08	2
Hornerin	Q86YZ3	282.22	10.20	1.68	1.16E-08	1
Ig gamma-1 chain C region	P01857	36.08	10.20	6.67	6.02E-08	1
Apolipoprotein C-III	P02656	10.84	10.18	16.16	2.73E-04	1
Actin, cytoplasmic 1	P60709	41.70	10.17	4.80	1.38E-06	1
Cartilage oligomeric matrix protein	P49747	82.80	10.15	2.11	2.41E-04	1
Dermcidin	P81605	11.27	10.15	12.73	2.65E-08	1
Vitronectin	P04004	54.27	10.14	3.10	5.06E-04	1
Hemoglobin subunit alpha	P69905	15.24	10.13	10.60	5.71E-07	3
Putative heat shock protein HSP 90-beta 2	Q58FF8	44.32	10.13	3.10	4.79E-06	1
Secreted phosphoprotein 24 OS=Homo sapiens GN=SPP2 PE=1 SV=1	Q13103	24.32	10.13	5.70	5.93E-05	1
Glial fibrillary acidic protein	P14136	49.84	8.15	2.50	4.64E-06	1

8.9 LDH Release from J774.A1 Macrophages after Exposure to 280 nm and 22nm Fe_2O_3 Particles (as described in 3.2.7)

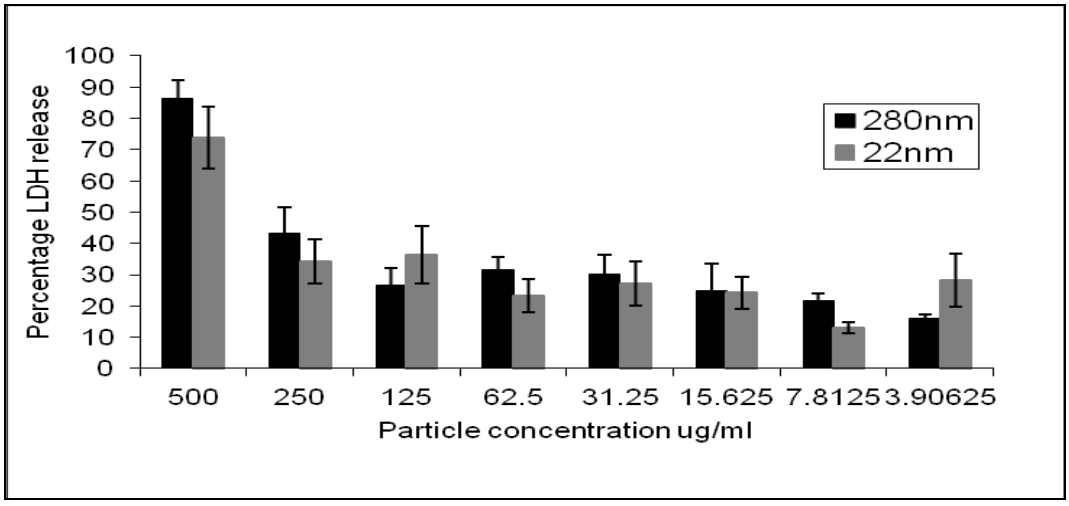

8.10 Percentage LDH Release from of J774.A1 Macrophages after Exposure to Fe_2O_3 280nm and 45NM Fe_3O_4 Particles for 4 Hours.

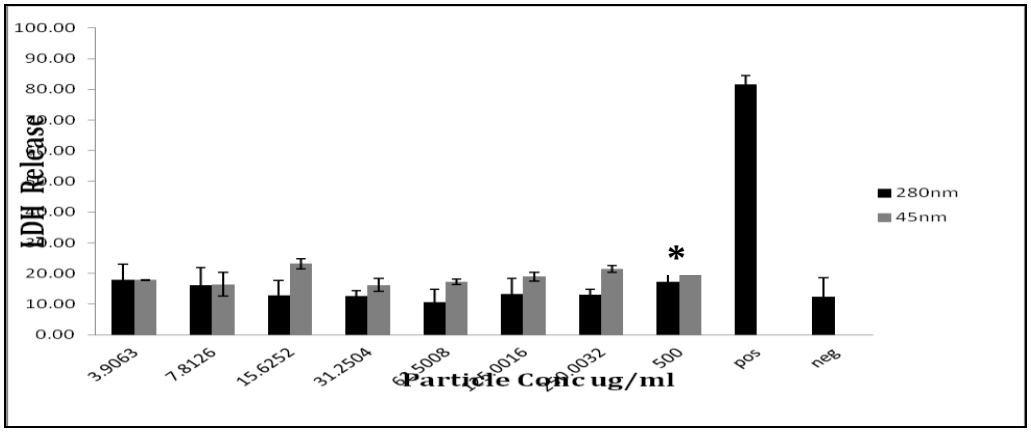

Figure 8.9 Values represent the means of 3 experiments ± SD There is no significant differences between exposure to the particle panel and the cells in media only expect at for the 45nm Fe_3O_4 Particles at 500µg/ml where P=0.0445

8.11 SDS-PAGE Gel Lanes (LLF)

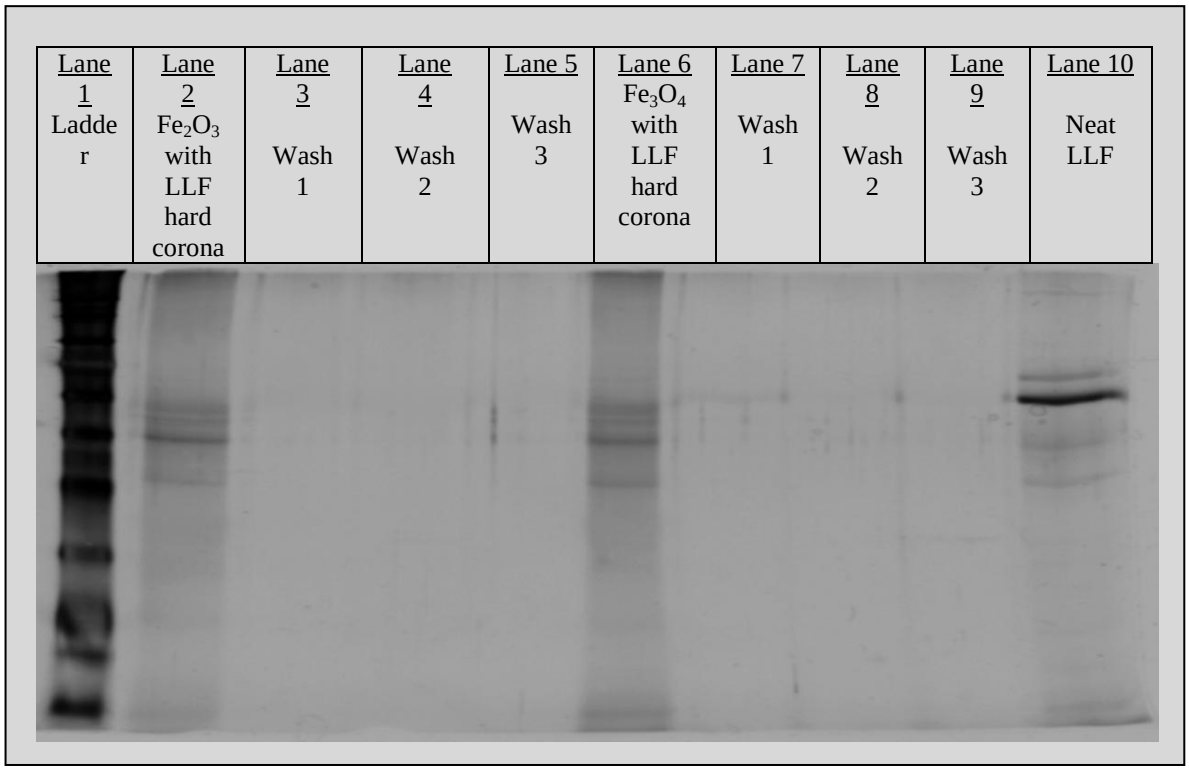

Figure 8.10 SDS-Gel lane shows Proteins Associated with 280nm Fe_2O_3 and the 45nm Fe_3O_4 LLF corona. Proteins were separated as described in materials and methods section 3.2.4 and 3.2.5.

8.12 Macrophage Migration in Transwell Chemotaxis Assay

(a)Macrophage migration in transwell chemotaxis assay towards RPMI culture media and RPMI with 10% FCS after 3 and 24 hours. (b) Macrophage (serum starved and non serum starved) migration in transwell chemotaxis assay towards serum treated with 65.5µg/ml Fe_2O_3 particles.

(a)

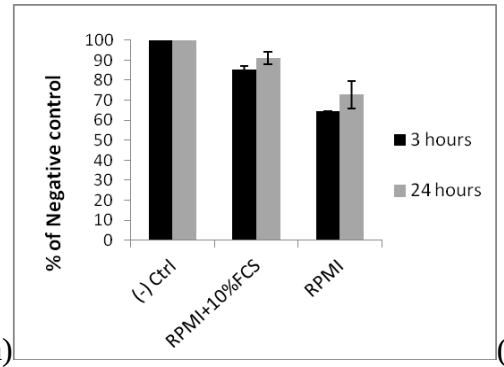

(b)

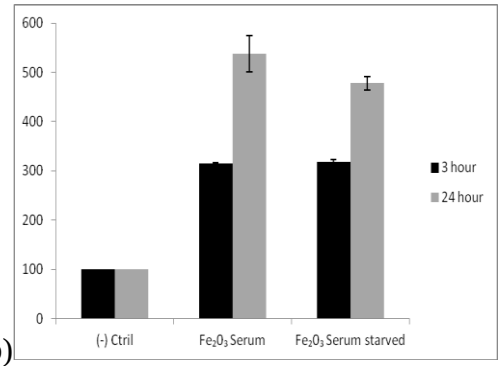

8.13 Experimental Chemotaxis Assay

(a)

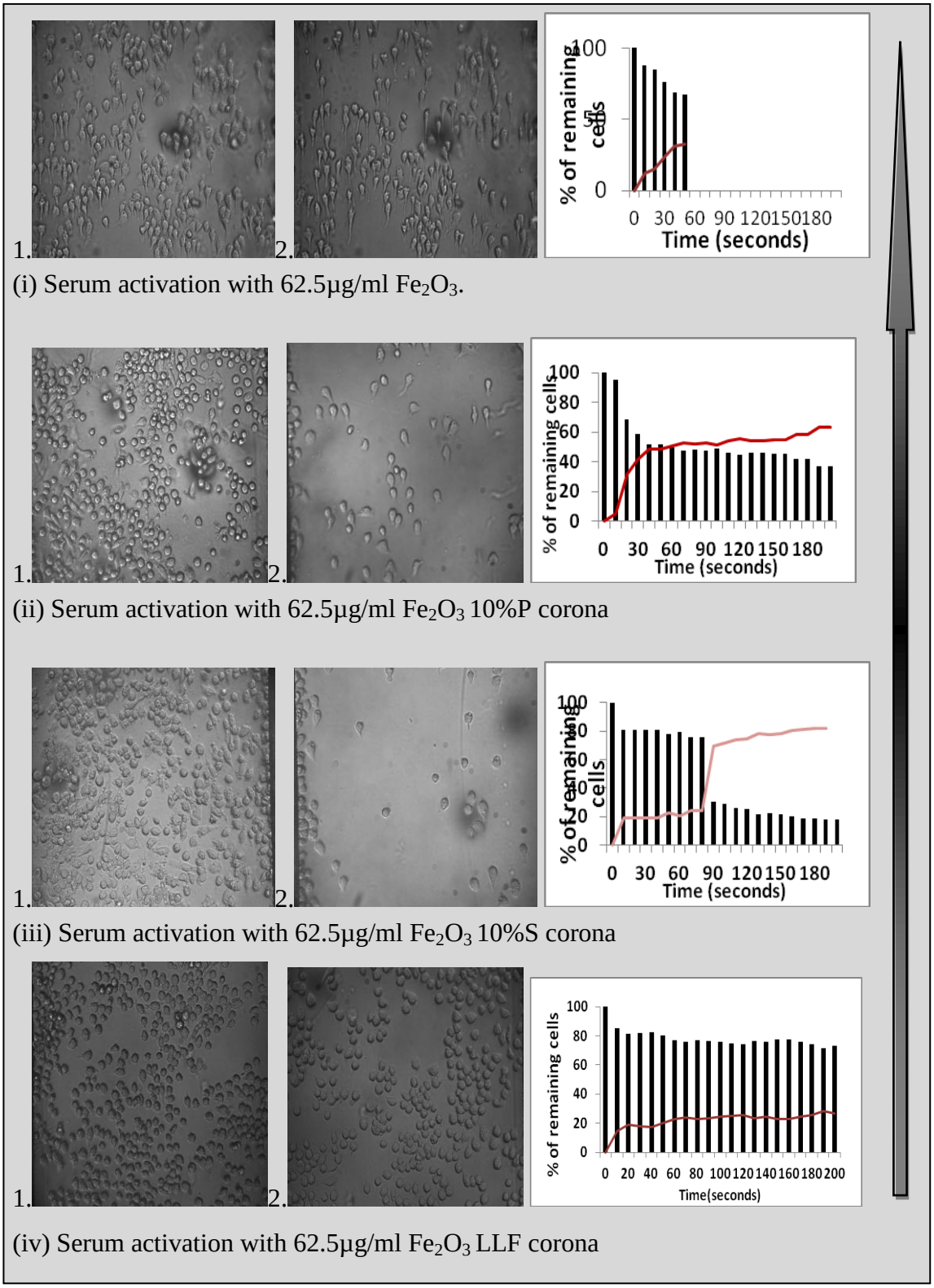

Figure 8.11(a) Microfluidic analysis of cells exposed to Fe_2O_3 particle activated serum. Image one at 0 seconds and image two at 200 Seconds. The graph shows the percentage of remaining cells, the red line represent the cells that migrated

(b)

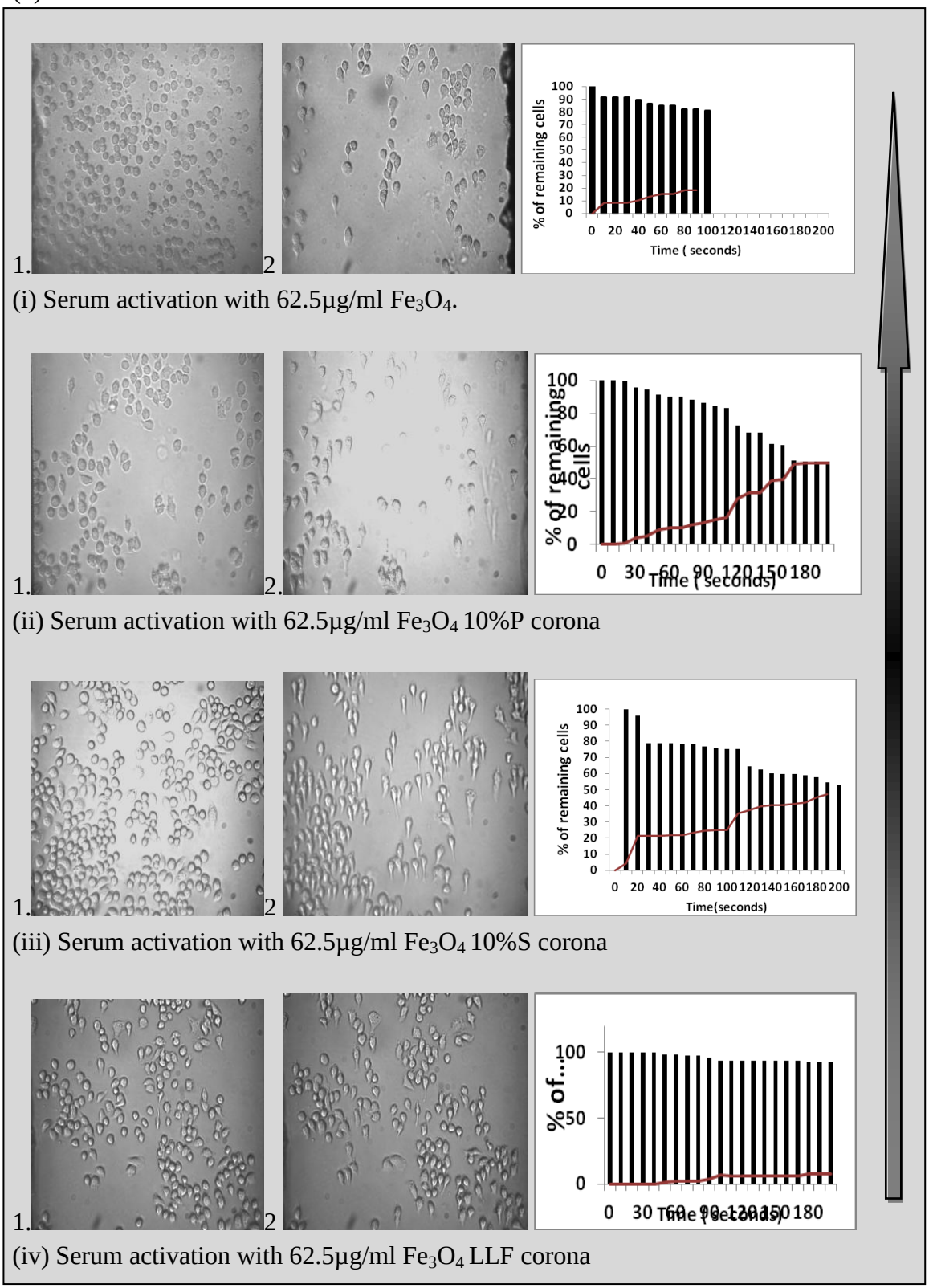

Figure 8.11(b) Microfluidic analysis of cells exposed to Fe_3O_4 particle activated serum. Image 1 at 0 Seconds and image 2 at 200 Seconds. The graph shows the percentage of remaining cells, the red line represent the cells that migrated.

(c)

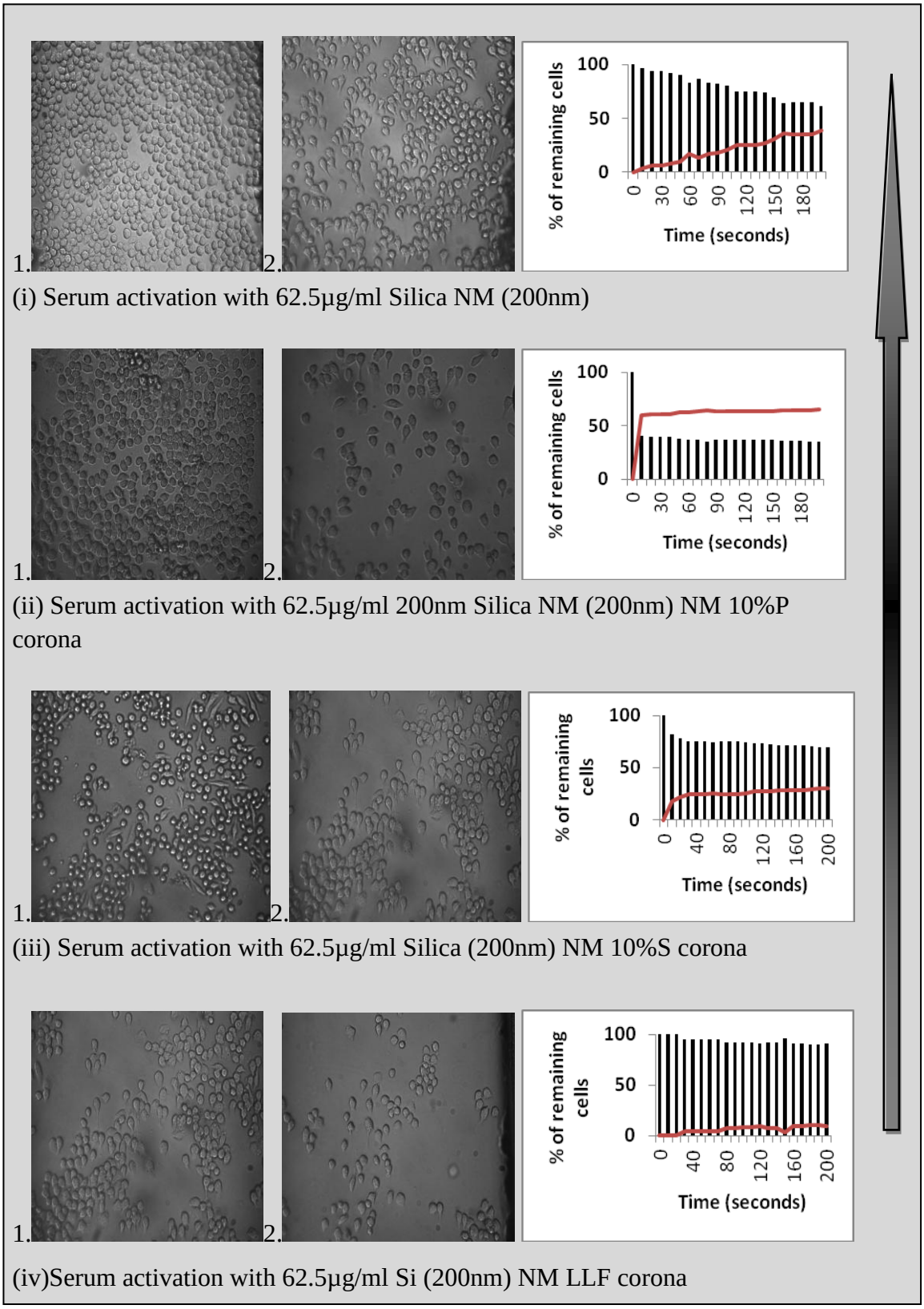

Figure 8.11(c): Microfluidic analysis of cells exposed to 200nm silica activated serum image 1 at 0 Seconds and image 2 at 200 Seconds. The graph shows the percentage of remaining cells, the red line represent the cells that migrated.

(d)

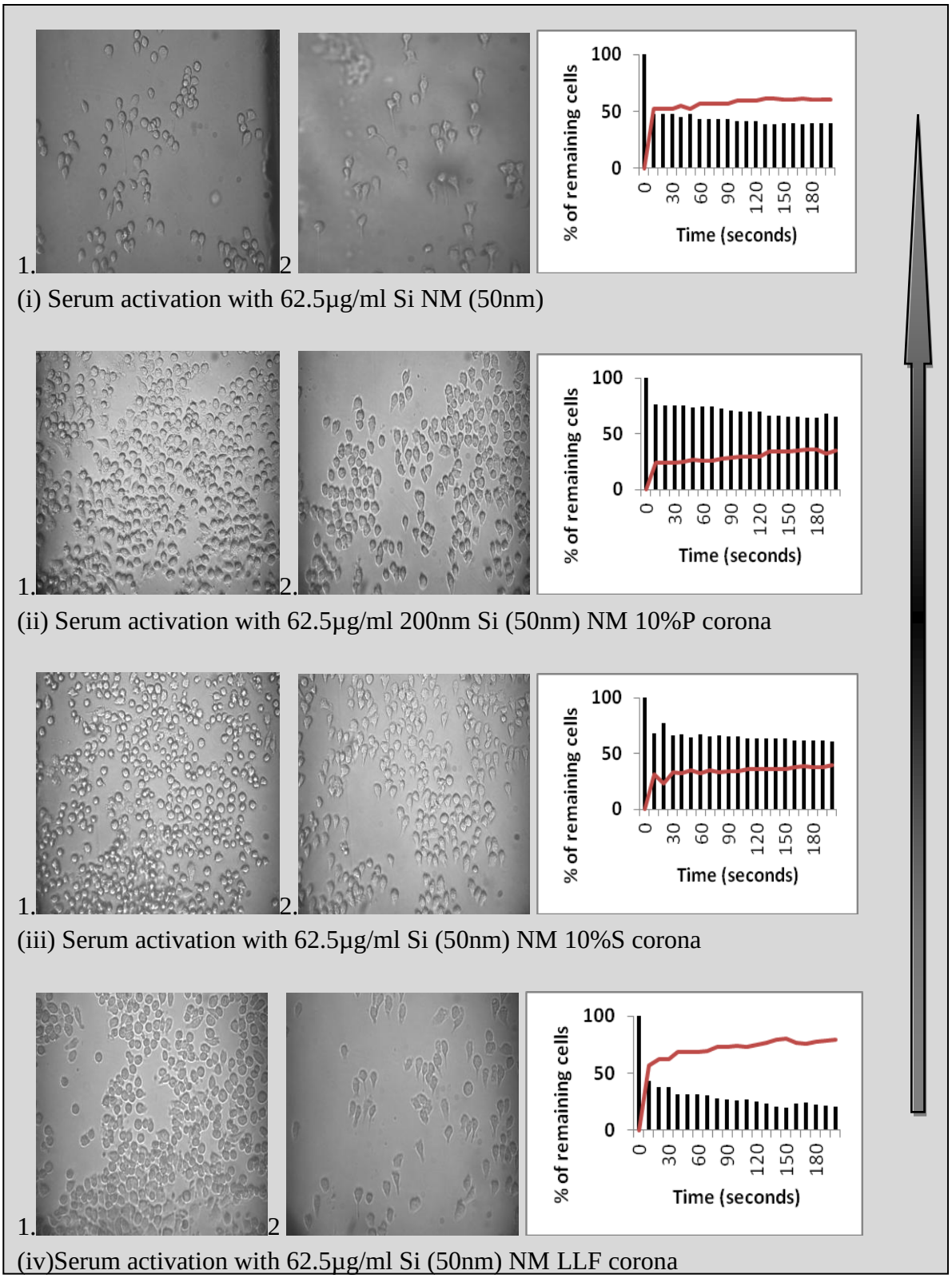

Figure 5.8(d) Microfluidic analysis of cells exposed to 50nm silica activated serum. Image 1 at 0 Seconds and image 2 at 200 Seconds. The graph shows the percentage of remaining cells, the red line represent the cells that migrate.

8.14 Confocal Image-Supplementary Data to Section 5.3.4

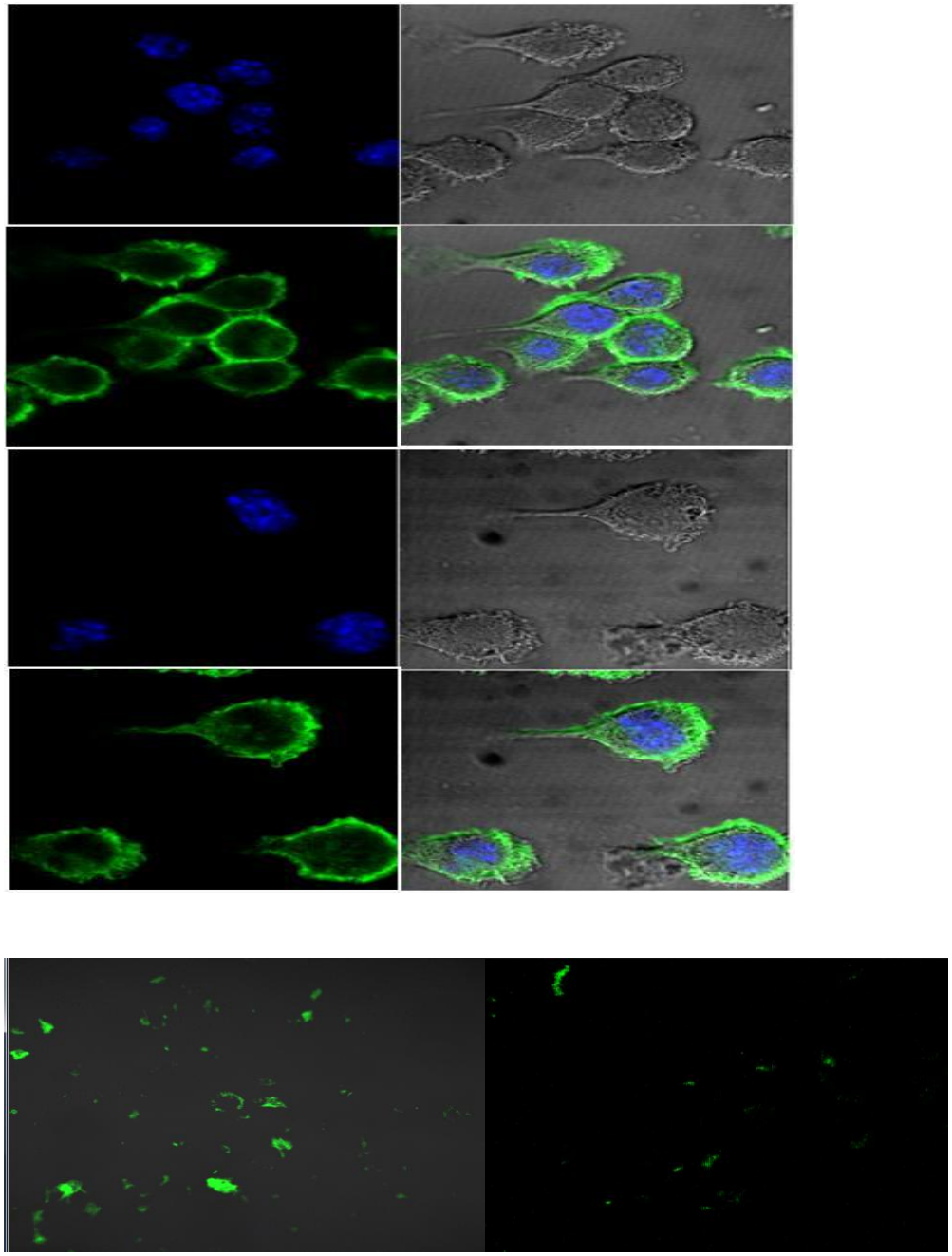

Figure 8.12 Confocal Imaging taken using 63X oil immersion lens showing J774.A1 cells exposed to serum activated with (a) Fe_2O_3 particles (b) Fe_3O_4 particles (c)Channel after cells have migrated. The cells imaged were those remaining on the microfluidic Cellix substrate chip from microfluidic analysis. Cells were fixed in 3.7% paraformaldehyde and stained with Phalloidin-FITC and Hoechst. Images were obtained on a Zeiss Laser Scanning Microscope (LSM 510 META from Zeiss, Germany).